AMINOETHYL-(α,α-DIMETHYL)-GLYCYL PNAs: SYNTHESIS AND INTERACTION STUDIES WITH DNA AND GOLD NANOPARTICLES

A THESIS SUBMITTED TO THE

UNIVERSITY OF PUNE

FOR THE DEGREE OF

DOCTOR OF PHILOSOPHY

IN

BIOTECHNOLOGY

BY

GOURISHANKAR RAJSHEKHAR ALAND

DIVISION OF ORGANIC CHEMISTRY (SYNTHESIS)

NATIONAL CHEMICAL LABORATORY

PUNE 411 008, INDIA

AUGUST 2006

CERTIFICATE

This is to certify that the work presented in the thesis entitled "**AMINOETHYL-(α,α-DIMETHYL)-GLYCYL PNAs: SYNTHESIS AND INTERACTION STUDIES WITH DNA AND GOLD NANOPARTICLES**" submitted by **Gourishankar Rajshekhar Aland** was carried out by the candidate at the National Chemical Laboratory, Pune, under our supervision. Such materials as obtained from other sources have been duly acknowledged in the thesis.

Dr. K. N. GANESH
(Research Guide)
Director, IISER, Pune-411008.

Dr. MURALI SASTRY
(Research Co-Guide) **AUGUST 2006**

CANDIDATE'S DECLARATION

I hereby declare that the thesis entitled "**AMINOETHYL-(α,α-DIMETHYL)-GLYCYL PNAs: SYNTHESIS AND INTERACTION STUDIES WITH DNA AND GOLD NANOPARTICLES"** submitted for the degree of Doctor of Philosophy in Biotechnology to the University of Pune has not been submitted by me to any other University or Institution. This work was carried out at the National Chemical Laboratory, Pune, India.

Gourishankar R. Aland
Senior Research Fellow (CSIR),
Division of Organic Chemistry (Synthesis),
National Chemical Laboratory,
Pune - 411 008, INDIA.

AUGUST 2006

Dedicated to my Parents &

To my Mentor, Dr. K. N. Ganesh

ACKNOWLEDGEMENTS

It gives me great pleasure to place on record my deep sense of gratitude to my research supervisor **Dr. K. N. Ganesh** for his encouragement and scientific temperament, which furthered my interest in bio-organic chemistry and Bio-nanotechnology. I wish to thank him for the confidence he had in me which allowed me near total freedom in pursuing avenues which I thought were interesting. His undying enthusiasm for science and unwavering support is always a source of inspiration. His integral view on research and mission for providing only high-quality work and not less, has made a deep impression on me. He had given me full of freedom- freedom to learn, freedom to discover my true potential, freedom to express myself, freedom to set my goals where I am free to aim for the sky. He is the one who gives me the tools, I call values, by which I live the rest of my lives.

My special thanks goes to my Co-guide Dr. Murali Sastry, formerly at Physical Chemistry Division, NCL, Pune (Presently Chief Scientist, TATA Chemicals Limited, Mumbai) for his encouragement, ideas, understanding and suggestions. Without his support, I would not have been able to complete work on nanotechnology.

I am very much grateful to Dr. Mrs. V. A. Kumar for her dedicated help, kind advice, inspiration, encouragement and continuous support throughout my tenure at NCL. The confidence she had in me, willingness to share new ideas, excitements helped me in a great sense to shape my research career and realistic life.

I owe much to Dr. Mrs. S. R. Deshpande, Dr. Mrs. A. P. Likhite, and Dr. Mrs. S. P. Maybhate who never failed to stop by and discuss interesting results. They truly helped shape and improve my thinking during my initial days of my research. Without their boundless love and support, I would not have been able to complete work on sterically hindered amino acid, α-aminoisobutyric acid.

I am equally indebted to Dr. S. D. Prasad for his help during the course of this work on thermodynamic calculations. My sincere thanks go to Mrs. Anita Gunjal for providing synthesized DNA and Dr. A. A. Natu & Dr. N. P. Argade for their valuable help during the course of this work.

I wish to thank Mrs. Shantakumari and Dr. Mahesh Kulkarni, NCL for their help in recording the LC-Ms and MALDI-TOF spectra. I wish to acknowledge Mrs. M. V. Mane and Mrs. S. S. Kunte for carting out the HPLC analysis and Mrs. Phalgune and Mr. Sathe for their assistance in recording the NMR. Also I wish to acknowledge Mrs. Renu Pasricha for recording the TEM images.

The KNG group has been my family for past few years. During this time, all members past and present have helped me, inspired me and entertained me. I was glad to be a member of such a diverse and lively group. Thanks to Moneesha, Meena, Ramesh, Pallavi, Dinesh, Nagendra, Govind, Pravin, Raman, Umashankar, Sunil, Smita, Madhuri, Khirud, Sushmita, Amit, Ashwani, Sridhar, Geetali, Roopa, Pradnya, Manaswini, Sachin, Mahesh and Sourabh from Nanoscience group for always willing to help and for making the lab a pleasant and productive place. I thank you all for your care and attention. I also thank OCS office staff- Mrs. Deshpande, Mr. P. V. Iyer, Pawar and Bhumkar for their assistance in many ways throughout my tenure at NCL.

I wish to thank many relatives, friends and colleagues who have helped in one way or other, especially Jayant, Meghraj, Avinash and all teaching staff of S. G. R. S. College of Pharmacy, Saswad, Pune and many in NCL who are not named in person, for their valuable friendship and helping hand.

I acknowledge The Council of Scientific and Industrial Research, New Delhi for providing me financial support in the form of a fellowship. I am grateful to the Director, NCL, for giving me the opportunity to work in this institute.

Finally I would like to thank in a special way to my Parents, my brothers - Santosh and Sidddheshwar and my wife, Shruti, who were extremely patient and tolerant towards my erratic hours of work and for being a source of unending love, extended support, encouragement and appreciation throughout my research work to excel in whatever I did.

Gourishankar

CONTENTS

CHAPTER 1:

INTRODUCTION TO PEPTIDE NUCLEIC ACIDS

CHAPTER 2:

MODIFIED *aeaib*- & *apaib*-PNAs:

SYNTHESIS AND DNA/RNA BINDING STUDIES

CHAPTER 3:

DNA/PNA NANOBIOTECHNOLOGY

CHAPTER 3: Section A

INTRODUCTION TO DNA/PNA NANOBIOTECHNOLOGY

CHAPTER 3: Section B
PRESENT WORK

Reprints of Publications

1. **Gourishankar A.**; Shukla S.; Ganesh K. N.; Sastry M. **Isothermal Titration Calorimetry Studies on the Binding of DNA Bases and PNA Base Monomers to Gold Nanoparticles.** *J. Am. Chem. Soc.* **2004**, *126*, 13186-13187.

   (No. of Citations = 10)

2. **Gourishankar A.**; Shukla S.; Sastry M.; Ganesh K. N. **DNA and PNA as templates for building nanoassemblies via electrostatic complexation with gold nanoparticles.** *Curr. Appl. Phys.* **2005**, *5,* 102-107.

   (No. of Citations = 1 and One out of Top 25 Hottest articles on ScienceDirect.com)

ABBREVIATIONS

β-ala	β-alanine
A	Adenine
aeg	Aminoethylglycine
aeaib	Aminoethyl-α-aminoisobutyric acid
aep	Aminoethylpropyl
AFM	Atomic Force Microscopy
aib	α-aminoisobutyric acid
ala	Alanine
ap	Antiparallel
apaib	Aminopropyl-α-aminoisobutyric acid
apg	aminopropylglycine
AS-ONs	Antisense Oligonucleotides
AuNP	Gold nanoparticles
Boc	Tertiary-butyloxycarbonyl
BMC	Biomolecular Computation
C	Cytosine
Cbz	benzyloxy carbonyl
CD	Circular Dichroism
CNT	Closed-carbon nanotube
CST	Critical solution temperature
dA	Deoxy-adenine
dAA	α,α-disubstituted α-amino acid
DCC	Dicyclohexylcarbodiimide
DCM	Dichloromethane
DCU	Dicyclohexyl urea
dG	2'-deoxyguanine

DIAD	Diisopropylazodicarboxylate
DIPCDI	Diisopropylcarbodiimide
DIPEA	Diisopropylethylamine
DMF	N,N-Dimethylformamide
DNA	2'-deoxyribonucleic acid
DSC	Differential Scanning Calorimetry
FAB	Fast atom bombardment
FDA	Food & Drug Administration
FISH	Fluorescence *in situ* hybridization
Fmoc	9-Fluorenylmethoxycarbonyl
FPLC	Fast Protein Liquid Chromatography
FTIR	Fourier Transform Infra-Red
g	Gram
G	Guanine
gly	Glycine
hr	Hours
HBTU	*O*-(1H-Benzotriazol-1-yl) *N*,*N*,*N*^{1},*N*^{1}-tetramethyl uronium hexafluorophosphate
HG	Hoogsteen
HIV	Human Immunodeficiency Virus
HOBt	1-Hydroxybenztriazole
HPLC	High Performance Liquid Chromatography
Hz	Hertz
ITC	Isothermal Titration Calorimetry
LNA	Locked Nucleic Acids
µM	Micromolar
MALDI-TOF	Matrix Assisted Laser Desorption Ionisation-Time Of Flight

MBO	Mixed Backbone Oligonucleotides
MBHA	4-methylbenzhydrylamine
MF	Merrifield Resin
Mg	Milligram
MHz	Megahertz
M	Molar
Ml	Milliliter
mM	Millimolar
Mmol	Millimoles
*m*RNA	messenger Ribonucleic acid
N	Normal
Nm	Nanometer
NMP	N-methyl pyrrolidine
NMR	Nuclear Magnetic Resonance
ODNs	Oligodeoxynucleotides
ONs	Oligonucleotides
p	Parallel
PARC	PNA assisted rare cleavage
PCR	Polymerase Chain Reaction
PPh_3	Triphenyl phosphine
PNA	Peptide Nucleic Acid
Pro	Proline
PS	Phosphorothioate
Pyr	pyrrolidinone
RAIR	Reflection Absorption Infra-Red
RNA	Ribonucleic acid
RISC	RNA inducing silencing complex

RP-HPLC	Reversed Phase HPLC
r.t.	Room temperature
ss	Single strand/ Single stranded
s	Seconds
SAM	Self-assembled monolayer
SAR	Structure Activity Relationship
S-DNA	Thiolated DNA
SERS	Surface Enhanced Raman Spectroscopy
SMCC	Succinimidyl-4-(*N*-maleimidomethyl)-cyclohexane-1-carboxylate
STM	Scanning Tunneling Microscopy
SWNT	Single-walled carbon nanotube
T	Thymine
TBTU	*O*-(1H-Benzotriazol-1-yl) *N*,*N*,N^{1},N^{1}-tetramethyl uronium tetrafluoroborate
TEA	Triethylamine
TEM	Transmission Electron Microscopy
TFA	Trifluroacetic acid
TFMSA	Trifluromethanesulphonic acid
THF	Tetrahydrofuran
UV-Vis	Ultraviolet- Visible
WC	Watson-Crick

ABSTRACT

The Thesis entitled "**Aminoethyl-(α,α-dimethyl)-glycyl PNAs: Synthesis and Interaction Studies with DNA and Gold nanoparticles**" is divided into four chapters.

Chapter 1 introduces background literature for undertaking the research work on peptide nucleic acids and defines the objectives.

Chapter 2 details the synthesis and DNA/RNA hybridization studies of *aeaib*- and *apaib*- PNAs.

Chapter 3 Section A introduces background literature for undertaking the research work on DNA/PNA based nanotechnology and defines the objectives. Section B describes interaction studies of DNA and PNA with gold nanoparticles by microscopy, spectroscopy and microcalorimetry.

Chapter 1: Introduction to Peptide Nucleic Acids (PNAs).

The potential of oligodeoxynucleotides to act as antisense agents that inhibit viral replication in cell culture was discovered by Zamecnik and Stephenson in 1978. Since then antisense technology has been developed as a powerful tool for target validation and therapeutic purposes. To be effective as medicinal agents, the therapeutic oligonucleotides should be made to cross the membrane and be stable to cellular nucleases. Among the several chemical modifications, PNAs are emerging as one of the potential candidates.

Peptide nucleic acids (PNAs), are a new class of DNA analogues invented 12 years ago, in which the charged sugar-phosphate backbone of DNA is replaced by a neutral and achiral polyamide backbone as shown in Figure 1. The monomeric unit consists of N-(2- aminoethyl) glycine units to which the nucleobases are attached through a conformationally rigid, tertiary acetamide linker group. The binding of PNA to the target DNA/RNA sequences occurs with high sequence specificity and affinity. Despite having several advantages like resistance to cellular enzymes such as nucleases and proteases, the major limitations confounding its application are ambiguity in orientational selectivity of binding (parallel/antiparallel), poor solubility in aqueous media and inefficient cellular uptake.

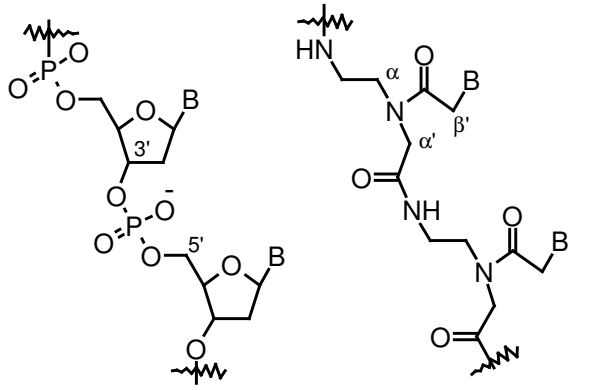

Chapter 2: Synthesis of *N*-(Boc-aminoethyl-α,α-dimethylglycyl)-thymine PNA and *N*-(Boc-aminopropyl-α,α-dimethylglycyl)-thymine PNA monomers: Synthesis and biophysical studies with DNA/RNA.

The deficiencies of PNA are addressed by rational structural modifications of PNA based on conformational preorganization of backbone using gem-dimethyl functionality in the glycine unit of *aeg*- and *apg*-PNA (Figure 2). In contrast to well-known strategies towards chiral and cyclic PNAs, an approach is to make them achiral and acyclic and also pre-organize the PNA backbone for favorable binding by constraining the conformation through substituents on the backbone. These analogues to some extent improved the solubility, affinity and orientational selectivity in DNA: PNA binding. The objective of this chapter is to carry out the synthesis of *N*-(Boc-aminoethyl-α,α-dimethylglycyl)-thymine PNA and *N*-(Boc-aminopropyl-α,α-dimethylglycyl)-thymine PNA monomers and biophysical studies with DNA/RNA.

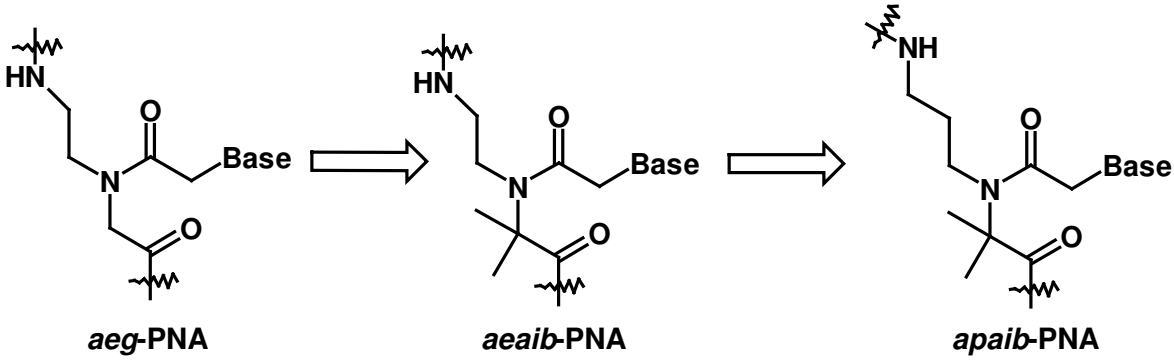

Figure 2. Structural modifications in *aeg*-PNA in present work

2.1. Synthesis of aminoethyl (α, α-dimethyl)-glycyl (*aeaib)* thymine monomer :

The synthesis of *aeaib* PNA monomer was carried out starting from the easily available 1,2-diaminoethane **1**. This was treated with Boc-anhydride to give the mono-protected derivative **2**, obtained by using a large excess of 1,2-diaminoethane over the Boc-anhydride. The di-Boc derivative obtained in very small amounts (< 5%), being insoluble in water, could be removed by filtration. The *N1*-Boc-1,2-diaminoethane **2** was then subjected to *N*-alkylation using ethyl-2-bromo-isobutyrate and potassium carbonate in dry acetonitrile. The aminoethyl (α,α-dimethyl) glycine ethyl ester **3** was treated with chloroacetyl chloride to yield the corresponding chloro derivative **4**. Thymine was reacted with ethyl *N*-(Boc-aminoethyl)-*N*-(chloroacetyl)- (α,α-dimethyl)glycine ethyl ester using K_2CO_3 to obtain the *N*-(Boc-aminoethyl-α,α-dimethylglycyl)-thymine ethyl ester **5**. The ethyl ester in the *aeaib*-PNA monomer was hydrolyzed by aqueous methanolic sodium hydroxide to yield the corresponding carboxylic acid **6**.

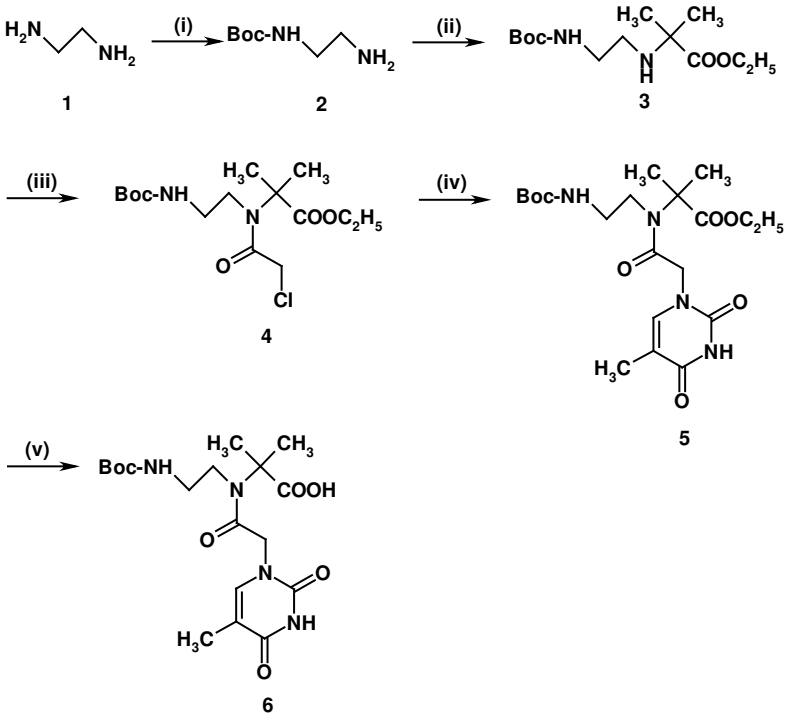

Scheme 1. Reagents and conditions : (i) boc-anhydride, dioxane: water (1:1), rt, 12hrs (ii) ethyl-2-bromo isobutyrate, dry acetonitrile, K_2CO_3, 50^0C, 6hrs (iii) $ClCH_2COCl$, Na_2CO_3, dioxane: water (1:1) (iv) thymine, K_2CO_3, dry DMF (v) NaOH, water, methanol.

2.2. Synthesis of aminopropyl (α, α-dimethyl)-glycyl (*apaib)* thymine monomer :

The synthesis of *apaib* PNA monomer was carried out starting from 1,3-diaminopropane **7** which was treated with Boc-anhydride to give the mono-protected derivative **8**, using a large excess of 1,3-diaminopropane over the Boc-anhydride. The di-Boc derivative obtained in very small amounts (< 5%), being insoluble in water, could be removed by filtration. The *N1*-Boc-1,3-diaminopropane **8** was subjected to *N*-alkylation using ethyl-2-bromo-isobutyrate and potassium carbonate in dry acetonitrile. The aminopropyl (α,α-dimethyl) glycine ethyl ester **9** was treated with chloroacetyl chloride to yield the chloro derivative **10**. Thymine was reacted with ethyl *N*-(Boc-aminopropyl)-*N*-(chloroacetyl)- (α,α-dimethyl)glycine ethyl ester using K_2CO_3 to obtain the *N*-(Boc-aminopropyl-α,α-dimethylglycyl)-thymine ethyl ester **11** in high yield. The ethyl ester group of the *apaib*PNA monomer was hydrolyzed by aqueous methanolic sodium hydroxide yield the corresponding carboxylic acid **12**.

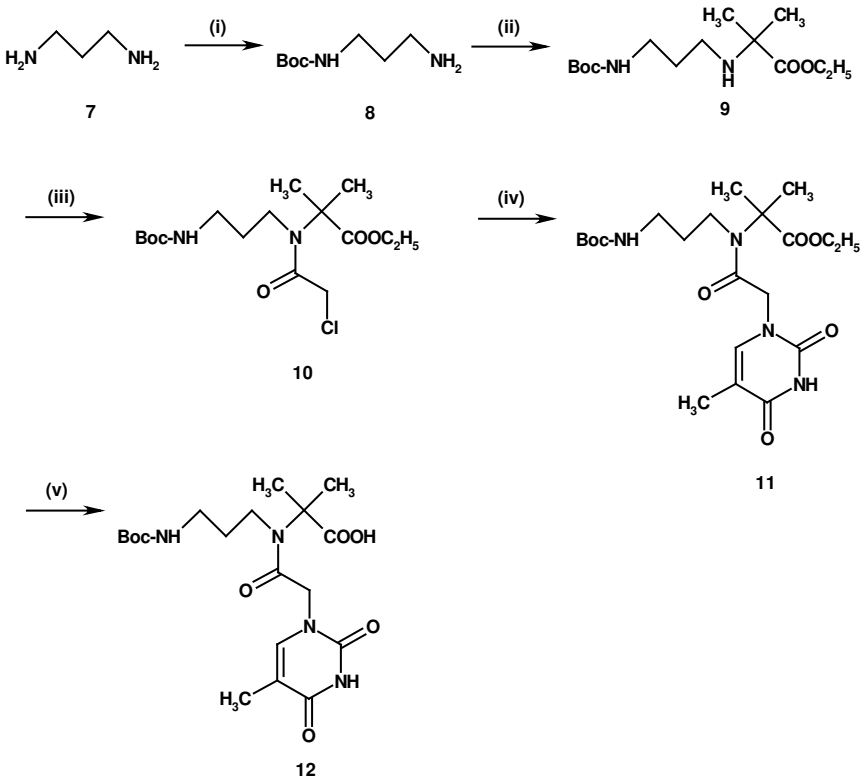

Scheme 2. Reagents and conditions : (i) boc-anhydride, dioxane: water (1:1), rt, 12hrs (ii) ethyl-2-bromo isobutyrate, dry acetonitrile, K_2CO_3, 50^0C, 6hrs (iii) $ClCH_2COCl$, Na_2CO_3, dioxane: water (1:1) (iv) thymine, K_2CO_3, dry DMF (v) NaOH, water, methanol.

2.3. Solid Phase Synthesis of *aeg-aepip*PNA Oligomers.

The *aeaib*- and *apaib*-PNA monomers **6** and **12** were incorporated into the PNA oligomer sequences at predefined positions to yield the modified *aeg*PNAs **2**-**11** and **13** & **14**. For control studies, the unmodified *aeg*PNA sequences **1** and **12** were used. PNAs (**1-14**) after cleavage from the resin were purified by HPLC on RPC-18 column and characterized by MALDI-TOF mass spectrometry. The complementary DNA oligomers **1-4** were synthesized on an automated DNA synthesizer. The RNA oligonucleotides **1-3** complementary to PNA oligomers were obtained commercially from Genomechanix, Gainesville, FL, along with the HPLC purity and mass spectral data.

2.4. Biophysical studies on PNA:DNA complexes.

The studies on DNA:PNA interactions are investigated by UV, CD and ITC. The CD of DNA complexes of *apaib* PNAs were similar to that of the *aeg*-PNA:DNA complexes. The PNA_2:DNA triplexes exhibited two maxima at 265nm and 280nm with a minimum at 246nm and crossover points between ~250- ~260nm. The double hump profile is characteristic of poly T:poly A:poly T triplexes as shown in Figure 12 (PNA **7**:DNA **1**).

The polypyrimidine PNA oligomers (**1-11**) are homopyrimidine sequences that are well known to form DNA:PNA_2 triplexes. The thermal stabilities of PNA_2:DNA complexes were studied by temperature dependent UV absorbance measurements. The mixed purine-pyrimidine *aeg-aeaib*PNA (**13**), *aeg-apaib*PNA (**14**) and control *aeg*PNA (**12**) oligomers were synthesized to examine the orientational selectivity in binding to DNA/RNA. Table **1** & **2** show the T_m values for PNA:DNA/RNA complexes derived from various *aeg*PNA, *aeg-aeaib*PNAs and *aeaib*PNA homothymine as well as mixed sequences with different degrees of modification which exhibited stabilization compared to the unmodified *aeg*PNA oligomer.

The T_m values from Table 1 & 2 indicates-

- The homopyrimidine-*aeg*PNA backbone comprising *aeaib*/*apaib* units effect stabilization of the resulting triplexes with complementary DNA/RNA strands depending upon the number of modified PNA monomer units.

- Three modified units in a mixed purine-pyrimidine duplex-forming oligomer discriminates between the *parallel* versus *antiparallel* DNA/RNA sequence much better than the unmodified *aeg*PNA.

Table 1. UV-T_m (^{0}C) of *aeaib*/*apaib*PNA:DNA complexes.*

Entry	PNA sequence	DNA	T_m in ^{0}C
1.	PNA **1** H – T T T T T T T T -Lys NH_2	**1**	43.0
2.	PNA **2** H – T T T T T T T **t** -Lys NH_2	**1**	51.1
3.	PNA **3** H – T T T T T **t** T **t** -Lys NH_2	**1**	57.9
4.	PNA **4** H – T T T **t** T **t** T **t** -Lys NH_2	**1**	64.7
5.	PNA **5** H – T **t** T **t** T **t** T **t** -Lys NH_2	**1**	79.6
6.	PNA **6** H – **t t t t t t t t** -Lys NH_2	**1**	>85
7.	PNA **7** H – T T T T T T T ***t*** – Lys NH_2	**1**	40.3
8.	PNA **8** H – T T T T T ***t*** T ***t*** – Lys NH_2	**1**	48.4
9.	PNA **9** H – T T T ***t*** T ***t*** T ***t*** – Lys NH_2	**1**	55.2
10.	PNA **10** H – T ***t*** T ***t*** T ***t*** T ***t*** – Lys NH_2	**1**	59.2
11.	PNA **11** H – ***t t t t t t t t*** – Lys NH_2	**1**	76.9
12.	PNA **12** H – G T A G A T C A C T – Lys NH_2	**3** (*ap*)	49.8
13.	PNA **12** H – G T A G A T C A C T – Lys NH_2	**4** (*p*)	37.5
14.	PNA **13** H – G **t** A G A **t** C A C **t**– Lys NH_2	**3** (*ap*)	80.9
15.	PNA **13** H – G **t** A G A **t** C A C **t** – Lys NH_2	**4** (*p*)	56.5
16.	PNA **14** H – G ***t*** A G A ***t*** C A C ***t***– Lys NH_2	**3** (*ap*)	72.8
17.	PNA **14** H – G ***t*** A G A ***t*** C A C ***t*** – Lys NH_2	**4** (*p*)	49.7

*DNA **1**= 5'GCAAAAAAAACG3'; DNA **3**= $^{5'}$AGTGATCTAC$^{3'}$ and DNA **4**= $^{5'}$CATCTAGTGA$^{3'}$ T=*aeg*PNA; **t** = *aeaib*PNA; ***t*** = *apaib*PNA Buffer: 10 mM sodium phosphate, pH 7.4.

Table 2. UV-T_m (^{0}C) of *aeaib*/*apaib*PNA:RNA complexes*.

Entry	PNA sequence	RNA	T_m in ^{0}C
1.	PNA **1** H – T T T T T T T T -Lys NH_2	**3**	53.8
2.	PNA **2** H – T T T T T T T **t** -Lys NH_2	**3**	55.2
3.	PNA **3** H – T T T T T **t** T **t** -Lys NH_2	**3**	64.7
4.	PNA **4** H – T T T **t** T **t** T **t** -Lys NH_2	**3**	67.4
5.	PNA **5** H – T **t** T **t** T **t** T **t** -Lys NH_2	**3**	72.8
6.	PNA **6** H – **t t t t t t t t** -Lys NH_2	**3**	>85
7.	PNA **7** H – T T T T T T T ***t*** – Lys NH_2	**3**	44.3
8.	PNA **8** H – T T T T T ***t*** T ***t*** – Lys NH_2	**3**	51.1
9.	PNA **9** H – T T T ***t*** T ***t*** T ***t*** – Lys NH_2	**3**	55.2
10.	PNA **10** H – T ***t*** T ***t*** T ***t*** T ***t*** – Lys NH_2	**3**	56.5
11.	PNA **11** H – ***t t t t t t t t*** – Lys NH_2	**3**	60.6
12.	PNA **12** H – G T A G A T C A C T – Lys NH_2	**1** (*ap*)	50.1
13.	PNA **12** H – G T A G A T C A C T – Lys NH_2	**2** (*p*)	40.5
14.	PNA **13** H – G **t** A G A **t** C A C **t**– Lys NH_2	**1** (*ap*)	72.3
15.	PNA **13** H – G **t** A G A **t** C A C **t** – Lys NH_2	**2** (*p*)	31.6
16.	PNA **14** H – G ***t*** A G A ***t*** C A C ***t***– Lys NH_2	**1** (*ap*)	64.7
17.	PNA **14** H – G ***t*** A G A ***t*** C A C ***t*** – Lys NH_2	**2** (*p*)	32.9

*RNA **1**= 5'polyrA3'; RNA **1**= $^{5'}$AGUGAUCUAC$^{3'}$ and RNA **2**= $^{5'}$CAUCUAGUGA$^{3'}$, T=*aeg*PNA; **t** = *aeaib*PNA; ***t*** = *apaib*PNA Buffer: 10 mM sodium phosphate, pH 7.4.

- The main contributing factor to the enhanced affinity however, remains the specific hydrogen bonding between the A-T and G-C nucleobases.
- The *gem*-dimethyl functionality in the glycine unit of *aeg*- and *apg*-PNA contributes to the high binding affinity due to steric lock.
- Thus overall, the *gem*-dimethyl functionality in *aeg*- and *apg*-PNA backbone fit into the *aeg*PNA backbone with increased T_m of the derived complexes with DNA/RNA.

It is demonstrated that isothermal titration calorimetry may be successfully employed to study the thermodynamic parameters of PNA:DNA complexes. The UV-T_m stabilization of modified PNAs (*apaib*PNA and *apaib*PNA) over *aeg*PNA confirms with the entropy-enthalpy compensation suggesting the preorganization of modified PNA.

Finally, an efficient synthesis of modified *aeaib* and *apaib* monomers was developed and incorporated into the oligomers at derived sites. These results emphasize that the chemical, biophysical and structural properties can be controlled by the right kind of rigidity without any chirality. In this regard, the *gem*-dimethyl functionality need to be explored more by introducing in the aminoethyl segment or aminoethyl and glycine, both segments.

Chapter 3.

Section 3A: Introduction to DNA/PNA Nano-Biotechnology

Organization of nanoparticles on structurally well-defined templates is a first step towards creating nanomachines. In this respect, nucleic acids are ideal structural templates and a variety of secondary structures realizable from DNA/RNA. DNA, well-known as the predominant chemical for duplication and storage of genetic information in biology, has also recently been shown to be highly useful as an engineering material for construction of special purpose computers and micron-scale objects with nanometer-scale feature resolution. Properly designed synthetic DNA can be thought of as programmable glue which, via specific hybridization of complementary sequences, will reliably self-organize to form desired structures and superstructures. Such engineered structures are inherently information-rich and are suitable for use directly as computers or as templates for imposing specific patterns on various other materials. DNA-based nanotechnology has generated interest in a number of applications due to the specificity, programmability and reproducibility of DNA interaction with nanoparticles. Gold nanoparticles (AuNPs) modified with DNA find use in diverse fields such as DNA chips, DNA

sensors, drug/DNA delivery, imaging and bio-diagnostics and in structured nanoparticle assemblies for electronics. Similar applications are envisaged for the DNA analogue, peptide nucleic acids (PNAs).

The remarkable utility and versatility of such systems is attributed to the very nature of AuNP-DNA interaction, which in turn is determined by the differential affinity of the nucleobases (adenine, guanine, thymine and cytosine), nucleosides, nucleotides and oligonucleotide sequences to the gold nanoparticles. Previous studies on understanding the nature of interaction of nucleotides with nanogold have made use of various spectroscopic techniques such as Surface Enhanced Raman Spectroscopy (SERS), Fourier Transform Infra-Red (FTIR), and Reflection Absorption Infra-Red (RAIR) spectroscopy, which are clearly indirect methods for estimation of the strength of the abovementioned interactions.

The directed assembly of nanoparticles (in particular gold nanoparticles, AuNPs) using DNA as a natural template is gaining increasing popularity. The base pairing interaction of complementary DNA strands, which is mediated by hydrogen bonds, facilitates this process in a straightforward manner. The use of DNA as a structural interconnect for gold nanoparticle assembly has a number of advantages: (1) DNA sequences may be suitably designed to precisely control the extent of aggregation and inter-particle separation and thereby, the collective optical properties of the assembly (such assemblies have important implications in nanomaterials science);

(2) DNA is an excellent anionic one-dimensional template for promoting the growing metal nanowires either by a process of ion entrapment and reduction or direct attachment of metal nanoparticles and

(3) The sequence-specific denaturation of DNA duplexes enables the use of gold nanoparticles as colorimetric DNA detectors with immense application in diagnosis of genetic disorders.

In all studies pertaining to the assembly of nanoparticles by DNA hybridization, conjugation of the single stranded DNA sequences with gold nanoparticles has been achieved by thiolation of the DNA at the 3' end of the sequence. While this has been shown to be an excellent strategy for anchoring DNA at a single point to the nanoparticle via the strong gold-thiolate covalent bond, it is now explored to bind DNA to the nanoparticles through the DNA bases. Direct binding of nucleobases to gold nanoparticles could provide an excellent strategy for using the particles as nanoelectrodes for sensing, electron transport studies and as carriers in gene therapy.

Section 3B: Studies on interactions of DNA:PNA-Gold nanoparticles by spectroscopy, microscopy and microcalorimetry

The objective of this chapter is to study the thermodynamic analysis for interaction of the nucleobases (Adenine, Guanine, Cytosine and Thymine) as well as the corresponding PNA monomers with AuNPs at molecular level. The binding affinity of nucleobases towards AuNPs was determined by Isothermal Titration Calorimetry (ITC). The differential binding strengths by ITC of the four nucleobases can be exploited to develop alternative strategies of designing oligonucleotides for gold nanoparticle complexation without the need to thiolate oligonucleotides. Also this describes the synthesis and characterization of DNA/PNA-gold nanoparticle composites using TEM and UV-*T*m techniques.

3.1. Studies on interactions of DNA-nucleobases and PNA acid monomers with Gold nanoparticles (AuNPs) by UV-visible spectroscopy

The gold nanoparticles were capped with PNA base monomers and nucleobases was achieved by stoicheiometric mixing. Figure 3A and 3B shows the UV-vis absorption spectra recorded from AuNPs capped with PNA base monomers and DNA bases, respectively. In the case of PNA base monomer interaction with AuNPs (Figure 3A), binding is indicated by the appearance of a longitudinal plasmon band at ca. 670 nm, indicative of aggregation of the nanoparticles. In the case of PNA-thymine monomer interaction with AuNPs, the 670 nm band does not arise, suggesting weak interaction with the particles. A similar trend is seen in the reaction of nucleobases with gold nanoparticles (Figure 3B). The absence of a longitudinal absorption band and the broadening of transverse plasmon band at ca. 520 nm was seen upon AuNP complexation with G, C, and A. These results show that both the thymine nucleobase and thymine- PNA monomer interact much more weakly with AuNPs than the other

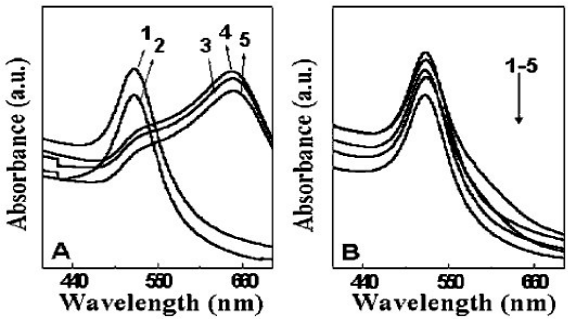

Figure 3. (A) UV-vis absorption spectra recorded from AuNPS modified with PNA base monomers. Curve 1 corresponds to as-prepared AuNPs. Curves 2-5 correspond to AuNP-PNA-T, AuNP-PNA-G, AuNPPNA- C, and AuNP-PNA-A solutions, respectively. (B) UV-vis absorption spectra of gold nanoparticles modified with DNA bases. Curves 1-5 correspond to the as-prepared AuNPs, AuNP-T, AuNP-A, AuNP-G, and AuNP-C solutions, respectively.

nucleobases/PNA base monomers. UV-vis spectroscopy is, however, unable to differentiate between the strength of interaction of the remaining three nucleobases/PNA monomers with AuNPs.

3.2. Studies on interactions of DNA-nucleobases and PNA acid monomers with Gold nanoparticles (AuNPs) by Transmission Electron Microscopy (TEM)

The TEM images are unable to highlight the differential binding affinities among the four nucleobases and the PNA monomers, but they support the higher binding affinities of the latter over the former as shown in Figure 4.

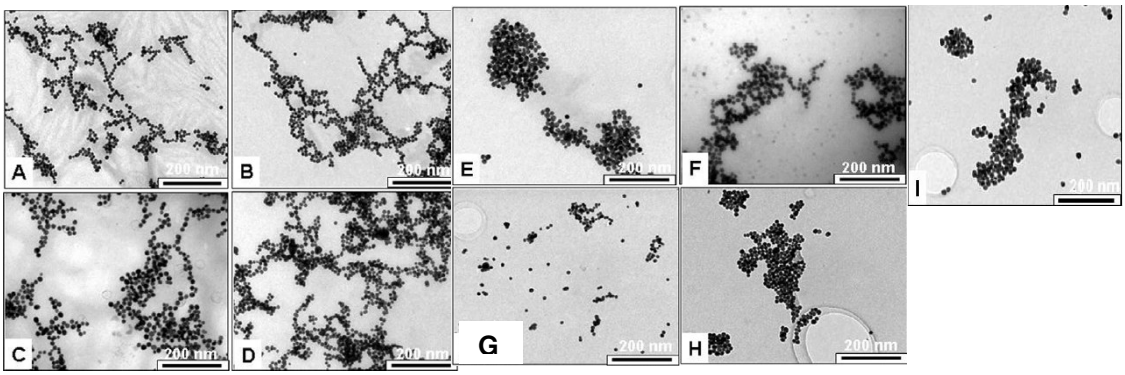

Figure 4. TEM images of Au-NP interaction with DNA bases and PNA monomers. Images A-D correspond to Au-NPs capped with cytosine, adenine, guanine and thymine respectively. Images E-H correspond to Au-NPs capped with PNA-cytosine, PNA-adenine, PNA-guanine and PNA-thymine respectively. Image I corresponds to as prepared Au-NPs.

3.3. Studies on interactions of DNA-nucleobases and PNA acid monomers with Gold nanoparticles (AuNPs) by Isothermal Titration Calorimetry (ITC)

ITC is a sensitive technique that measures the heat of reaction of two aqueous solutions when one is titrated against the other and has emerged as a powerful tool for studying the thermodynamic as well as kinetic aspects of complexation in biological systems. ITC has been used with much success in studies related to protein-protein interactions, protein-DNA interactions, protein-lipid interactions, etc. It is shown here that ITC may be used to directly observe the energetics of interaction of the nucleobases as well as the corresponding PNA base monomers with AuNPs. The results suggest that the binding affinity of nucleobases toward AuNPs is different from those obtained in earlier studies. The ITC results recorded for titration of the nucleobases and *aeg*-PNA base monomers with the AuNPs show that the interaction is exothermic. The three nucleobases C, A, and G and the corresponding PNA monomers show a classical binding behavior with a sigmoidal response while T and the PNA analogue did not elicit

a strong calorimetric response. Thus C, G, and A and their PNA base analogues bind strongly with gold nanoparticles, while T binds much more weakly in the order C > G > A > T. This suggests that amine groups of C, G and A interact strongly with aqueous AuNPs while T without an amine group weakly interacts with nanoparticles.

The thermodynamic data (Table 3) suggests that the *aeg*PNA monomers bind much more strongly to the AuNPs than the nucleobases.

Table 3. AuNP-DNA/PNA Interaction Exothermicity in cal/mol

Entry		Nucleobases	PNA monomers
1.	Cytosine	- 732.19	- 2444.92
2.	Guanine	- 427.18	- 1147.97
3.	Adenine	- 249.29	- 0518.45
4.	Thymine	-----	-----

3.4. Interaction of DNA and PNA with AuNPs

The gold nanoparticle solution (10 mM) was added to single stranded DNA-A_8 (10 μM) or PNA-T_8 and the solution was kept for 2 hr to enable the assembly. The hybridization of Au-DNA-A_8 and PNA-T_8, resulted in a color change from raspberry-red to purple. Figure 5 shows TEM images of uncapped gold nanoparticles complexes with DNA (dA_8), PNA–T_8 and dA_8:PNA-T_8.

Interestingly, the single stranded DNA-A_8 induces a uniformly packed nanoorganization of gold particles while the uncharged PNA-T_8 exhibits clusters in an aggregated form with no particular ordering of gold nanoparticles. Upon mixing the two complementary strands, some bit of order is restored, but no linear superclustered assemblies were seen as in case of DNA:DNA duplexes. The UV-Visible spectra showed a weak and broad red shifted surface plasmon band at 538 nm. Thus charges present on DNA and gold nanoparticles seem to be the driving factors for formation of highly ordered linear superclusters by electrostatic complexation.

3.5. DNA-PNA-gold hybrids

In order to examine the effect of gold particle complexation on thermal stability of DNA:PNA hybrids, temperature dependent UV absorbance were done at 260 nm. The DNA:PNA duplexes both free and in gold complexes showed sigmoidal transitions characteristic of two phases and the T_m, obtained from first derivative melting curves is shown in Table 4.

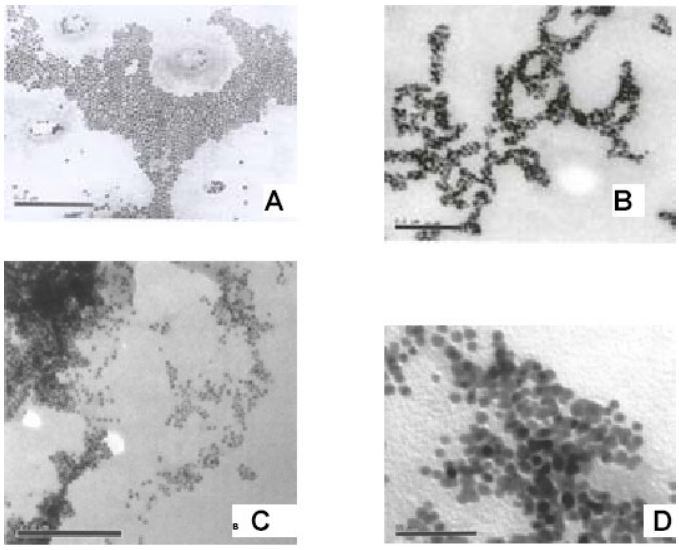

Figure 5. TEM images of uncapped gold nanoparticle complexes with (A) DNA-A_8 (B) PNA-T_8 and (C) DNA-A_8:PNA-T_8. D is a magnified image of asection of C.

Table 4. UV-*T*m of DNA:PNA hybrids

Entry	DNA:PNA (1:2)	T_m in ^{0}C	ΔT_m in ^{0}C
1.	dA_8:PNA-T_8	39.1	-----
2.	AuNP-dA_8:PNA-T_8	74.2	35.1
3.	AuNP-dA_8:AuNP-PNA-T_8	76.9	37.8
4.	Lys-AuNP-dA_8:PNA-T_8	58.7	19.6

Significant stabilization of DNA:PNA hybrids occurs upon complexation with gold nanoparticles. When Au-DNA-A_8 is mixed with PNA–T_8, the stability is enhanced by about 35^{0}C (Entry 1 and 2), while mixing of DNA and PNA strands, both in gold complexed form had an improvement of about 37.8^{0}C suggesting that even one strand complexation with gold nanoparticle is good enough to effect a large stabilization of hybrids. When lysine capped gold nanoparticles were used, the stability enhancement was much less (ΔTm = 19.6^{0}C), perhaps due to the repulsive effects of positively charged lysine and the N-terminus of PNA.

In conclusion, it is shown the non-thiolic polyanionic DNA can act as a template for organizing lysine capped cationic gold nanoparticles into linear superstructures. PNA:DNA hybrids generated upon gold nanoparticles also remarkably stabilize the DNA:PNA hybrids against thermal denaturation.

PUBLICATIONS/ CONFERENCES/SYMPOSIA PARTICIPATED

PUBLICATIONS

- Isothermal Titration calorimetry Studies on the binding of DNA bases and PNA base monomers to Gold nanoparticlesfor building nanoassemblies via electrostatic complexation with gold nanoparticles. **A. Gourishankar**; Sourabh Shukla; Krishna N. Ganesh and Murali Sastry. *J. Am. Chem. Soc.*, **2004**, *126,* 13186-13187.

- DNA and PNA templates for building nanoassemblies via electrostatic complexation with gold nanoparticles. **A. Gourishankar**; S. Shukla; R. Pasricha; M. Sastry and K. N. Ganesh. *Curr. Appl. Phys.*, **2005**, *5,* 102-107.

- Thermodynamics of the interaction of gold nanoparticles with DNA bases: an isothermal titration calorimetry analysis. **A. Gourishankar**; S. Shukla; S. D. Prasad; K. N. Ganesh and M. Sastry. **2006** (Manuscript under preparation).

- Synthesis and Biophysical studies of gem-dimethyl substituted Peptide Nucleic Acids. **A. Gourishankar** and K. N. Ganesh. **2006** (Manuscript under preparation).

SYMPOSIA/CONFERENCES ATTENDED

- **A. Gourishankar**; M. Sastry; K. N. Ganesh. **Interaction of DNA/ PNA monomers and oligomers with Gold nanoparticles studied by Spectroscopy, Microscopy and Microcalorimetry**. RSC-student symposium, West India section, held at IIT-Bombay from 24^{th}-25^{th} Sept 2004. **(Oral Presentation)**.

- **A. Gourishankar**; S. Shukla; M. Sastry; K. N. Ganesh. **Interaction of DNA nucleobases/ *aeg*PNA monomers and their oligomers with Gold nanoparticles:**

Studies by Spectroscopy, Microscopy and Microcalorimetry. National Science day held at NCL, Pune on 27th February 2005. **(Poster Presentation- Best Poser Award)**.

- **A. Gourishankar**; S. Shukla; M. Sastry; K. N. Ganesh. **Interaction of DNA nucleobases/ *aeg*PNA monomers and their oligomers with Gold nanoparticles: Studies by Spectroscopy, Microscopy and Microcalorimetry**. Nanoscience & Technology Conference, held at NCL, Pune from 7th-8th March 2005. **(Poster Presentation)**.

- **A. Gourishankar**; K. N. Ganesh. **Synthesis and Biophysical Studies of *gem*-dimethyl substituted Peptide Nucleic Acids**. ACS & CSIR Conference, held at NCL, Pune from 7th-8th January 2006. **(Poster Presentation)**.

- **A. Gourishankar** and K. N. Ganesh. **Interaction of DNA nucleobases/ *aeg*PNA monomers and their oligomers with Gold nanoparticles: Studies by Spectroscopy, Microscopy and Microcalorimetry**. International Nanoscience conference held at Indian Institute of Sciences, Bangalore from 20th-25th August 2006. **(Oral Presentation)**.

Chapter 1

Introduction

Good Order is the foundation of all things.

PNA

1. INTRODUCTION

Self-recognition by the nucleic acids through complementary base pairing is one of the fundamental processes in biological recognition and preservation of genetic information. DNA, is the predominant chemical for duplication and storage of genetic information in biology and has also recently been shown to be highly useful as an engineering material for construction of special purpose computers and micron-scale objects with nanometer-scale feature resolution. Properly designed synthetic DNA can be thought of as programmable glue, which, via specific hybridization of complementary sequences, will, reliably self-organize to form desired structures and superstructures. Such engineered structures are inherently information-rich and are suitable for use directly as computers or as templates for imposing specific patterns on various other materials. In theory, DNA can be used to create any desired pattern in two or three dimensions and simultaneously to guide the assembly of a wide variety of other materials into any desired patterned structure. Given diverse mechanical, chemical, catalytic, and electronic properties of these specifically patterned materials, DNA self-assembly techniques hold great promise for bottom-up nanofabrication in a large number of potential applications in wide ranging fields of technology. Starting with background for understanding why the physical, chemical, and biological properties of DNA make it extremely useful as a "smart" material for nanoengineering projects. The development of DNA-based nanofabrication, outlines its major successes, and presents some possible future applications in fields as diverse as electronics, combinatorial chemistry, nano-robotics, and gene therapy, DNA-based nanoengineering as a field is related to

computational biology, bioinformatics, and genome informatics rather tangentially; it is more closely allied with biomolecular computation (BMC) – the engineering of biological macromolecules for production of artificial information processing systems. Rather than using binary, electronic computers for analyzing information extracted from biological systems, BMC seeks to utilize biomolecules directly as active parts of engineered computers.

1.2. CHEMISTRY AND BIOLOGY OF DEOXYRIBO NUCLEIC ACID (DNA)

DNA (deoxyribonucleic acid) is a linear polymer whose monomeric residues are made up of a sugar group (deoxyribose), linked to a phosphate group, and one of the four nitrogenous bases (either adenine, cytosine, guanine, or thymine; designated A, C, G, and T, respectively) as shown in Figure 1.

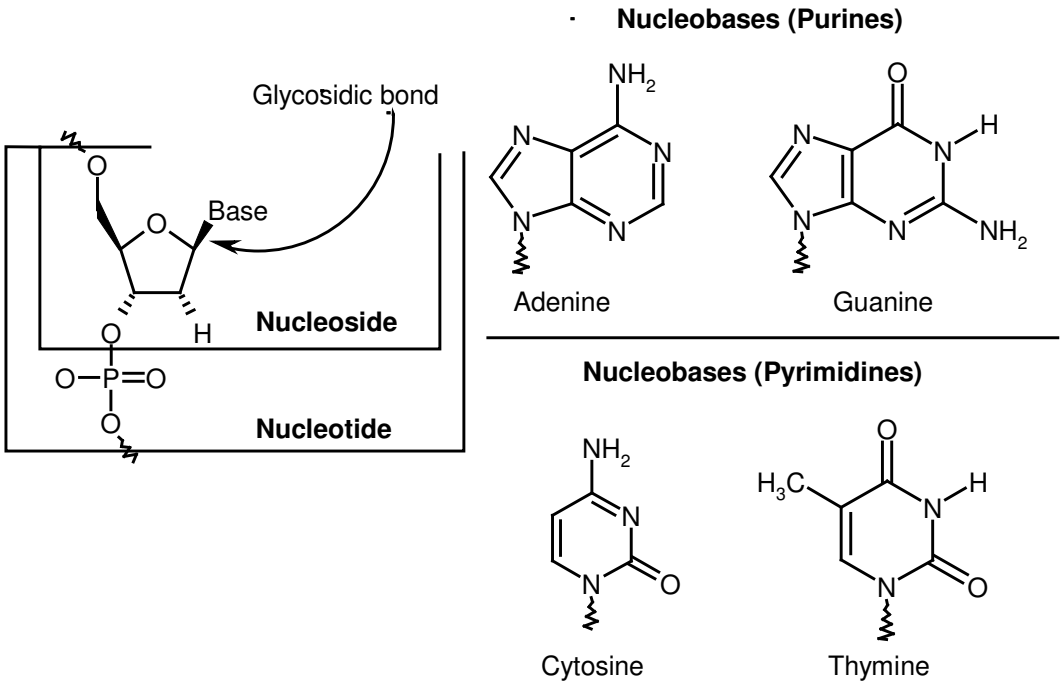

Figure 1. Chemical structures of DNA unit

The neighboring residues are joined by a chemical bond between the n^{th} phosphate and the $(n + 1)^{th}$ sugar group such that a polymeric backbone is formed of alternating sugar and phosphate groups. The backbone has chemical directionality due to asymmetry in the placement of phosphate groups on the sugar, with each sugar having one phosphate bound to its 5' carbon and one phosphate bound to its 3' carbon. This asymmetry gives the entire polynucleotide chain two distinct ends – the 5' and the 3', as shown in Figure 2. Two complementary DNA strands hybridize (form hydrogen bonds) to one another in anti-parallel fashion, with the 5' end of one-strand pointing towards the 3' end of its complementary strand to form the famous Watson-Crick double-stranded/duplex coiled as a helix. The second pertinent point regarding the chemical

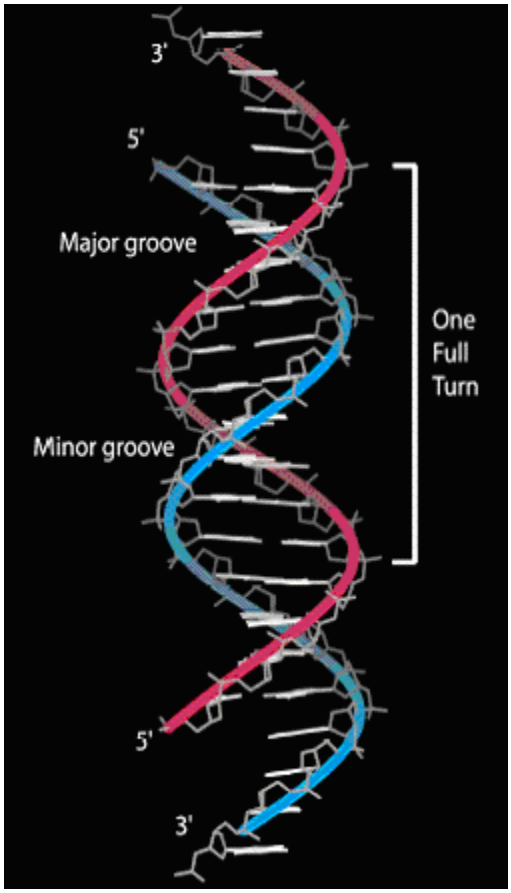

Figure 2. Double-stranded DNA shown in the standard, right handed, B-form double helix with four base ssDNA sticky-ends appended to the 3' ends of both strands. Strand backbones are highlighted with colored ribbons; bases (light gray) are viewed edgewise and can be seen to point toward their hydrogen bonding partner on the opposite strand. One full turn of DNA has a length of 3.4 nm along the vertical helix axis and contains on average 10.5 bases; the helix diameter is approximately 2 nm. The concave faces of the helix are known as the major and minor grooves; they are geometrically distinct and can be used to identify strand polarity – for example, when looking into the minor groove, the strand on the bottom (in this orientation) always has its 3' end pointing down (toward the bottom of the page). Understanding the geometric constraints of DNA structure is essential to successful design of DNA-based objects and materials

nature of DNA is that the nitrogenous bases (nucleobases) form hydrogen bonded pairs in tongue-and-groove fashion providing specificity for annealing. The base pairs linking the sugar-phosphate backbones on opposite strands have a regular spacing along the helix axis and provide the physicochemical energy of stacking which zips the DNA together in its helical structure.

In double helical DNA (or double-stranded DNA), the nucleobases are paired (Figure 3): Guanine (G) pairs specifically with Cytosine (C) and Adenine (A) pairs with Thymine (T). G and C are said to be complementary, as are A and T. DNA strands of exact Watson-Crick complementarity form stable hydrogen-bonded structures under standard temperature and solution conditions.

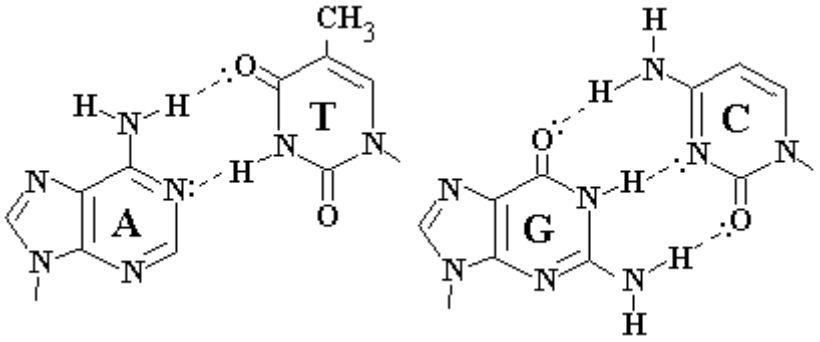

Figure 3. Base pairing structures of A-T and C-G.

Some alternative base pairings have been found to form fairly stable hydrogen bonding, however, careful design of the sequences, as well as very slow annealing protocols, can successfully avoid alternative pairings and ensure that perfectly complementary strand matchings are highly favored. The third important point stems directly from the exceptional stability and specificity of dsDNA. If a short segment of single-strand (ssDNA) is appended to a longer strand, which participates in a double

helical domain, the ssDNA will act as “smart glue”, binding specifically to a complementary ssDNA segment located on another ds-domain. These ssDNA segments are known as “sticky-ends”. Complementary sticky-end pairs therefore act as address labels and can be used to specify which dsDNA domains are allowed to anneal to one another.

Finally, the “folding rules” which dictate the three-dimensional (3D) structure of DNA in solution are simple compared to other biological macromolecules, making DNA a more salutary engineering material than proteins, for example, whose folding rules have yet to be completely understood. Given proper pH and cation concentration, dsDNA can reliably adopt standard B-form helical structure with predictable dimensions.

In summary, the important points of DNA structure include: *antiparallel* alignment of backbones in hybridized strands, base-pairing specificity for high-fidelity annealing of sequences to their complements, and annealing by heating and slow cooling for double helix formation.

The task of engineering specific physical structures from DNA benefits from the tools evolved during the eons of biological evolution. The recognition of DNA or RNA sequences by complementary oligonucleotides is a central theme of molecular biology, which deals with the molecular basis of biological or genetic specificity.

1.3. ANTISENSE TECHNOLOGY

During the process of transcription, the double-stranded DNA separates into individual strands and the sense DNA strand carrying genetic information, then serves as the template for the transcription into *m*RNA as shown in Figure 4. The antisense sequences corresponding to complement regions of *m*RNA were first described as naturally occurring sequences wherein endogenous antisense RNA complementary to a cellular *m*RNA result in a repression of gene expression.[1-5] Antisense binding is sequence specific and occurs when the bases A, G, T and C of the antisense oligonucleotides align in a precise, sequence-specific manner with a complementary sequence of bases on the target RNA. Inhibition of gene expression occurs because the modified *m*RNA which is sterically blocked by complementation is no longer available for translation and the resultant protein synthesis.

Although most traditional pharmaceuticals act by targeting enzymes or other receptor proteins, antisense technology involves the blocking of genetic messages to turn

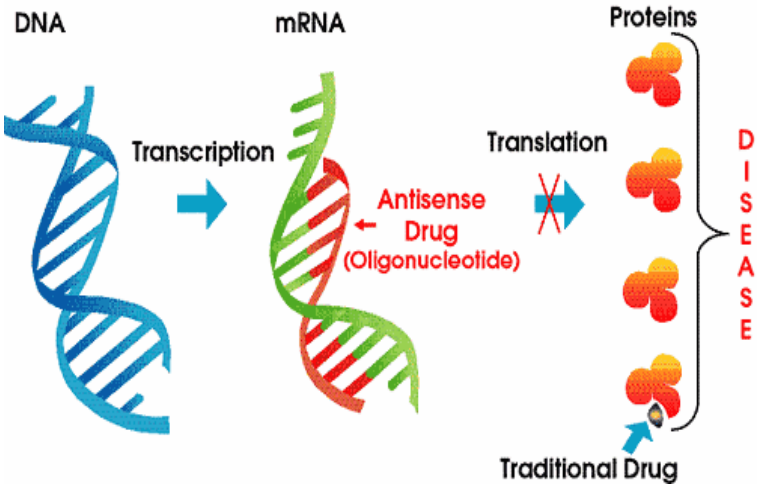

Figure 4. Antigene and Antisense technology

off the production of disease producing proteins at the source.[6-9] These potential genetic-code blocking drugs might control disease by inhibiting deleterious or malfunctioning genes. This is different from gene therapy, which inserts the corrected genes into cells. Among the potential therapeutic targets for antisense therapy are viruses (HIV, herpes simplex, human papillomavirus) and oncogenes *(c-myb, c-ras)*. A related approach is to block specific genes is via triple helix (triplex) technology in which short oligodeoxynucleotides (ODNs) of 15 to 27 nucleotides in length can bind to polypurine/polypyrimidine stretches in duplex DNA. The resulting triple helices can sterically inhibit DNA replication.

Hurdles to antisense drug development include difficulties in cell permeation of the negatively charged, highly lipophobic molecules and problems due to sensitivity to degradation of the phosphodiester linkages in ODNs by endogenous cellular nucleases.[10,11] Chemical modification of oligonucleotides by substituting for negatively charged oxygen on the phosphodiester linkages with sulfur, methyl or nitrogen results in phosphorothioate, methyl phosphonate, and phosphoamidate analogs, each possessing an additional chiral center, which increase resistance to nucleases and enhance lipophilicity. Derivatives containing 3' -5' formacetal linkers have advantage of not creating additional chiral centers that make enantiopurification difficult.[8,10,12]

1.4. ANTISENSE OLIGONUCLEOTIDES– CONCEPT AND MECHANISMS

Conceptual simplicity, the possibility of rational design, relatively inexpensive cost, and gene information from the sequencing of human genome have led to the use of short fragments of nucleic acid, commonly called oligonucleotides, either as therapeutic agents

or as tools to study specific gene function. In the past decade, the development of antisense oligonucleotide technologies as therapeutics agents has led to Food and Drug Administration approval for the commercialization of the first antisense oligonucleotide, Vitravene for cytomegalovirus retinitis[13,14] and to numerous ongoing clinical trials of therapeutic oligonucleotides.[15] The concepts underlying antisense technology shown in Figure 5D is relatively straightforward: the use of a sequence, complementary to a specific *m*RNA can inhibit its expression and then induce a blockade in the transfer of genetic information from DNA to protein. The principle mode of action of these modified oligonucleotides (ODNs) is through binding *via* Watson-Crick base pairing[16] to a specific mRNA sequence coding for a protein associated with a diseased state. The subsequent inhibition of the translational event leads to inhibition of synthesis of corresponding disease causing protein (antisense strategy).[17] In addition, the binding of an ODN can also inhibit transcription to a duplex DNA *via* formation of triple helix (antigene

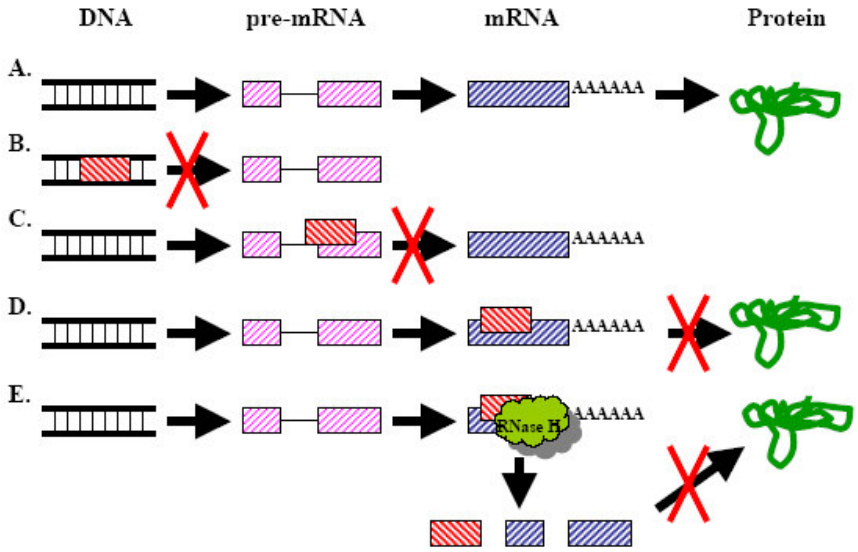

Figure 5. Summary of the strategies available for antisense knock-down or knock-out of a specific genetic message. **A.** The normal process of transcription and translation. **B.** Prevention of transcription by DNA-targeted agents. **C.** Prevention of mature mRNA formation by pre-mRNA targeting. **D.** Prevention of translation by interruption of the translational apparatus. **E.** Prevention of translation by RNase H digestion of the mRNA.

strategy)[18] (Figure 5B).

In the 'antigene' concept, proceeding through triple helix mode, the therapeutic oligonucleotide is targeted to the complementary duplex DNA principally through Hoogsteen base pairing (Figure 6). This leads to inhibition of DNA transcription and

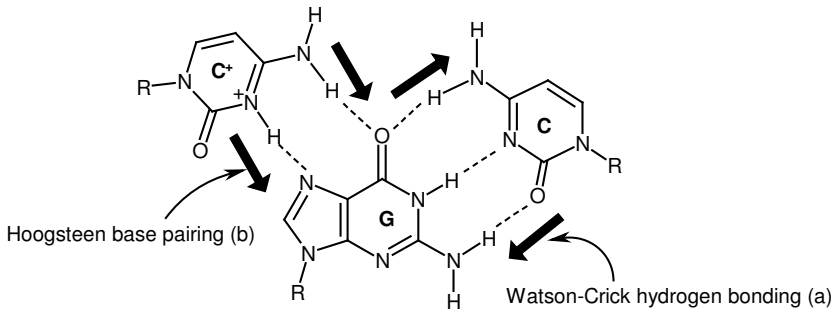

Figure 6. a) Watson-Crick hydrogen-bonding scheme for G: C base pairs and b) Hoogsteen base pairing scheme for C:G base pairs.

replication. In general, the antisense oligonucleotides are relatively short (13–25 nucleotides) and hybridize to a unique sequence in the total pool of targets present in cells. Although it is easy to synthesize phosphodiester oligonucleotides on automated machines, their use is limited as they are rapidly degraded by the intracellular exonucleases, usually via 3'-5' activity.[19-21] Although oligonucleotides are designed to specifically block the transfer of the genetic information to protein, other mechanisms by which these induce a biological effects and complex rigorous proof for additional mechanisms are still lacking.

As illustrated in Figure 7, the two major mechanisms contribute to antisense activity. On the basis of mechanism of action, two classes of antisense oligonucleotides can be discerned: (*a*) the steric-blocker oligonucleotides, which physically prevent or inhibit the progression of splicing or the translational machinery and (*b*) the RNaseH

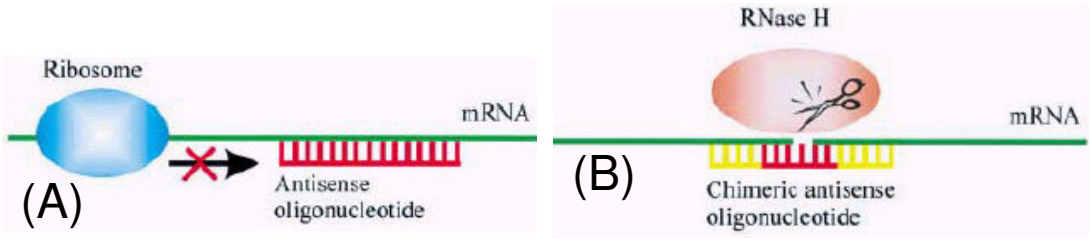

Figure 7. Mechanisms of antisense activity
(A) Blocking of Translation: Translational arrest by blocking the ribosome.
(B) RNase H cleavage: RNase H cleavage induced by (chimeric) antisense-oligonucleotides.

dependent oligonucleotides, which induce the degradation of *m*RNA in the RNA-DNA hybrid. RNaseH is a ubiquitous enzyme that hydrolyzes the RNA strand of an RNA/DNA duplex. Oligonucleotide-assisted RNaseH dependent reduction of targeted RNA expression can be quite efficient, reaching 80–95% down-regulation of protein and *m*RNA expression. Furthermore, in contrast to the steric-blocker oligonucleotides, RNaseH dependent oligonucleotides can inhibit protein expression when targeted to virtually any region of the *m*RNA. Most steric-blocker oligonucleotides are efficient only when targeted to the 5'- or AUG initiation codon region. Phosphorothioate oligonucleotides can inhibit protein expression when targeted to widely separated areas in the coding region.[23,24]

1.4.1. Advantages of Oligonucleotides for Chemical Genetics

For manipulating cellular processes, nucleic acids possess significant advantages as chemical genetic tools.[25,26] The most obvious advantage is use of a target gene sequence to design the complementary oligonucleotide as a high-affinity ligand. Among the several possible sequences, particular sequences are chosen based on some empirical rules or by "*m*RNA walking" protocols of various sequences for activity. The single

stranded *m*RNA folds into secondary structures, limiting the access to some regions of *m*RNA. The automated synthesis of ODNs makes it possible to obtain hundreds of oligonucleotides for large-scale investigations of genome function, whereby potent inhibitory oligonucleotides are identified and tested. Oligonucleotides that contain mismatched bases can serve as controls to establish the mechanism and specificity of the observed phenotype. A practical hope for therapeutic development is that one oligonucleotide, Fomivirsen, is FDA approved antisense drug, demonstrating the "proof of concept" of this class of molecules to advance through the stringent regulatory process, while several others are in clinical trials. Clinical experience demonstrates that oligonucleotides can be efficacious and can be synthesized on large scale for systemic administration. Oligonucleotides have become a realistic option for therapy, and their favorable properties will reduce the time needed to translate a lead compound into a drug that can be tested in the clinic. Once the chemical class is identified, simple terms, in antisense therapeutic strategy a different "drug" means a different "sequence" of oligonuleotide.

1.5. MODIFICATIONS IN ANTISENSE OLIGONUCLEOTIDES

In order to meet all the requirements for successful antisense/antigene oligonucleotides, it is necessary for standard oligonucleotides to be chemically modified in a suitable manner (Figure 8). Many types of chemically modified AS-ONs have been produced and tested to date. Modifications range from changes in the overall electronic charge of the oligonucleotide to the incorporation of non-phosphate oligonucleotide backbones. They are commonly grouped into three 'generations' based upon the type of

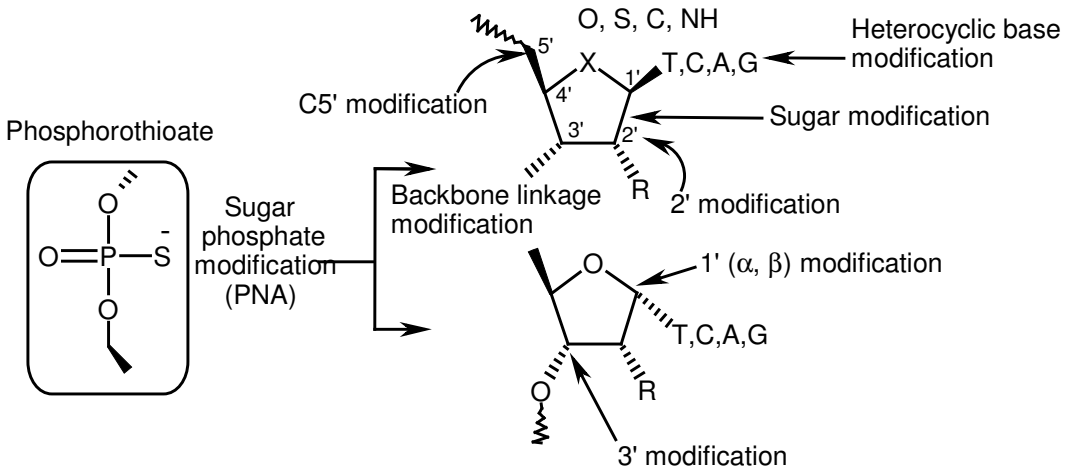

Figure 8. Structurally possible DNA modification sites.

modification: AS-ON analogues with altered phosphate backbones, modified sugars (especially at the 2' position of the ribose), or AS-ONs containing unnatural bases.27 The major technological goals for gene silencing platforms in all cases are : resistance to nuclease digestion, good cellular uptake, satisfactory hybridization affinity to the target nucleic acids, binding specificity and low toxicity.

i) First generation' antisense-oligonucleotides

These were designed to make the internucleotide linkages, the backbone to which the nucleotide bases are covalently attached, more resistant to nuclease attack. They were modified by replacing one of the non-bridging oxygen atoms in the phosphate group with either sulfur or a methyl group. Those DNA analogues with a sulfur group are known as phosphorothioate oligodeoxynucleotides (PS-ODNs) Figure 9, and are most widely used AS-ON to date. The main advantages of PS-ODNs are resistance against nucleases; ability to recruit RNase H to cleave targets mRNA, ease of synthesis and attractive pharmacokinetic properties. The drawback of PS-ODNs include lower binding affinity

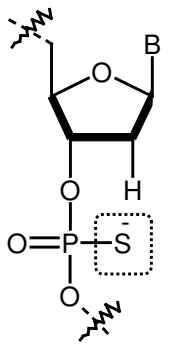

Figure 9. Phosphorothioate DNA

than its corresponding phosphodiester oligonucleotide as measured by melting temperature (T_m) and a tendency to exhibit generally undesirable sequence-independent properties *in vivo*, such as immune stimulation, complement activation and cellular toxicity.[28,29,30] PS-ODNs have been studied in a number of disease models, both in vivo and in vitro, with promising results.[28] The first FDA-approved antisense drug, Vitravene from Isis (Carlsbad, CA, USA) and the majority of antisense compounds in clinical trials to date are based on this chemistry. Another major disadvantage of PS oligodeoxynucleotides is their non-specific binding to certain proteins, particularly those that interact with polyanions such as heparin-binding proteins. Phosphorothioates are chiral at P and this leads to problems in stereo-specific synthesis.

ii) 'Second generation' antisense-oligonucleotides

These contain nucleotides with alkyl modification at the 2' position of the ribose. 2'-O-methyl and 2'-O-methoxy-ethyl RNAs (Figure 10), are the most important representatives. The significant improvements are a reduction in general toxicity, increased hybrid stability, and increased nuclease resistance. However, these desirable properties are counterbalanced by the fact that 2'-O-methyl RNA cannot induce RNase H

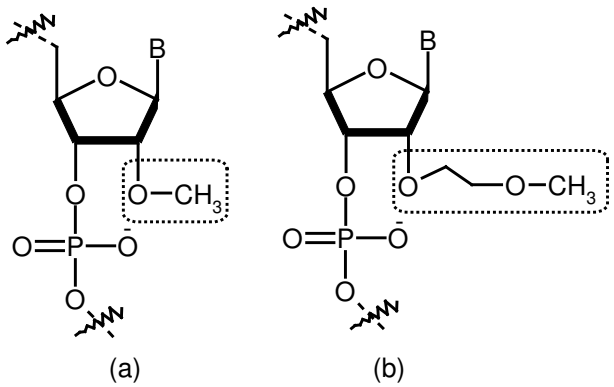

Figure 10. (a) 2'-O-methyl RNA (b) 2'-O-ethoxy-ethyl RNA

cleavage of the target mRNA. For most early antisense approaches, target RNA cleavage by RNase H was deemed necessary to achieve sufficient antisense potency. Use of RNAs with only the 2'-O-alkyl modification has been largely discontinued. In order to induce RNase H cleavage, mixed backbone (MBOs) ONs were developed by surrounding a phosphorothioate-modified deoxyribose core that retains RNase H activity with nuclease-resistant arms, such as 2'-O-methyl (OMe) ribonucleotides.[31,32] The choice of oligonucleotide modification and its placement is critical to their properties. Combining appropriate oligonucleotide segments can modulate the antisense activity, pharmacokinetics, in vivo degradation and safety profile of an MBO and backbone modifications at defined sites; this can lead to improved therapeutic effectiveness. GEM231, which targets RI_a /PKA, is built on an MBO platform and is being developed by Hybridon (Cambridge, MA, USA) as a cancer therapeutic.[33] It is an 18-mer oligonucleotide with four -OMe ribonucleosides at both the 3'- and 5'- ends surrounding the remaining deoxynucleosides, all with phosphorothioate internucleotide linkages. Phase I and II clinical trials using GEM231 are being conducted to treat solid cancers, either as a monotherapy or in combination with other marketed chemotherapeutics.

iii) 'Third generation' antisense-oligonucleotides

These are DNA and RNA analogues with modified phosphate linkages or riboses as well as nucleotides with a completely different chemical moiety replacing the furanose ring. Locked nucleic acids (LNAs), morpholino phosphoroamidates (MF) and peptide nucleic acids (PNA), as shown in Figure 11 are three interesting RNA/DNA analogues in this

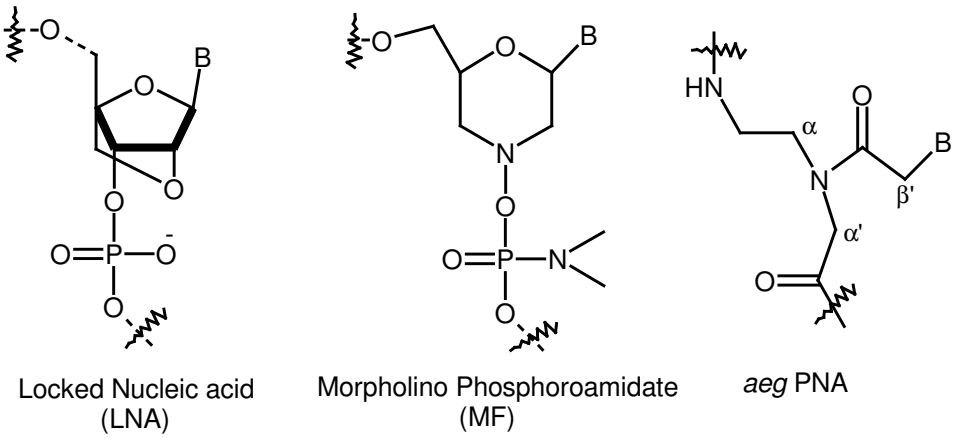

Figure 11. Third generation antisense oligonucleotides.

class that attract much attention. These compounds are essentially nuclease resistant while maintaining good hybridization affinity with their complementary mRNA.

LNA, also known as bridged nucleic acid (BNA) is a type of novel high-affinity molecule that provides major improvements in a number of key properties. LNA contains a methylene bridge connecting the 2'-oxygen of the ribose with the 4' –carbon. This design leads to improved binding to complementary DNA and RNA sequences.[34]

Like other 2' modifications, the 2'-4' linkage reduces or eliminates activation of mRNA cleavage by RNase H. However, because LNA bases are added by standard DNA/RNA synthesis protocols, it is straightforward to design chimeric 'gapmer', in

which a central DNA portion is flanked by LNA in order to enhance the stability of binding. Such chimeric LNA-containing ONs allow the high affinity of LNA binding to be combined with the ability of DNA to recruit RNase H.

In the first *in vivo* study reported for an LNA, an efficient knock-down of the rat delta opioid receptor was achieved in the absence of any detectable toxic reactions in rat brain.[35] Subsequently, full LNA ONs have been successfully used *in vivo* to block the translation of an RNA polymerase.[36] These ONs inhibited tumor growth in a xenograft model with an effective concentration that was five times lower than was found previously for corresponding PS-ODNs.

MFs and PNAs represent a more radical approach to the nuclease-resistance problem, as the phosphodiester linkage is completely replaced with polyamide (peptide) or phosphoroamidate backbone.[37,38] They both form tight bonds with their RNA targets and probably exert their effects by blocking translation, as neither molecule effectively activate RNaseH. Whether it is necessary to preserve the ability of these molecules to activate RNaseH is controversial, but many workers in this field still believe that molecules with such a capability are likely to be more effective, at least in clinical settings. Uncharged backbones prevent PNAs and MFs from binding to proteins that normally recognize polyanions, which are a major source of nonspecific interactions. However, the electrostatic neutral property, solubility and cellular uptake are serious problems. Improved intracellular delivery could be obtained by coupling these ONs with certain ligands (e.g. a four-lysine tail) or by mechanical disturbance of the cell membrane (e.g. electroporation).

According to the *in vivo* studies performed to date, PNA (See next section) appear to be nontoxic and can target a broad range of mRNA sequences effectively, but the clearance *in vivo* is rapid compared with that of PS-ODN or MBO, thus limiting *in vivo* effectiveness. The seemingly negative property of binding to certain proteins protects PS-ODN or MBO from filtration, thus increasing their serum half-life. Whereas PNAs do not appear to have gene silencing advantages over other chemically modified ONs, their ability to recognize duplex DNA makes PNAs promising candidates for modulating gene expression or inducing mutations by strand invasion of chromosomal duplex DNA.[39] Effective gene knock-down by antisense MFs *in vivo* has been shown, and therapeutic compounds are being developed. Some of third generation antisense oligonucleotides like LNA, MF and PNA have shown new promising biological activity with high potential for development as antisense drugs shown in Table 1.

Currently some of third generation antisense oligonucleotides like LNA, MF and PNA have shown the promising potential to substantively improve the drug discovery and development feasibility and value of gene silencing with applicability to *in vivo* target validation, diagnostics and therapeutics. However, inefficient delivery and stability, causing limited efficacy, as well as undesired side effects, have stood in the way of broader uptake of antisense gene silencing for drug discovery and development.

Table 1. Antisense-oligonucleotides approved or in clinical trials

Product	Company	Target	Disease	Chemistry	Status
Vitravene (Fomivirsen)	ISIS Pharmaceuticals	CMV- IE2	CMV retinitis	PS DNA	Approved
Affinitac (ISIS 3521)	ISIS	PKC-a	Cancer	PS DNA	Phase III
Genasense	Genta Bcl2	Bcl2	Cancer	PS DNA	Phase III
Alicaforsen (ISIS 2302)	ISIS	ICAM-1	Psoriasis,Crohn's disease, Ulcerative colitis	PS DNA	Phase II/III
ISIS 14803	ISIS	Antiviral	Hepatitis C	PS DNA	Phase II
ISIS 2503	ISIS	H-ras	Cancer	PS DNA	Phase II
MG98 DNA	Methylgene	DNA methyl transferase	Solid tumors	PS DNA	Phase II
EPI-2010	EpiGenesis Pharmaceuticals	Adenosine A1 receptor	Asthma	PS DNA	Phase II
GTI 2040	Lorus Therapeutics	Ribonucleotide reductase (R2)	Cancer	PS DNA	Phase II
ISIS 104838	ISIS	TNF α	Rheumatoid Arthritis,Psoriasis	2nd generation	Phase II
Avi4126	AVI BioPharma	c-myc	Restenosis,cancer, Polycystic kidney disease	3rd generation	Phase I/II
Gem231	Hybridon	PKA RIα	Solid tumors	2nd generation	Phase I/II
Gem92	Hybridon	HIV gag	AIDS	2nd generation	Phase I
GTI 2051	Lorus Therapeutics	Ribonucleotide reductase (R1)	Cancer	PS DNA	Phase I
Avi4557	AVI BioPharma	CYP3A4	Metabolic redirection of approved drugs	3rd generation	Phase I

1.6. PEPTIDE NUCLEIC ACID (PNA): A NEW MOLECULAR TOOL

Much efforts have been invested in the development of synthetic oligonucleotide analogues with the goal of obtaining antisense drugs with properties superior to those of natural oligo-(deoxy)-ribonucleotides, in particular with respect to biostability, hybridization efficacy, specificity and cellular uptake. None of these analogues have found their way into general use molecular biology, although phosphothioates are occasionally being used for antisense gene knockout experiments.

Peptide nucleic acid (PNA), Figure 12-II, have recently found increasing applications. PNA is a linear polymer that, unlike DNA (Figure 12-I), contains a neutral, achiral backbone of repeating *N*-(2-aminoethyl)-glycine units linked by amide bonds, with the purine and pyrimidine bases attached by methylene carbonyl linkages. In other words, it is a sequence made up of derivatives of the four nucleobases found in DNA but without 2'-deoxy-D-ribose residues and phosphodiester bonds. It has instead a neutral backbone that reduces the electrostatic repulsion during duplex formation. PNA forms hybrids with complementary DNA stabilized by hydrogen bonding and base stacking

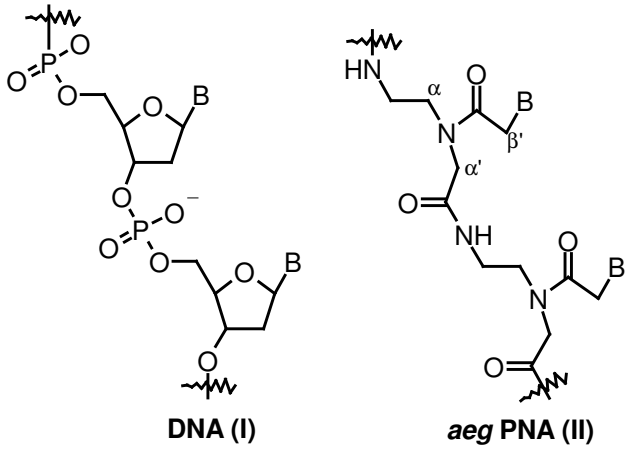

Figure 12. Structures of DNA and a*eg*PNA

with distances similar to the DNA double helix structure but, unlike DNA/DNA hybrids, PNA/DNA hybrids are resistant to nuclease and protease attack due to the inability of nuclease and proteolytic enzymes to recognize the peptide backbone. The PNA:DNA hybrids have higher thermal stability, with their melting temperature (T_m) approximately 10^0C higher than the corresponding DNA/DNA duplex, and are relatively insensitive to ionic strength, due to the neutral charge of PNA. Additionally, single base mismatched PNA:DNA duplexes are less stable than their corresponding DNA/DNA hybrids, a fact that makes them perfectly suitable for specific mutation detection. Due to the major differences between PNA chemistry and oligonucleotide chemistry, PNA has chemical, physical and biological properties that differ significantly from those of oligonucleotides, although the hybridization efficiency and specificity is retained or even improved.[38]

Not surprisingly, the very simple structure of PNA in combination with its impressive DNA mimicking properties was an immediate inspiration and open invitation for synthetic organic chemists to make derivatives and analogues of aminoethyl-glycinyl PNA. The aim was towards a better understanding of the physico-chemical properties of this molecule as well as efforts to improve its "biological" properties.[41] PNAs recognize complementary DNA/RNA by Watson-Crick hydrogen bonding and are true DNA mimics in terms of base-pair recognition. PNAs being peptides possess amine and carboxy termini instead of 3' to 5' polarity of DNA and can bind DNA/RNA in either parallel or antiparallel modes. Although PNA does not show predominant preferences for binding DNA/RNA in either direction, in general the antiparallel mode is slightly preferred over the parallel one.[42] In the antiparallel mode the PNA 'N' terminus is towards the 3'- end and the 'C' terminus, towards the 5'- end of the complementary DNA/RNA

oligonucleotide. The parallel mode of binding consists of PNA 'N' terminus being towards the 5'- end with the 'C' terminus towards the 3'- end of the complementary DNA/ RNA oligonucleotide (Figure 13).

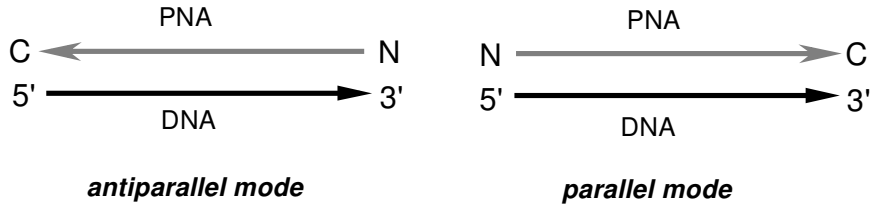

Figure 13. Parallel and antiparallel modes of PNA-DNA binding.

1.6.1. Peptide Nucleic Acid (PNA): Targeting Double Stranded DNA

PNA was originally conceived as a mimic of a triplex forming oligonucleotide.[43] However, despite being an extremely efficient structural mimic of DNA (or RNA), homopyrimidine PNAs do not bind very efficiently to double stranded DNA targets by triplex formation, but through a very interesting alternating mechanism: duplex invasion[44] (Figure 14). During this process, the complementary PNA binds to duplex and displaces the existing complementary DNA strand followed by binding of a second PNA strand to form PNA_2:DNA triplexes.[45]

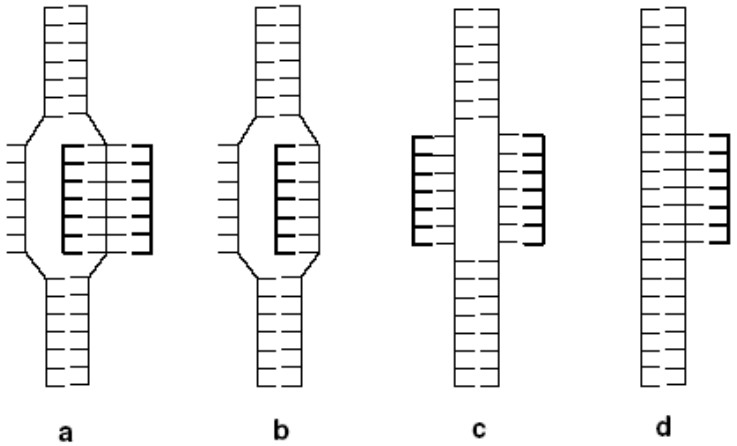

Figure 14. Strand invasion complexes **a.** Triplex invasion **b.** duplex invasion **c.** Double duplex invasion **d.** Third strand binding forming a PNA2:DNA complex.

1.6.2. Stability of PNA complexes: Sequence effects

Duplexes between PNA and DNA or RNA are in general thermally more stable than the corresponding DNA-DNA or DNA-RNA duplexes.[42,46] The sequence dependence of the stability is, however, more complex than that found for DNA-DNA complexes because of the inherent asymmetry of the duplex. In fact PNADNA duplexes show significantly increased stability when the purines are in the PNA strand. Thus on top of the dependence on G-C content, the stability of PNA+DNA duplexes also depends on the purine fraction of the PNA strand as expressed in the empirical formula recently derived for the thermal stability of PNA-DNA duplexes.[47] In general, it is also observed that the thermal stability of PNA-PNA duplexes exceeds that of PNA-RNA duplexes which again are more stable than PNA-DNA duplexes.

Significantly the stability of PNA-DNA duplexes are almost unaffected by the ionic strength of the medium (actually the stability decreases slightly with increasing Na+ concentration due to counter-ion release upon duplex formation). This is in sharp contrast, of course, to the behavior of DNA-DNA (or RNA) duplexes, the stability of which decreases dramatically at low ionic strength because of the requirement of counter-ion shielding of the phosphate backbone.[48] PNA hybridization kinetics have been studied by BIAcore technology and the results indicate - although they cannot be considered conclusive – no major difference in on rates of PNA and DNA duplex formation.[46] Most importantly, PNA-DNA-PNA triplexes exhibit extraordinary high stability. However, the rate of formation of such ternary triplexes is slow giving rise to significant hysteresis of the thermal transition.

1.6.3. Structure of PNA complexes

So far the three dimensional structures of four PNA complexes have been determined. The PNA-RNA[49] and PNA-DNA[50] duplex structures were determined by NMR methods, while the structures of a PNA_2:DNA triplex[51] and a PNA:PNA duplex[52] were solved by X-ray crystallography.

Several general conclusions can be drawn from these structural studies (Figure 15). In general, the PNA is able to adapt to its partner to a great extent. In the PNA-RNA and PNA-DNA duplexes the oligonucleotide adopts closely to its natural A- and B-conformation respectively in terms of sugar puckering, while the helix parameters have both A- and B-form characteristics. The PNA does, however, prefer a unique, different helix form, the P-form, which is predominant in the PNA_2:DNA triplex and is of course fully developed in the PNA-PNA duplex. This helix is very wide (28 Å diameter) and has a very large pitch (18 base pairs). In terms of base pair conformations it is a very regular helix, and the base pairs are virtually perpendicular to the helix axis.

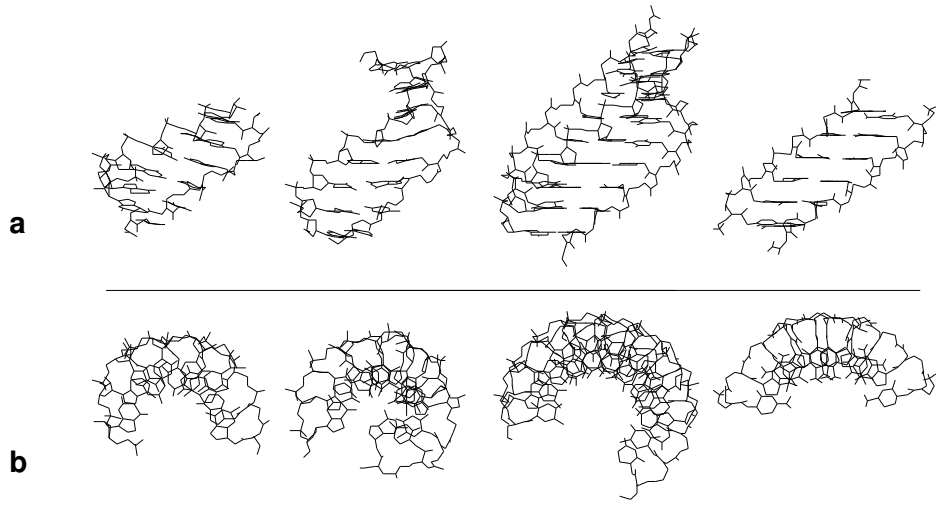

Figure 15. Structures of PNA complexes shown in side view (**a**) and top view (**b**). The complexes from left to right are PNA:RNA, PNA:DNA, PNA:DNA:PNA and PNA:PNA.

1.7. CHEMICAL MODIFICATIONS OF PNA

Being a relatively simple structure, PNA monomers are good targets for chemical modifications. The structure of the classical PNA monomer[41] has been subjected to a variety of rational modifications with the aim of understanding the structure activity relationship (SAR), (Figure 16). In this class of DNA mimics as well as in PNA

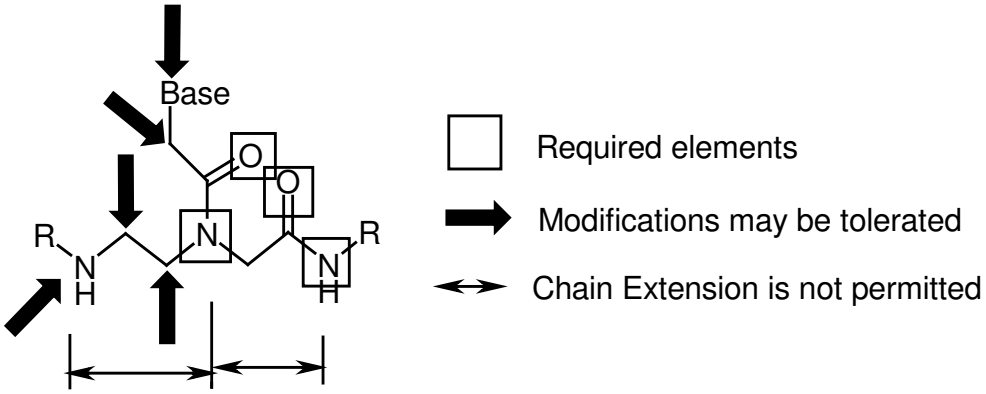

Figure 16. Towards the SAR of an acyclic backbone-based Peptide Nucleic acid

oligomers, the goal is to specifically improve properties required for various applications within medicine, diagnostics, molecular biology etc. These limitations include low aqueous solubility, ambiguity in DNA binding orientation and poor membrane permeability. Structurally, the analogues can be derived from modifications in the ethylenediamine or glycine sector of the monomer, linker to the nucleobase, the nucleobase itself or a combination of the above. The strategic rationale behind the modifications are as follows: (i) introduction of chirality into the achiral PNA backbone to influence the orientational selectivity in complementary DNA binding, (ii) rigidification of PNA backbone via conformational constrain to pre-organize the PNA structure and thereby entropically drive the duplex formation, (iii) introduction of

cationic functional groups directly in the PNA backbone, in a side chain substitution or at the N or C terminus of the PNA, (iv) modulate nucleobase pairing either by modification of the linker or the nucleobase itself and (v) conjugation with 'transfer' molecules for effective penetration into cells. In addition to improving the PNA structure for therapeutics, several modifications are directed towards their applications in diagnostics. Some of the modifications are discussed below.

The earliest and the simplest of the modifications involved extension of the PNA structure with a methylene group individually in each of the structural sub-units (aminoethyl,[53] glycine[54] and base linker[54]) of the PNA monomer. These resulted in PNAs with N-(2-aminoethyl)-β-alanine (Figure 17a) and N-(3-aminopropyl)glycine (Figure 17b) backbone and ethylene carbonyl linked nucleobase (Figure 17c). However, these modifications resulted in a significant lowering of Tm of the derived PNA:DNA hybrids. The deleterious consequences of such subtle changes to the PNA structure suggested the high structural organization to which the original PNA structure is inherently tuned for

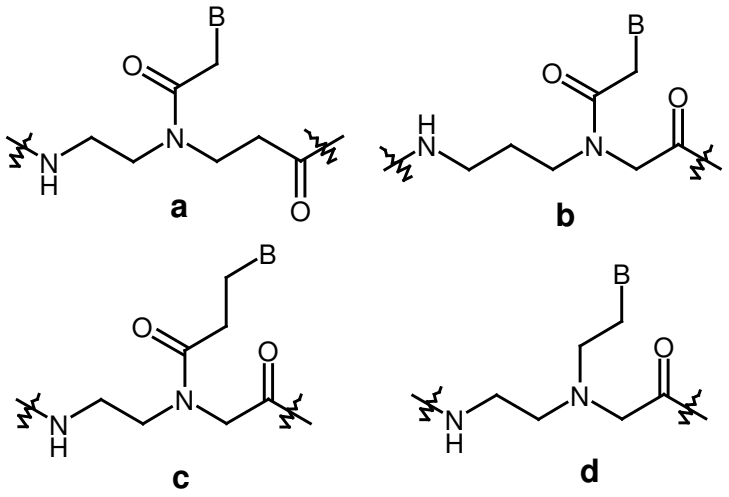

Figure 17. PNA modifications.

interaction with DNA. The replacement of the tertiary amide carbonyl by a methylene group leading to a flexible, cationic tertiary amine monomer (Figure 17d) resulted in a large destabilization of the PNA:DNA hybrids.[55] The necessity of such a pseudo rigid amide group pointed to the importance of constrained flexibility in the backbone.

Improvement of aqueous solubility of PNAs has been achieved by the introduction of charges within the molecule or by the introduction of ether linkages in the backbone (Figure 18).

Making PNA anionic also aided in increasing the water solubility as in the case of the phosphonate analogs, but was accompanied by a decrease in the binding affinity to complementary nucleic acid sequence.[56,57,58,59,60] (Figure 19).

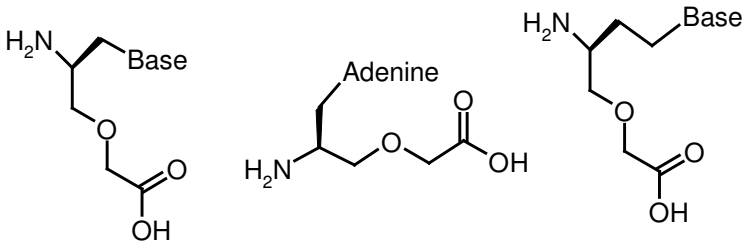

Figure 18. Ether-linked PNA (OPNA).

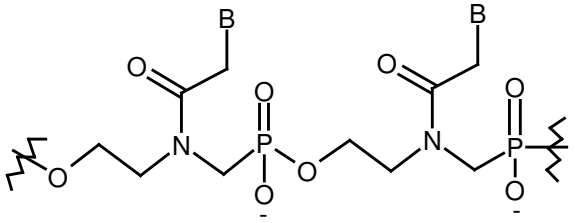

pPNA-O

Figure 19. Phosphonate PNA.

The chiral versions of these analogs similar to original PNAs led to excellent aqueous solubility properties. PNAs composed of monomers derived from serine and homoserine coupled by ether linker with glycine or alanine, were able to bind sequence specifically to RNA, though with much weaker affinity.[61,62]

Novel class of cationic PNA (DNG/PNA), which binds to DNA/RNA targets with high affinity, has been also reported[63] (Figure 20a). In another report, guanidium functional group was introduced into the PNA backbone, which exhibited remarkable cellular uptake properties while maintaining Watson-Crick recognition with complementary DNA strand[64] (Figure 20b).

Another type of modification involved interchanges of various CO and NH groups on the peptide linkages leading to retero inverse, [65,66] peptoid[66] and heterodimeric analogs[67] (Figure 21). Except for the heterodimer analogue (Figure 21c), these exhibited a lower potency for duplex formation with complementary DNA/RNA suggesting that in addition to geometric factors, other subtle requirements such as hydration and dipole-dipole interactions influencing the environment of backbone, may be involved in effecting efficient PNA: DNA hybridization.

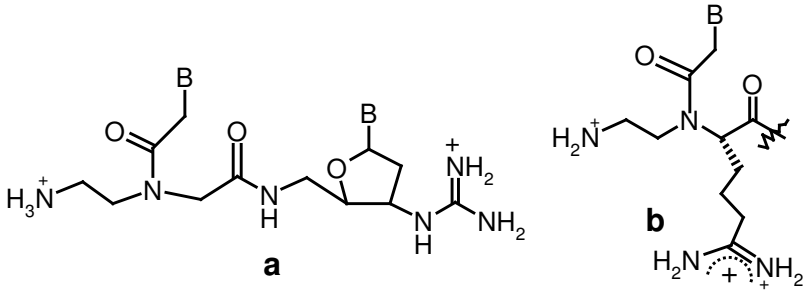

Figure 20. a) PNA-DNG chimera b) GPNA.

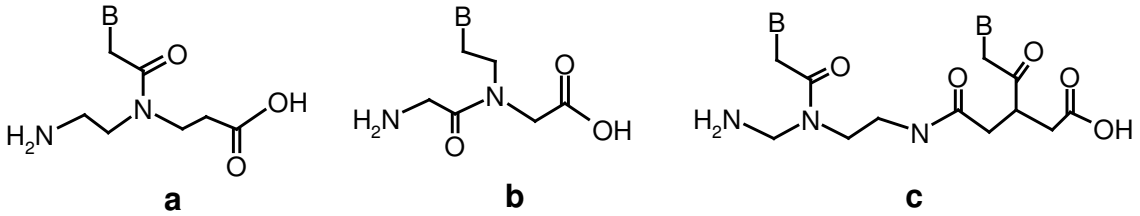

Figure 21. (a) Retero-inverso, (**b)** Peptoid and **(c)** Heterodimeric PNA.

1.7.1. Construction of bridged PNA structures

Any favorable structural pre-organization of PNA may trigger the shift in the equilibrium towards the desired complex form because of the reduced entropy loss upon complex formation, provided that the enthalpic contributions suitably compensate. This may be achieved if the conformational freedom in *aeg*PNA is curtailed by bridging the aminoethyl or glycyl acetyl linker arms (Figure 22) to give rise to cyclic analogues with pre-organized structures without affecting the nucleobase recognition ability through hydrogen bonding.

Additionally, the introduction of chemical bridges into *aeg*PNA to provide cyclic structures may help in controlling the rotameric populations by fixing the nucleobase orientation and also in directional selective binding by virtue of the chirality in the

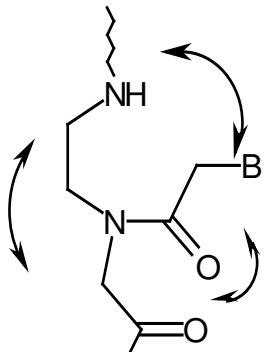

Figure 22. Possible positions for introduction of methylene or ethylene bridges.

backbone. Such a structural pre-organization approach using additional conformational constraint has been extremely successful in the case of DNA analogues. Prominent examples are conformationally locked nucleic acids[68] or conformationally frozen hexitol[69] and altritol[70] nucleic acids (Figure 23), which have pre-organized 3'-*endo* sugar conformations as prevalent in highly stable DNA-RNA duplexes.

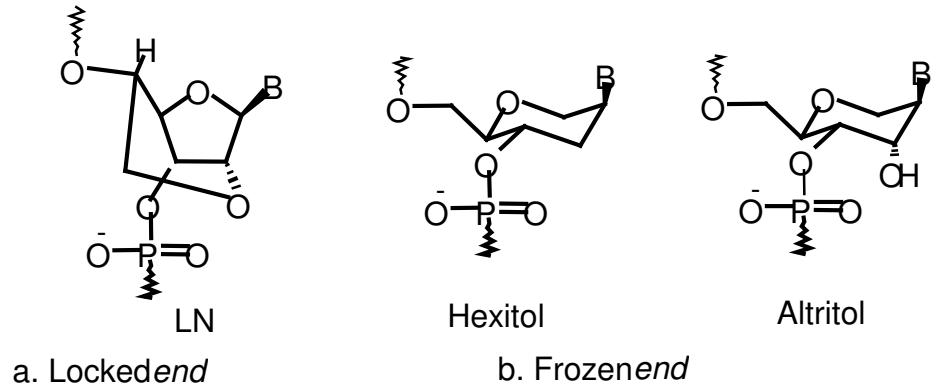

Figure 23. a) Locked 3'-*endo* conformation in LNA; b) frozen 3'-*endo* conformation in hexitol and altritol NA.

1.7.2. PNA with five-membered nitrogen heterocycles

The naturally occurring amino acid *trans*-4-hydroxy-proline, a five-membered nitrogen heterocycle with useful substitutions and well known and easily manipulated stereochemistry, [71,72] is a versatile, commercially available starting material amenable for creating structural diversity to mimic the DNA/PNA structures. Many researchers have exploited *trans*-4-hydroxy-L-proline for the synthesis of a wide variety of chiral, constrained and structurally pre-organized PNAs.

1.7.2.1. Aminoprolyl PNA

The introduction of a methylene bridge between the β- carbon atom of the aminoethyl segment and the α' -carbon atom of the glycine segment of the *aeg*PNA resulted in 4- aminoprolyl PNA, with the introduction of two chiral centers (Figure 24). [73]

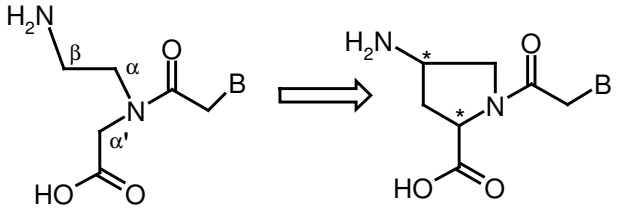

Figure 24. Aminoprolyl PNA.

The incorporation of single chiral D-*trans*- and L-*trans*-prolyl PNA monomeric units in the PNA oligomers at the N-terminus resulted in discrimination of parallel/antiparallel binding orientation preferences towards the target DNA sequences. A backbone combining *aeg*PNA alternating with L-*trans*-4-aminoprolyl PNA was later shown to bind to the target sequences with higher affinity than the pure *aeg*PNA oligomers.[74] Efforts directed towards releasing the structural strain in aminoprolyl PNA resulted in the synthesis of prolyl carbamate nucleic acids. Here a carbamate linkage, extended by two additional atoms[75] in comparison to the unmodified aegPNA oligomers, replaced the backbone amide bond.

1.7.2.2. Gly-Pro-Peptide PNA

Lowe *et al.*[75] used 4-Hydroxyproline for the synthesis of a novel chiral prolylglycyl PNA. The methylene bridge was inserted between the α'-carbon atom of the glycine unit and the β'-carbon atom of the nucleobase linker of *aeg*PNA (Figure 25).[76,77]

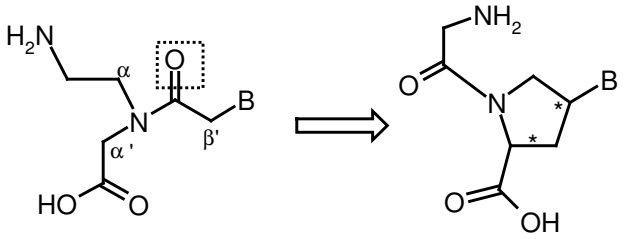

Figure 25. Gly-pro peptide PNA.

The tertiary amide bond in the backbone between proline and glycine units replaced the aminoethylglycyl backbone. The oligomers with such a backbone did not bind to the target sequences, the geometry imposed by the rigidity of the system probably being inappropriate for correct recognition. The sequences with *aeg*PNA alternating with the proline-glycine PNA unit showed reduced binding to the target sequences, unlike the 4-aminoproline PNA.

1.7.2.3. Aminoethylprolyl PNA, *aep*PNA

A proline-based PNA in which a pyrrolidine ring would replace the tertiary amide linker to the nucleobase might balance the flexibility and rigidity in the PNA backbone. The α'-carbon atom of the glycine unit and the β'-carbon atom of the nucleobase linker were joined through a methylene bridge (Figure 26). [78]

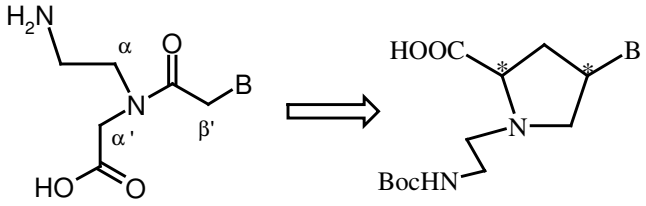

Figure 26. *aep*PNA.

The flexibility in the aminoethyl segment of *aeg*PNA was retained, unlike that in the proline-glycine PNA. The oligomers comprising 4-(*S*)-2-(*S*/*R*) *aep*PNA thymine units showed very favourable binding properties towards the target sequences without compromising the specificity. The stereochemistry at the C-2 centre did not exert any significant effect on the binding ability of the homooligomeric sequences.

1.7.2.4. Pyrrolidinone PNA

Another conformationally restricted cyclic PNA analogue was derived from a pyrrolidinone ring system. A methylene bridge was inserted between the a-carbon atom of the aminoethyl segment and the b'-carbon atom of the acetyl linker to the nucleobase of *aeg*PNA[79] (Figure 27). The carbonyl group of the nucleobase linker was retained and was forced to point towards the carboxy terminus of the backbone. The hybridization properties of PNA decamers containing this analogue with complementary DNA, RNA

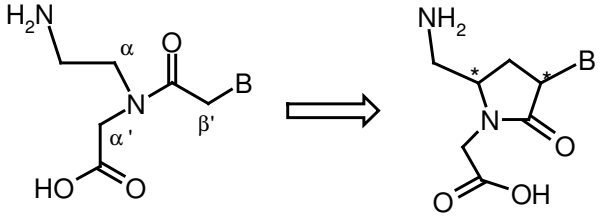

Figure 27. Pyrrolidinone PNA.

and PNA strands were investigated. The oligomers incorporating the (3*S*,5*R*) isomer were shown to have the highest affinity towards RNA in comparison with DNA.[80]

1.7.2.5. *aepone*PNA

In order to get the best characteristics from both the *aeg*PNA and the *aep*-PNA, monomer was synthesized restoring the amide character to the pyrrolidine ring nitrogen *via* selective C5 oxidation of *aep*-proline derivatized intermediate[81] (Figure 28). *aepone*-PNA oligomer stabilizes the derived triplexes with DNA but destabilizes the complexes formed with poly (rA).

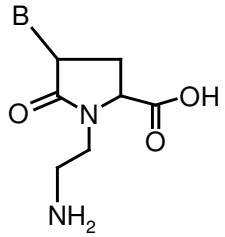

Figure 28. *aepone*PNA.

1.7.2.6. Prolyl-(β-amino acid) peptide PNA

The conformational strain in the alternating proline-glycine backbone was released by replacement of the α amino acid residue by different β amino acid spacers with appropriate rigidity.[82] Novel pyrrolidinyl PNAs comprising alternate units of nucleobases modified with D-proline, either D/L aminopyrrolidine 2 carboxylic acid, (1*R*, 2*S*) –2-aminocyclopentanecarboxylic acid or β alanine were synthesized (Figure 29).[83]

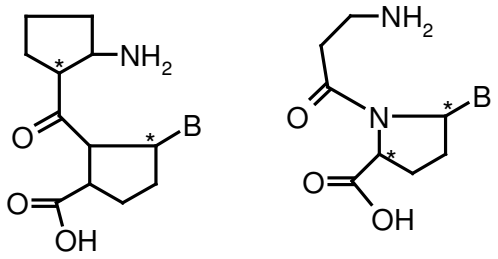

Figure 29. a) Prolyl-2-amino-cyclopentanecarboxylic acid, **b**) Prolyl-β-alanine.

1.7.2.7. Pyrrolidine PNA and pyrrolidine PNA-DNA chimera

Insertion of a methylene bridge in *aeg*PNA, linking the α-carbon atom of the aminoethyl segment and the β'-carbon atom of the tertiary amide linker, afforded the pyrrolidine PNA.[84] A fully modified (2*R*,4*S*) pyrrolidine PNA decamer formed very stable complexes with both DNA and RNA targets. The incorporation of the (2*S*, 4S) thymine monomer into oligomers and mixed pyrimidine oligomers resulted in a decreased binding efficiency with the target DNA/RNA sequences. The (2*R*, 4R) isomer was incorporated into a PNA: DNA dimer amenable to the synthesis of PNA: DNA chimeras. The chimeric PNA: DNA bound to the target DNA with decreased efficiency relative to the native DNA.

Comparative complexation of PNA oligomers incorporating diastereomeric pyrrolidine monomers[85] having nucleobases T, A, G and C with complementary DNA and RNA sequences, It is found that (i) (2*R*, 4*S*)-PNA oligomers that stabilize PNA_2:DNA homopyrimidine:homopurine triplexes destabilize the mixed pyrimidine:homopurine duplexes, (ii) the presence of (2*S*, 4*R*) and (2*R*, 4*R*) stereoisomers

affects enhanced DNA duplex stability, (iii) *cis*-(2*S*, 4*S*) and -(2*R*, 4*R*) remarkably enhance PNA:RNA duplex stability.

1.7.2.8. A cyclopentane conformational restraint for a peptide nucleic acid

Based on molecular modelling studies (*S*, *S*) cyclopentadiamine ring was used for conformational restraint of the C2-C3 dihedral angle of the PNA backbone. The *trans* cyclopentane modification improves the stability of PNA-DNA triplexes and PNA-RNA duplexes for a poly-T PNA.[86] Recently cyclopentyl PNAs[87, 88] having *cis* and *trans* isomers have been reported (Figure 30). The results suggest that these have a stereochemistry dependent stabilization effect on binding both DNA and RNA. The *cp*PNAs have a better selectivity for mismatch DNA sequence and a higher binding to complementary DNA sequence than the unmodified PNA.

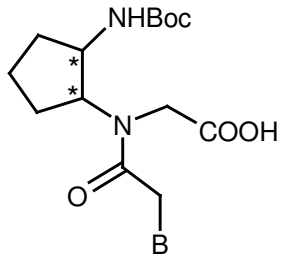

Figure 30. Cyclopentyl PNA.

1.7.2.9. *bep*PNA

One-carbon extended conformationally constrained pyrrolidine PNA monomer (*bep*PNA) has been synthesized, incorporated into PNA sequences at predefined positions, and showed selective RNA binding properties (Figure 31).[89]

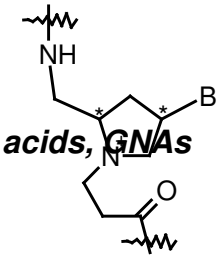

1.7.3.1. Glucosamine nucleic acids, GNAs

Figure 31. *bep*PNA.

1.7.3. PNA with six membered ring structures

Six-membered ring structures exhibit unique conformational preferences, and the binding abilities of hexose sugar phosphate containing oligonucleotide have been extensively studied by Eschenmoser *et al*.[90] The ability of morpholino, [91] hexitol, [92] and cyclohexene oligonucleotides[93] to bind to DNA/RNA are well established and are dictated by the conformational preferences of the six membered ring structures. Conformations in the six membered ring structures are rigid, in contrast to the relatively flexible five membered ring, and hence their influence on the stability of the resulting PNA-DNA/RNA complexes may be expected to make important contributions to the stabilities of the DNA/RNA complexes.

The six membered glucosamine ring appeared to fulfill the requirement of optically pure and constrained conformational scaffolding for the attachment of nucleobases (Figure 32). The homopyrimidine and mixed base sequences using GNA monomer were constructed. The binding affinities and selectivities of these oligomers to DNA and RNA targets indicated selective recognition of RNA by Watson–Crick hydrogen bonding.[94] The entropy changes were found to be smaller for GNA-DNA/RNA

than for DNA-DNA/RNA, consistent with idea that the GNA oligomer was pre-organized for binding to the target sequences.

1.7.3.2. Piperidinone PNA

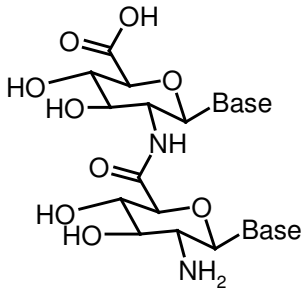

Figure 32. GNA.

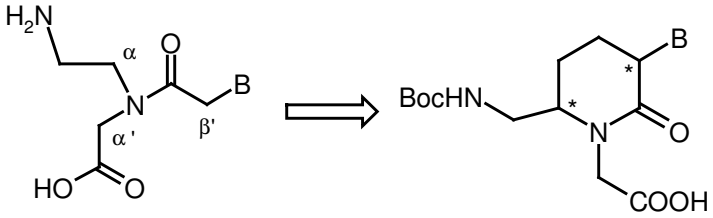

Figure 33. Piperidinone PNA.

Introduction of an ethylene bridge between the α carbon atom in the ethylene diamine and β' carbon atom and acetyl linker resulted in a six-membered ring structure-piperidinone PNA[95] (Figure 33). (3*R*, 6*R*) and (3*S*, 6*R*) adenine monomers were synthesized and incorporated into *aeg*PNA, which resulted in a large decrease in the duplex stability.

1.7.3.3. Cyclohexyl PNA

Introduction of conformational constraint in the *aeg*PNA resulted in the chiral cyclohexyl-derived backbone[96] (Figure 34). The aminoethyl segment of the *aeg*PNA was replaced with a 1,2 diaminocyclohexyl moiety, either in the (*S*,*S*) or (*R*,*R*) configuration. The oligomers with (*S*,*S*)-cyclohexyl residues were able to hybridize with DNA or RNA, with little effect on thermal stability. Molecular modeling studies reveled that (*S*,*S*) isomer can be accommodated more easily in duplex than (*R*,*R*) isomer. In contrast, incorporation of the (*R*,*R*) isomer resulted in a drastic decrease in the stability of PNA-DNA/RNA complexes. The complexes formed by the two isomers were of the opposite handedness, as evident from CD spectroscopy.

Recently, synthesis of ethyl *cis*–(1*S*,4*R*/1*R*,2*S*)-2-aminocyclohex-1-yl-*N*-(thymin-1-yl-acetyl)glycinate *via* enzymatic resolution of the *trans*-2 azido cyclohexanols has been reported.[97] The crystal structure of intermediate showed equatorial disposition of the tertiary amide group, with the torsion angle β in the range 60°-70°. UV-Tm experiments showed that (1*S*, 2*R*) isomer preferred to bind RNA and (1*R*, 2*S*) isomer showed higher affinity towards DNA in homothymine sequences leading to stereo-discrimination in recognition of DNA and RNA.[86]

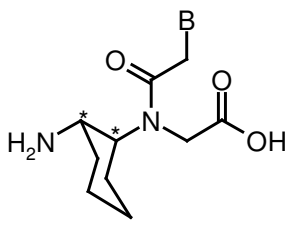

Figure 34. Cyclohexyl PNA.

1.7.3.4. Chiral piperidine PNA

This PNA analog takes advantage of the conformationally frozen six-membered ring (Figure 35) having substituents in definite preferred orientations with respect to each other. [98] DNA complementation studies of the modified PNAs by UV-Tm measurements indicate that these PNAs form stable PNA_2: DNA complexes. The tertiary ring nitrogen is protonatable at physiological pH and may add favorable therapeutic features to the oligomers, as the positive charges in the backbone are known to aid cellular uptake.

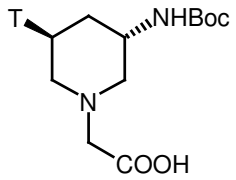

Figure 35. Chiral piperdine PNA.

1.7.3.5. [(Aminoethyl)-amino]-cyclohexanoic acid

Rigidity was introduced into the *aeg*PNA by replacing the glycyl segment in the backbone by α amino cyclohexanoic acid[99] (Figure 36). Incorporation of these monomers into oligomers and their DNA/RNA binding properties has not yet been reported.

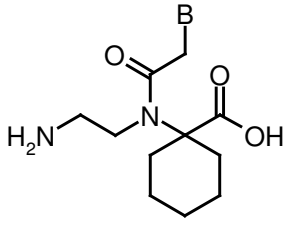

Figure 36. [(Aminoethyl) amino]cyclohexanoic acid.

1.7.3.6. Morpholino PNA

The set of morpholino analogues with phosphonate esters, amide or ester linkages between the morpholino nucleoside residues was synthesized. Preliminary results indicated that amide-linked morpholino PNAs were better accommodated in the complexes than the ester or the phosphonate linked oligomers**.**

1.8. MODIFIED NUCLEOBASES

Non-natural nucleobases could aid in understanding of the recognition process between the natural nucleobase-pairs in terms of factors such as hydrogen bonding and internucleobase stacking. They could also generate new recognition motifs with potential applications in diagnostics. Only a few nucleobase modifications have been reported in the PNA context

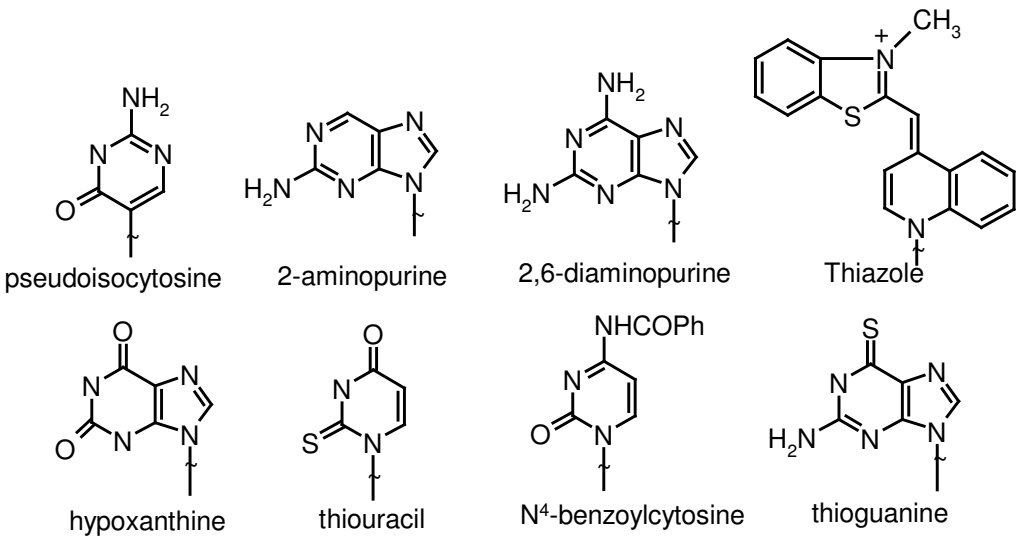

Figure 37. Modified nucleobases.

(Figure 37). Pseudoisocytosine mimics the C^+ recognition pattern[100] for triplex formation and 2,6-diaminopurine offers increased affinity and selectivity for thymine.[101] 2-Aminopurine[102] can hydrogen bond with uracil and thymine in the reverse

Watson-Crick mode and being inherently fluorescent, can be used to study the kinetics of the hybridization process with complementary nucleic acids. Replacement of *aeg*PNA with thiazole orange afforded a PNA probe that fluoresced upon hybridization.[103]

The E-base,[104] hypoxanthine,[105] N^4-benzoylcytosine[106] and 6-thioguanine[107] represent some more examples of modified nucleobases. Thiouracil along with 2,6-diaminopurine has been utilized as a non-natural base pair in PNA-DNA recognition and was shown for the first time to lead to a phenomenon termed as 'double duplex invasion'. Therefore, the scientific literature has an ample range of examples reporting PNA modifications to get better understanding of the structural and biological features of native nucleic acids.

1.9. BIOLOGICAL APPLICATIONS OF PNA

Antigene and Antisense applications of PNA

Peptide nucleic acids have promise as candidates for gene therapeutic drugs design. They require well-identified targets and a well-characterized mechanism for their cellular delivery. In principle, two general strategies can be adapted to design gene therapeutic drugs. Oligonucleotides or their potential analogs are designed to recognize and hybridize to complementary sequences in a particular gene whereby they should interfere with the transcription of that particular gene (antigene strategy). Alternatively, nucleic acid analogs can be designed to recognize and hybridize to complementary sequences in mRNA and thereby inhibit its translation (antisense strategy). PNAs are chemically and biologically stable molecules and have significant effects on replication, transcription, and translation processes, as revealed from *in vitro* experiments. Moreover, no sign of any general toxicity of PNA has so far been observed.[108, 109,110]

1.9.1. Inhibition of transcription

Peptide nucleic acids should be capable of arresting transcriptional processes by virtue of their ability to form a stable triplex structure or a strand-invaded or strand displacement complex with DNA (Figure 38).

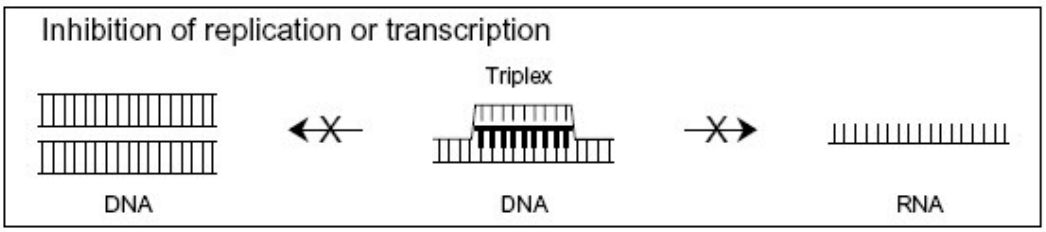

Figure 38. Mechanism of inhibition of replication or transcription.

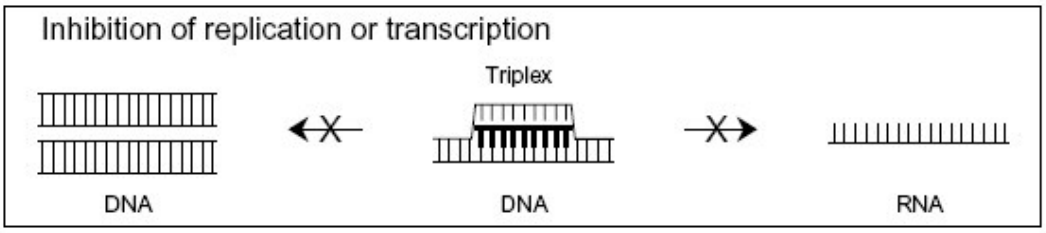

Figure 38. Mechanism of inhibition of replication or transcription.

Such complexes can create a structural hindrance to block the stable function of RNA polymerase and thus are capable of working as antigene agents. Evidence from *in vitro* studies supports the idea that such complexes are indeed capable of affecting the process of transcription involving both prokaryotic and eukaryotic RNA polymerases. Nielsen *et al.*[111] have demonstrated that even an 8-mer PNA (T_8) is capable of blocking phage T3 polymerase activity. The presence of a PNA target within the promoter region of IL-2Ra gene has been used to understand the effect of PNA binding to its target on this gene expression.[112, 113] The PNA_2:DNA triplex arrests transcription *in vitro* and is capable of acting as an antigene agent. But one of the major obstacles to applying PNA as an antigene agent is that the strand invasion or the formation of strand displacement complex is rather slow at physiological salt concentrations.[114,115] Several modifications of PNA have shown improvement in terms of binding. Modifications of PNA by chemically linking the ends of the Watson-Crick and Hoogsteen PNA strands to each other, introducing pH-independent pseudoisocytosines into the Hoogsteen strand,[116] incorporating intercalators, or positively charged lysine residues[117] in PNA strand can drastically increase the association rates with dsDNA. Lee *et al.*[118] have demonstrated that PNA as well as the PNA–DNA chimera complementary to the primary site of the

HIV-I genome can completely block priming by $tRNA_3Lys$. Consequently, *in vitro* initiation of the reverse transcription by HIV-1 RT is blocked. Thus, oligomeric PNAs targeted to various critical regions of the viral genome are likely to have a strong therapeutic potential for interrupting multiple steps involved in the replication of HIV-1.

1.9.2. Inhibition of translation

The basic mechanism of the antisense effects by oligodeoxynucleotides is considered to be either a ribonuclease H (RNase H) -mediated cleavage of the RNA strand in oligonucleotide-RNA heteroduplex or a steric blockage in the oligonucleotide–RNA complex of the translation machinery[119] (Figure 39). Oligodeoxynucleotide analogs such as phosphorothioates activate RNase H and thus hold promise of working as antisense agents. However, they also exhibit some non-specificity in their action. PNA/RNA duplexes, on the other hand, cannot act as substrates for RNase H. Normally, the peptide nucleic acid antisense effect is based on the steric blocking of either RNA processing, transport into cytoplasm, or translation. It has been concluded from the results of *in vitro* translation experiments involving rabbit reticulocyte lysates that both

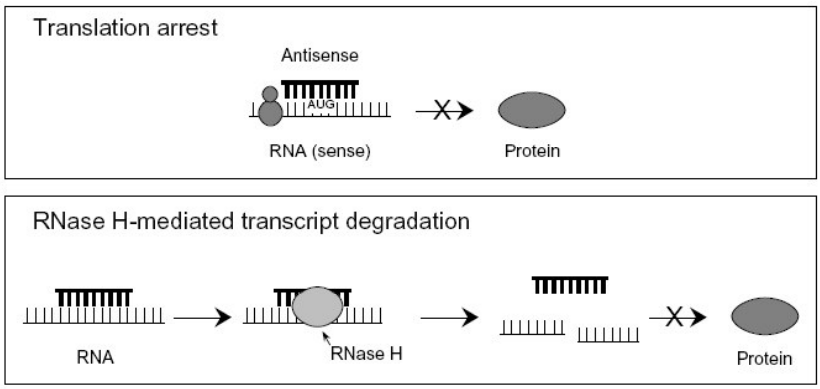

Figure 39. Mechanisms of inhibition of translation. (A) Translational arrest by blocking the ribosome. (B) RNase H cleavage induced by antisense-oligonucleotides.

duplex- (mixed sequence) and triplex forming (pyrimidine-rich) PNAs are capable of inhibiting translation at targets overlapping the AUG start codon. Triplex-forming PNAs are able to hinder the translation machinery at targets in the coding region of *m*RNA. However, translation elongation arrest requires a PNA_2: RNA triplex and thus needs a homopurine target of 10–15 bases.

In contrast, duplex-forming PNAs are incapable of this. Triplex-forming PNAs can inhibit translation at initiation codon targets and ribosome elongation at codon region targets. Triple helix-forming PNAs can also hinder the translation process. Bis-PNA or clamp-PNA structures are capable of forming internal triple helical constructs. In principle, if targeted against the coding region of mRNA, PNA_2: RNA triple helix forming derivatives can also cause a stop in translation, which can be easily verified by the detection of a truncated protein. However, this methodology requires a sequence optimization for each new target. Recent studies show that *E. coli* cells are somewhat permeable for PNA molecules. Good and Nielsen[120, 121] have shown that it is possible to achieve PNA antisense effects in the 'leaky' mutant strains of *E. coli*. PNAs targeted

against the AUG region of the mRNA corresponding to β-galactosidase and β-lactamase genes were indeed capable of down-regulating the expression of these two genes.

1.9.3. Inhibition of replication

It is also possible to use PNA for inhibiting the elongation of DNA primers by DNA polymerase. Further, the inhibition of DNA replication should be possible if the DNA duplex is subjected to strand invasion by PNA under physiological conditions or if the DNA is single stranded during the replication process. Efficient inhibition of extrachromosomal mitochondrial DNA, which is largely single-stranded during replication, has been demonstrated by Taylor *et al.*[122] The PNA-mediated inhibition of the replication of mutant human mitochondrial DNA is a novel (and also potential) approach toward the treatment of patients suffering from ailments related to the heteroplasmy of mitochondrial DNA. Here wild type and mutated DNA are both present in the same cell. Experiments have shown that PNA is capable of inhibiting the replication of mutated DNA under physiological conditions without affecting the wild-type DNA in mitochondria.

1.9.4. Interaction of PNA with enzymes

RNase H

The activation of the intracellular enzyme RNase H by oligonucleotides to cleave RNA bound to deoxyribonucleic acid oligomers depends on the chemical structure of RNase H-stimulating oligonucleotides. The antisense oligonucleotide with an RNase H

activity (e.g., phosphorothioate oligos) is considered a better antisense molecule (inhibitor) than one without the activity (methylphosphonates and hexitol nucleic acids).[123] Despite their remarkable nucleic acid binding properties, PNAs generally are not capable of stimulating RNase H activity on duplex formation with RNA. However, recent studies have shown that DNA/PNA chimeras are capable of stimulating RNase H activity. On formation of a chimeric RNA double strand, PNA/DNA can activate the RNA cleavage activity of RNase H (Figure 40). Cleavage occurs at the ribonucleotide parts base paired to the DNA part of the chimera. Moreover, this cleavage is sequence specific in such a way that certain sequences of DNA/PNA chimeras are preferred over others. They are also reported to be taken up by cells to a similar extent as corresponding oligonucleotides. Thus, PNA/DNA chimeras appear by far the best potential candidates for antisense PNA constructs.

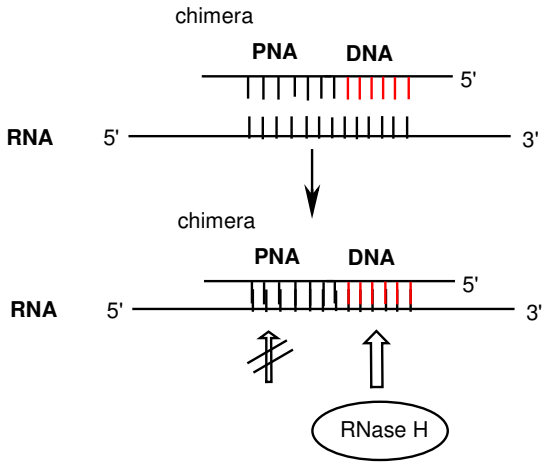

Figure 40. Schematic representation of Rnase H- mediated cleavage activity after the binding of PNA-DNA chimera to target RNA.

Polymerase and reverse transcriptase

In general, there is no direct interaction of PNA with either DNA polymerase or reverse transcriptase. However, different groups have shown indirect involvement of PNA in inhibiting these enzyme functions (activity) under *in vitro* conditions. For example, PNA oligomers are capable of terminating the elongation of oligonucleotide primers by either binding to the template strand or directly competing with the primer for binding to the template. Primer extension by MMLV reverse transcriptase has been shown to be inhibited by introducing a PNA oligomer. In another experiment, Nielsen *et al*.[124] demonstrated that the primer extension catalyzed by *Taq*-polymerase can be terminated by incorporating a PNA oligomer (PNA-H (t) $_{10}$ into the system. The latter can bind to a (dA) $_{10}$ sequence in the template and thereby terminate the primer extension. Moreover, the reverse transcription of *gag* gene of HIV I is also inhibited *in vitro* by PNAs.[125] The inhibition has been achieved by using a bis-PNA construct, which is more efficient than the corresponding mono PNA construct.[126] Also, the reverse transcription can be completely inhibited by a pentadecameric antisense PNA, using a molar ratio of 10:1 (PNA/RNA), without any noticeable RNase H cleavage of the RNA. PNA oligomers that are complementary to the RNA primer-binding site can inhibit the telomerase activity. Studies have shown that the telomerase inhibition activity of PNA is better than that of corresponding activity of phosphorothioate oligonucleotides. This is mainly due to a higher binding affinity of PNA compared to phosphorothioates.[127] Corey and co-workers[128] have demonstrated an efficient inhibition of telomerase after lipid-mediated delivery of template- and non-template -directed PNA into the cell.

1.9.5. PNA as a molecular-biological tool

Peptide nucleic acids also exhibit potential for use as a tool in biotechnology and molecular biology. Here we will mainly present indications of PNA becoming an important molecular biology tool.

Enhanced PCR amplification

The polymerase chain reaction (PCR) has been widely used for various molecular genetic applications including the amplification of variable number of tandem repeat (VNTR) loci for the purpose of genetic typing.[129, 130] PNA has been used to achieve an enhanced amplification of VNTR locus D1S80.[131] Small PNA oligomers are used to block the template, and the latter becomes unavailable for intra- and inter-strand interaction during reassociation. On the other hand, the primer extension is not blocked; during this extension, the polymerase displaces the PNA molecules from the template and the primer is extended toward completion of reaction (Figure 41). This approach shows the potential of PNA application for PCR amplification where fragments of different sizes are more accurately and evenly amplified.

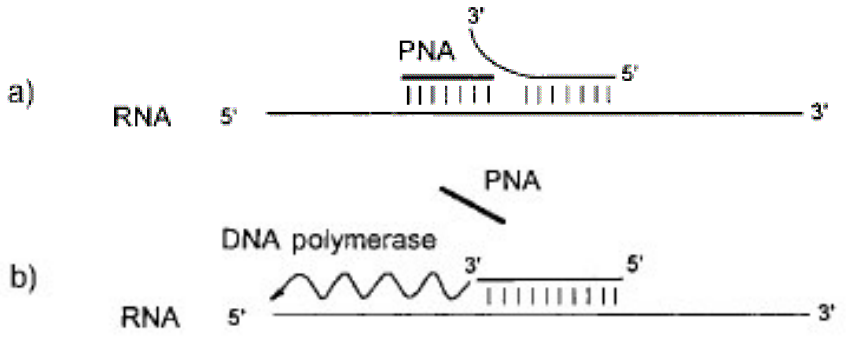

Figure 41. Schematic representation of "PCR clamping"

1.9.6. PNA hybridization as alternative to Southern hybridization

Southern hybridization is perhaps one of the most widely used techniques in molecular biology. Despite its great potential to predict both size and sequence information and information regarding the genetic context, there are certain disadvantages of this process. It requires a laborious multistep washing procedure and there could sometimes be poor sequence discrimination between closely related species. PNA pre-gel hybridization simplifies the process of Southern hybridization by reducing the required time, as the cumbersome post separation, probing, and washing steps are eliminated. Labeled (fluoresceinated) PNA oligomers are used as probes and allowed to hybridize to a denatured DNA sample at low ionic strength. The mixture is thereafter subjected directly to electrophoresis for size separation and ssDNA fragments separated on the basis of length. The charge-neutral PNA allows hybridization at low ionic strength and renders higher mobility to the complex compared to the excess unbound PNA. The DNA-PNA hybrids are blotted (transferred) onto a nylon membrane, dried, UV cross-linked, and detected using standard chemiluminescent techniques.[132] Alternatively, the bound PNA can be detected by using capillary electrophoresis (*vide infra*), which can make use of the direct fluorescence detection method. Under the same conditions, a normal DNA–DNA duplex will tend to disrupt whereas the PNA–DNA duplex will remain intact due to the strong binding of PNA to DNA. This allows specific sequence detection with simultaneous size separation of the target DNA following a simple and straightforward protocol. Consequently, the analysis is much faster than the conventional Southern hybridization technique.

1.9.7. PNA-assisted rare cleavage

Peptide nucleic acids, in combination with methylases and other restriction endonucleases, can act as rare genome cutters.[133] The method is called PNA-assisted rare cleavage (PARC) technique. It uses the strong sequence-selective binding of PNAs, preferably bis-PNAs, to short homopyrimidine sites on large DNA molecules, e.g., yeast or λ-DNA. The PNA target site is experimentally designed to overlap with the methylation/ restriction enzyme site on the DNA, so a bound PNA molecule will efficiently shield the host site from enzymatic methylation whereas the other, unprotected methylation/restriction sites will be methylated. After the removal of bis-PNA, followed by restriction digestions, it is possible to cleave the whole DNA by enzymes into limited number of pieces. DNA is efficiently protected from enzymatic digestion due to methylation in most of the sites except for those previously bound to PNA. Thus, short PNA sequences, particularly positively charged bis-PNAs in combination with various methylation/restriction enzyme pairs or recently reported pseudo-complementary PNA[134] (*pc*PNAs, which completely cover the desired methylation/restriction site) (Figure 42), can constitute an extraordinary new class of genome rare cutters.

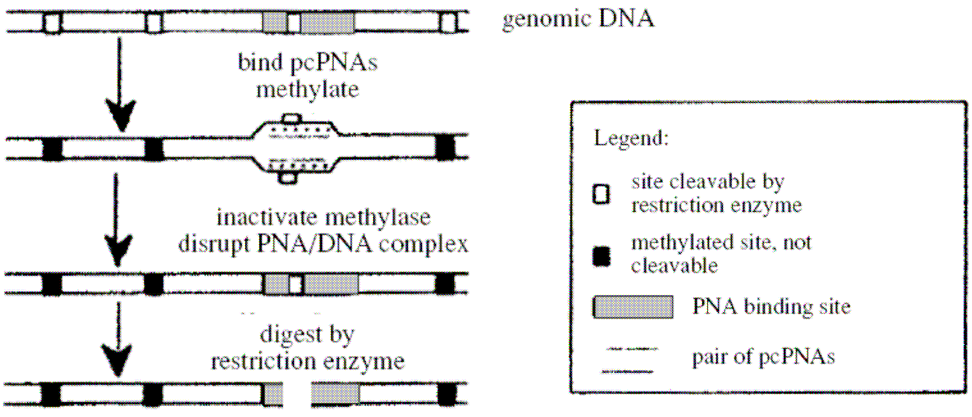

Figure 42. Schematics of the PARC method involving pcPNAs.

1.9.8. Artificial restriction enzyme system

S1 nuclease cleaves single-stranded nucleic acids releasing 5'-phosphoryl mono- or oligonucleotides. It removes the single-stranded overhangs of DNA fragments and can be used in RNA transcript mapping and construction of unidirectional deletions. PNA in combination with S1 nuclease can work as an 'artificial restriction enzyme' system. Homopyrimidine PNA oligomers hybridize to the complementary targets on dsDNA via a strand invasion mechanism, leading to the formation of looped-out non-complementary DNA strands. The enzyme nuclease S1 can degrade this single-stranded DNA part into well-defined fragments. If two PNAs are used for this purpose and allowed to bind to two adjacent targets on either the same or opposite DNA strands, it will essentially open up the entire region, making the substrate accessible for the nuclease digestion and thereby increasing the cleavage efficiency (Figure 43). [135]

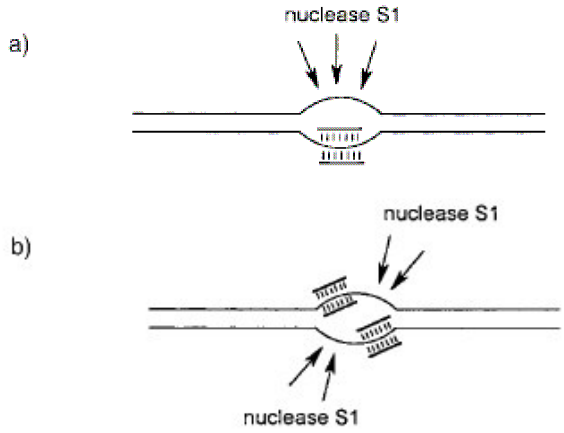

Figure 43. Artificial restriction enzymes: a) Single strand cleavage by PNA b) double strand cleavage by double PNA clamping.

1.9.9. Determination of telomere size

The conventional method for the determination of telomere length involves Southern blot analysis of genomic DNA and provides a range for the telomere length of all chromosomes present. The modern approach uses fluorescein-labeled oligonucleotides and monitor *in situ* hybridization to telomeric repeats. However, a more delicate approach resulting in better quantitative results is possible by using fluorescein-labeled PNAs, as shown by Lansdorp *et al*.[136] This PNA-mediated approach permits accurate estimates of telomeric length. *In situ* hybridization of fluorescein-labeled PNA probes to telomeres is faster and requires a lower concentration of the probe compared to its DNA counterpart. Low photobleaching and an excellent signal-to-noise ratio make it possible to quantitate telomeric repeats on individual chromosomes in this way. Experiments suggest that variations of this approach can possibly be applied to other repetitive sequences.

1.9.10. Nucleic acid purification

Based on its unique hybridization properties, PNAs can also be used to purify target nucleic acids. PNAs carrying six histidine residues have been used to purify target nucleic acids using nickel affinity chromatography (Figure 44). [137] Also, biotinylated PNAs in combination with streptavidin-coated magnetic beads may be used to purify *Chlamydia trachomatis* genomic DNA directly from urine samples. However, it appears

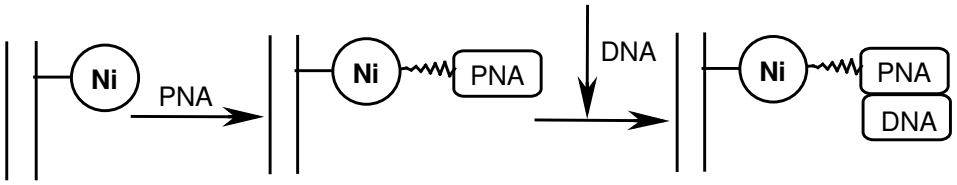

Figure 44. Nucleic acid purification by Ni affinity chromatography.

that this simple, fast, and straightforward 'purification by hybridization' approach has certain drawbacks. It requires the knowledge of a target sequence and depends on a capture oligomer to be synthesized for each different target nucleic acid. Such target sequences for the short pyrimidine PNA, i.e., the most efficient probe for strand invasion, are prevalent in large nucleic acids. Thus, short PNAs can also be used as generic capture probes for purification of large nucleic acids. It has been shown that a biotin tagged PNA-thymine heptamer could be used to efficiently purify human genomic DNA from whole blood by a simple and rapid procedure.

1.9.11. PNA as a diagnostic tool

The high-affinity binding of PNA oligomers has led to the development of new applications of PNA, especially as a diagnostic probe for detecting genetic mutations: Applications are possible for the detection of genetic mutation and mismatch analysis that can use its unique hybridization properties. The ensuing sections will highlight some of the recent developments related to the use of PNA as a probe to detect genetic mutations and corresponding mismatch analysis confirming its potential as a diagnostic tool for clinical applications.

Single base pair mutation analysis using PNA directed PCR clamping

Amplification of the target nucleic acid by the PCR technique is considered an important step for detection of genetic diseases. The higher specificity of PNA binding to DNA, higher stability of a PNA–DNA duplex compared to the corresponding DNA–DNA duplex, and its inefficiency to act as a primer for DNA polymerases are the basis

for this novel technique. This strategy includes a distinct annealing step involving the PNA targeted against one of the PCR primer sites. This step is carried out at a temperature higher than that for conventional PCR primer annealing where the PNA is selectively bound to the DNA molecule. The PNA/DNA complex formed at one of the primer sites effectively blocks the formation of a PCR product. PNA is also able to discriminate between fully complementary and single mismatch targets in a mixed target PCR. Sequence-selective blockage by PNA allows suppression of target sequences that differ by only one base pair. Also, this PNA clamping was able to discriminate three different point mutations at a single position.[138, 139] One major advantage of this PNA-mediated PCR clamping is that it allows detection of mutations stretched over 4–6 bp regions in a single reaction, and this could also be used to detect other hot-spot mutations.

Molecular Beacons

Molecular beacons are single-stranded oligonucleotide hybridization probes that form a stem-and-loop structure, Figure 45. The loop contains a probe sequence that is complementary to a target sequence, and the stem is formed by the annealing of complementary arm sequences that are located on either side of the probe sequence. A

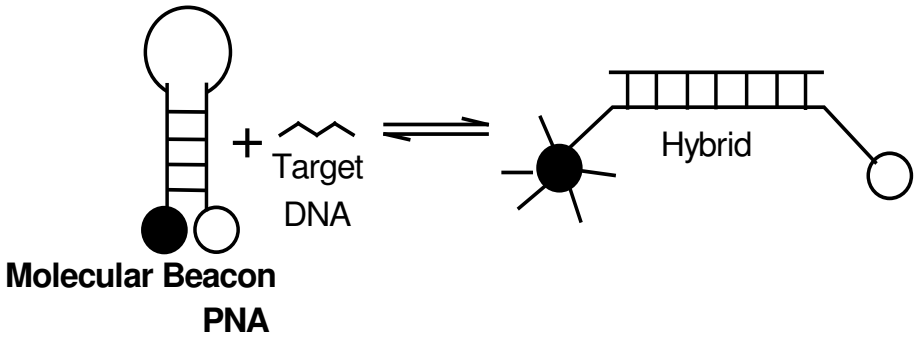

Figure 45. Schematic Presentation of Molecular Beacons

fluorophore is covalently linked to the end of one arm and a quencher is covalently linked to the end of the other arm. Molecular beacons do not fluoresce when they are free in solution. However, when they hybridize to a nucleic acid strand containing a target sequence they undergo a conformational change that enables them to fluoresce brightly.[140] Molecular beacons can be used as amplicon detector probes in diagnostic assays. Because non-hybridized molecular beacons are dark, it is not necessary to isolate the probe-target hybrids to determine the number of amplicons synthesized during an assay.

Molecular beacons have three key properties that enable the design of new and powerful diagnostic assays: 1) they only fluoresce when bound to their targets, 2) they can be labeled with a fluorophore of any desired color, and 3) they are so specific that they easily discriminate single-nucleotide polymorphisms.[141] PNA offers an opportunity of advancing biosensor technology, especially with regard to sensitivity, automation and system integration.[142]

1.10. ANTI-CANCER AGENT

PNA-peptide duplexes, which can penetrate into cells, have been used in anti-cancer applications. In this manner, telomerase activity in human melanoma cells and tumor specimens was inhibited by PNA conjugated with Antennapedia derived peptide (Antp) at nm concentrations.[143] Since telomerase is almost ubiquitously expressed in human tumors, the data point out the potential use of PNAs as anticancer drugs. Applications of PNAs as anticancer agents were also reported with PNA complementary to various sequences of bcl-2 .[144]

1.11. CELLULAR UPTAKE OF PNA

It is essential for any therapeutic agent to have good bioavailability. The activity of the antisense oligonucleotides is crucially affected by how well they reach their site of action unmetabolized. The protein biosynthesis apparatus of the cell is located in the cytoplasm where thousands of enzymes carry out the biosynthesis of sugars, fatty acids, nucleotides, amino acids, and proteins. The mRNA produced in the nucleus by transcription of the DNA is translated into the corresponding protein on the ribosomes in the cytoplasm. In order for the antisense oligonucleotides to be able to stop translation by hybridization, they must pass through the plasma membrane to enter interior of the cell. The plasma membrane is a natural barrier to many large or negatively charged molecules. It might therefore be supposed that this membrane barrier would form a bottleneck in the antisense oligonucleotide concept.[145, 146]

It is important to understand the effect of peptide nucleic acids on intact cells and problems related to its delivery into the cell. The cellular uptake of this unique nucleic acid analog is very slow, which is still the major challenge that needs to be overcome before it can be used as a therapeutic drug. So far, there is hardly any report of the antisense activity of PNA in cell culture without the use of brute techniques to help bypass the membrane barrier. Effects of PNA on intact cells have been demonstrated by cellular microinjection; antisense activity against a transfected gene has also been established in this way.[147] Serious efforts are being made to increase the cellular uptake of PNA, particularly by modifying the molecule itself or conjugating to it suitable potential ligand molecules that could enhance a physical or receptor-mediated cellular

uptake.[148, 149,150] Incorporation of a 'guide' sequence or some 'vector' peptides is one potential approach whereby PNA is attracted to the cell membrane and helped in docking into it (Figure 46).

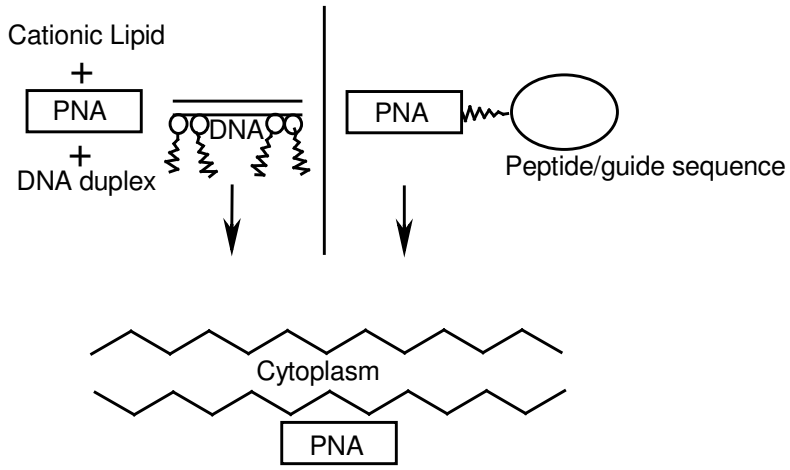

Figure 46. Methods for cellular uptake of PNA.

Several methods have been proposed to facilitate the uptake of PNAs in eukaryotic cells. These include transient permeabilization with streptolysin O, cell membrane permeabilization by lysolectin or detergents like Tween, or conjugation with peptides capable of being internalized easily.[151] Aldrian-Herrada *et al.*[152] showed that peptide nucleic acids are rapidly internalized in cultured neurons when coupled to a delivery peptide (retro p-Antp peptide). His result is promising and demonstrates that PNAs guided by suitable vector peptides could work as antisense agents. Corey and co-workers[153] have reported a novel method for *in vitro* cellular delivery of peptide nucleic acids using a cationic lipid. The cationic lipid is capable of associating with the negatively charged phosphodiester backbone of DNA and RNA and fusing with the cell membrane to allow the oligonucleotide to enter into the cell through an endocytotic

pathway. This technique has been improvised for the delivery of PNA molecules into the cells. Desired PNA oligomers are hybridized to overlapping oligonucleotides and the complex is mixed with cationic lipid. The cationic lipid–DNA–PNA complex thus formed can be internalized, and the partially hybridized PNA is imported into the cell as a passive cargo. On passive delivery into the cell, peptide nucleic acid is expected to dissociate itself from the complex.[154] Another strategy that has been adapted to improvise the delivery of PNA *in vitro* is to incorporate it into delivery vehicles (vesicles), e.g., liposomes. There are also some reports of direct PNA uptake.

1.12. G-PNA

In the past few years fusion of the human HIV-1 Tat transduction domain (GRKKRRQRRR) to a number of different moieties including proteins31 and synthetic molecules[155] has led to their efficient uptake by cells. Subsequently, replacement of this Tat domain by a homoarginine peptide as well as various unnatural peptoid constructs containing guanidinium groups retained the ability to promote efficient uptake.[156] Based on these findings, Ly *et al* synthesized PNA oligomers based on the previously reported 2-aminoethylarginine backbone.[157] Incorporation of the arginine side chain (*i.e.* the guanidinium functional group) into the PNA backbone at the a-position caused efficient uptake of the PNA by human colon and osteosarcoma cell lines. The disadvantage to G-PNA is currently the need to synthesize the monomers, which are not commercially available.

1.13. *In situ* HYBRIDIZATION (PNA-FISH)

The efficiency of PNAs as hybridization probes has also been demonstrated in fluorescence *in situ* hybridization (FISH) applications. Because of their neutral backbone, PNA probes present *in situ* a high specificity and require low concentrations and short hybridization time. Additional *in situ* benefits of using PNA probes are reduced background binding, low photobleaching and mild washing procedure. *In situ* labeling can efficiently be obtained with a single 15-mer PNA oligomer carrying a single label.

The PNA-FISH technique was first developed for quantitative telomere analysis. Using a unique fluorescein labeled PNA probe, Lansdorp *et. al.* [158] performed the *in situ* labelling of human telomeric repeat sequences and the data obtained allowed accurate estimates of telomere lengths. Subsequently, telomeric PNA probes were used in several *in situ* studies of cancer and ageing.[159, 160] Further developments were focused on the *in situ* specific identification of human chromosomes on both metaphases and interphase nuclei, using PNA probes specific for satellite repeat sequences of various chromosomes. Multicolour PNA experiments were thus reported on lymphocytes, amniocytes and fibroblasts from normal subjects and patients with numerical abnormalities.[161, 162] These experiments demonstrated the superiority of PNA probes over satellite DNA probes in both intensity and sequence discrimination.

Recently, PNA-FISH has been adapted to *in situ* chromosomal analysis of the human sperm.[163] Comparative estimates of disomies X, Y and 1 were performed in sperm from healthy subjects using FISH, PRINS and PNA procedures in parallel. An equivalent quality of *in situ* nuclear labelling and similar results were obtained with the three

methods. However, the hybridization timing of PNA probes (i.e. 45 min) appeared to be significantly shortened in comparison with FISH reaction on sperm. The fast hybridization kinetics of PNA was similar to the kinetics of PRINS reaction. The similarity between PNA and PRINS might be essentially due to the small size of both PNA probes and PRINS primers, which do not exceed 30 bases in length. The data point out the importance of the probe size for *in situ* assays and consequently the great potentiality of the PNA approach, since high specific binding can be obtained with a short, unique PNA oligomer. This study also demonstrates the efficiency of multicolour PNA procedure and shows that PNA could be a powerful alternative to FISH and PRINS for *in situ* chromosomal investigations.

1.14. RECENT ADVANCES IN GENE THERAPEUTICS

1.14.1. RNAi

Only recently, research in the antisense field increased in impact by the discovery of RNA interference (RNAi). This naturally occurring phenomenon as a potent sequence specific mechanism for post-transcriptional gene silencing was first described for the nematode worm *Caenorhabditis elegans*.[164] RNA interference is initiated by long double-stranded RNA molecules, which are processed into 21–23 nucleotides long RNAs by the Dicer enzyme. This RNase III protein is thought to act as a dimer that cleaves both strands of dsRNAs and leaves two nucleotide, 3' overhanging ends. These small interfering RNAs (siRNAs) are then incorporated into the RNA induced silencing complex (RISC), a protein-RNA complex, and guide a nuclease, which degrades the

target RNA. The 21 nucleotide-long siRNA duplexes with 3' overhangs can specifically suppress gene expression in mammalian cells.[165] So it is thought to provide a significantly higher potency compared to traditional antisense approaches. Not only short double stranded RNA molecules but also short hairpin RNAs (shRNAs), i.e. fold-back stem-loop structures that give rise to siRNA after intracellular processing, can induce RNA interference.

An alternative approach to prolong siRNA-mediated inhibition of gene expression is the introduction of modified nucleotides into chemically synthesized RNA, despite the fact that even unmodified short double-stranded RNA revealed an unexpectedly high stability in cell culture and *in vivo*. For certain applications, however, further enhancement of the siRNA stability might be desirable.[166] Taken together, first promising *in vivo* experiments with siRNA have already been performed and further therapeutically important genes are expected to be targeted soon. No toxic reactions after siRNA application have been observed in the studies performed to date, but great care has to be taken to rule out severe side effects of long-term induction of RNAi before trials can be started to treat human diseases. Because silencing of gene expression by siRNAs is similar to traditional antisense technology, researchers will be able to benefit from the lessons learned for more than a decade such as the requirement to use proper controls to proof a specific knock-down of gene expression and a careful analysis of possible unspecific effects mediated by the immune system.

1.14.2. miRNA

A group of small RNA molecules, distinct from but related to siRNAs, have been identified in a variety of organisms. These small RNAs, called microRNAs (miRNAs), are transcribed as parts of longer RNA molecules that can be as long as 1000 nt. The RNAs are processed in the nucleus into hairpin RNAs of 70-100 nt by the dsRNA-specific ribonuclease Drosha. The hairpin RNAs are transported to the cytoplasm via a transportin-5 dependent mechanism where they are digested by a second, double-strand specific ribonuclease called Dicer. A complex that is similar to the RNA-Induced Silencing Complex (RISC) that participates in RNA interference (RNAi) binds the resulting 19-23-mer miRNA. In animals, the complex-bound, single-stranded miRNA binds specific mRNAs through sequences that are significantly, though not completely, complementary to the mRNA. By a mechanism that is not fully characterized - but which apparently does not involve mRNA degradation as in RNAi— the bound mRNA remains untranslated, resulting in reduced expression of the corresponding gene.[167, 168,169]

1.14.3. Ribozymes

Ribozymes are molecular scissors that cut RNA, the molecular messages given by genes in order to produce proteins. These molecular scissors provide a very useful means of studying gene function since by cutting the RNA with a ribozyme; a gene can be effectively turned off. Cech first discovered the earliest reports of these ribozymes or catalytic RNAs in 1987. This was seen as a major discovery, since until then proteins were thought to be the only entity capable of behaving as enzymes. Ribozymes can be

used to study gene function most notably in the study of HIV, the AIDS virus, and in Cancer research.[170, 171]

Table 2. Chemically synthesized ribozymes in ongoing clinical trials

Entry	Product	Target	Disease	Status
1.	ANGIOZYME	VEGF-receptor-1	Metastatic colorectal cancer	Phase II
2.	HERZYME	HER-2	Cancer	Phase I

1.15. PRESENT WORK

The preceding sections give an overview of the peptide nucleic acids (PNAs), the synthetic copycat of natural nucleic acids that are DNA analogues with a homomorphous but chemically different backbone consisting of *N*-(2-aminoethyl)-glycine units in contrast to the sugar-phosphate backbone of DNA. In spite of this, PNAs bind to complementary nucleic acid oligomers obeying the Watson-Crick hydrogen bonding rules for PNA:DNA duplexes and Hoogsteen hydrogen bonding mode for third strand binding in a triplex. The attractive binding properties of PNAs, both in terms of affinity and specificity, coupled with their strand invasion potential have promoted PNA as a useful tool in molecular biology, diagnostics, and as a possible candidate for antisense/ antigene drug therapy.

The major drawbacks like poor water solubility, inefficient cell uptake, self-aggregation and ambiguity in directionality of binding restrict its applications. In order to overcome these limitations, several modifications of PNA have been carried out which were chiral and cyclic. PNAs have also been linked to helper molecules in various chimerae in an endeavor to improve its favorable properties. In contrast to well known

strategies towards chiral and cyclic PNAs, the approach in the present thesis is to make them achiral and acyclic.

The α-amino isobutyric acid, Figure 47a, α, α-disubstituted glycine is a naturally occurring amino acid. The α-amino isobutyric acid (Aib), residues in peptides are known to stabilize helix structures. The stereochemical consequences of introducing Aib into peptide chains limits the range of accessible conformations; nucleates helical structures and facilitates crystallization presumably by restricting conformational flexibility in solution.

α,α-dialkylated amino acids possess significant steric bulk which makes their incorporation into peptides is difficult. Peptides containing these hindered residues are of significant biological importance. Hence the objective was to incorporate *gem*-dimethyl groups at glycyl unit into aminoethylglycyl- and aminopropylglycyl- PNA backbone as conformational constrain elements. The presence of the extra methyl groups at C^{α} atom restricts conformational space accessible to Aib and forces peptide chain into left or right-handed conformation. The synthesized PNA oligomers can be evaluated for their hybridization with DNA/RNA, (Figures 47b and 47c) are the target molecules for synthesis.

Understanding the secondary structures of peptides and proteins, for example, the α-helix, β-sheet and reversed turn, is important as they play a vital role in molecular biology, the life sciences and drug discovery. Replacement of the α-hydrogen atom of an α-amino acid with an alkyl substituent results in an α, α-disubstituted α-amino acid (dAA), such as α-aminoisobutyric acid (Aib), diethylglycine (Deg), 1-

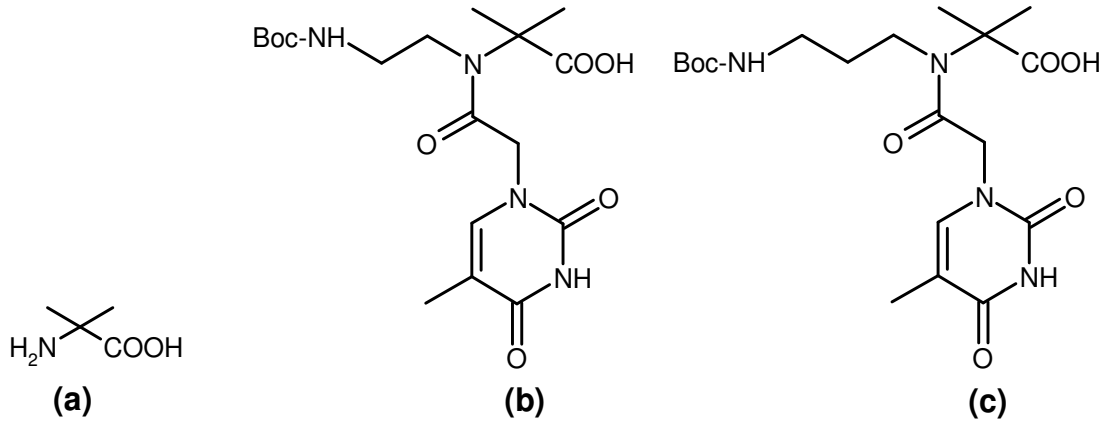

Figure 47. (a) Alpha-amino-isobutyric acid (b) and (c) Target molecules for PNA synthesis

aminocycloalkanecarboxylic acid (Ac_nc, n = ring size), and isovaline. The α,α-dialkylated amino acid residues have acquired considerable importance as a means of introducing backbone conformation constraints in synthetic peptides. The prototype residue α-aminoisobutyric acid (Aib) is a strong helix-promoting residue, a property predicted by early conformational energy calculations, which can be studied by Isothermal Titration Calorimetry (ITC).

1.16. REFERENCES

[1] W. Bains, *Biotechnology from A to Z*, Oxford, Oxford University Press, **1993**, 19.

[2] Zamecnik, P. C.; Stephenson, M. L. Inhibition of Rous sarcoma virus replication and cell transformation by a specific oligodeoxynucleotide. *Proc. Natl. Acad. Sci. USA.*, **1978**, *75*, 280-284.

[3] Weintraub H. M. Antisense RNA and DNA. *Sci. Am.*, **1990**, *262*, 40.

[4] Helene, C.; Toulme, J. J. Specific regulation of gene expression by antisense, sense and antigene nucleic acids. *J. Biochim. Biophys. Acta*, **1990**, *1049*, 99-125.

[5] Green, P. J.; Pines, O.; Inouye, M. The role of antisense RNA in gene regulation. *Annu. Rev. Biochem.*, **1986**, *55*, 569-597.

[6] Bass, B.L.; Weintraub H. M. An unwinding activity that covalently modifies its double-stranded RNA substrate. *Cell*, **1988**, *55*, 1089-1098.

[7] Wagner, J. A.; McDonald, T. V.; Nghiem, P. T.; Lowe, A. W.; Schulman, H.; Gruenert, D. C; Stryer, L.; Gardner, P. Antisense oligodeoxynucleotides to the cystic fibrosis transmembrane conductance regulator inhibit cAMP activated but not calcium-activated chloride currents. *Proc. Natl. Acad. Sci. USA*, **1992**, *89*, 6785-6789.

[8] Thayer, A. M., *Chem. Eng. News, Dec. 3*, **1990**, 17.

[9] Uhlmann E.; Peymann, A. Antisense oligonucleotides: a new therapeutic principle. *Chem. Rev.*, **1990**, *90*, 543-584.

[10] Milligan, J. F.; Matteucci, M. D.; Martin J. C. Current concepts in antisense drug. *J. Med. Chem.*, **1993**, *36*, 1923-1937.

[11] Toulme, J., in *Antisense RNA and DNA*, Murray, J. A. H., Ed., New York, Wiley-Liss, NY, **1992**, 175.

[12] Mohan, P. in *Biotechnology and Pharmacy*, Pezzuto J. M., et. al., Eds., New York, Chapman & Hall, **1993**, 256.

[13] Orr, R. M. Technology evaluation: fomivirsen. Isis Pharmaceuticals Inc/CIBA vision. *Curr. Opin. Mol. Ther.*, **2001**,*3*, 288–294.

[14] Roehr, B. Fomivirsen approved for CMV retinitis. *J. Int. Assoc. Physicians AIDS Care*, **1998**, *4*, 14–16.

[15] Agrawal, S., and Kandimalla, E. R. Antisense therapeutics: is it as simple as complementary base recognition? *Mol. Med. Today*, **2000**, *6*, 72–81.

[16] Watson, J. D.; Crick, F. H. C. Molecular structure of nucleic acid. A structure for deoxyribose nucleic acid. *Nature,* **1953**, *171*, 737-738.

[17] Crooke, S. T. *Therapeutic Applications of oligonucleotides*, **1995,** Springer-Verlag:Heidolbery.

[18] Soyfer, V. N.; Potman, V. N. *Triple- Helical Nucleic Acids*, **1996,** Springer-Verlag: NewYork.

[19] Wickstrom, E. Oligodeoxynucleotide stability in subcellular extracts and culture media. *J. Biochem. Biophys*. Methods, **1986**, *13*, 97–102.

[20] Akhtar, S.; Kole, R.; and Juliano, R. L. Stability of antisense DNA oligodeoxynucleotide analogs in cellular extracts and sera. *Life Sci.*, **1991**, *49*, 1793–1801.

[21] Eder, P. S.; DeVine, R. J.; Dagle, J. M.; Walder, J. A. Substrate specificity and kinetics of degradation of antisense oligonucleotides by a 3' exonuclease in plasma. *Antisense Res. Dev.*, **1991**, *1*, 141–151.

[22] Kurreck, J. Antisense technologies oligonucleotides Improvement through novel chemical modifications. *Eur. J. Biochem.* **2003**, *270*, 1628-1644.

[23] Dean, N. M., McKay, R., Condon, T. P., and Bennett, C. F. Inhibition of protein kinase C-α expression in human A549 cells by antisense oligonucleotides inhibits induction of intercellular adhesion molecule 1 (ICAM-1) mRNA by phorbol esters. *J. Biol. Chem.*,**1994**, *269*: 16416–16424.

[24] Larrouy, B., Blonski, C., Boiziau, C., Stuer, M., Moreau, S., Shire, D., and Toulme, J. J. RNase H-mediated inhibition of translation by antisense oligodeoxyribonucleotides: use of backbone modification to improve specificity. *Gene*, **1992**, *121*, 189–194.

[25] Opalinska, J. B.; Gewirtz, A. M. Nucleic-acid therapeutics: basic principles and recent applications. *Nat. Rev. Drug Discov.* **2002**, *1*, 503–514.

[26] Braasch, D. A.; Corey, D. R. Novel antisense and peptide nucleic acid strategies for controlling gene expression. *Biochemistry,* **2002**, *41*, 4503–4510.

[27] Mickelfield, J. Backbone modification of nucleic acids: Synthesis, structure and therapeutic applications. *Current Med. Chem*. **2001**, *8*, 1157-1179.

[28] Crooke, S. T. Progress in antisense Technology:the end of the beginning. *Methods Enzymol.*, **2000**, *313*, 3-45.

[29] Hogrefe, R. I. An antisense oligonucleotide primer, *Antisense Nucleic Acid Drug Dev.*, **1999**, *9*, 351-357.

[30] Levin, A. A. A review of the issues in the pharmacokinetics and toxicology of phosphorothioate antisense oligonucleotides. *Biochim. Biophys Acta*, **1999**, *1489*, 69-84.

[31] Agrawal, S.; Zhao, Q. Mixed backbone oligonucleotides: improvements in oligonucleotides-induced toxicity *in vivo*. *Antisense Nucleic Acid Drug Dev.*, **1998**, *8*, 135-139.

[32] Shen, L. X. et al. Impact of mixed-backbone oligonucleotides on target binding affinity and target cleaving specificity and selectivity by *Escherichia coli* RNase H. *Bioorg Med. Chem.* **1998**, *6*, 1695-1705.

[33] Goel, S. et al. A safety study of mixed-backbone oligonucleotides (GEM231) targeting the type I regulatory subunit alpha of protein kinase A using a continuous infusion schedule in patients with refractory solid tumors. *Clin. Cancer Res.* **2003**, *9*, 4069-4076.

[34] Braasch, D. A.; Corey, D. R. Locked Nucleic Acid (LNA): fine-tuning the recognition of DNA and RNA. *Chem. Biol.* **2001**, *8*, 1-7.

[35] Wahlestedt, C. et al. Potent and nontoxic antisense oligonucleotides containing locked nucleic acids. *Proc. Natl. Acad. Sci. U. S. A.* **2000**, *97*, 5633-5638.

[36] Fluiter, K. et al. In vivo tumor growth inhibition and biodistribution studies of locked nucleic acid (LNA) antisense oligonucleotides. *Nucleic Acids Res.* **2003**, *31*, 953-962.

[37] Summerton, J. Morpholino oligomers: the case for an Rnase H-independent structural type. *Biochim. Biophys. Acta.* **1999**, *1489*, 141-158.

[38] Nielsen, P. E.; Egholm, M. An introduction to peptide nucleic acid. *Curr. Issues Mol. Biol.* **1999**, *1*, 89-104.

[39] Braasch, D. A.; Corey, D. R. Novel antisense and peptide nucleic acid strategies for controlling gene expression. *Biochemistry* **2002**, *41*, 4503-4510.

[40] Kurreck, J. Antisense technologies. Improvements through novel chemical modifications. *Eur. J. Biochem.* **2003**, *270*, 1628-1644.

[41] Nielsen, P.E.; Egholm, M.; Berg, R. H.; Buchardt, O. Sequence selective recognition of DNA by strand displacement with a thymine substituted ployamide. *Science,* **1991,** *254*, 1497-1500.

[42] Egholm, M.; Buchardt, O.; Christensen, L.; Behrens, C.; Freier, S. M.; Driver, D. A.; Berg, R. H.; Kim, S. K.; Nordén, B.; Nielsen, P. E. PNA hybridizes to complementary oligonucleotides obeying the Watson-Crick hydrogen bonding rules. *Nature,* **1993**, *365*, 566-568.

[43] Petersen, M.; Nielsen, C. B.; Nielsen, K. E.; Jensen, G. A.; Bondensgaard, K.; Singh, S. K.; Rajwanshi, V. K.; Koshkin, A. A.; Dahl, B. M.; Wengel, J.; Jacobsen, J. P. The conformations of locked nucleic acids (LNA). *J. Mol. Recognit.* **2000**, *13*, 44– 53.

[44] Bentin, T.; Nielsen, P. E. In Triple Helix Forming Oligonucleotides (Malvy, C., Barel-Bellan, A., Pritchard, L., eds.) Kluwer Academic Publishers, pp. 245-255.

[45] Lohse, J.; Dahl, O.; Nielsen, P.E. Double duplex invasion by peptide nucleic acid:A general principle for sequence-specific targeting of double stranded-DNA. *Proc.Natl. Acad. Sci. USA.* **1999**, *96*, 11804-11808.

[46] Jensen, K.K.; Ørum, H.; Nielsen, P.E.; Norden, B.*Biochemistry* **1997**, *36*, 5072.

[47] Giesen, U. Kleider, W.; Berding, C.; Geiger, A.; Ørum, H. and Nielsen, P. E. *Nucleic Acids Res.* **1998**, *26*, 5004.

[48] Tomac, S.; Sarkar, M.; Ratilainen, T.; Wittung, P.; Nielsen, P.E.; Nordén, B.; Gräslund, A. *J. Amer. Chem. Soc.* **1996**, *118*, 5544.

[49] Brown, S.C.; Thomson, S.A.; Veal, J.M.; Davis. D.G. NMR Solution structure of a Peptide nucleic acid complexed with RNA. *Science* **1994**, *265*, 777.

[50] Eriksson, M. & Nielsen, P.E. Solution structure of a peptide Nucleic Acid-DNA duplex. *Nature Structural Biology* **1996**, *3*, 410.

[51] Betts, L.; Josey, J.A.; Veal, J.M.; Jordan, S.R. A nucleic acid triple helix formed by a Peptide Nucleic Acid-DNA complex. *Science* **1995**, *270*, 1838.

[52] Rasmussen, H.; Kastrup, J.S.; Nielsen, J.N.; Nielsen, J.M.; Nielsen, P.E. Crystal structure of a Peptide Nucleic acid (PNA) duplex at 1.7 A Resolution. *Nature Structural Biology* **1997**, *4***,** 98.

[53] Hyrup, B.; Egholm, M.; Rolland, M.; Nielsen, P. E.; Berg, R. H.; Buchardt, O. Modification of the binding affinity of peptide nucleic acids (PNA). PNA with extended backbones consisting of 2-aminoethyl-b-alanine or 3-aminopropylglycine units. *J. Chem. Soc. Chem. Commun.* **1993**, 518-519.

[54] Hyrup, B.; Egholm, M.; Nielsen, P.E.; Wittung, P.; Nordén, B.; Buchardt, O. Structure-activity studies of the binding of modified peptide nucleic acids (PNAs) to DNA. *J. Amer. Chem. Soc*. **1994,** *116*, 7964-7968.

[55] Hyrup, B.; Egholm, M.; Buchardt, O.; Nielsen, P. E. A flexible and positively charged PNA analogue with an ethylene-linker to the nucleobase: Synthesis and hybridization properties. *Bioorg. Med. Chem. Lett*. **1996**, *6*, 1083-1087.

[56] Efimov, V. A.; Choob, M. V.; Buryakova, A. A.; Chakhmakhcheva, O. G. Synthesis and binding study of phosphonate analogues of PNAs and their hybrids with PNA. *Nucleosides Nucleotides,* **1998**, *17*, 1671-1679.

[57] Efimov, V. A.; Buryakova, A. A.; Choob, M. V.; Chakhmakhcheva, O. G. Phosphonate analogues of peptide nucleic Acids and related compounds: synthesis and hybridazation properties. *Nucleosides Nucleotides,* **1999**, *18*, 1393-1396.

[58] Van der Laan, A. C.; Strömberg, R.; Van Boom, J. H.; Kuyl-Yeheskiely, E.; Chakhmakhcheva, O. G. An approach towards the synthesis of oligomers containing a N-2 hydroxyethyl-aminomethyl phosphonate backbone: A novel PNA analogue. *Tet. Lett.* **1996**, *37*, 7857-7860.

[59] Peyman, A.; Uhlmann, E.; Wagner, K.; Augustin, S.; Breipohl, G.; Will, D. W.; Schäffer, A.; Wallmeier, H. Phosphonic ester nucleic acids (PHONAs): oligonucleotide analogues with an achiral phosphonic acid ester backbone. *Angew. Chem. Int. Ed. Engl.* **1996**, *35*, 2636-2638.

[60] Kehler, J.; Henriksen, U.; Vekbjerg, H.; Dahl, O. Synthesis and hybridization properties of an acyclic phosphonate PNA analogues. *Bioorg. Med. Chem.* **1998**, *6*, 315-322.

[61] Altmann,K. H.; Chiesi, S.; Echevevria, C. Polyamide based nucleic acid analogues and 2013, 2013: Synthesis of d amino acids with nucleic acid bases bearing side chains. *Bioorg. Med. Chem. Lett.* **1997**, *7*, 1119-1122.

[62] Kuwahara, A. M.; Sisido, M. Novel PNA that shows high sequence specificity and all- or none type hybridization with the complementary DNA. *J. Am, Chem. Soc*. **1999**, *121*, 256-257.

[63] Barawkar, D.; Bruice, T. Deoxynucleic guanidines/PNA(DNG/PNA) chimeras: Oligonucleoside analogues containing cationic guanidium and neutral amide linkages. *J. Am. Chem. Soc*. **1999**, *121*, 10418-10419.

[64] Zhou, P.; Wang, M.; Du, L.; Fisher, G. W.; Waggoner A.; Ly, W. H. Novel binding and efficient cellular uptake of guanidine-based peptide nucleic acids (GPNA). *J. Am. Chem. Soc*. **2003,** *125*, 6878-6879.

[65] Krotz, A. H.; Buchardt, O.; Nielsen P. E. Synthesis of retro-inverso peptide nucleic acids: chracterisation of the monomer. *Tetrahedron Lett.* **1995**, *36*, 6937-6940.

[66] Almarison, O.; Bruice, T. C. Peptide Nucleic Acids (PNA) conformation and polymorphism in PNA-DNA and PNA-RNA hybrids. *Proc. Natl. Acad. Sci*. USA **1993**, *90*, 9542-9546.

[67] Lagriffoule, P. H.; Egholm, M.; Nielsen, P. E.; Berg, R. H.; Buchardt, O. The synthesis, co-oligomerization and hybridization of thymine-thymine heterodimer containing peptide Nucleic Acid. *Bioorg. Med. Chem. Lett*. **1994**, *4*, 1081-1082.

[68] Wengel, J. Synthesis of 3'-*C*- and 4'-*C*-Branched Oligodeoxynucleotides and the Development of Locked Nucleic Acid (LNA). *Acc. Chem. Res.* **1999**, *32*, 301-310.

[69] Lescrinier, E.; Esnouf, R.; Schraml, J.; Busson, R.; Heus, H. A.; Hilbers, C. W.; Herdewijn, P. Solution structure of a HNA–RNA hybrid. *Chem. Biol.* **2000**, *7*, 719-731.

[70] Allart, B.; Khan, K.; Rosemeyer, H.; Schepers, G.; Hendrix, C.; Rothenbacher, K.; Seela, F.; Van Aerschot, A.; Herdewijn, P. D-altritol nucleic acids (ANA): hybridisation properties, stability, and initial structural analysis. *Chem. Eur. J.* **1999**, *5*, 2424-2431.

[71] Robinson, D. S.; Greenstein, J. P. Stereoisomers of hydroxyproline. *J. Biol. Chem.***1952**, *195*, 383-388.

[72] Webb, T. R.; Eigenbrot, C. Conformationally restricted arginine analogs. *J. Org. Chem.* **1991**, *56*, 3009-3016.

[73] Gangamani. B. P.; Kumar, V. A.; Ganesh, K. N. Synthesis of N-(purinyl/pyrimidinyl acetyl)-4-aminoproline diastereomers with potential use in PNA synthesis. *Tetrahedron,* **1996**, *52*, 15017-15030.

[74] Jordan, S.; Schwemler, C.; Kosch, W.; Kretschmer, A.; Schwenner, E.; Milke, B. New hetero-oligomeric peptide nucleic acids with improved binding properties to complementary DNA. *Bioorg. Med. Chem. Lett.* **1997**, *7*, 687-692.

[75] Meena; Kumar, V. A.; Ganesh, K. N. Synthesis and evaluation of prolyl carbamate nucleic acids (PrCNA). *Nucleosides, Nucleotides, Nucleic Acids,* **2001**, *20*, 1193-1196.

[76] Lowe, G.; Vilaivan, T. Amino acids bearing nucleobases for the synthesis of novel peptide nucleic acids. *J. Chem. Soc. Perkin Trans 1,* **1997**, 539-546.

[77] Lowe, G.; Vilaivan, T. Solid phase synthesis of novel peptide nucleic acids. *J. Chem. Soc. Perkin Trans I* **1997**, 555-560.

[78] D'Costa, M.; Kumar, V. A.; Ganesh, K. N. Aminoethylprolyl peptide nucleic acids(*aep*PNA) : chiral PNA analogues that forms highly stable DNA:*aep*PNA_2 triplexes. *Org. Lett*. **1999**, *1*, 1513-1516.

[79] Puschl, A.; Boesn, G.; Zuccarello, G.; Dahl, O.; Pitsch, S.; Nielsen, P. E. Synthesis of pyrrolidinone PNA: A novel conformationally restricted peptide nucleic acid analogues. *J. Org. Chem.* **2001**, *66*, 707-712.

[80] Samuel, T. H.; David, T.; Hickman, T.; Morral, J.; Beadham, I. G.; Micklefield, J. Nucleic acid binding properties of thyminyl and adeninyl pyrrolidine-amide oligonucleotide mimics (POM). *Chem. Comm*. **2004**, 516-517.

[81] Sharma, N. K.; Ganesh, K. N. Expanding the repertoire of pyrrolidyl PNA analogues for DNA/RNA hybridization selectivity: aminoethylpyrrolidinone PNA (*aepone*-PNA) *Chem. Commun.* **2003**, 2484-2485.

[82] Vilaivan, T.; Khongdeesameor, C.; Harnyuttanokam, P.; Lowe, G. Synthesis and properties of novel pyrrolidinyl PNA carrying b amino acid spacers. *Tetrahedron Lett.* **2001**, *42*, 5533-5536.

[83] Vilaivan, T.; Khongdeesameor, C.; Harnyuttanokam, P.; Lowe, G. J. A novel pyrrolidinyl PNA showing high sequence specificity and preferential binding to DNA over RNA. *J. Am. Chem. Soc.* **2002,** *124,* 9326-9327.

[84] Puschl, A.; Tedeschi, T.; Nielsen, P. E. Pyrrolidine PNA: A novel conformationally restricted PNA analogues. *Org. Lett.* **2000**, *2*, 4161-4163.

[85] Lonkar, P. S.; Ganesh, K. N.; Kumar, V. A. Chimeric (*aeg*-pyrrolidine)PNAs: synthesis and stereodiscriminative duplex binding with DNA/RNA. *Org. Biomol. Chem.***2004**, *2*, 2604-2611.

[86] Michael, C. Mark, M.; Witschi, A.; Larionova, N.; John, M.; Russell; Haynes, D.; Toshiaki, H.; Grajkowski, A.; Appella, D. H. A cyclopentane conformational restraint for a Peptide Nucleic Acid: Design, asymmetric synthesis and improved binding affinity to DNA & RNA. *Org. Lett.* **2003**, *5*, 2695-2698.

[87] Govindaraju, T.; Kumar, V. A.; Ganesh, K. N. *cis*-Cyclopentyl PNA (*cp*PNA) as constrained chiral PNA analogues: stereochemical dependence of DNA/RNA hybridization. *Chem. Commun*. **2004**, *7*, 860-861.

[88] Pokorski, J. K.; Witschi, M. A.; Purnell, B. L.; Appella, D. H. *(S,S)-trans-c*yclopentane constrained peptide nucleic acids. A general backbone modification that improves binding affinity and sequence specificity. *J. Am. Chem. Soc.* **2004**, *126*, 15067-15073.

[89] Govindaraju, T.; Kumar, V. A. Backbone-extended pyrrolidine peptide nucleic acids (*bep*PNA): design, synthesis and DNA/RNA binding studies. *Chem. Commun.***2005**, 4, 495-497.

[90] Schoning, K.; Scholz, P.; Guntha, S.; Wu, X.; Krishnamurthy, R.; Eschenmoser, A. Chemical etiology of nucleic acid structure: The–threofuranosyl (3'-2) oligonucleotide system. *Science,* **2000**, *290*, 1347-1351.

[91] Summerton, J. D.; Weller. Morpholino antisense oligomers: design, preparation and properties. *Antisense Nucleic Acid Druug Dev.* **1997,** *7*, 187-195.

[92] Lescrinier, E.; Esnouf, R.; Schraml, J.; Busson, R.; Heus, H. A.; Hilbers, C. W.; Herdewijn, P. Solution structure of HNA-RNA hybrid. *Chem. Biol*. **2000**, *7,* 719-731.

[93] Wang, B.; Verbeure, I.; Luyten, E.; Lescrinier, M.; Froeyen, C.; Hendrix, H.; Rosemeyer, F.; Seela, A.; Van-Aerschot.; Herdwijn, P. Cyclohexene nucleic

acids(CeNA): Serum stable oligonucleotides that activate RNase H and increase duplex stability with complementary RNA. *J. Am. Chem. Soc*. **2000,** *122*, 8595-8602.

[94] Goodnow, R. A.; Tam, S.; Pruess, D. L.; McComas, W. Oligomer synthesis and DNA/RNA recognition properties of a novel oligonucleotide backbone analog: Glucopyranosyl nucleic amide (GNA). *Tetrahedron Lett.* **1997,** *38*, 3199-3202.

[95] Puschl, A.; Boesen, T.; Tedeschr, T.; Dahl, O.; Nielsen, P. E. Synthesis of (3*R*,6*R*)- and (3*S*,6*R*)-piperidinone PNA. *J. Chem. Soc. Perkin 1* **2001,** 2757-2763.

[96] Lagriffoule, P.; Wittung, P.; Eriksson, M.; Jensen, K. K.; Norden, P.; Buchardt, O.; Nielsen, P. E. Peptide nucleic acids with a conformationally constrained chiral cyclohexyl-derived backbone. *Chem. Eur. J.* **1997**, *3*, 912-919.

[97] Govindaraju, T. G.; Ganesh, K. N.; Kumar, V. A. Synthesis and evaluation of (1*S*,2*R*/1*R*,2*S*)-aminocyclohexylglycyl PNAs as conformationally preorganised PNA analogues for DNA/RNA recognition. *J. Org. Chem.* **2003**, *69*, 1858-1865.

[98] Lonkar, P. S.; Kumar, V. A. Design and synthesis of conformationally frozen peptide nucleic acid backbone: chiral piperidine PNA as a hexitol nucleic acid surrogate. *Bioorg. Med. Chem. Lett.* **2004**, *14*, 2147–2149.

[99] Maison, W.; Schlemminger, I.; Westterhoff, O.; Martens. J. Modified PNAs : A simple method for the synthesis of monomeric building blocks. *Bioorg. Med. Chem. Lett*. **1999**, *9*, 581-584.

[100] Egholm, M.; Christensen, L.; Dueholm, K.; Buchardt, O.; Coull, J.; Nielsen, P. E. Efficient pH-independent sequence-specific DNA binding by pseudoisocytosine containing bis-PNA. *Nucleic Acids Res.* **1995**, *23*, 217-222.

[101] Haaima, G.; Hansen, H. F.; Christensen, L.; Dahl, O.; Nielsen, P. E. Increased DNA binding and sequence discrimination of PNA oligomers containing 2,6-diaminopurine. *Nucleic Acids Res.* **1997**, *25*, 4639.

[102] Gangamani, B. P.; Kumar, V. A.; Ganesh, K. N. 2-Aminopurine peptide nucleic acids (2-*ap*PNA): intrinsic fluorescent PNA analogues for probing PNA–DNA interaction dynamics. *J. Chem. Soc. Chem. Commun.* **1997**, 1913-1914.

[103] Kohler, O; Seitz, O. Thiazole orange as fluorescent universal base in PNA. *Chem. Commun.* **2003**, 2938-2939.

[104] Eldrup, A. B.; Dahl, O.; Nielsen, P. E. A novel Peptide Nucleic Acid monomer for recognition of thymine in triple helix structure. *J. Am. Chem. Soc.* **1997**, *119*, 11116.

[105] Timar, Z.; Bottka, S.; Kovacs, L.; Penke, B. Synthesis and preliminary thermodynamic investigation of hypoxanthine-containing peptide nucleic acids. *Nucleosides Nucleotides* **1999**, *18*, 1131-1133.

[106] Bergmann, F.; Bannwarth, W.; Tam, S. Solid phase synthesis of directly linked PNA-DNA hybrids. *Tetrahedron Lett.* **1995**, *36*, 6823-6826.

[107] Nielsen, P. E.; Egholm, M.; Berg, R. H.; Buchardt, O. Sequence specific inhibition of DNA restriction enzyme cleavage by PNA. *Nucleic Acids Res*. **1993**, *21*, 197-200.

[108] Pooga, M..; Soomets, U.; Hällbrink, M.; Valkna, A.; Saar, K.; Rezaei, K.; Kahl, U.; Hao, Jing-Xia; Xu, Xiao-Jun; Weisenfeld-Hallin, Z.; Hökfelt, T.; Bartfai, T.; Langel, Ü. Cell penetrating PNA constructs regulate galanin receptor levels and modify pain transmission *in vivo*. *Nat. Biotech.* **1998**, *16*, 857-861.

[109] Hamilton, S. E.; Simmons, C. G.; Kathiriya, I. S.; Corey, D. R. Cellular delivery of peptide nucleic acids and inhibition of human telomerase. *Chem. Biol.* **1999,** *6,* 343-347.

[110] Fraser, G. L.; Holmgren, J.; Clarke, P. B.; Wahlestedt, C. Antisense inhibition of d-opioid receptor gene function in vivo by peptide nucleic acids. *Mol. Pharmacol.* **2000,** *57*, 725-731.

[111] Nielsen, P. E.; Egholm, M.; Buchardt, O. Sequence specific transcription arrest by peptide nucleic acid bound to the DNA template strand. *Gene,* **1994**, *149*, 139–145.

[112] Hanvey, J. C.; Peffer, N. C.; Bisi, J. E.; Thomson, S. A.; Cadilla, R.; Josey, J. A.; Ricca, D. J.; Hassman, C. F.; Bonham, M. A.; Au, K. G.; Carter, S. G.; Bruckenstein, D. A.; Boyd, A. L.; Noble, S. A.; Babiss, L. E. Antisense and antigene properties of peptide nucleic acids. *Science,* **1992**, *258*, 1481–1485.

[113] Praseuth, D.; Grigoriev, M.; Guieysse, A. L.; Pritchard, L. L.; Harel-Bellan, A.; Nielsen, P. E.; Helene, C. Peptide nucleic acids directed to the promoter of the alphachain of the interleukin-2 receptor. *Biochim. Biophys. Acta,* **1996**, *1309***,** 226–238.

[114] Tomac, S.; Sarkar, M.; Ratilainen, T.; Wittung, P.; Nielsen, P. E.; Norden, B.; Graslund, A. Ionic effects on the stability and conformation of peptide nucleic acid complexes. *J. Am. Chem. Soc.* **1996**, *118*, 5544–5552.

[115] Bentin, T.; Nielsen, P. E. Enhanced peptide nucleic acid binding to supercoiled DNA: possible implications for DNA 'breathing' dynamics. *Biochemistry,* **1996**, *35*, 8863–8869.

[116] Egholm, M.; Christensen, L.; Dueholm, K. L.; Buchardt, O.; Coull, J.; Nielsen, P. E. Efficient pH-independent sequence-specific DNA-binding by pseudoisocytosine containing bis-PNA. *Nucleic Acids Res.* **1995**, *23*, 217–222.

[117] Kuhn, H.; Demidov, V. V.; Frank-Kamenetskii, M. D.; Nielsen, P. E. Kinetic sequence discrimination of cationic bis-PNAs upon targeting of double-stranded DNA. *Nucleic Acids Res.* **1998**, *26*, 582–587.

[118] Lee, R.; Kaushik, N.; Modak, M. J.; Vinayak, R.; Pandey, V. N. Polyamide nucleic acid targeted to the primer binding site of the HIV-1 RNA genome blocks *in vitro* HIV-1 reverse transcription. *Biochemistry,* **1998**, *37*, 900–910.

[119] Knudsen, H.; Nielsen, P. E. Antisense properties of duplex- and triplex-forming PNAs. *Nucleic Acids Res.* **1996**, ***24,*** 494–500.

[120] Good, L.; Nielsen, P. E. Inhibition of translation and bacterial growth by peptide nucleic acid targeted to ribosomal RNA. *Proc. Natl. Acad. Sci. USA.* **1998**, *95*, 2073–2076.

[121] Good, L.; Nielsen, P. E. Antisense inhibition of gene expression in bacteria by PNA targeted to mRNA. *Nat. Biotech.* **1998**, *16*, 355–358.

[122] Taylor, R. W.; Chinnery, P. F.; Turnbull, D. M.; Lightowlers, R. N. Selective inhibition of mutant human mitochondrial DNA replication *in vitro* by peptide nucleic acids. *Nature Genet.* **1997**, *15*, 212–215.

[123] Uhlmann, E.; Peyman, A.; Breipohl, G.; Will, D. W. PNA: synthetic polyamide nucleic acids with unusual binding properties. *Angew. Chem. Int. Ed.* **1998***, 37*, 2796–2823.

[124] Nielsen, P. E.; Egholm, M.; Berg, R. H.; Buchardt, O. Peptide nucleic acids (PNAs): potential antisense and antigene agents. *Anti-Cancer Drug Design,* **1993**, *8,* 53–63.

[125] Koppelhus, U.; Zachar, V.; Nielsen, P. E.; Liu, X.; Eugen-Olsen, J.; Ebbesen, P. Efficient in vitro inhibition of HIV-1gag reverse transcription by peptide nucleic acid (PNA) at minimal ratios of PNA/RNA. *Nucleic Acids Res.* **1997**, *25*, 2167–2173.

[126] Mologni, L.; leCoutre, P.; Nielsen, P. E.; Gambacorti-Passerini, C. Additive antisense effects of different PNAs on the *in vitro* translation of the PML/RARa gene. *Nucleic Acids Res.* **1998**, *26*, 1934–1938.

[127] Norton, J. C.; Piatyszek, M. A.; Wright, W. E.; Shay, J. W.; Corey, D. R. Inhibition of human telomerase activity by peptide nucleic acids. *Nat. Biotech.* **1996**, *14*, 615–620.

[128] Hamilton, S. E.; Simmons, C. G.; Kathiriya, I. S.; Corey, D. R. Cellular delivery of peptide nucleic acids and inhibition of human telomerase. *Chem. Biol.* **1999**, *6*, 343– 351.

[129] Petersen, M. B.; Economou, E. P.; Slaugenhaupt, S. A.; Chakravarti, A.; Antonarakis, S. E. Linkage analysis of the human HMG14 gene on chromosome 21 using a GT dinucleotide repeat as polymorphic marker. *Genomics,* **1990**, *7*, 136–138.

[130] Pena, S. D.; Chakraborty, R. Paternity testing in the DNA era. *Trends Genet.* **1994**, *10*, 204–209.

[131] Demers, D. B.; Curry, E. T.; Egholm, M.; Sozer, A. C. Enhanced PCR amplification of VNTR locus D1S80 using peptide nucleic acid (PNA). *Nucleic Acids Res.* **1995**, *23,* 3050–3055.

[132] Perry-O'Keefe, H.; Yao, X. W.; Coull, J. M.; Fuchs, M.; Egholm, M. Peptide nucleic acid pre-gel hybridization: an alternative to Southern hybridization. *Proc. Natl. Acad. Sci. USA.* **1996**, *93*, 14670–14675.

[133] Veselkov, A. G.; Demidov, V.; Nielsen, P. E.; Frank-Kamenetskii, M. D. A new class of genome rare cutters. *Nucleic Acids Res.* **1996**, *24*, 2483–2487.

[134] Frank-Kamenetskii, M. D.; Demidov, V. V. PNA directed genome rare cutting: new developments. *http://www.bu.edu/cab*

[135] Demidov, V.; Frank-Kamenetskii, M. D.; Egholm, M.; Buchardt, O.; Nielsen, P. E. Sequence specific double strand DNA cleavage by peptide nucleic acid (PNA) targeting using nuclease S1. *Nucleic Acids Res.* **1993**, *21*, 2103–2107.

[136] Lansdorp, P. M.; Verwoerd, N. P.; van de Rijke, F. M.; Dragowska, V.; Little, M. T.; Dirks, R. W.; Raap, A. K.; Tanke**,** H. J. Heterogeneity in telomere length of human chromosomes. *Hum. Mol. Genet.* **1996**, *5*, 685–691.

[137] Orum, H.; Nielsen, P. E.; Jorgensen, M.; Larsson, C.; Stanley, C.; Koch, T. Sequence-specific purification of nucleic acids by PNA-controlled hybrid selection. *BioTechniques,* **1995**, *19*, 472–480.

[138] Orum, H.; Nielsen, P. E.; Egholm, M.; Berg, R. H.; Buchardt, O.; Stanley, C. Single base pair mutation analysis by PNA directed PCR clamping. *Nucleic Acids Res.* **1993**, *21*, 5332–5336.

[139] Thiede, C.; Bayerdorffer, E.; Blasczyk, R.; Wittig, B.; Neubauer, A. Simple and ensitive detection of mutations in the ras proto-oncogenes using PNA-mediated PCR clamping. *Nucleic Acids Res.* **1996**, *24*, 983–984.

[140] Bonnet, G.; Tyagi, S.; Libchaber, A.; Kramer, F. R. Thermodynamic basis of the enhanced specificity of structured DNA probes. *Proc. Natl. Acad. Sci.* USA, **1999**, *96*, 6171-6176.

[141] Marras, SAE.; Kramer, F. R.; Tyagi, S. Efficiencies of fluorescence resonance energy transfer and contact-mediated quenching in oligonucleotide probes. *Nucleic Acids Res.* **2002**, *30*, 122-127.

[142] Brandt, O.; Hoheisel, J. D. Peptide nucleic acids on microarrays and other biosensors. *Trends Biotech.* **2004**, *22*, 617-622.

[143] Norton JC, Piatyszek MA, Wright WE, Shay JW and Corey DR: Inhibition of human telomerase activity by peptide nucleic acids. Nat Biotechnol 14: 615-618, 1996.

[144] Mologni L, Nielsen PE and Gambacorti-Passerini C: *In vitro* transcriptional and translational block of the bcl-2 gene operated by peptide nucleic acid. Biochem Biophys Res Commun 264: 537-543, 1999.

[145] Miller, P. S.; McParland, K. B.; Jayaraman, K.; Ts'O, P. O. P. Biochemical and biological effects of nonionic nucleic acid methylphosphonates. *Biochemistry,* **1981,** *20*, 1874.

[146] Marcus-Secura, C. J.; Woerner, A. M.; Shinozuka, K.; Zon, G.; Quinnan, G. V. Jr. Comparative inhibition of chloramphenicol acetyltransferase gene expression by antisense oligonucleotide analogues having alkyl phosphotriester, methylphosphonate and phosphorothioate linkages. *Nucleic Acids Res.* **1987**, *15*, 5749.

[147] Nielsen, P. E. Sequence-specific recognition of double stranded DNA by peptide nucleic acids. *Adv. DNA Sequence-Specific Agents,* **1998**, *3*, 267–278.

[148] Faruqi, A. F.; Egolm, M.; Glazer, P. M. Peptide nucleic acid-targeted mutagenesis of a chromosomal gene in mouse cells. *Proc. Natl. Acad. Sci. USA.***1997**, *95*, 1398–1403.

[149] Pooga, M.; Soomets, U.; Hallbrink, M.; Valkna, A.; Saar, K.; Rezaei, K.; Kahl, U.; Hao, J. X.; Xu, X. J.; Wiesenfeld-Hallin, Z. Cell penetrating PNA constructs regulate galanin receptor levels and modify pain transmission *in vivo. Nat. Biotech.* **1998**, *16*, 857–861.

[150] Basu, S.; Wickstrom, E. Synthesis and characterization of a peptide nucleic acid conjugated to a D-peptide analog of insulin-like growth factor 1 for increased cellular uptake. *Bioconj. Chem.* **1997**, *8*, 481–488.

[151] Simmons, C. G.; Pitts, A. E.; Mayfield, L. D.; Shay, J. W.; Corey, D. R. Synthesis and permeability of PNA-peptide conjugates. *Bioorg. Med. Chem. Lett.* **1997**, *7*, 3001–3007.

[152] Aldrian-Herrada, G.; Desarmenien, M. G.; Orcel, H.; Boissin-Agasse, L.; Mery, J.; Brugidou, J.; Rabie, A. A peptide nucleic acid (PNA) is more rapidly internalized in culture neurons when coupled to a retro-inverso delivery peptide. The antisense activity depresses the target mRNA and protein in magnocellular oxytocin neurons. *Nucleic Acids Res.***1998**, *26*, 4910–4916.

[153] Hamilton, S. E.; Simmons, C. G.; Kathiriya, I. S.; Corey, D. R. Cellular delivery of peptide nucleic acids and inhibition of human telomerase. *Chem. Biol.* **1999**, *6*, 343–351.

[154] Kaihatsu, K.; Huffman, K. E.; Corey D. R. Intracellular Uptake and Inhibition of Gene Expression by PNAs and PNA-Peptide Conjugates. *Biochemistry,* **2004**, *43,* 14340-14347.

[155] Ratilainen, T.; Holmen, A.; Tuite, E.; Haaima, G.; Christensen, L.; Nielsen, P. E.; Norden, B. Hybridization of peptide nucleic acid. *Biochemistry,* **1998**, *37*, 12331–12342.

[156] Holmen, A.; Norden, B. Thermodynamics of PNA-nucleic acid interactions. In *Peptide Nucleic Acids: Protocols and Applications* (Nielsen, P. E., and Egholm, M., eds) 1999, pp. 87–97, Horizon Press, Wymondham, U.K.

[157] Marky, L. A.; Breslauer, K. J. Calculating thermodynamic data for transitions of any molecularity from equilibrium melting curves. *Biopolymers,* **1987**, *26*, 1601–1620.

[158] Lansdorp, P.M.; Verwoerd, N.P.; van de Rijke, F. M.; *et al:* Heterogeneity in telomere length of human chromosomes. *Hum. Mol. Genet.*, **1996**, *5*, 685-691.

[159] Boei, J. J. W. A.; Vermeulen, S.; Natarajan, A. T. Analysis of radiation-induced chromosomal aberrations using telomeric and centromeric PNA probes. *Int. J. Radiat. Biol.*, **2000**, *76*, 163-167.

[160] Mathioudakis, G.; Storb, R.; McSweeney, P. A.; *et al.* Polyclonal hematopoiesis with variable telomere shortening in human longterm allogeneic marrow graft recipients. *Blood*, **2000,** *96*, 3991-3994.

[161] Chen, C.; Wu, B.; Wei, T.; Egholm, M.; Strauss, W. M. Unique chromosome identification and sequence-specific structural analysis with short PNA oligomers. *Mamm. Genome*, **2000,** *11*: 384-391.

[162] Taneja, K. L.; Chavez, E. A.; Coull, J.; Lansdorp, P. M. Multicolor fluorescence *in situ* hybridization with peptide nucleic acid probes for enumeration of specific chromosomes in human cells. *Genes Chromosomes Cancer*, **2001**, *30*, 57-63.

[163] Pellestor, F.; Andréo, B.; Taneja, K.; Williams, B. PNA on human sperm: a new approach for *in situ* aneuploidy estimation. *Eur. J. Hum. Genet.*, **2003**, *11*, 337-341.

[164] Fire, A.; Xu, S. Q.; Montgomery, M. K.; Kostas, S. A.; Driver, S. E.; Mello, C. C. Potent and specific genetic interference by double-stranded RNA in *Caenorhabditis elegans*. *Nature*, **1998**, *391*, 806–811.

[165]Yu, J. Y.; DeRuiter, S. L.; Turner, D. L. RNA interference by expression of short interferencing and hair pin RNAs in mammalian cells. *Proc. Natl. Acad. Sci.*, **2002**, *99*, 6047-6052.

[166] Amarzguioui, M.; Holen, T.; Babaie, E.; Prydz, H. Tolerance for mutations and chemical modifications in a siRNA. *Nucleic Acids Res.* **2003**, *31*, 589-595.

[167] Carrington, J. C.; Ambros, V. Role of microRNAs in plant and animal development. *Science* **2003**, *301*, 336-338.

[168] Ambros, V. MicroRNA pathways in flies and worms: growth, death, fat, stress, and timing. *Cell,* **2003**, *113*, 673-676.

[169] Xu, P.; Vernooy, S. Y.; Guo, M.; Hay, B. A. The Drosophila microRNA mir-14 suppresses cell death and is required for normal fat metabolism. *Curr. Biol*. **2003**, *13*, 790-795.

[170] Tang, J.; Breaker, R. R. Structural diversity of self-cleaving ribozymes. *Proc. Natl. Acad. Sci.* USA, **2000**, *97*, 5784-5789.

[171] Winkler, W. C.; Nahvi, A.; Roth, A.; Collins, J. A.; Breaker, R. R. Control of gene expression by a natural metabolite-responsive ribozyme. *Nature,* **2004,** *428,* 281-286.

Chapter 2

Modified *aeaib*- and *apaib*-PNAs:

Synthesis and Biophysical Studies

2.1. INTRODUCTION

Chapter 1 described how the search for effective antigene/antisense agents has led to the development of novel DNA/RNA analogues in the past decade.[1-8] One of the most prominent outcome of this search is the Peptide Nucleic Acids (PNAs).[9-14] In this class of compounds, the entire negatively charged sugar-phosphate backbone of DNA is replaced by a neutral and achiral polyamide backbone consisting of *N*-(2-aminoethyl)glycine units. The nucleobases are attached to the backbone through a methylene carbonyl linkage as shown in Figure 1-II. PNA binding to the target DNA/RNA sequences occurs with high

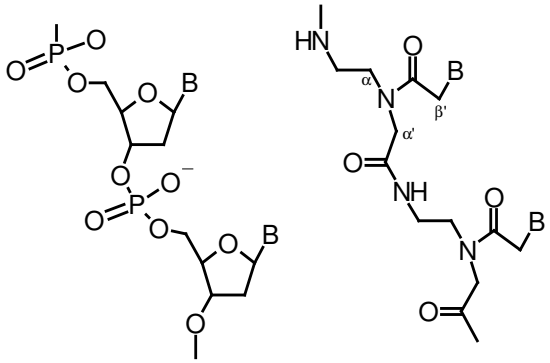

Figure 1. The basic structures of DNA (I) and PNA (II)

sequence specificity and affinity.[15] Despite having several advantages like resistance to cellular enzymes like nucleases and proteases, the major limitations perplexing its application are ambiguity in orientational selectivity of binding, poor solubility in aqueous media and inefficient cellular uptake.[16] To improve the properties of *aeg*PNA and achieve optimal fine-tuning of aminoethylglycyl (*aeg*PNA) backbone, previous efforts[17-19] from this laboratory and that of others[20] has resulted in a number of five-membered pyrrolidyl PNA analogues. The *aeg*PNA backbone is highly flexible due to

the presence of 2-aminoethyl and glycyl segments that slowly reorganize to the preferred conformations during complex formation with DNA/RNA. Pre-organizing the *aeg*PNA backbone into "hybridization competent conformations" is expected to have entropic advantages for binding DNA/RNA. In contrast to well-known strategies towards chiral and cyclic PNAs, attempts have been herein made to introduce *gem*-dimethyl functionality into the glycine unit of PNA, leading to an achiral and acyclic backbone but still possessing conformational constraints to pre-organize it for favorable binding to complementary DNA/RNA.

Glycine, (Figure 2a) the least hindered amino acid has the small propensity to adopt helix conformation, perhaps due to the large flexibility of this residue.[21] On the other hand, some non-coded α-amino acid residues are known to be excellent helix formers. In particular, an α-aminoisobutyric acid, (Figure 2b) (*Aib*; also denoted α-methylalanine or α,α-dimethylglycine) has been extensively used in peptidomimetics.

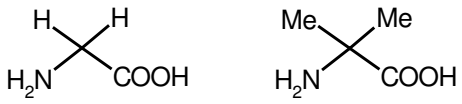

(**a**) (**b**)

Figure 2. Structures of **(a)** natural amino acid, Glycine and **(b)** non-coded amino acid, α-aminoisobutyric acid.

The two methyl groups at C^{α} -atom of *Aib* restricts the conformational space [ϕ and ψ (Ramachandran plot)] accessible to *Aib* and forces the peptide chain into left or right handed conformations.[21] In peptides containing such non-standard residues, α-substituents influence the geometry of the peptide bond, converting linear peptides that

are often difficult to crystallize to stiff and rigid structures, which are prone to crystallization. Other example is α,β-dehydroamino acids[22], having a rigid side chain orientation and change in α-carbon geometry causes this also a perturbation in the electronic distribution of the adjacent -CO-NH- bonds, inducing conjugation with the π electron of the $C^{\alpha} = C^{\beta}$ double bond. In the case of the dialkylglycines, the Thorpe-Ingold distortion of the C^{α} geometry may affect the peptide bond geometry in a subtle manner. The main consequence of such changes is the severe steric hindrance that restricts conformation to small areas within the α-left and α-right handed regions of the Ramachandran plot.[22]

2.2. PRESENT WORK: A RATIONALE

In most of the PNA backbone modifications hitherto known, introduction of constrain is always associated with introduction of chirality. In order to introduce rigidity without any chirality, which may have interesting consequences, aminoethyl-α-aminoisobutyric acid PNA monomer (Figure 3b), was designed by incorporating *gem*-dimethyl group into the α-glycyl carbon of *aeg*-PNA backbone. The choice of the dimethyl group was dictated by its preferences to form helices in polypeptides. Further, to release the constrain in a different part of PNA backbone, a methylene group was introduced into the ethylenediamine segment to make it propylenediamine, leading to aminopropyl-α-aminoisobutyric acid PNA monomer (Figure 3c).

The present chapter reports on the synthesis of modified aminoethyl-α,α-dimethylglycine PNA or *aeaib*-PNA (Figure 4a) and aminopropyl-α,α-dimethylglycine

PNA or *apaib*-PNA (Figure 4b), their oligomerization and the thermal stability of hybrids between the modified PNA oligomers and DNA/RNA.

The specific objectives of this chapter are:

(i) Synthesis of *N*-Boc-(aminoethyl-α,α-dimethylglycyl)-thymine PNA and *N*-Boc-(aminopropyl-α,α-dimethylglycyl)-thymine PNA monomers.

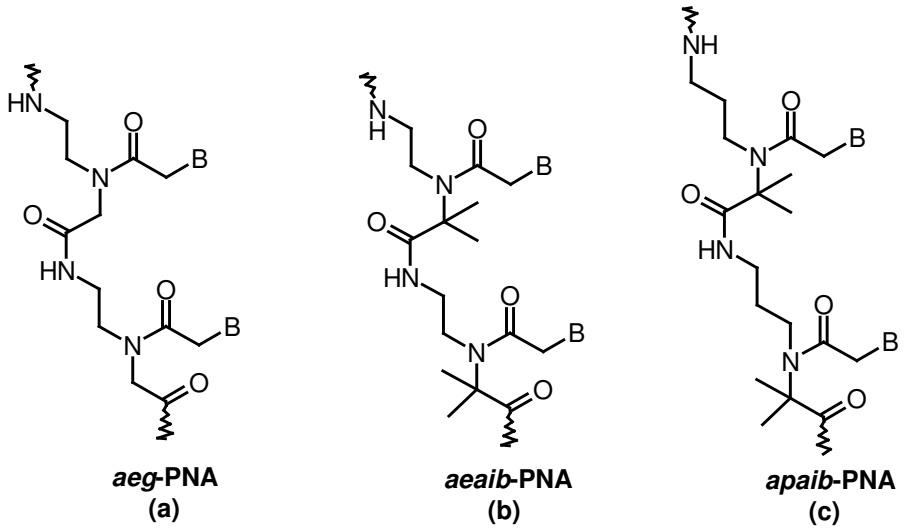

Figure 3. Design of *aeaib and apaib*-PNA.

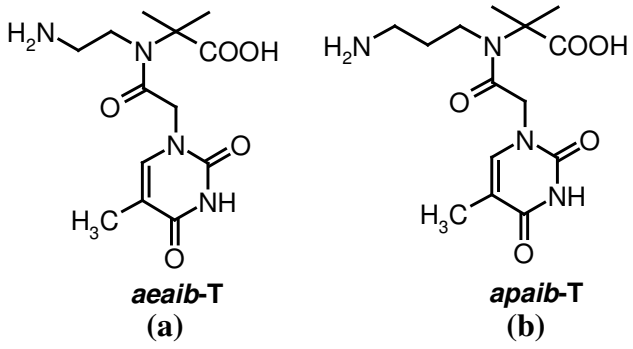

Figure 4. Target molecules for the synthesis of modified PNA monomers.

(ii) Solid phase peptide synthesis of PNA oligomers incorporating *aeg* and/or *aeaib*-PNA or *apaib*-PN

(iii) Cleavage from solid support and purification and characterization of *aeg*PNA and modified PNA oligomers.

(iv) Biophysical studies of *aeaib*-PNA:DNA/RNA and *apaib*-PNA:DNA/RNA hybrids using UV-T_m, CD and Isothermal Titration calorimetry.

2.3 RESULTS AND DISCUSSION

2.3.1. Synthesis of Aminoethyl-(α,α-dimethyl)-glycyl-(*aeaib*)–PNA Monomer

Various strategies were attempted for the synthesis of *aeaib*-PNA monomer and these are shown in Scheme 1 and 2. The synthesis began with the mono-*N*-protected derivative **2**, obtained by using a large excess of 1,2-diaminoethane over the boc-anhydride. The *N1, N2*-di-Boc derivative was obtained in very small amounts (< 5%), and the major product was the mono-*N*-protected derivative **2**. The di-Boc derivative, being insoluble in water, could be easily removed by filtration. The formation of *N*-Boc-Gly-Weinreb amide **4** from *N*-Boc-glycine **2** and *N,O*-dimethylhydroxylamine salt **3** shown in Scheme 1. Employing *N*,*N*-diisopropyl-carbodiimide as a condensing agent in this amide bond forming reaction allowed access to pure **4** (at one tenth cost of the commercially available material). The reduction of a Boc-protected α-amino Weinreb amide with lithium aluminium hydride to give an aldehyde has been well established.[22a] Reaction **4** with lithium aluminium hydride cleanly afforded the *N*-Boc-glycinal **5** in good yield without any need to perform column purification that could degrade the aldehyde. *N*-Boc-glycinal **5** was immediately used in the reductive amination with aib-ethyl-ester salt **6** using sodium triacetoxyborohydride. This reaction did not proceed to

yield the expected compound **7** perhaps due to unfavorable steric interactions between the reacting substituents and *gem*-dimethyl groups.

An alternative approach was attempted as shown in Scheme 2, the attempts continued with the starting material as the protected ethanolamine **8**. Initially, the amine functionality of ethanolamine was protected with different protecting groups like Boc, phthalimido, mono-benzyl and di-benzyl with the intention of converting it later into the mesyl-, tosyl- or bromo- derivatives **9** for alkylating *aib*-ethyl-ester salt to get the compound **7**. However, all attempts to synthesize the compound **7** from compounds **9** and **6** failed.

The observed results are a direct consequence of the 'scissor movement', i.e. bulky groups like the methyl group replacing hydrogen atoms require more space in

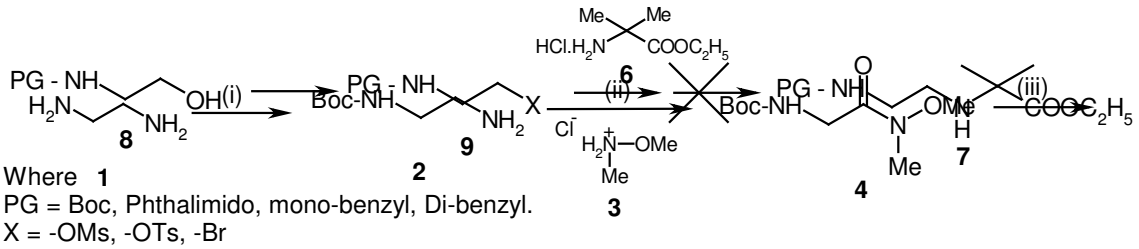

Scheme 2. Strategy attempted for the synthesis of *aeaib*-PNA monomer

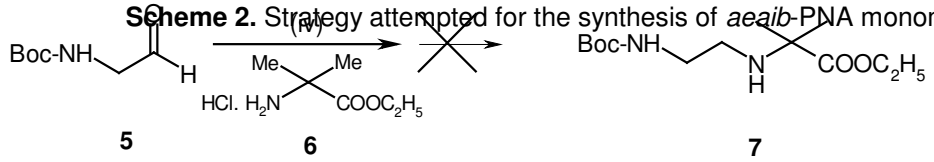

Scheme 1. Reagents and conditions: (i) Boc-anhydride, dioxane: water (1:1), rt, 12hrs (ii) *N, N*-diisopropylcarbodiimide, triethylamine, dry DCM, 19 hrs. (iii) $LiAlH_4$, 40 min. (iv) $NaBH(OAc)_3$, Triethylamine.

transition state and result in a larger CH_3-C-CH_3 bond angle. This increase in bond angle

consequently leads to a deformation of opposite bond angle, which is subsequently reduced.

In the third approach, the synthesis of aminoethyl-(α,α-dimethyl)-glycyl (*aeaib*) PNA monomer was carried out by reverting the amine and alkylating agent as in Scheme 3. The *N1*-Boc-1,2-diaminoethane **2** was subjected to *N*-alkylation using ethyl-2-bromo-isobutyrate and potassium carbonate in dry acetonitrile to obtain the aminoethyl-(α,α-dimethyl)-glycine ethyl ester **7**. This reaction proceeded neatly to give 77% yield of the much sought compound **7**. The formation of compound **7** was supported by observance of (singlet) signals for ($\underline{CH_3}$)$_2$C- at 1.34 δ in ^{1}H NMR in addition to N-$C\underline{H_2}$ signal and at 28.13 δ in ^{13}C NMR. The observed mass for compound **7** is 275.21 (M+1) was in agreement with the calculated mass 274. Compound **7** was treated with chloroacetyl chloride to yield the corresponding *N*-alkylated chloro derivative **10**. Thymine was *N*-alkylated with compound **10** using K_2CO_3 to obtain *N*-Boc-aminoethyl-(α,α-dimethyl)-glycyl-thymine ethyl ester **11** which was characterized by ^{1}H NMR, ^{13}C NMR and Mass spectroscopy. The formation of compound **11** was supported by observance of signals for ($C\underline{H_3}$)$_2$C- at 1.48 δ in ^{1}H NMR in addition to N$\underline{H}$- of thymine at 6.94δ and ($\underline{C}H_3$)$_2$C- at 23.98 δ in ^{13}C NMR. In ^{13}C NMR for compound **11**, chemical shift of ($\underline{C}$H$_3$)$_2$C- shifted to upfield by 4.15 δ in comparison to compound **7**. The observed mass for compound **11** is 463 (M+Na) was in agreement with calculated mass 440.

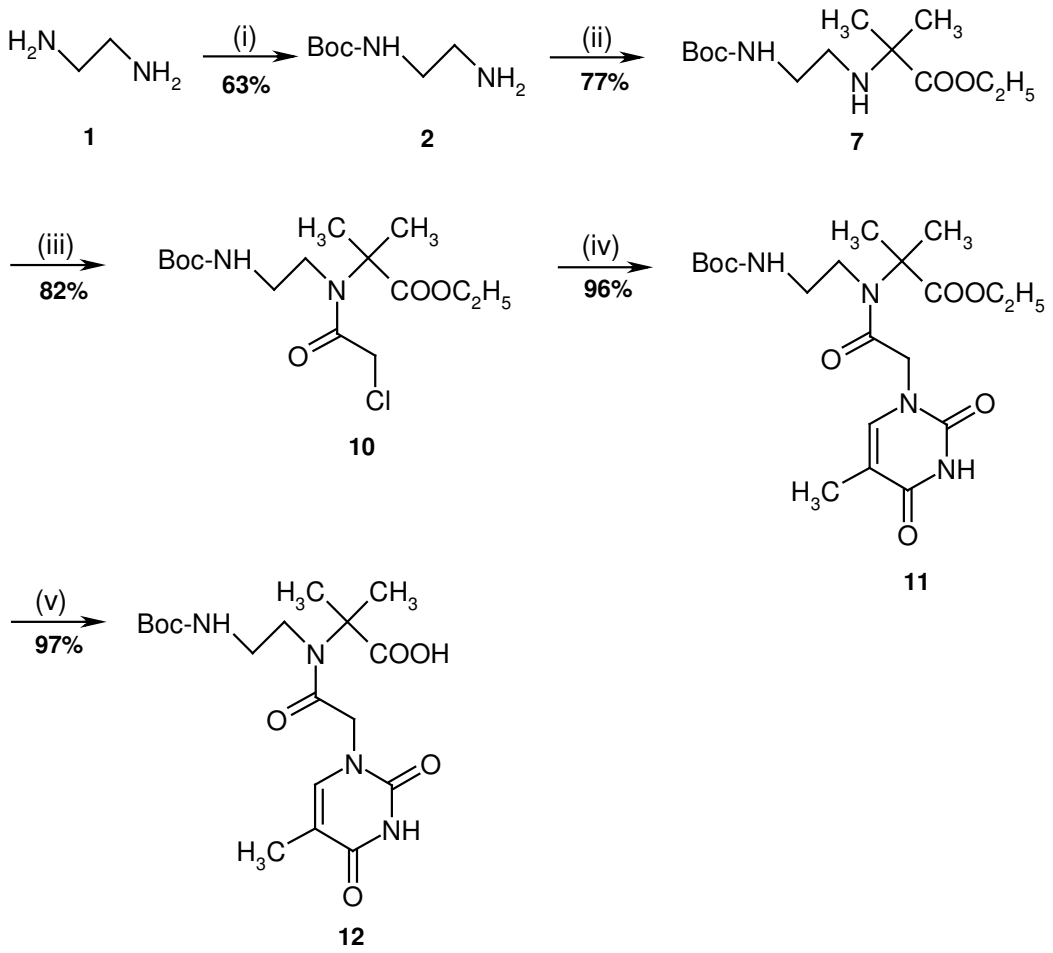

Scheme 3. Reagents and conditions: (i) Boc-anhydride, dioxane: water (1:1), rt, 12hrs (ii) ethyl-2-bromoisobutyrate, dry acetonitrile, K_2CO_3, 50^0C, 6hrs (iii) $ClCH_2COCl$, Na_2CO_3, dioxane: water (1:1) (iv) thymine, K_2CO_3, dry DMF (v) NaOH, water, methanol.

2.3.2. Synthesis of Aminopropyl-(α,α-dimethyl)-glycyl-(*apaib*)–PNA Monomer

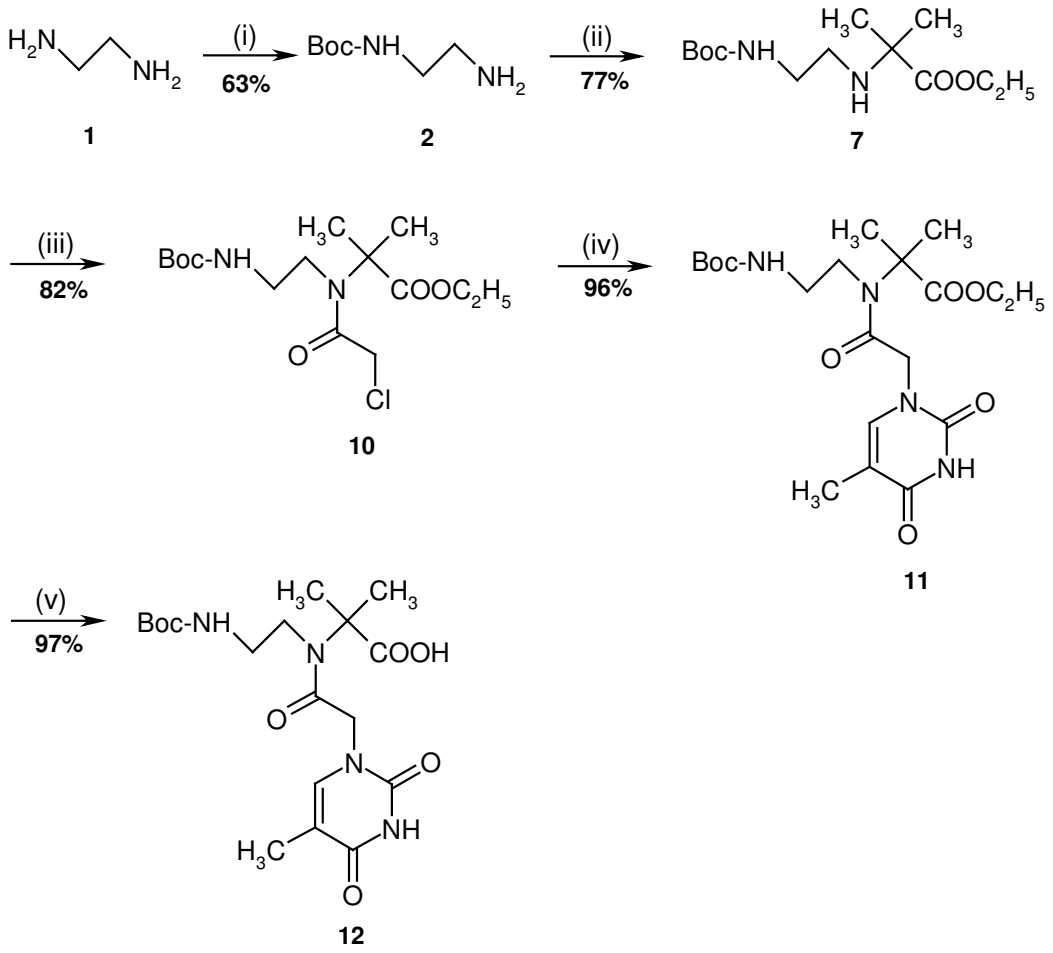

Scheme 3. Reagents and conditions: (i) Boc-anhydride, dioxane: water (1:1), rt, 12hrs (ii) ethyl-2-bromoisobutyrate, dry acetonitrile, K_2CO_3, 50^0C, 6hrs (iii) $ClCH_2COCl$, Na_2CO_3, dioxane: water (1:1) (iv) thymine, K_2CO_3, dry DMF (v) NaOH, water, methanol.

Scheme 4 describes the synthesis of *apaib* PNA monomer **18** having an additional methylene group in backbone starting from 1,3- diaminopropane **13,** which was treated with boc-anhydride to give the *N*-mono protected derivative **14**, as a major product using a large excess of 1,3-diaminopropane over the boc-anhydride. The *N1,N3*-di-Boc derivative obtained in very small amounts (< 5%) being insoluble in water, was removed by filtration. The *N1*-Boc-1,3-diaminopropane **14** was *N*-alkylated using ethyl-2-bromo-isobutyrate and potassium carbonate in dry acetonitrile. The formation of compound **15**

was supported by observance of signals for ($\underline{CH_3}$)$_2$C- at 1.26 δ in ^{1}H NMR and at 25.27 δ in ^{13}C NMR. The calculated mass for compound **15** is 288 while the observed mass is 289.14 (M+1). The *N*-Boc-aminopropyl-(α,α-dimethyl)-glycine ethyl ester **15** was treated with chloroacetyl chloride to yield the *N*-alkylated chloro derivative **16**. Thymine was reacted with compound **16** and K_2CO_3 to obtain the *N*-Boc-aminopropyl-(α,α-dimethyl)-glycyl-thymine ethyl ester **17** in high yield which was characterized by ^{1}H NMR, ^{13}C NMR and mass spectroscopy. The formation of compound **17** was supported by observance of signals for ($C\underline{H_3}$)$_2$C- at 1.47 δ in ^{1}H NMR along with N$\underline{H}$- of thymine signal at 6.98δ and in ^{13}C NMR observance of signals for ($\underline{C}H_3$)$_2$C- at 23.94 δ. The ^{13}C chemical shift of ($\underline{C}H_3$)$_2$C- shifted to upfield by 1.33 δ in comparison to compound **15**. The observed mass for compound **17** is 477.18 (M+Na) in agreement with calculated mass 454. The crystal structure of the intermediate **15** was further confirmed by X-ray crystallography. The X-ray crystal structure for Compound **15** is as shown Figure 5.

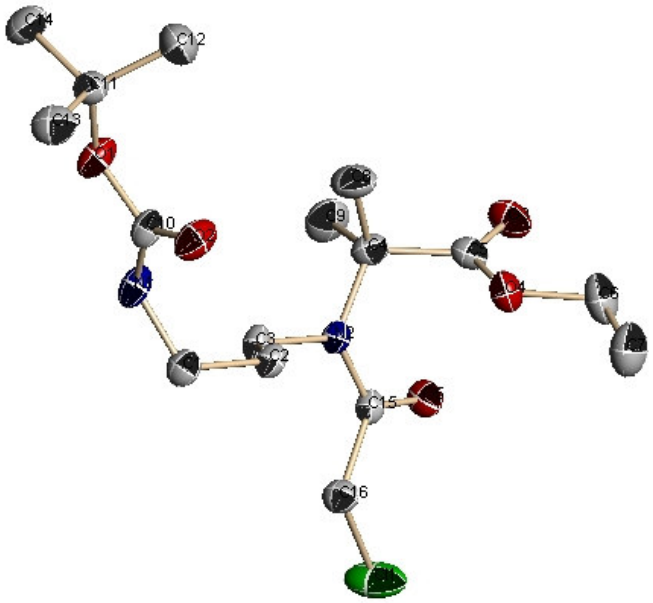

Figure **5.** X-ray crystal structure for Compound **15**

2.3.3. Hydrolysis of Esters

Solid phase peptide synthesis of target PNA analogues *aeaib*PNA and *apaib*PNA requires *N*-protected free carboxylic acids. The ethyl ester groups of the *aeaib*PNA and *apaib*PNA monomers were subjected to saponification by sodium hydroxide in water-methanol mixture to yield the corresponding carboxylic acid.

2.3.3a. Hydrolysis of Aminoethyl-(α,α-dimethyl)-glycyl-(*aeaib*)–PNA-Thymine ester and Aminopropyl-(α,α-dimethyl)-glycyl-(*apaib*)–PNA-Thymine ester Monomers

The hydrolysis of the ethyl esters **11** and **17** was achieved in a single step, upon treatment with 1M NaOH in methanol: water. As followed by TLC, the ester was found to be hydrolyzed to acid within 5 hrs. Neutralization of the excess alkali with Dowex 50 H^+ and work-up gave aminoethyl-(α,α-dimethyl)-glycyl-(*aeaib*)-PNA-thymine acid **12** (Figure 6a) and aminopropyl-(α,α-dimethyl)-glycyl-(*apaib*)-PNA-thymine acid **18** (Figure 6b) in quantitative yields (> 95%).

2.3.4. Synthesis of Aminoethylglycyl (*aeg*)-PNA Monomers

The synthesis of unmodified *aeg*PNA monomers was necessary for synthesis of control *aeg*PNA and was carried out according to the literature procedures[25] as shown in

Scheme 5. The synthesis was carried out starting from the easily available 1,2-diaminoethane **1**. This was treated with boc-azide to give the mono-*N*-protected derivative, obtained by using a large excess of 1,2-diaminoethane over the boc-azide in

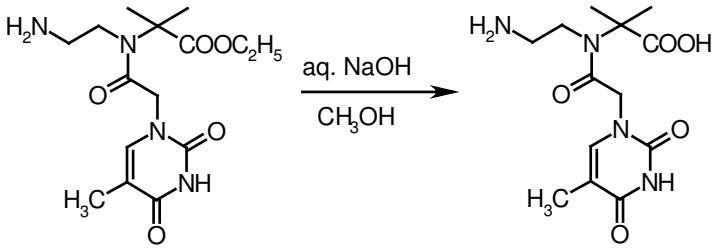

11 **12**

Figure 6a. Hydrolysis of Aminoethyl-(α,α-dimethyl)-glycyl-(*aeaib*)–PNA-T-ester **11** to acid monomer **12**.

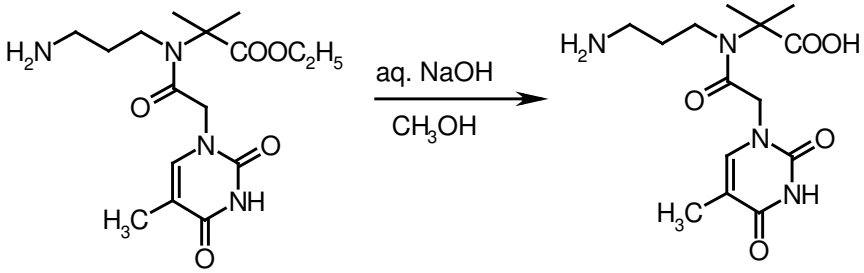

17 **18**

Figure 6b. Hydrolysis of Aminopropyl-(α,α-dimethyl)-glycyl-(*apaib*)–PNA-T-ester **17** to acid monomer **18**.

high dilution. The *N1*,*N2*-di-boc derivative obtained in very small amounts (< 5%) being insoluble in water, was removed by filtration. The *N1*-Boc-1,2-diaminoethane **2** was *N*-alkylated using ethyl-bromoacetate and KF-Celite[26] in dry acetonitrile. The use of KF-Celite was found to be advantageous over K_2CO_3 both, in terms of the yield of the product, as well as the ease of work-up. The aminoethylglycine ethyl ester **19** was further treated with chloroacetyl chloride to yield the corresponding chloro-derivative **20** in good

yield. The use of triethylamine as the base in this reaction gave poor yields. However, when Na_2CO_3 was used as the base in aqueous dioxane, the desired product was obtained in good yield. The ethyl *N*-Boc-(aminoethyl)-*N*-(chloroacetyl)-glycinate **20** was used as a common intermediate in the preparation of all the *aeg*PNA monomers with different nucleobases.

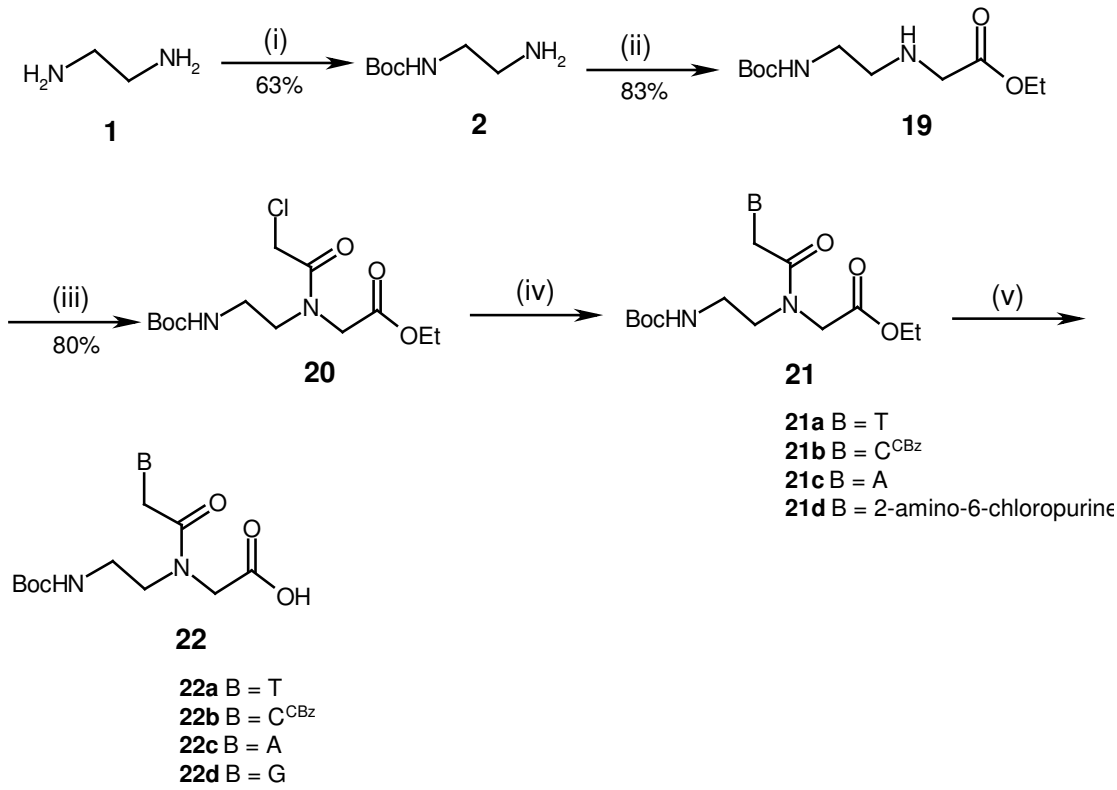

Scheme 5. Reagents and conditions: (i) Boc-azide, dioxane: water (1:1), rt, 12hrs (ii) ethyl-2-bromoacetate, dry acetonitrile, K_2CO_3, 50^0C, 6hrs (iii) $ClCH_2COCl$, Na_2CO_3, dioxane: water (1:1) (iv) T/C^{cbz}/ A/ G (v) NaOH, water, methanol.

Thymine was reacted with ethyl-*N*-Boc-(aminoethyl)-*N*-(chloroacetyl)-glycinate using K_2CO_3 as a base to obtain the *N*-Boc-(aminoethylglycyl)-thymine ethyl ester **21a** in high yield. In the case of cytosine, the *N4*-amino group was protected as its benzyloxycarbonyl derivative, and used for alkylation employing sodium hydride (NaH) as the base to provide the *N1*-substituted product **21b**. The *N1*-alkylation of thymine and cytosine with ethyl-*N*-Boc-(aminoethyl)-*N*-(chloroacetyl)-glycinate is regio-specific. Although adenine is known to undergo both *N7*- and *N9*-substitution, *N7*-alkylation was not observed when NaH was used as the base. It reacted with adenine forming sodium adenylide, which then reacts with ethyl-*N*-Boc-(aminoethyl)-*N*-(chloroacetyl)-glycinate

to obtain *N*-Boc-(aminoethylglycyl)-adenine ethyl ester **21c** in moderate yield. The alkylation of 2-amino-6-chloropurine with ethyl-*N*-Boc-(aminoethyl)-*N*-(chloroacetyl)-glycinate was facile with K_2CO_3 as the base and yielded the corresponding *N*-Boc-(aminoethylglycyl)-(2-amino-6-chloropurine)-ethyl ester **21d** in excellent yield. All the compounds exhibited ^1H and ^{13}C NMR spectra consistent with the reported data.[25] The ethyl esters were hydrolyzed using aqueous NaOH to give the corresponding acids, **22a-22d** which were used for solid phase synthesis. There is no need for protection of the exocyclic amino groups of adenine and guanines, as these are known to be unreactive under the conditions used for peptide coupling.

2.3.5. SOLID PHASE PEPTIDE SYNTHESIS

2.3.5a. General Protocols for PNA Synthesis.

The synthesis of PNAs was done using solid phase peptide synthesis protocols by incorporating the modified monomers *aeaib* **12** and *apaib* **18** instead of *aeg* **21a** at desired sites in the oligomer sequence. PNA synthesis was done from the *C*-terminus to the *N*-terminus using monomeric units with protected amino and carboxylic acid function. The most commonly used *N*-protecting groups for solid phase peptide synthesis are the *t*-butyloxycarbonyl (*t*-Boc) and the 9-fluorenylmethoxycarbonyl (Fmoc) groups. The fmoc protection strategy has a drawback in PNA synthesis since under the basic deprotection conditions using piperidine, the terminal free amine generated attacks the tertiary amide leading to acyl migration.[27] Hence, the Boc-protection strategy was preferred for the present work.

MBHA resin (4-methyl-benzhydrylamine resin) was used as the solid support on which the PNA oligomers were built and the monomer-acids were coupled by *in situ* activation with HBTU/HOBt.[28] This resin yields the peptides with *C*-terminal amides upon cleavage at the end of the synthesis. During the synthesis of all oligomers, the orthogonally protected (Boc/Cl-Cbz) L-Lysine was used as the *C*-terminal spacer amino acid and was first linked to the resin through an amide bond. The amine content on the resin was determined by the picrate assay and found to be 0.85 mmol/gm. Since high loading causes incomplete reactions, the loading was lowered to about 0.25 mmol/gm by partial acetylation of amino groups using calculated amount of acetic anhydride. The PNA oligomers were synthesized using repetitive cycles, with each cycle comprising the following steps:

(i) *N*-Deprotection of Boc-group using 50% TFA in CH_2Cl_2.

(ii) Neutralization of the TFA salt formed with di-isopropyl-ethylamine (DIPEA) (5% DIPEA in CH_2Cl_2) to liberate the free amine.

(iii) Coupling of the free amine with the carboxylic acid group in the incoming monomer. The coupling reaction was carried out using 3-4 equivalents of excess monomers in presence of *O*-(Benzotriazol-1-yl)-*N*,*N*,*N*′,*N*′-tetramethyl-uronium hexafluorophosphate (HBTU) and 1-hydroxybenzotriazole (HOBt), for suppressing racemization, in DMF and/or NMP as the solvent. The deprotection of the *N*-Boc protecting group and the coupling reactions were monitored by Kaiser's test[29] in which the intensity of blue color is proportional to the amount of the free amino groups present on the resin bead.

(iv) Capping of the unreacted amino groups using acetic anhydride in pyridine: CH_2Cl_2. A typical synthesis cycle is depicted in Scheme 6.

The modified aminoethyl-(α,α-dimethyl)-glycyl thymine monomer **12** and aminopropyl-(α,α-dimethyl)-glycyl thymine monomer **18** were incorporated into PNA sequences at desired sites as shown in Table 1.

Various homothymine PNA oligomers incorporating modified monomers were synthesized in order to study their triplex formation and stability with DNA/RNA (Table 1, Entry 1-11).

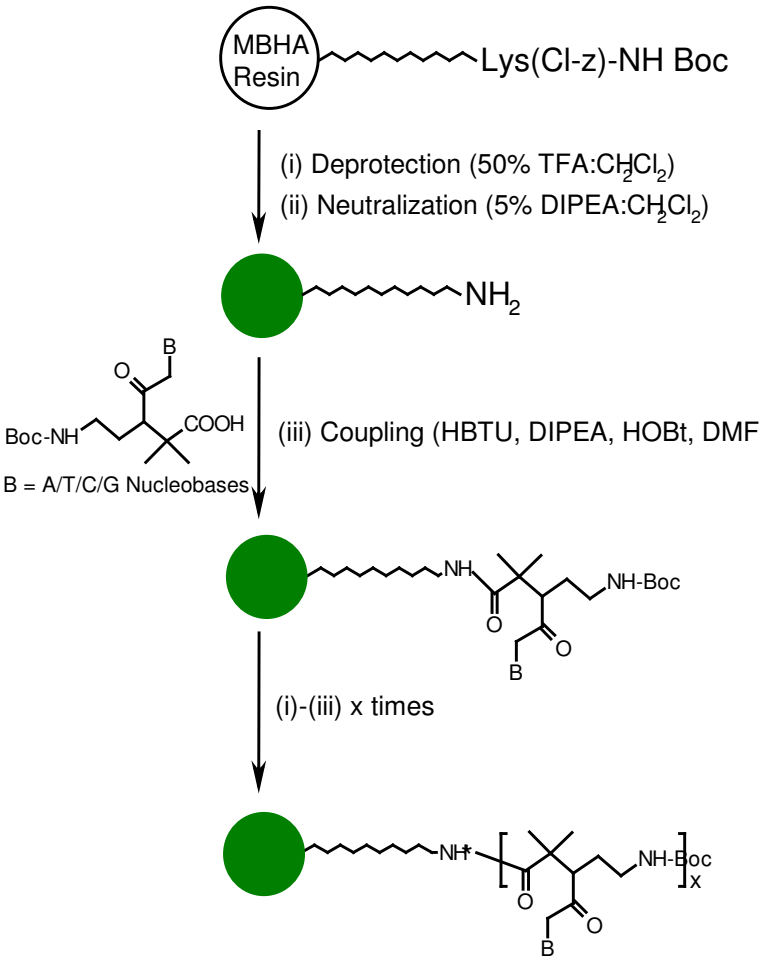

Scheme 6. Schematic representation of solid phase peptide synthesis using the Boc-protection strategy.

In order to study the potential for duplex formation and discrimination in DNA/RNA complementary sequences by the *aeaib*/*apaib* containing PNAs, it was necessary to synthesize the mixed base sequences incorporating both purines and pyrimidines. Such sequences were synthesized by incorporating *aeg*PNA (A/T/C/G) monomers and *aeaib*PNA (**t**) or *apaib*PNA (***t***) monomers at specific positions of 10-mer PNA sequences (Table 1, Entry 12-14). The coupling time was 24 hrs for first four monomeric units, after which the coupling efficiency get reduced and the time was increased to 48-72 hrs for coupling the modified monomers.

Table 1. PNA sequences synthesized in the present study*

Entry	Sequence Code	PNA sequences
		Homothymine Sequences
1.	*aeg*PNA **1**	H – T T T T T T T T – $LysNH_2$
2.	*aeaib*PNA **2**	H – T T T T T T T **t** – $LysNH_2$
3.	*aeaib*PNA **3**	H – T T T T T **t** T **t** – $LysNH_2$
4.	*aeaib*PNA **4**	H – T T T **t** T **t** T **t** – $LysNH_2$
5.	*aeaib*PNA **5**	H – T **t** T **t** T **t** T **t** – $LysNH_2$
6.	*aeaib*PNA **6**	H – **t t t t t t t t** – $LysNH_2$
7.	*apaib*PNA **7**	H – T T T T T T T ***t*** – $LysNH_2$
8.	*apaib*PNA **8**	H – T T T T T ***t*** T ***t*** – $LysNH_2$
9.	*apaib*PNA **9**	H – T T T ***t*** T ***t*** T ***t*** – $LysNH_2$
10.	*apaib*PNA **10**	H – T ***t*** T ***t*** T ***t*** T ***t*** – $LysNH_2$
11.	*apaib*PNA **11**	H – ***t t t t t t t t*** – $LysNH_2$
		Mixed Sequences
12.	*aeg*PNA **12**	H – G T A G A T C A C T – $LysNH_2$
13.	*aeaib*PNA **13**	H – G **t** A G A **t** C A C **t** – $LysNH_2$
14.	*apaib*PNA **14**	H – G ***t*** A G A ***t*** C A C ***t*** – $LysNH_2$

*A/T/C/G, **t** and ***t*** indicating *aeg*, *aeaib* and *apaib*-PNA monomers respectively.

2.3.6. Cleavage of the PNA oligomers from the solid support

The oligomers were cleaved from the solid support, using trifluoromethane sulphonic acid (TFMSA) in presence of trifluoroacetic acid (TFA), which yielded PNA oligomers having L-lysine amide at *C*-terminus. Using a cleavage time of 2.5 hrs at room temperature, the side chain protecting groups of lysine were also removed during this process. After cleavage reaction, the PNA oligomers obtained in solution were precipitated from methanol by addition of dry diethyl ether.

2.3.7. Purification of the PNA oligomers

All the cleaved oligomers were subjected to initial gel filtration over sephadex NAP column to remove low molecular weight impurities. The purity of the so obtained PNA oligomers was checked by analytical RP-HPLC (C18 column, Acetonitrile:water system), and was found to be more than 70-80 % purity. These were subsequently purified by reverse phase HPLC on a semi-preparative C18 column to give oligomers in 95-99 % purity as ascertained by analytical RP-HPLC. The HPLC profiles for all PNA sequences are shown in Appendix I (Entry 26, 27, 30, 31 & 34). The integrity of PNA oligomers was confirmed by MALDI-TOF mass spectrometric analysis. For control and modified PNA sequences, MALDI-TOF mass spectra are shown in Appendix I (Entry 28, 29, 32, 33 & 35). Table 2 shows the retention time with calculated and observed mass of synthesized homothymine and mixed PNA sequences.

The observed mass for *aeg*PNA **1** is 2275 (M+1) in agreement with calculated mass 2274. In case of, *aeg-aeaib*PNA **2-5** and *aeaib*PNA **6**, an additional mass of 28 was

seen for each modified *aeaib*-PNA unit, whereas, in *aeg-apaib*PNA **7**-**10** and *apaib*PNA **11**, an additional mass of 42 was present for each modified *apaib*-PNA unit. This increase in the mass observed is in agreement with the calculated mass for all modified homopyrimidine PNAs **2**-**11**.

Table 2. HPLC and MALDI-TOF mass spectral analysis of modified PNAs

Entry	PNA strand	Retention Time (mins) HPLC	$M_{calculated}$	$M_{observed}$
1.	*aeg*PNA **1**	07.337	2274	2275.47
2.	*aeaib*PNA **2**	08.019	2302	2300.86
3.	*aeaib*PNA **3**	08.319	2330	2334.60
4.	*aeaib*PNA **4**	08.955	2358	2364.68
5.	*aeaib*PNA **5**	09.293	2386	2389.82
6.	*aeaib*PNA **6**	10.315	2498	2505
7.	*apaib*PNA **7**	8.632	2316	2316.78
8.	*apaib*PNA **8**	8.787	2358	2363.74
9.	*apaib*PNA **9**	9.484	2400	2405.58
10.	*apaib*PNA **10**	10.167	2442	2452.21
11.	*apaib*PNA **11**	10.906	2610	2613.21
12.	*aeg*PNA **12**	9.890	2852	2860.93
13.	*aeaib*PNA **13**	13.368	2936	2941.47
14.	*apaib*PNA **14**	14.472	2978	2978.59

The observed mass for mixed sequences PNA **12,** PNA **13** and is 2861 (M+9), 2942 (M+6) and 2979 (M+1), in agreement with calculated mass 2852, 2936 and 2978 respectively.

2.3.8. Synthesis of Complementary Oligonucleotides (DNA & RNA)

The DNA oligonucleotides **1-4** (Table 3) complementary to PNA oligomers (**1**-**14**) were synthesized on Applied Biosystems ABI 3900 high throughput DNA synthesizer using standard β-cyanoethyl phosphoramidite chemistry. The oligomers were synthesized in the 3' to 5' direction on polystyrene solid support, followed by ammonia treatment. The oligonucleotides were desalted by gel filtration and the purity ascertained

by RP HPLC on C18 column was more than 98% and so were used without further purification for biophysical studies with PNAs. The RNA oligonucleotides **1-3** (Table 3) complementary to PNA oligomers (**1**-**14**) were obtained commercially from Genomechanix, Gainesville, FL, along with the HPLC purity and mass spectral data.

Table 3. DNA/RNA Oligonucleotides used in the present work

Entry	Sequence Code	Sequences	Type (Corresponding PNA)
		DNA sequences 5' to 3'	
1.	DNA **1**	G C A A A A A A A A C G	Match (**1**-**11**)
2.	DNA **2**	G C A A A A A C A A C G	Mismatch (**1**-**11**)
3.	DNA **3**	A G T G A T C T A C	Antiparallel (**12**-**14**)
4.	DNA **4**	C A T C T A G T G A	Parallel (**12**-**14**)
		RNA sequences 5' to 3'	
5.	RNA **1**	A G U G A U C U A C	Antiparallel (**12**-**14**)
6.	RNA **2**	C A U C U A G U G A	Parallel (**12**-**14**)
7.	RNA **3**	Poly rA	Match (**1**-**11**)

2.3.9. Biophysical Studies of *aeaib*- and *apaib*-PNA:DNA/RNA Complexes

The studies on binding affinity, specificity and discrimination of *aeaib*/*apaib*PNA:DNA/RNA towards complementary DNA and RNA were done by determination of T_m, the melting temperature of duplexes and triplexes. The stoichiometry of the *aeaib*PNA:DNA and *apaib*PNA:DNA complexes was determined using Job's method. The CD spectra of corresponding PNA complexes with complementary DNA were studied to understand the conformational changes upon modification. Isothermal Titration Calorimetry of the complexation of the *aeaib*/*apaib*PNAs to complementary DNA, gave information on the energetics of the binding processes.

2.3.10. Biophysical Spectroscopic techniques for studying PNA:DNA Interactions

2.3.10a. UV-Studies

Monitoring the UV absorption at 260nm as a function of temperature has been extensively used to study the thermal stability of various nucleic acid complexes including PNA-DNA/RNA hybrids.[30] Increasing the temperature perturbs PNA/DNA hybrids, inducing a structural melting of the duplexes/triplexes by disrupting the hydrogen bonds between the base pairs and leading to a loss of secondary/tertiary structures. This is evidenced by an increase in the UV absorption at 260nm, termed as 'hyperchromicity'. The magnitude of hyperchromicity is a measure of the extent of the secondary structure present in nucleic acids. The process is co-operative and the plot of the absorbance at 260nm Vs temperature is sigmoidal (Figure 7a). This corresponds to a two-state "all or none" model for nucleic acid melting, i.e., the nucleic acids exist in only two states, either as duplexes or as single strands and at varying temperatures, the relative proportions change. A non-sigmoidal (e.g., linear) transition with low hyperchromicity is a consequence of non-duplexation (non-complementation). In many cases, the transitions are broad and the exact T_ms are obtained from the peak in the first derivative plots. This technique has provided valuable information regarding complementary interactions in nucleic acid hybrids involving DNA, RNA and PNA.

The stoichiometry of binding in PNA:nucleic acid complexes can be determined from either UV-mixing or UV-titration experiments. The UV-mixing experiments are carried out by mixing the appropriate oligomers in different mole ratios, keeping the total concentration constant. The UV-absorbance of these samples is plotted as a function of

the mole fraction of one of the components, in what is termed as a Job's plot[31] (Figure 7b). The absorbance steadily decreases until all the strands present are involved in complex formation as a result of the hypochromic effect, and then rises afterwards when one strand is present in excess. The stoichiometry of the complexation is derived from the

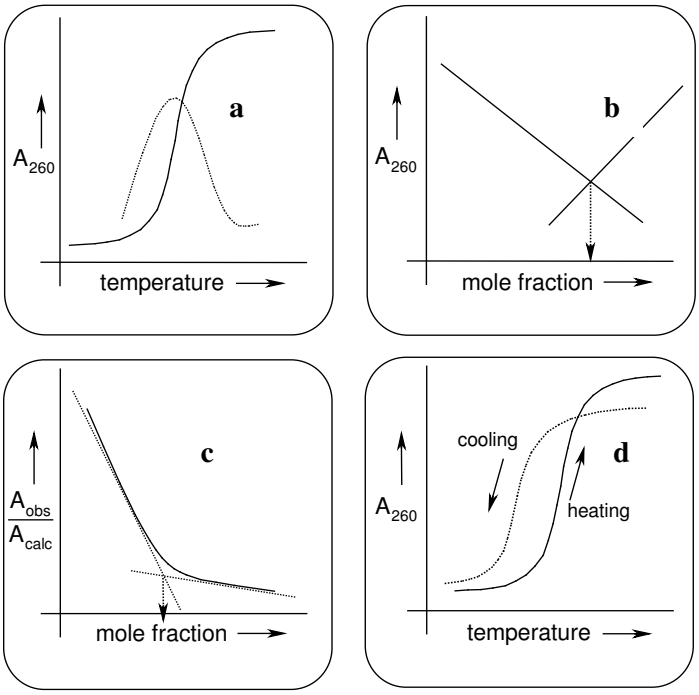

Figure 7. Schematic representation of **a**. UV-melting (thermal stability), **b**. UV-mixing, **c**. UV-titration (stoichiometry) and **d**. Hysteresis (rate of hybridization).

minimum in such a plot.

The stoichiometry of complexation can also be determined by UV-titration (Figure 7c). In this method, one of the strands involved in complexation is sequentially added in aliquots to a fixed amount of the complementary component and the UV-absorbance is recorded at each addition. Upon successive addition of the complementary strand, complex formation results in hypochromicity, which leads to a progressive

decrease in the ratio of the observed to the calculated absorbance. After the first strand present in the buffer is completely bound as duplex, the absorbance reaches a plateau and the stoichiometric point at which the plateau is reached indicates the stoichiometry of complexation.

PNA/DNA strands bearing charged groups could be tested for hysteresis by thermal dissociation Vs re-association plots. The experiment consists of recording the UV absorbance by first heating the duplexes/triplexes (UV-melting) followed by cooling the sample while recording the absorbance (re-association, cooling curve). In DNA:DNA complexes, the cooling curve does not reversibly follow the melting curve and exhibits a hysteresis (Figure 7d). This is due to the fact that the re-association of duplexes or triplexes is much slower than melting due to the interstrand repulsion on account of the negative phosphate groups. When one of the strands bears cationic charges, the net repulsion between the two strands is reduced and the re-association rates are positively enhanced leading to a lower hysteresis in the heating-cooling plots.

The fidelity of base pairing in the PNA:DNA complexes can be examined by challenging the PNA oligomer with a DNA strand bearing a mismatch at a desired site, preferably opposite the site of modification. The base mismatch leads to incorrect hydrogen bonding between the bases and causes a drop in the measured melting temperature. A modification of the PNA structure is considered good if it gives a significantly lower T_m with DNA sequences containing mismatches as compared to that with unmodified PNA. It is to be pointed out that in all biophysical experiments described herein, the modified PNAs are always evaluated against the unmodified control PNA.

Homopyrimidine thymine PNA sequences bind to the complementary homopurine DNA sequence forming PNA_2:DNA triplexes in which it is difficult to distinguish the PNA strand that binds to the central DNA strand by WC hydrogen bonding from that which binds by HG hydrogen bonding. Mixed base sequences form duplexes of *antiparallel* or *parallel* orientations that can be selected by proper design of the complementary DNA sequences. By convention (Figure 8), *antiparallel* PNA:DNA

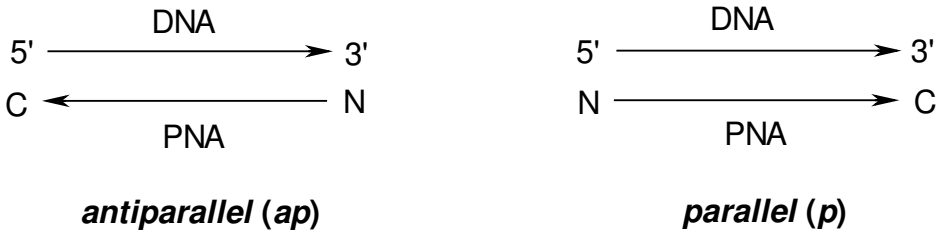

Figure 8. Schematic representation of the *antiparallel* and *parallel* modes of complexation of PNA with complementary DNA.

complexes are defined as those in which the 'N' terminal of the PNA faces the 3'-end of the DNA with the 'C' terminal facing the 5'-end and parallel PNA:DNA complexes are those in which the 'C' terminal of PNA faces the 3'-end of DNA with the 'N' terminal towards the 5'-end of the DNA.[32]

2.3.10b. Circular Dichroism

Circular Dichroism (CD) is a well-established tool used to study the conformational aspects of nucleic acids.[33,34] A CD curve is a plot of the molecular ellipticity [θ] versus the wavelength λ. The CD effect results from the fact that the right circularly polarized ray is absorbed differently from the left circularly polarized beam of light.

The molecular ellipticity is defined as-

$$[\theta] = 3{,}300.\Delta\varepsilon, \qquad \Delta\varepsilon = \varepsilon_L - \varepsilon_R$$

where $\Delta\varepsilon$ is the differential dichroic absorption and ε_L and ε_R are the molar extinction coefficients for the left and right rays.

Upon comparison with reference samples of known conformational state, CD spectra can provide reliable and useful data concerning the conformational states of the system under study. However, CD does not give detailed molecular structural data as obtained from X-ray crystallography or NMR, but it can be used as a complementary tool

to UV spectroscopy to evaluate the overall base-stacking patterns. The differences in secondary structure and handedness of helices can be differentiated conformationally through changes in CD profiles.

CD of nucleic acids arises predominantly as an effect of coupling between the transition moments of adjacent nucleobases due to continuous stacking. The PNA backbone is inherently achiral. However, PNA, a polyamide, can be expected to form helices *via* intramolecular hydrogen bonding leading to a racemic mixture of right- and left-handed helices and no net CD is observed.[35] Upon complexation with DNA/RNA, which are chiral molecules, PNA:DNA/RNA duplexes/triplexes exhibit strong CD signals.

Thus, the complex formed as a consequence of the binding of achiral PNA and chiral DNA leads to the formation of a chiral complex. CD thus, assumes importance in the characterization of such complexes.

2.3.11c. Gel Electrophoresis

Electrophoretic gel shift assay is used to establish the binding of different PNAs to the complementary DNA. The neutral PNAs do not migrate in gel electrophoresis. However, upon complexation with DNA, the resulting PNA:DNA complexes are overall negative and hence migrate in electrophoretic gel. The modified PNAs and the control PNA are individually treated with complementary oligonucleotides and the complexation is monitored by non-denaturing gel electrophoresis at 10°C. The spots can be visualized on a TLC with fluorescent background. The formation of PNA_2:DNA triplexes is accompanied by the disappearance of the single strand DNA and appearance of a slower

migrating band due of the PNA_2:DNA complexes. The migration of modified PNA_2:DNA complexes can be compared with that of the unmodified PNA:DNA complex. The PNA_2:DNA triplexes show more retardation as compared to PNA:DNA duplexes. This is attributed to the increased molecular weight upon formation of triplex, and the overall less net negative charge.

2.3.10d. Differential scanning calorimetry

Differential scanning calorimetry (DSC) is used to study thermally induced order-disorder transitions in nucleic acids. A DSC instrument measures, as a function of temperature (T), the excess heat capacity (C^{ex}_p) of a nucleic acid solution relative to the same amount of buffer solution. A single DSC profile provides a wealth of thermodynamic information, much of which cannot be obtained by any other techniques. Specifically, from a single curve of C^{ex}_p versus T, one can derive the following information: the transition enthalpy (ΔH), entropy (ΔS), free energy (ΔG), and heat capacity (ΔC_p); the state of the transition (two-state versus multistate); and the average size of the molecule that melts as a single thermodynamic entity (i.e., the size of the cooperative unit). This technique has been employed to generate a substantial and rapidly expanding database of DNA:PNA interactions. It is apparent that thermodynamic as well as structural information is required to develop a clear understanding of the complex relationships between structure, energetics and biological function.

2.3.10e. Isothermal titration calorimetry

Isothermal titration calorimetry (ITC) is used to study the hybridization of nucleic acid molecules at constant temperature. In a typical ITC experiment, small aliquots of a titrant DNA solution are added to an analyte PNA solution at 4^0C (with the analyte PNA being complementary to the titrant DNA) and the released heat is monitored. Judicious selection of nucleic acid concentrations and buffer conditions results in a titration curve that can be analyzed to yield the stoichiometry of the association reaction (n), the enthalpy of association (ΔH), the equilibrium association constant (K), and thus the free energy of association (ΔG). Once ΔH and ΔG are known, the entropy of association (ΔS) can also be obtained. Thus, a single ITC experiment yields a wealth of thermodynamic information about the association reaction. Repetition of the ITC experiment at a number of different temperatures yields the ΔC_p for the association reaction from the temperature dependence of ΔH.

2.4. RESULTS

In the present Chapter, studies on PNA-DNA interactions as investigated by UV, CD and Isothermal Titration Calorimetry techniques are presented with discussion on the effect of introducing *gem*-dimethyl functionality in the *aeg*- and *apg*-PNA of glycine unit on duplex/triplex formation.

2.4.1. Homopyrimidine PNA Sequences: UV Studies

2.4.1a. *aeaib*PNA:DNA and *apaib*PNA:DNA binding stoichiometry

The Job's plots were generated from individual stoichiometric mixtures of *aeaib*PNA **2** and *apaib*PNA **7** with DNA **1** having varying relative molar ratios of (PNA **2/7**:DNA **1**) 0:100, 10:90, 20:80, 30:70, 40:60, 50:50, 60:40, 70:30, 80:20, 10:90, 100:0.

The UV absorbances recorded at wavelength (λ_{max} 260 nm) for different mixtures were plotted against mole fractions of PNA **2** and **7**. Figure 9 and 10 show the change in absorbance at λ_{max} observed for the mixtures of different molar fractions of *aeaib*-PNA **2** and *apaib* PNA **7** respectively with DNA **1**. There is a shift in the λ_{max} to higher value when

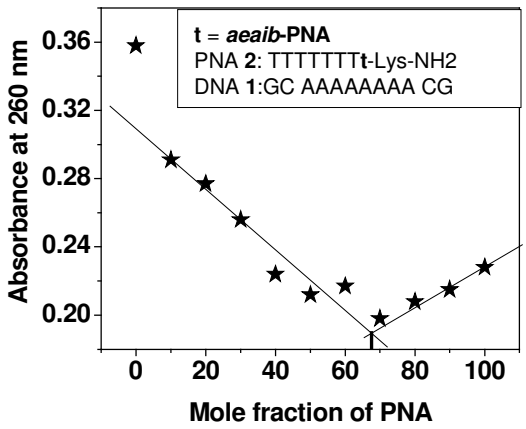

Figure 9. UV-titration of DNA **1** with PNA **2**

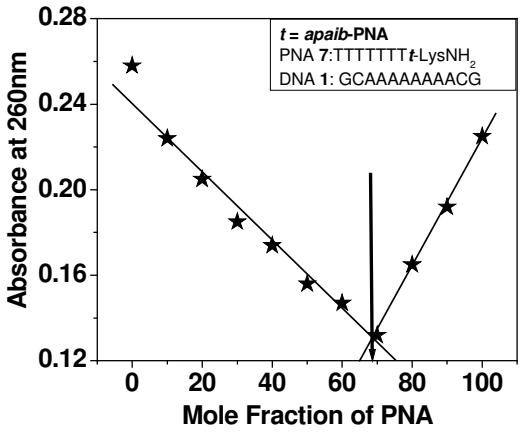

Figure 10. UV-titration of DNA **1** with PNA **7**

concentration of PNA **2** and **7** with further addition, increased absorbance. A gradual decrease in absorbance with addition of PNA **2** or **7** was observed till the PNA mole fraction reached to about 65%. The UV absorbance-molar ratio plot showed a minimum around 2:1 stoichiometry in both *aeaib* and *apaib* PNAs suggesting the formation of PNA_2:DNA triplexes for both complexes.

2.4.2. CD spectroscopic studies of *aeaib*- and *apaib*-PNA_2:DNA Triplexes

PNA being non-chiral, does not show any CD spectrum. However, PNA:DNA complexes exhibit characteristic CD signatures due to chirality induced by DNA complement. It is known that formation of PNA triplexes is accompanied by appearance of positive CD bands at 258 nm and 285 nm that are not present in CD of single stranded DNA.

The *aeaib*-PNA monomer was sequentially incorporated one at a time into triplex forming homopyrimidine *aeg*PNA-T_8 sequences starting from *N*-terminus at alternate sites to obtain PNA **2**- **6** to study any patterns in the structural pre-organization of PNA due to preferential base stacking. Although the CD spectra of the *aeaib*PNA-T_8 single strands differed depending on the number of *aeaib*PNA units (PNA **2**:DNA **1**), upon complex formation with the complementary DNA oligomer, the CD was similar to that of the control *aeg*PNA_2:DNA triplex (Figure 11).

The CD of DNA complexes of *apaib* PNAs **7-11** were similar to that of the *aeg*-PNA **1**:DNA **1** complexes (Figure 12). The PNA_2:DNA triplexes exhibited two maxima at 265nm and 280nm with a minimum at 246nm and crossover points between ~250-~260nm. The double hump profile is characteristic of poly T:poly A:poly T triplexes as shown in Figure 12 (PNA **7**:DNA **1**).

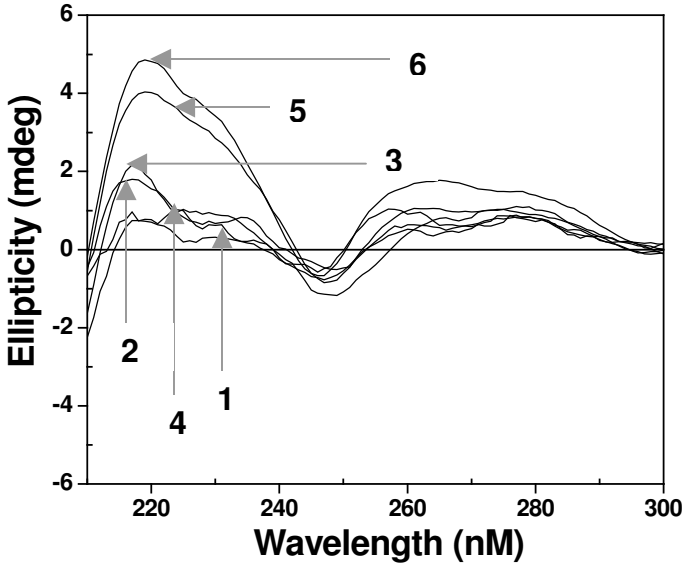

Figure 11. CD profiles of *aeaib*-$(PNA)_2$:DNA **1** triplexes
The numbers with arrow correspond to PNA sequences

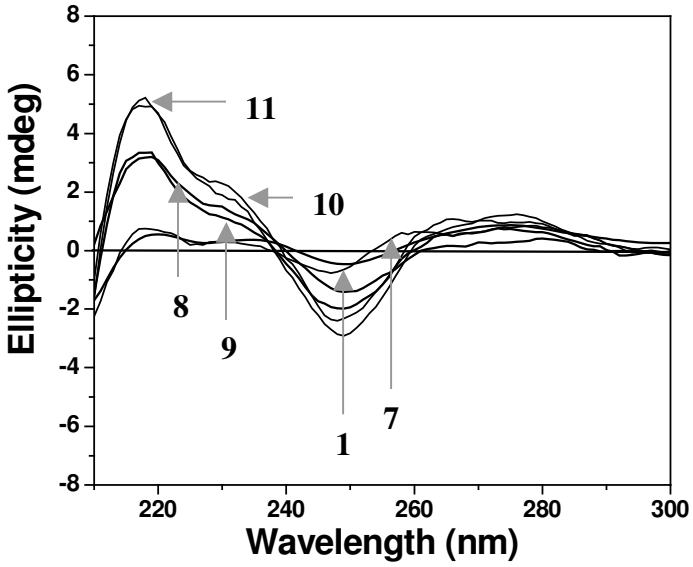

Figure 12. CD profiles of *apaib*-$(PNA)_2$:DNA **1** triplexes
The numbers with arrow correspond to PNA sequences

2.4.3.

PNA_2:DNA/RNA TRIPLEXES: UV-T_m STUDIES

2.4.3a. *aeaib*PNA_2:DNA Triplexes: UV- T_m Studies

The thermal stabilities of PNA_2:DNA complexes (Figure 13) were studied by temperature dependent UV absorbance measurements. Table 4 shows the T_m values for PNA_2:DNA complexes derived from various *aeg*PNA, *aeg-aeaib*PNAs and *aeaib*PNA homothymine sequences containing different degrees of modification.

The first derivative plots (Figure 13) of all PNA_2:DNA triplexes indicated a single transition, characteristic of both PNA strands dissociating simultaneously from DNA in a single step. The T_m values (Entry 2-6, Table 4) indicate that the incorporation of *aeaib*PNA oligomers exhibited stabilization compared to the unmodified *aeg*PNA-T_8 homooligomer **1**. As the number of incorporation of *aeaib*PNA units increases, there is a systematic elevation of thermal stability of the consistent PNA_2:DNA triplexes with enhancement in T_m of 7-8^{0}C per modification.

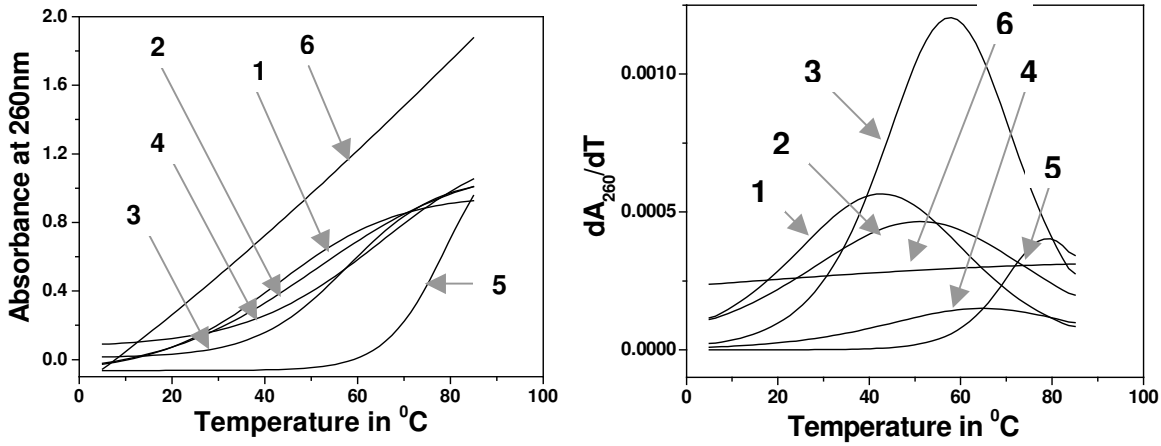

Figure 13. Melting profiles for PNA_2:DNA complexes of *aeg*PNA **1**, *aeg-aeaib*PNA **2**-**5** and *aeaib*PNA **6** with DNA **1**. Conditions: 10mM Phosphate Buffer, 10mM NaCl, pH 7.4
The numbers with arrow correspond to PNA sequences.

Table 4. UV-T_m (^{0}C) of *aeaib*PNA_2:DNA triplexes.*

Entry	PNA sequence	DNA	T_m in ^{0}C	ΔT_m in ^{0}C
1.	PNA **1** H – T T T T T T T T T -Lys NH_2	**1**	43.0	----
2.	PNA **2** H – T T T T T T T **t** -Lys NH_2	**1**	51.1	+ 08.1

3.	PNA **3**	H – T T T T T **t** T **t** -Lys NH_2	**1**	57.9	+ 14.9
4.	PNA **4**	H – T T T **t** T **t** T **t** -Lys NH_2	**1**	64.7	+ 21.7
5.	PNA **5**	H – T **t** T **t** T **t** T **t** -Lys NH_2	**1**	79.6	+ 36.6
6.	PNA **6**	H – **t t t t t t t t** -Lys NH_2	**1**	>85	>42.0

*Buffer: 10mM sodium phosphate, pH 7.4. T_m values are accurate to (±) 0.5°C. Experiments were repeated at least thrice and the T_m values were obtained from the peaks in the first derivative lots. T and **t** indicating *aeg* and *aeaib*-PNA respectively. DNA **1** $^{5'}$ GCAAAAAAAACG $^{3'}$

2.4.3b. *aeaib*PNA_2: RNA Triplexes: UV-Tm Studies

The thermal stabilities of PNA_2:RNA complexes (Figure 14) were studied by temperature dependent UV absorbance measurements. Table 5 shows the T_m values for PNA_2:RNA complexes derived from various *aeg*PNA, *aeg-aeaib*PNAs and *aeaib*PNA homothymine sequences with different degrees of modification.

The first derivative plots for PNA_2:RNA triplexes (Figure 14) showed a single transition, characteristic of both PNA strands dissociating simultaneously from RNA in a

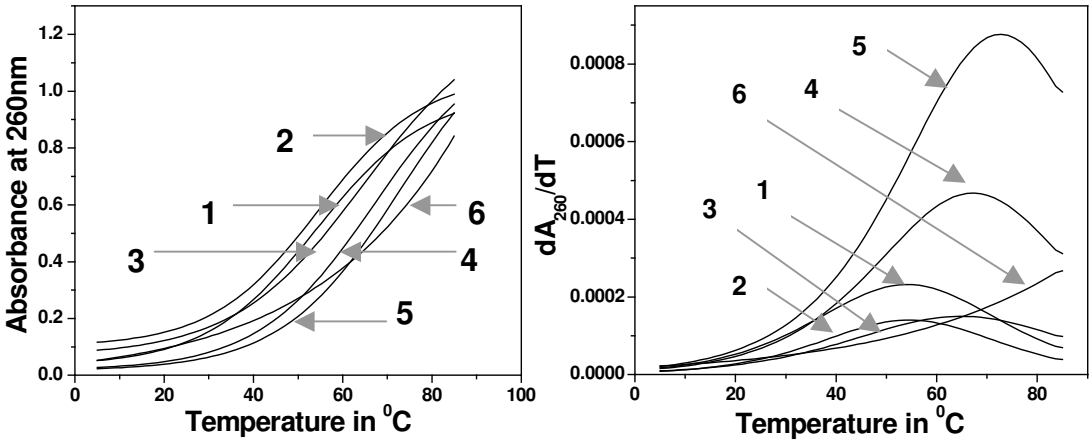

Figure 14. Melting profiles for PNA_2:RNA complexes of *aeg*PNA, *aeg-aeaib*PNA and *aeaib*PNA with RNA **3**. Conditions: 10mM Phosphate Buffer, 10mM NaCl, pH 7.4
The numbers with arrow correspond to PNA sequences.

Table 5. UV-T_m (^{0}C) of *aeaib*PNA_2:RNA triplexes.*

Entry	PNA sequence	RNA	T_m in ^{0}C	ΔT_m in ^{0}C
1.	PNA **1** H – T T T T T T T T – Lys NH_2	**3**	53.8	----
2.	PNA **2** H – T T T T T T T **t** – Lys NH_2	**3**	55.2	+01.4
3.	PNA **3** H – T T T T T **t** T **t** – Lys NH_2	**3**	64.7	+10.9
4.	PNA **4** H – T T T **t** T **t** T **t** – Lys NH_2	**3**	67.4	+13.6
5.	PNA **5** H – T **t** T **t** T **t** T **t** – Lys NH_2	**3**	72.8	+19.0
6.	PNA **6** H – **t t t t t t t t** – Lys NH_2	**3**	>85	>31.2

*Buffer: 10mM sodium phosphate, pH 7.4. T_m values are accurate to (±) 0.5°C. Experiments were repeated at least thrice and the T_m values were obtained from the peaks in the first derivative plots. T and **t** indicating *aeg* and *aeaib*-PNA respectively. RNA **1** Poly rA

single step. The T_m values (Entry 2-6, Table 5) indicate that the incorporation of *aeaib*PNA units exhibited stabilization of the derived oligomers compared to the unmodified *aeg*PNA-T_8 homooligomer **1**. As the number of incorporation of *aeaib*PNA units in oligomers increases, there is enhancement of thermal stability with RNA.

2.4.3c. *apaib*PNA_2:DNA Triplexes: UV-T_m Studies

The thermal stabilities of *apaib*-PNA_2:DNA complexes (Figure 15) were studied by temperature dependent UV absorbance measurements. Table 6 shows the T_m values for PNA_2:DNA complexes derived from various *aeg*PNA, *aeg-apaib*PNAs and *apaib*PNAs of homothymine sequences with different degrees of modification.

The first derivative plots (Figure 15) for *apaib*-PNA_2:DNA triplexes indicated a single transition, characteristic of both PNA strands dissociating simultaneously from DNA in a single step. The T_m values (Entry 2-6, Table 6) indicate that the incorporation of *apaib*PNA oligomers exhibited stabilization of all *apaib*PNA_2:DNA complexes compared to that of the unmodified *aeg*PNA-T_8 homooligomer **1** except the complex **7:1**. The slight destabilization observed with one modification (Entry 2, T_m = 40.3 ^{0}C ; ΔT_m =

-2.7 ^{0}C) disappeared in presence of a second modification (Entry 3) leading to regaining of the stability. As the number of incorporated *apaib*PNA units increased, a systematic elevation of thermal stability of the derived complexes with DNA was observed, with an increase in T_m of 5-6 ^{0}C per modification for homothymine sequences.

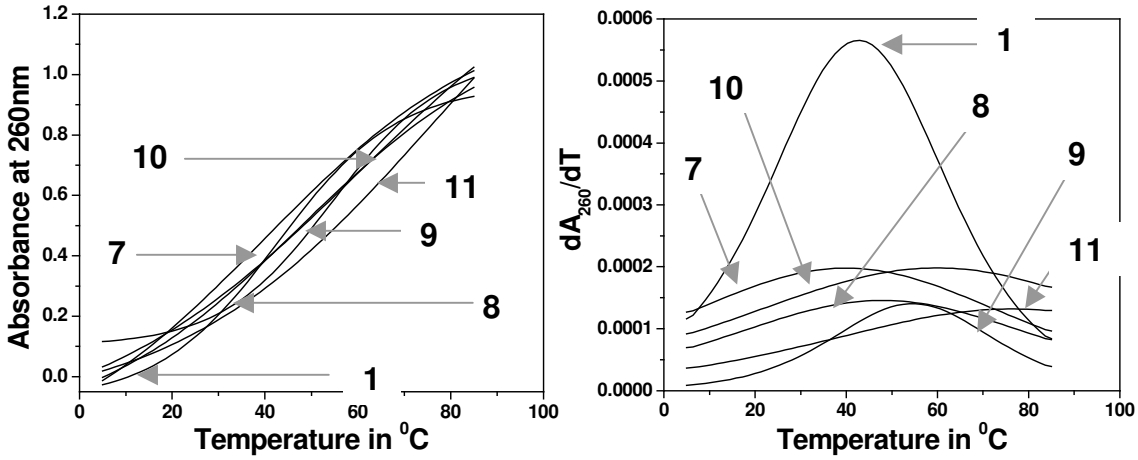

Figure 15. Melting profiles for PNA_2:DNA complexes of *aeg*PNA, *aeg-apaib*PNA and *apaib*PNA with DNA **1**. Conditions: 10mM Phosphate Buffer, 10mM NaCl, pH 7.4
The numbers with arrow correspond to PNA sequences.

Table 6. UV-T_m (^{0}C) of *apaib*PNA_2:DNA triplexes.*

Entry		PNA sequence	DNA	T_m in ^{0}C	ΔT_m in ^{0}C
1.	PNA **1**	H – T T T T T T T T – Lys NH_2	**1**	43.0	----
2.	PNA **7**	H – T T T T T T T ***t*** – Lys NH_2	**1**	40.3	- 02.7
3.	PNA **8**	H – T T T T T ***t*** T ***t*** – Lys NH_2	**1**	48.4	+ 05.4
4.	PNA **9**	H – T T T ***t*** T ***t*** T ***t*** – Lys NH_2	**1**	55.2	+ 12.2
5.	PNA **10**	H – T ***t*** T ***t*** T ***t*** T ***t*** – Lys NH_2	**1**	59.2	+ 16.2
6.	PNA **11**	H – ***t t t t t t t t*** – Lys NH_2	**1**	76.9	+ 33.9

*Buffer: 10mM sodium phosphate, pH 7.4. T_m values are accurate to (±) 0.5°C. Experiments were repeated at least thrice and the T_m values were obtained from the peaks in the first derivative plots. T and ***t*** indicating *aeg* and *apaib*-PNA respectively. DNA **1** $^{5'}$ GCAAAAAAAACG $^{3'}$

2.4.3d. *apaib*PNA$_2$: RNA Triplexes: UV-T_m Studies

The thermal stabilities of *apaib*-PNA$_2$:RNA complexes (Figure 16) were studied by temperature dependent UV absorbance measurements. Table 7 shows the T_m values for PNA$_2$:RNA complexes derived from various *aeg*PNA, *aeg-apaib*PNAs and *apaib*PNAs homothymine sequences with different degrees of modification.

The first derivative plots (Figure 16) for PNA$_2$:RNA triplexes indicated a single transition, characteristic of both PNA strands dissociating simultaneously from RNA in a single step. The T_m values (Entry 2-6, Table 7) indicate that the incorporation of *apaib*PNA units in PNA oligomers caused stabilization of derived complexes with RNA compared to the unmodified *aeg*PNA-T$_8$ homooligomer **1**. As the number of incorporated *apaib*PNA units increases, a concommittal enhancement of thermal stability with RNA was observed.

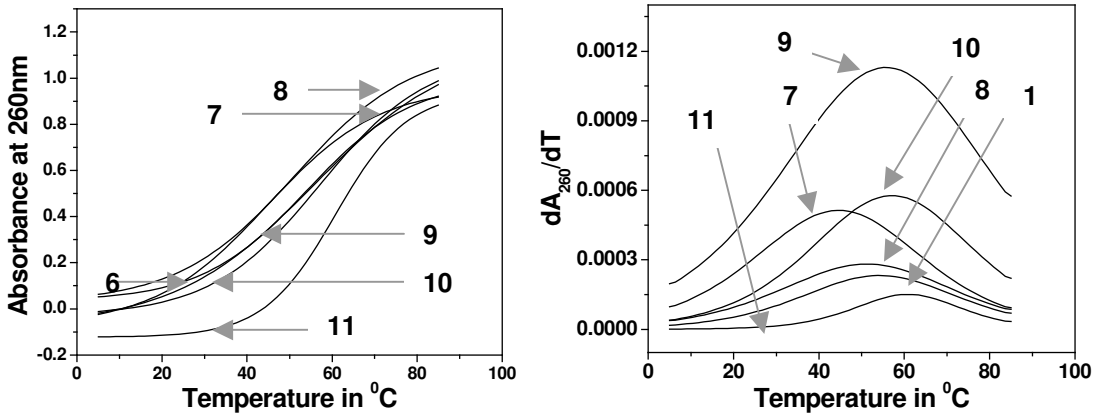

Figure 16. Melting profiles for PNA$_2$:RNA complexes of *aeg*PNA, *aeg-apaib*PNA and *apaib*PNA with RNA **3**. Conditions: 10mM Phosphate Buffer, 10mM NaCl, pH 7.4
The numbers with arrow correspond to PNA sequences.

Table 7. UV-T_m (^{0}C) of *apaib*PNA$_2$:RNA triplexes.*

Entry	PNA sequence	RNA	T_m in ^{0}C	Δ T_m in ^{0}C
1.	PNA **1** H – T T T T T T T T – Lys NH_2	**3**	53.8	----
2.	PNA **7** H – T T T T T T T ***t*** – Lys NH_2	**3**	44.3	- 09.5
3.	PNA **8** H – T T T T T ***t*** T ***t*** – Lys NH_2	**3**	51.1	- 02.7
4.	PNA **9** H – T T T ***t*** T ***t*** T ***t*** – Lys NH_2	**3**	55.2	+ 01.4
5.	PNA **10** H – T ***t*** T ***t*** T ***t*** T ***t*** – Lys NH_2	**3**	56.5	+ 02.7
6.	PNA **11** H – ***t t t t t t t t*** – Lys NH_2	**3**	60.6	+ 06.8

*Buffer: 10mM sodium phosphate, pH 7.4. T_m values are accurate to (±) 0.5°C. Experiments were repeated at least thrice and the T_m values were obtained from the peaks in the first derivative plots. T, **t** and ***t*** indicating *aeg*, *aeaib* and *apaib*-PNA respectively. RNA **1** Poly rA.

2.4.3e. Mismatch Studies

The enhanced thermal stability observed for *aeg-aeaib*PNA and *aeaib*PNA as well as *aeg-apaib*PNA and *apaib*PNA complexes with DNA should not result at the cost of losing base pairing specificities (Figure 17). This was examined by complexation of PNAs **6** & **11** with DNA **2** (dGCAAAACAAACG) that carry a single mismatch at the middle position.

The ΔT_m values for the mismatched complex with control *aeg*PNA **1** was –12.2^{0}C (Entry 1 & 2, Table 8), while that of *aeaib*PNA and *apaib*PNA were higher. The destabilization was > -66.4^{0}C for *aeaib*PNA homothymine sequence (Entry 3 & 4, Table 8) while > -63.7^{0}C for *apaib*PNA homothymine sequence (Entry 5 & 6, Table 8). The lower mismatch tolerance and higher binding affinities to matched complementary DNA **1** reflects the sequence recognition efficiency of RNA/DNA by *aeaib*PNA and *apaib*PNA.

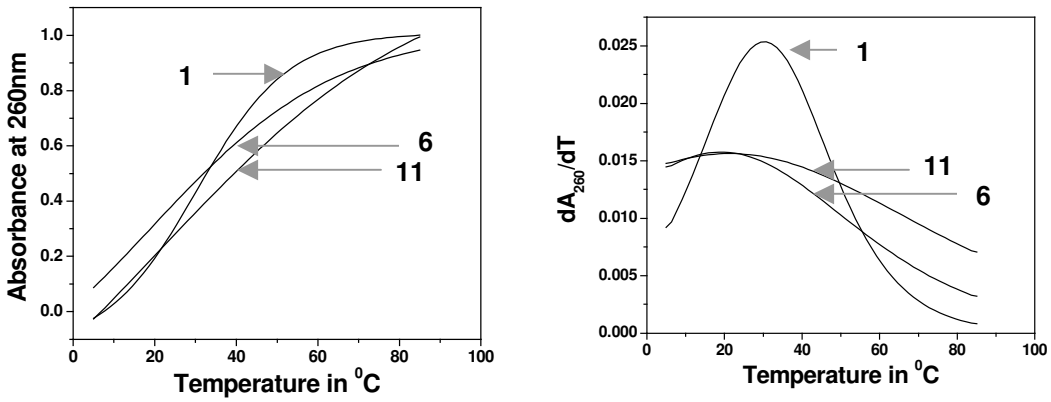

Figure 17. Melting profiles for PNA_2:DNA complexes of *aeg*PNA, *aeaib*PNA and *apaib*PNA with mismatch DNA **2**. Conditions: 10mM Phosphate Buffer, 10mM NaCl, pH 7.4.
The numbers with arrow correspond to PNA sequences.

Table 8. UV-T_m (^{0}C) of PNA_2:DNA mismatch complexes.*

Entry	PNA sequence	DNA	T_m in ^{0}C	ΔT_m in ^{0}C
1.	PNA **1** H – T T T T T T T T -Lys NH_2	**1**	43.0	----
2.	PNA **1** H – T T T T T T T T -Lys NH_2	**2**	30.8	-12.2
3.	PNA **6** H – **t t t t t t t t** -Lys NH_2	**1**	>85	----
4.	PNA **6** H – **t t t t t t t t** -Lys NH_2	**2**	18.6	> -66.4
5.	PNA **11** H – ***t t t t t t t t*** -Lys NH_2	**1**	>85	----
6.	PNA **11** H – ***t t t t t t t t*** -Lys NH_2	**2**	21.3	> -63.7

*Buffer: 10mM sodium phosphate, pH 7.4. T_m values are accurate to (±) 0.5°C. Experiments were repeated at least thrice and the T_m values were obtained from the peaks in the first derivative plots**.** T**, t** and ***t*** indicating *aeg*, *aeaib* and *apaib* PNA respectively. DNA **1** $^{5'}$ GCAAAAAAAACG $^{3'}$ and DNA **2** $^{5'}$ GCAAAACAAACG $^{3'}$

2.4.4. UV-T_m Studies of Duplexes with DNA

The oligothymine sequences described above form triplexes in which the identity of *parallel-antiparallel* binding orientation of the two PNA strands involved in complex formation does not matter. This is due to the fact that one of its PNA strands is always *parallel* and other *antiparallel*.

In order to study the inherent *parallel/antiparallel* orientational preferences of PNA:DNA binding induced by the modifications, mixed purine-pyrimidine sequences were synthesized. The mixed PNA sequences such as **12**-**14** form duplexes with the

complementary DNA in both *antiparallel*, (DNA **3**) and *parallel* (DNA **4**) directions and hence useful to examine the orientational selectivity in binding to DNA. Hence, T_m studies of PNA:DNA duplexes of these oligomers containing *aeaib*- and *apaib*-PNA units were carried out.

The duplexes were constituted by mixing equimolar amounts of *aeg*PNA **12,** *aeaib*PNA **13** and *apaib*PNA **14** individually with the complementary DNA oligomers **3** and **4** designed to bind in *antiparallel* and *parallel* orientations respectively. The UV-T_m profiles of complexes of PNAs **12**-**14** with DNA sequences **3** and **4** in phosphate buffer at pH 7.4 are shown in Figure 18 and the T_m values given in Table 9. With all PNAs, the *antiparallel* duplexes (Entry 1, 3, & 5) were found to be more stable than the corresponding *parallel* duplexes (Entry 2, 4 & 6). However, the modified *aeg-aeaib* **13** and *aeg-apaib* **14** stabilized the *antiparallel* duplexes with DNA **3** by 24.4 ^{0}C and 23.1 ^{0}C respectively compared to the 12.3^{0}C by *aeg*PNA over *parallel* duplexes with DNA **4**.

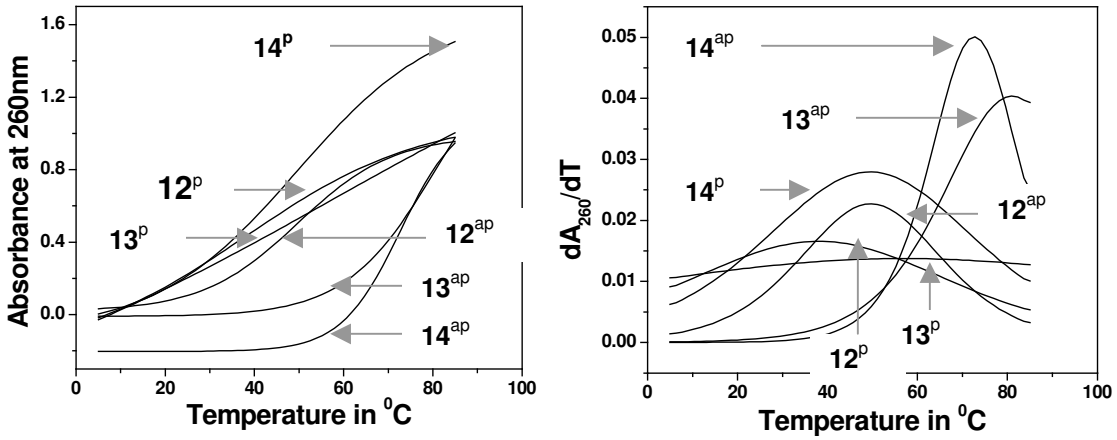

Figure 18. Melting profiles for mixed PNA:DNA complexes of *aeg*PNA, *aeg-aeaib*PNA and *aeg-apaib*PNA with *antiparallel* DNA **3** and *parallel* DNA **4**. Conditions: 10mM Phosphate Buffer, 10mM NaCl, pH 7.4. The number with arrow corresponds to PNA sequence.

Table 9. UV-T_m (^{0}C) of PNA:DNA duplexes containing the nucleobases A/T/C/G.*

Entry	PNA sequence	DNA	T_m in ^{0}C	ΔT_m in ^{0}C (*ap-p*)	ΔT_m in ^{0}C w.r.t. *aeg*PNA
1.	PNA **12** H – G T A G A T C A C T – Lys NH_2	**3** (*ap*)	49.8	----	----
2.	PNA **12** H – G T A G A T C A C T – Lys NH_2	**4** (*p*)	37.5	12.3	----
3.	PNA **13** H – G **t** A G A **t** C A C **t**– Lys NH_2	**3** (*ap*)	80.9	----	31.1
4.	PNA **13** H – G **t** A G A **t** C A C **t** – Lys NH_2	**4** (*p*)	56.5	24.4	----
5.	PNA **14** H – G ***t*** A G A ***t*** C A C ***t***– Lys NH_2	**3** (*ap*)	72.8	----	23.0
6.	PNA **14** H – G ***t*** A G A ***t*** C A C ***t*** – Lys NH_2	**4** (*p*)	49.7	23.1	----

*Buffer: 10mM sodium phosphate, pH 7.4. T_m values are accurate to (±) 0.5°C. Experiments were repeated at least thrice and the T_m values were obtained from the peaks in the first derivative plots. **t** and ***t*** indicating *aeaib* and *apaib* PNA respectively. DNA **3** $^{5'}$ AGTGATCTAC $^{3'}$ and DNA **4** $^{5'}$ CATCTAGTGA $^{3'}$

2.4.5. UV-T_m Studies of Duplexes with RNA

In order to study the *parallel/antiparallel* orientational preferences in PNA:RNA duplexes, mixed purine-pyrimidine PNA sequences were studied. The mixed PNA sequences such as **12**-**14** form duplexes with the complementary RNA in both *antiparallel* (RNA **1**) and *parallel* (RNA **2**) ways and are useful to examine the orientational selectivity in binding to RNA (Figure 19 & 20). Hence, T_m studies of PNA:RNA duplexes comprised of oligomers containing *aeaib- and apaib*-PNA units were carried out.

The duplexes were constituted by mixing equimolar amounts of *aeg*PNA **12,** *aeaib*PNA **13** and *apaib*PNA **14** individually with complementary RNA oligomers **1** & **2** in phosphate buffer at pH 7.4. The UV-T_m profiles of complexes of PNAs **12-14** with RNA sequences **1** and **2** designed to bind in *antiparallel* and *parallel* orientations respectively, are shown in Figure 19 & 20 and the T_m values given in Table 10. With all PNAs, the *antiparallel* PNA:RNA duplexes (Entry 1, 3, & 5, Table 10) were found to be more stable than the corresponding *parallel* PNA:RNA duplexes (Entry 2, 4 & 6, Table

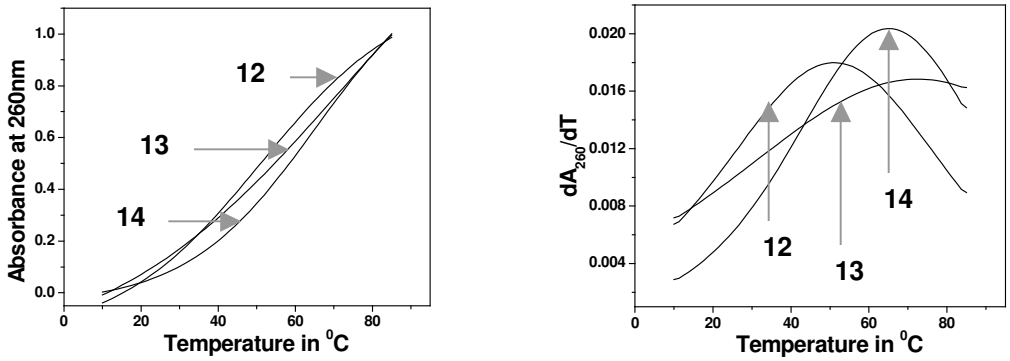

Figure 19. Melting profiles for mixed PNA:RNA complexes of *aeg*PNA, *aeg-aeaib*PNA and *aeg-apaib*PNA with *antiparallel* RNA **1**. Conditions: 10mM Phosphate Buffer, 10mM NaCl, pH 7.4. The numbers with arrow corresponds to PNA sequence. RNA **1** $^{5'}$ AGUGAUCUAC $^{3'}$

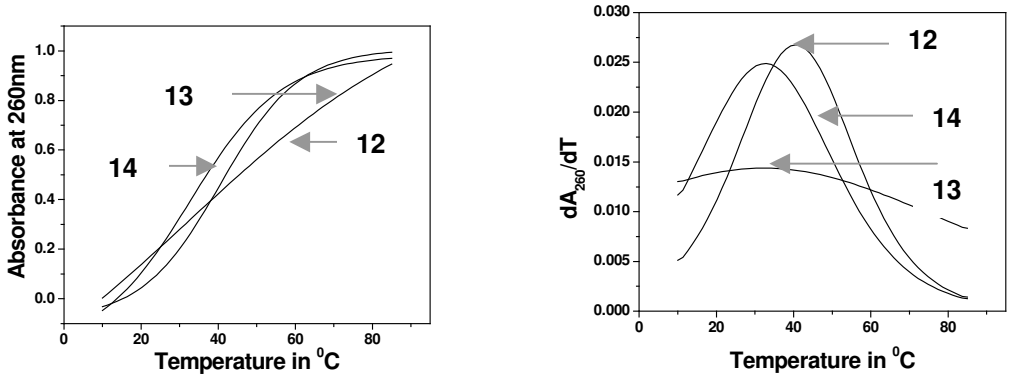

Figure 20. Melting profiles for PNA:RNA complexes of *aeg*PNA, *aeg-aeaib*PNA and *aeg-apaib*PNA with *parallel* RNA **2**. Conditions: 10mM Phosphate Buffer, 10mM NaCl, pH 7.4
The number with arrow corresponds to PNA sequence. RNA **2** $^{5'}$ CAUCUAGUGA $^{3'}$

Table 10. UV-T_m (^{0}C) of PNA:RNA duplexes.*

Entry	PNA sequence	RNA	T_m in ^{0}C	ΔT_m in ^{0}C (*ap-p*)	ΔT_m in ^{0}C w.r.t. *aeg*PNA
1.	PNA **12** H – G T A G A T C A C T – Lys NH_2	**1** (*ap*)	50.1	----	
2.	PNA **12** H – G T A G A T C A C T – Lys NH_2	**2** (*p*)	40.5	09.6	09.6
3.	PNA **13** H – G **t** A G A **t** C A C **t** – Lys NH_2	**1** (a*p*)	72.3	----	22.2
4.	PNA **13** H – G **t** A G A **t** C A C **t** – Lys NH_2	**2** (*p*)	31.6	40.7	40.7
5.	PNA **14** H – G ***t*** A G A ***t*** C A C ***t*** – Lys NH_2	**1** (*ap*)	64.7	----	14.6
6.	PNA **14** H – G ***t*** A G A ***t*** C A C ***t*** – Lys NH_2	**2** (*p*)	32.9	31.8	31.8

*Buffer: 10mM sodium phosphate, pH 7.4. T_m values are accurate to (±) 0.5°C. Experiments were repeated at least thrice and the T_m values were obtained from the peaks in the first derivative plots. **t** and ***t*** indicating *aeaib* and *apaib* PNA respectively. RNA **1** $^{5'}$ AGUGAUCUAC $^{3'}$ and RNA **2** $^{5'}$ CAUCUAGUGA $^{3'}$

10). However, the modified *aeg-aeaib*PNA **13** and *aeg-apaib*PNA **14** stabilized the *antiparallel* duplexes with RNA **1** by 40.7^0C and 31.8^0C respectively compared to the 9.6^0C by *aeg*PNA **12** over *parallel* duplexes with RNA **2**.

2.4.6. Isothermal Titration calorimetric analysis of the Thermodynamic parameters of *aeaib*- and *apaib*-PNA_2:DNA triplexes

Isothermal Titration calorimetry (ITC) is a thermodynamic technique that allows the study of two species. When these two interacting species interact, heat is either generated or absorbed. By measuring these interaction heats, binding constants (K), reaction stoichiometry (n) and thermodynamic parameters including enthalpy (ΔH) and entropy (ΔS) can be accurately determined. In addition, varying the temperature of the experiment allows the determination of the heat capacity (ΔC_p) for the reaction. In ITC, a solution of a ligand is titrated against a solution of a binding partner at constant temperature. The heat released upon their interaction (ΔH) is monitored over time. As successive amounts of the ligand are titrated into the cell, the quantity of heat absorbed or released is in direct proportion to the amount of binding occurring. As the system reaches saturation, the signal diminishes until only heats of dilution are observed. A binding curve is then obtained from a plot of the heats from each injection against the ratio of ligand and binding partner in the cell.

A PC controlled Microcal VP-ITC system was used. All samples used in the ITC experiments were performed on 10 mM sodium phosphate buffer (10mM NaCl, pH = 7.4). The temperature of the cell was held constant at 4^0c for all experiments. A solution

of one of the strands (PNA or DNA respectively), usually in these experiments 1.33 μM PNA **1**-**11** was placed in the cell (volume 1.43 ml) and the titrant solution (3.99 μM DNA **1,** 300μL) in the syringe, whose needle is designed as peddle-shaped stirrer rotating at 400 rpm. The plunger is controlled by a stepping motor, allowing precise injections. Typically 30 injections of 10 μL each and 20 sec apart made. Various models are available for regression of the ITC data. In the present work, the sequential binding with two sites is used to carry out all thermodynamic parameters. The data summarized in Table 11.

PNA **DNA**

Table 11. Thermodynamic parameters of the formation of PNA:DNA complexes from Isothermal titration calorimetry at temperature 277 K

Two set of binding model		**K** (x6 M^{-1})	**-ΔH** ($KJmol^{-1}$)	**N** (KJ/K/mol)	**-ΔG** ($KJmol^{-1}$)	**-TΔS** ($KJmol^{-1}$)	**T_m** in ^0C
1	**1**	1.8	35.9	0.85±0.07	19.1	16.8	43.0
2	**1**	2.1	37.8	0.86±0.02	19.9	17.9	51.1
3	**1**	3.7	56.2	0.88±0.05	34.7	21.5	57.9
4	**1**	7.6	72.2	0.99±0.06	50.4	21.8	64.7
5	**1**	15.4	85.0	0.86±0.06	57.5	27.5	79.6
6	**1**	42.2	245.6	1.09±0.08	102.8	142.8	>85
7	**1**	1.9	26.5	0.86±0.01	14.1	12.4	40.3
8	**1**	2.8	46.6	0.89±0.09	18.7	27.9	48.4
9	**1**	4.2	59.5	0.94±0.02	29.8	29.7	55.2
10	**1**	8.8	62.3	0.98±0.09	30.5	31.8	59.2
11	**1**	27.4	135.4	1.07±0.03	68.7	66.7	76.9

The standard uncertainities were determined from imprecision in the runs and systematic errors.

Each negative peak shown in the heat signal curves from PNA-DNA (Appendix I) represents an exothermic process, which denotes the heat released in one injection of the DNA into the PNA solution as a function of time. The upper panel corresponds to the raw calorimetric data obtained during titration, while lower panel are plots of the integrated enthalpy response obtained from the raw data plotted against the total volume of DNA

solution added to the reaction vessel containing the PNA solution. It is well known that the calorimetric response during dilution of the injectant can be quite prominent and capable of obscuring the calorimetric response during reaction and must be carefully taken into account. It should be pointed out that the data shown here (and in all subsequent measurements) has been corrected for effects arising due to dilution of the DNA during titration.

Lower panels correspond to binding isotherms of the PNAs **1**-**11** with their complementary DNA **1** (See Appendix I). A non-linear, least squares minimization software program (Origin 5.0 from Microcal Inc.) was used to fit the data using two set of binding model for PNA_2:DNA triplexes. The ITC results show that the PNA binding affinities (K) are in the range of 1.8 x 10^6 M^{-1} to 42.2 x 10^6 M^{-1} which is in agreement with literature values 1.8 x 10^6 M^{-1} to 4.15 x 10^7 M^{-1} for PNAs[25]. Thermodynamic parameter, enthalpy (ΔH) for PNA **1**-**11** with its complementary DNA **1** follows a systematic trend. As the number of incorporation of *aeaib-/apaib*-PNAunits in oligomers increases, there is increase in enthalpy (ΔH).

The free energy change, ΔG for PNA **6 and 11** were 42.2 and 27.4$KJmol^{-1}$ which much more higher than *aeg*PNA **1**. The free energy change, ΔG also becomes more negative suggesting favorable binding with increase in the number of modifications. The ΔS did not show much significant variation, except for PNA **6** and **11**, which are modified homo-oligomers.

2.5. DISCUSSION

*aeg*PNA is a DNA mimic with an achiral, uncharged pseudo-peptide backbone. Oligomer synthesis and the properties of PNA containing several modified analogs have been reviewed in the literature.[36] Introduction of chirality and functionality into the backbone have been studied by substituting natural amino acids like alanine, lysine, serine, D-glutamic acid, L-aspartic acid or L-isoleucine for glycine. Substituting chiral amino acids for glycine showed only a moderate loss of binding affinity to DNA and RNA. Besides this, several modifications achieved by introducing the chirality and rigidity in the *aeg*PNA backbone have shown success in binding with DNA/RNA. Also various chiral, cyclic analogues of PNA have been designed as conformationally locked PNAs to achieve specific hybridization with DNA or RNA with aims to increase the binding strength without compromising the binding specificity.[37]

In order to introduce rigidity without any chirality, in the present work the *aeg*PNA backbone was modified by substituting the glycine component by comformationally restricted α-aminoisobutyric acid (*Aib*) having *gem*-dimethyl functionality. Stereochemically constrained α,α-dimethylglycine residues are known to strongly favor certain backbone conformations and stabilize specific secondary structures in designed peptides. α-Aminoisobutyric acid (*Aib*) and related achiral homologs facilitate stable helix formation in oligopeptides as exemplified by a large number of crystal structure determinations in the solid state.[38] The ability to design conformationally rigid helical modules has been exploited in attempts to design structurally well-characterized helix-linker-helix motifs.

gem-Dialkyl Effect

From a synthetic perspective, α,α-disubstituted amino acids are particularly challenging because of the propensity for diketopiperazine formation. The steric effects have an important role in either helping or hindering various reactions and in particular, make these residues less reactive to standard peptide coupling techniques. These effects are result of *gem*-dialkyl effect which is an extension of the Thorpe-Ingold effect, arising due to 'angle compression'. This is a combination of many factors, the main one being the introduction of conformational relaxation into systems, for example, acceleration of a cyclisation reaction due to the substitution of two alkyl groups for two geminal hydrogen atoms on one of the carbon atoms in a chain that links the two reactive centers.

The gem-dialkyl functionality alters the bond angle (θ) thus bringing the ends of the chain closer in space. The ground state energy around the associated chain bonds is raised so that the conformational energy barrier for rotation about these bonds in minimized. All stagger conformers are readily populated, compared to unsubstituted chains for which the antiperiplanar conformer (extended chain conformer) is highly preferred. In effect, the decrease in entropy for the rotationally active (substituted) molecule upon going to the transition state will be less than that required for the unsubstituted parent. Thus the mutual steric repulsion in *gem*-dialkylated series overcomes the normal preference for chains to adopt the extended chain conformations and as a consequence, the two reacting components at the ends of the chain are both nearer and can meet more often, so leading to an enhanced rate of cyclisation. Therefore, dialkyl substituents force the peptide from its preferred straight chain, antiperiplanar conformation into staggered conformation, decreasing the bond angle in the chain and facilitating ring formation. Diketopiperazine formation is especially problematic in the synthesis of peptides containing disubstituted amino acids. This is in part due to these residues exhibiting a greater preference for the Z-amide.[24]

α-Aminoisobutyric acid (*Aib*), the prototype of α,α-disubstituted glycine, is a non-coded amino acid found in membrane channel-forming peptides of microbial origin.

The presence of the extra-methyl group at the C^{α} atom dramatically restricts the conformational space accessible to *Aib* and forces the peptide chain into a left- or right-handed helical conformation. Due to the stringency of the steric requirements, as well as to the high stability and crystallizability of its peptide derivatives, *Aib* has been often used to study the relationships existing between structure, stability and function in bioactive peptides, long polypeptide chains, and even proteins.

The target *aeaib*/*apaib* backbone can be prepared by *N*-alkylating either the ethylenediamine/propylenediamine by *aib* reagents or alkylation of *aib*-NH group by *C2*/*C3* alkylating agents. The alkylation can be done directly or via reductive amination, which were tried as shown in scheme 1 and 2. A direct alkylation of *aib* with mesyl-, tosyl- or halo derivatives of aminoethyl or aminopropyl did not work perhaps due to the bulky α,α-dimethyl substitution (gem-dialkyl effect). The aldehyde generated by Weinreb amide, was reacted with NH_2 group of *aib*, with the aim of getting the corresponding schiff base, but with no success. However, interchanging the amine and alkyl components of the alkyation reaction lead to success. The mono-protected diamine upon treatment with ethyl-bromoisobutyrate, lead to successful *N*-alkylation in moderate yields.

The incorporation of sterically hindered Aib, amino acid into short peptides is associated with poor yields in both solution and solid-phase synthesis using standard coupling reagents i.e. DCC/HOBt, even for prolonged reaction times. Other methods used, such as active esters, mixed anhydrides, also were found to give consistently unsatisfactory results. Better yields were obtained using condensing agents such as BOP, PyBOP, PyBrOP and BrOP. These limitations prompted the exploration of novel

experimental conditions for solid phase peptide synthesis, to improve the coupling efficiency of *aib*-containing *aeaib*- and *apaib*-PNA monomers and reduce the reaction times. Therefore, standard coupling reagent i.e. DCC/HOBt/HBTU in DMF:NMP (1:1) were used in excess equivalent with 4 equivalents of modified *aeaib*/*apaib* monomers. The coupling time was 24 hrs for the first four monomeric units, which further reduced the coupling efficiency, instead of 48hrs.

The effect of PNA backbone modification in the form of *aeaib*-PNA and *apaib*-PNA is expected to significantly affect the PNA:DNA thermal stability on triplexes as well as duplexes. The UV-T_m, CD and Isothermal Titration Calorimetry data presented suggested that the *aeaib*- and *apaib*-PNA:DNA/RNA interaction is significantly diversified.

2.5.1. UV-Spectroscopy

2.5.1a Comparison of *aeaib* with *aeg*PNA

*aeg*PNA homopyrimidine sequences comprising thymine units are known to form PNA_2:DNA triplexes. UV-titration experiments and Job's plot indicated a 2:1 binding stoichiometry (PNA_2:DNA) for PNA oligomers of *aeg-aeaib* units (PNA **2-6**)**.** The percent hyperchromicity Vs temperature plots derived from the UV-melting data indicated a single transition, characteristic of PNA_2:DNA triplex melting, wherein both the PNA strands dissociate from the DNA strand simultaneously, in a single step. The stabilizing effect of the *aeaib*-PNA units on the derived PNA_2:DNA complex

progressively increased with an increase in the number of *aeaib*-PNA units. There is a systematic increase in T_m of 7-8 ^{0}C per *aeaib*-PNA unit in homothymine sequences.

The stabilizing effect of the *aeaib*-PNA units on the derived PNA_2:RNA triplexes also progressively increased with an increase in the number of *aeaib*-PNA units. From comparative UV-melting studies *aeaib*-PNA units show preference for binding to complementary DNA stronger than that with complementary RNA. Thus it is seen that ΔT_m per modification is higher for binding complementary DNA compared to that for complementary RNA (Figure 21).

More importantly, the specificity is retained in all these cases. This is evident from the mismatch studies, wherein the presence of a single C-T mismatch (DNA **2**) in the center of the sequence made the *aeg*PNA_2:DNA complexes less stable compared to duplex with matched DNA **1**. The ΔT_m (match-mismatch) observed for *aeaib*-PNA **6** was much lower compared to *aeg*PNA:DNA duplexes as shown in Table 12. Thus higher binding is achieved without sacrificing the specificity of binding.

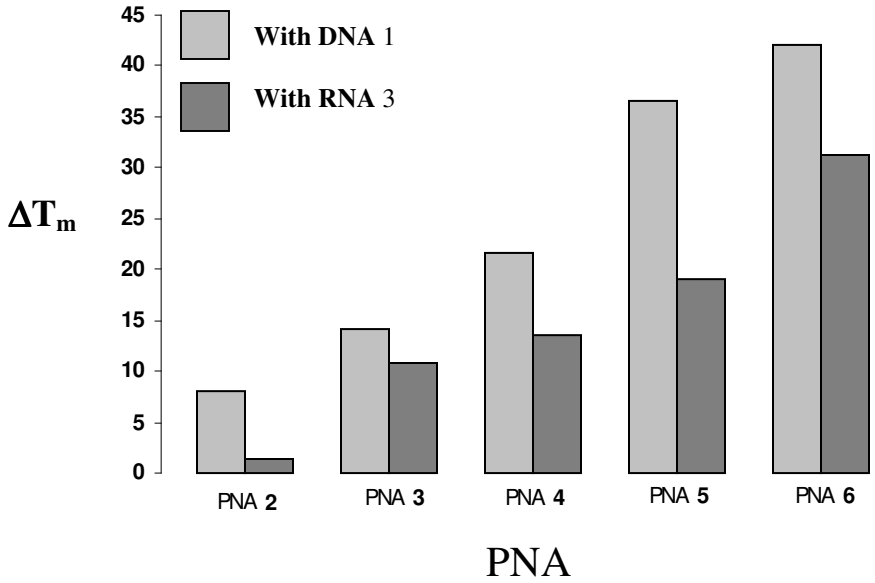

Figure 21. ΔT_m values in ^{0}C for *aeaib*PNA_2:DNA/RNA triplexes. The upper case letters on X-axis refer to the modified PNA sequence indicated by the number (Table 1).

Table 12. Comparative ΔT_m (^{0}C) of PNA_2:DNA between matched[†] and mismatched[††] complexes.*

Entry	PNA sequence	ΔT_m in ^{0}C (Matched – Mismatched)
1.	PNA **1** H – T T T T T T T T -Lys NH_2	12.2
2.	PNA **6** H – **t t t t t t t t** -Lys NH_2	>66.4

[†]DNA **1** $^{5'}$ GCAAAAAAAACG $^{3'}$ and [††]DNA **3** $^{5'}$ GCAAAACAAACG $^{3'}$

The preferences in binding orientations (*parallel* / *antiparallel*) effects of modified backbone of *aeaib*-PNA while hybridizing to complementary DNA sequences is not so important for homopyrimidine (T_8) sequences. These form triplexes with one strand of PNA in *parallel* and another *antiparallel* with respect to middle strand complementary DNA. It becomes importantly relevant in duplexes for determining the specificity of binding orientation. The mixed purine-pyrimidine sequences (PNA **12** & **13**) form duplexes and hence were examined to determine the preferential effect of the *aeaib*-backbone on the directionality of binding. The *aeaib*-PNA units in mixed *aeg*-PNA oligomers with DNA **3** stabilized the *antiparallel* duplexes more effectively than *parallel* duplexes (DNA **4**) as compared to control complexes. Thus, the presence of three units of *aeaib*-PNA in a mixed purine-pyrimidine duplex-forming oligomer discriminates the *parallel* versus *antiparallel* DNA sequence much better than the unmodified *aeg*PNA (Table 13, entry 1-4). The conformationally rigid dimethyl functionality in structures thus

Table 13. ΔT_m (^{0}C) of *aeaib*PNA:DNA duplexes containing the nucleobases A/T/C/G.*

Entry	PNA sequence	DNA	T_m in ^{0}C	ΔT_m in ^{0}C (*ap-p*)	ΔT_m in ^{0}C w.r.t. *aeg*PNA
1.	PNA **12** H – G T A G A T C A C T – Lys NH_2	**3** (*ap*)	49.8	----	----
2.	PNA **12** H – G T A G A T C A C T – Lys NH_2	**4** (*p*)	37.5	12.3	----
3.	PNA **13** H – G **t** A G A **t** C A C **t**– Lys NH_2	**3** (*ap*)	80.9	----	31.1
4.	PNA **13** H – G **t** A G A **t** C A C **t** – Lys NH_2	**4** (*p*)	56.5	24.4	12.1

DNA **3** $^{5'}$ AGTGATCTAC $^{3'}$ and DNA **4** $^{5'}$ CATCTAGTGA $^{3'}$

amplifies the selection of *parallel/antiparallel* modes of binding to DNA.

2.5.1b Comparison of *apaib*PNA with *aeaib*PNA and *aeg*PNA

DNA Vs RNA

Classical *aeg*PNA being flexible can easily attain competent conformation to hybridize with DNA as well as RNA and has near equal binding to both as measured by T_m (Table 9 & 10, Entry 1). UV-titration experiments, Job's plots indicated a 2:1 binding stoichiometry (PNA_2:DNA) for PNA oligomers of *aeg-aeaib* units (PNA **2**-**6**) and *aeg-apaib* units (PNA **7 - 11**)**.** The % hyperchromicity Vs temperature plots derived from the UV-melting data indicated a single transition, characteristic of PNA_2:DNA triplex melting, wherein both the PNA strands dissociate from the DNA strand simultaneously, in a single step. The stabilizing effect of the *apaib*-PNA units on the derived PNA_2:DNA complex progressively increased with an increase in the number of *aeaib*-PNA units. There is a systematic increase in T_m of 5-6 ^{0}C per *apaib*-PNA, homothymine sequences as compared with that of 7 – 8^{0}C *aeaib*-PNA units in homothymine sequences. This higher binding of *apaib*-PNAs, is perhaps a consequence of the pre-organizational conformational effects imposed by the dimethyl functionality in the glycine unit of *apg*-PNA. The favorable comformational features as shown in Figure 22 of these monomers are co-operatively transmitted to the oligomeric level.

The stabilizing effect of the *apaib*-PNA units on the derived PNA_2:DNA triplexes progressively increased with an increase in the number of *apaib*-PNA units. From UV-melting studies, it was observed that *aeaib*-PNA units have higher binding than that with *apaibPNAs* units to complementary DNA **1** as shown in Figure 23.

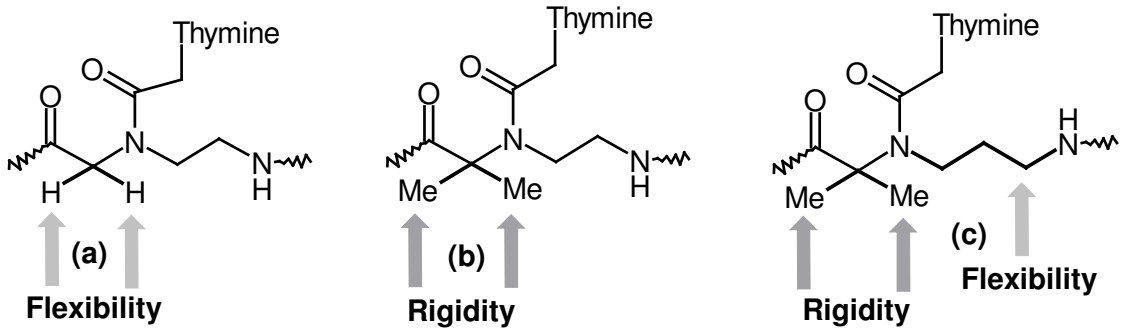

Figure 22. (a) Flexible *aeg*PNA (b) Introducing rigidity in glycine unit, *aeaib*PNA (c) Introducing rigidity as well as flexibility, *apaib*PNA.

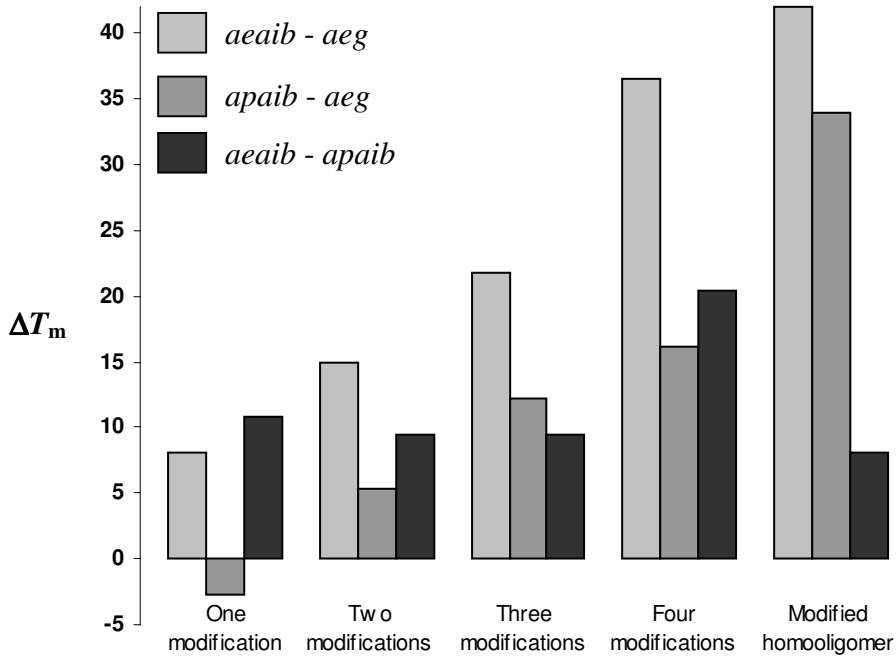

Figure 23. Comparative ΔT_m values in ^{0}C for *aeg*PNA, *aeaib*PNA, *apaib*PNA triplexes with complementary DNA **1**. The lower case letters on X-axis refer to the modified PNA sequence with number of modifications (Table 1).

The stabilizing effect of the *apaib*-PNA units on the derived PNA_2:RNA triplexes progressively increased with increase in the number of *apaib*-PNA units. From UV-melting studies, it follows that *aeaib*-PNA units have higher binding than that with *apaibPNAs* units to complementary RNA **3** as shown in Figure 24.

More importantly, the specificity is retained in all these cases. This was evident from the mismatch studies, where the presence of a single C-T mismatch (DNA **2**) in the center of the sequence made the PNA_2:DNA complexes unstable as compared to matched complexes with DNA **1**. This reveals that the mismatch in the center of the sequence result in mismatched hydrogen bonding and effecting steric incompatibility of fully modified sequence for DNA binding.

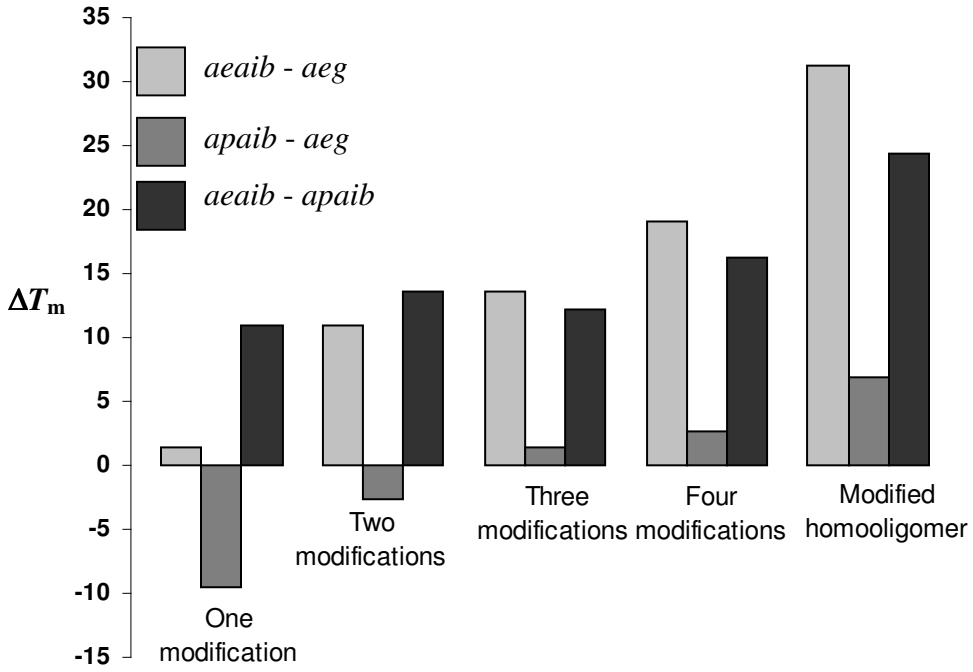

Figure 24. Comparative ΔT_m values in ^{0}C for *aeg*PNA, *aeaib*PNA, *apaib*PNA triplexes with complementary RNA **3**. The lower case letters on X-axis refer to the modified PNA sequence with number of modifications (Table 1).

Hyperchromicity

A useful parameter of interest is the hyperchromicity change accompanying the melting transitions that can be measured from UV-melting curves. The duplexes of *aeaib*PNA **13** and *apaib*PNA **14** having purines generally exhibited higher

hyperchromicity with *antiparallel* DNA **3** than with parallel DNA **4**. Generally higher T_ms were accompanied by larger % hyperchromicities though the hyperchromicity changes could not always be directly correlated with the thermal stabilities. However, in maximum cases, these were slightly higher than the control *aeg*PNA **1**. Since these reflect the extent of base-stacking, the observed pattern of changes suggest variable base stacking effects depending on the base type, conformation and relative orientations of strands in duplexes and triplexes. The percent hyperchromicity accompanying the melting of the mismatched PNA:DNA complexes was very much lower than that accompanying the melting of the fully complementary duplexes.

Parallel Vs Antiparallel

The preferences in binding orientations (*parallel*/*antiparallel*) of modified backbone of *apaib*-PNA while hybridizing to complementary DNA sequences is not so significant in homopyrimidine (T_8) sequences that form triplexes with one strand of PNA in *parallel* and another *antiparallel* with respect to complementary DNA. This becomes importantly relevant in duplexes to determine the specificity of binding orientation. The mixed purine-pyrimidine sequences (PNA **12** & **14**) form duplexes and hence were examined to determine the preferential effect of the *apaib*-backbone on the directionality of binding in duplexes. The *apaib*-PNA units in mixed *aeg*-PNA oligomers with DNA **3** stabilized the *antiparallel* duplexes more effectively than *parallel* duplexes (DNA **4**) as compared to control complexes. Thus, the presence of three units of *aeaib*-PNA of a mixed purine-pyrimidine duplex-forming oligomer discriminates the *parallel* versus *antiparallel* DNA sequence much better than the unmodified *aeg*PNA. The

comformationally rigid dimethyl functionality in structures led to excellent selection in *parallel*/*antiparallel* modes of binding to DNA. The modified *aeg*-*aeaib*-PNA **13** and *aeg*-*apaib*-PNA **14** show prominent stabilization with *antiparallel* DNA **3** over *parallel* DNA **4** by an increase in the T_m of 31.1 ^{0}C and 23.0 ^{0}C as compared to *aeg*PNA as shown in Figure 25.

The higher binding of *aeaib*-PNAs, is perhaps a consequence of the pre-organizational conformational effects imposed by the dimethyl functionality in the glycine unit of *aeg*-PNA. The favorable conformational features of the monomers are co-operatively transmitted to the oligomeric level. The results on *aeaib*-PNAs presented here support the idea of improving the stability and DNA/RNA binding selectivity *via* rational conformational tuning of classical PNA to achieve pre-organization.

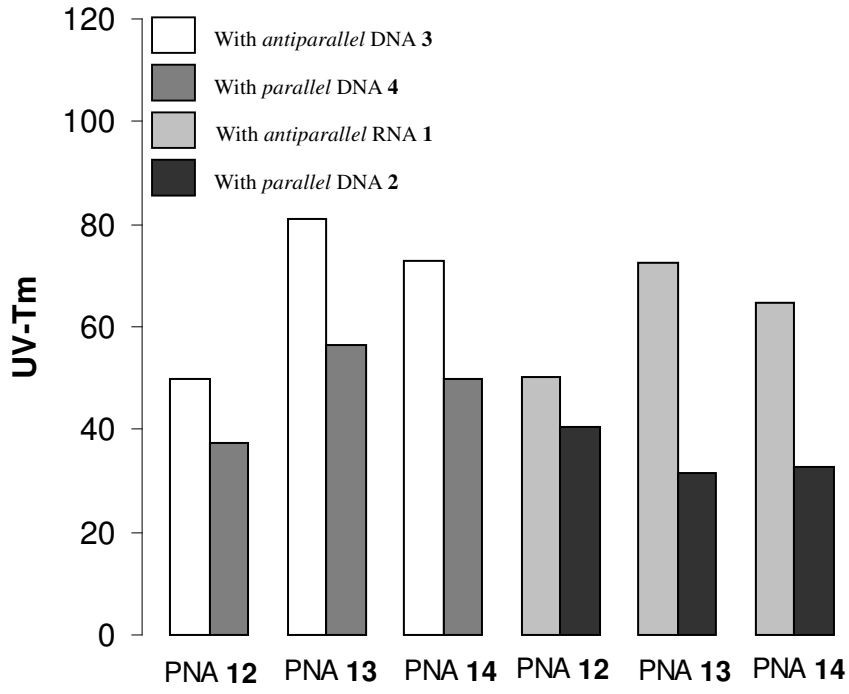

Figure 25. UV-Tm values for *aeg*/*aeaib*/*apaib*PNA:DNA/RNA *parallel* and *antiparallel* complexes. The upper case letters on X-axis refer to the PNA sequences indicated by number (Table 1).

2.5.2. CD Spectroscopy

*aeg*PNA is inherently achiral. However, upon complexation with complementary chiral nucleic acids, the complex is rendered chiral and exhibits an induced CD signal. Chirality can be induced in the achiral PNA strand by linking chiral moieties like amino acids, peptides, or oligonucleotides to the PNA termini. PNA has also been rendered chiral by the incorporation of chiral amino acids or modified PNA chiral units in its backbone. The CD in nucleic acids is predominantly an effect of influence of the chiral sugar on the transition moments of the nucleobases and subsequent coupling of the transition moments of adjacent stacked bases in the helical structures.

The introduction of rigidity in the backbone allows the investigation of specifically positioned centers within the achiral PNA oligomer. Thus, it is of general interest to investigate how much sterically hindered functionality inserted at different positions of a PNA oligomer can coherently induce a preferred handedness of the single or double stranded PNA. Eventual pre-organization of PNAs can favour the DNA/RNA recognition process. It has been suggested that mechanisms for immobilization of the rotation around the bonds of the α-carbon of the amino acid influence the pre-organization and the *gem*-dimethyl substituents on α-carbon is effective in this pre-organization.

PNA-T_8 oligomers were demonstrated to form PNA_2:DNA triplexes with the DNA polypurine strand as the central strand. In such cases, CD supported the fact that a right handed triplex is formed as PNA_2:DNA complex.

The effects on CD induced by the *aeaib*-PNA and *apaib*-PNA units in the PNA upon complexation with complementary DNA are marginal. Significantly, these CD profiles were similar to those of the control achiral *aeg*PNA complexes. Thus, in a PNA:DNA complex, it is the CD of the DNA that dominates over any inherent CD of the PNA involved in the structure.

The PNA_2:DNA triplexes exhibited two maxima at 265nm and 280nm, a minimum at 246nm and crossover points around ~250- ~260nm. The double hump profile is characteristic of poly T:poly A:poly T triplexes as shown in Figure 11 (PNA **7**:DNA **1**).

Significantly, these CD profiles were similar to those of the control achiral a*eg*PNA complexes. Thus, in a PNA:DNA complex, it is the CD of the DNA that dominates over any inherent CD of the PNA involved in the structure.

2.5.3. Isothermal Titration calorimetry

It is demonstrated that isothermal titration calorimetry may be successfully employed to study the thermodynamic parameters of PNA:DNA complexes. Although one expected major entropic contributions to binding, there is more from enthalpic component in free energy, rather than significance from entropic factors.

2.6. SUMMARY

In summary, this chapter promulgates the design and synthesis of novel N-(Boc-aminoethyl-α,α-dimethyl glycyl)-thymine acid and N-(Boc-aminopropyl-α,α-dimethyl glycyl)-thymine acid derived PNA analogues. *aeg*PNA homopyrimidine sequences are known to form triplexes. UV-mixing experiments indicated a 2:1 binding stoichiometry (PNA_2:DNA) for homopyrimidine *aeaib*/*apaib*PNA:DNA complexes, while 1:1 stoichiometry was observed for purine-pyrimidine mixed sequences.

The homopyrimidine-*aeg*PNA backbone comprising *aeaib*/*apaib* units effect stabilization of the resulting triplexes with complementary DNA strands depending upon the number of modified PNA monomers and position of the modified unit. A single modified unit in a mixed purine-pyrimidine duplex-forming oligomer discriminates between the *parallel* versus *antiparallel* DNA sequence much better than the unmodified *aeg*PNA. The *gem*-dimethyl functionality in the glycine unit of *aeg*- and *apg*-PNA contributes to the high binding affinity due to steric lock. The main contributing factor to the enhanced affinity however, remains the specific hydrogen bonding between the A-T and G-C nucleobases.

Finally, an efficient synthesis of modified *aeaib* and *apaib* monomers was developed and incorporated into the oligomers at derived sites. These results emphasize that the chemical, biophysical and structural properties can be controlled by the right kind of rigidity without any chirality. In this regard, the *gem*-dimethyl functionality need to be explored more by introducing in the aminoethyl segment or aminoethyl and glycine, both segments.

2.7. EXPERIMENTAL

2.7.1. Synthetic strategy

The chemicals used were of laboratory or analytical grade. All the solvents used were purified according to the literature procedures. Thin Layer Chromatography (TLC) monitored all the reactions for completion. Usual work-up implies sequential washing of the organic extract with water and brine followed by drying over anhydrous sodium sulphate and evaporation under vacuum.

Column chromatography was performed for purification of compounds on Spectrochem silica gel (60-120 mesh). TLCs were carried out on pre-coated silica gel GF_{254} aluminium sheets (Merck 5554). TLCs were run in either dichloromethane with an appropriate quantity of methanol or in petroleum ether with an appropriate quantity of added ethyl acetate for most compounds. Free acids were chromatographed on TLC using a solvent system of *iso*-propanol: acetic acid: water in the proportion 9:1:1. The compounds were visualized with UV light and/ or by spraying with ninhydrin reagent subsequent to Boc-deprotection (exposing to HCl vapors) and heating.

^{1}H (200MHz/300MHz/500MHz) and ^{13}C (500MHz) NMR spectra were recorded on a Bruker ACF 200 spectrometer fitted with an Aspect 3000 computer and all the chemical shifts are referred to internal TMS for ^{1}H and chloroform-d for ^{13}C. The chemical shifts are quoted in δ (ppm) scale.

CD spectra were recorded on a JASCO J715 spectropolarimeter. Mass spectra were recorded on a Finnigan-Matt (LCMS) mass spectrometer, while MALDI-TOF spectra were obtained from a KRATOS PCKompact and Applied Biosystems instrument.

***N1-(Boc)-1,2-diaminoethane* (2)**

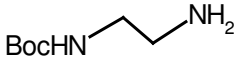

1,2-diaminoethane **1** (20g, 0.33mol) was taken in dioxane: water

(1:1, 500ml) and cooled in an ice-bath. Boc-azide (5g, 35mmol) in dioxane (50ml) was slowly added with stirring and the pH was maintained at 10.0 by continuous addition of 4M NaOH. The mixture was stirred for 8h and the resulting solution was concentrated to 100ml. The *N*1, *N*2-di-Boc derivative not being soluble in water, precipitated, and it was removed by filtration. The corresponding *N*1-mono-Boc derivative was obtained by repeated extraction from the filtrate in ethyl acetate. Removal of solvents yielded the mono-*N*-Boc-diaminoethane **2** (3.45g, 63% yield).

^{1}H NMR ($CDCl_3$) δ: 5.21 (br s, 1H, N*H*), 3.32 (t, 2H, J=8 Hz), 2.54 (t, 2H, J=8 Hz), 1.42 (s, 9H, C(C*H*$_3$)$_3$).

Ethyl N--Boc-(aminoethyl)- α,α-dimethylglycinate **(7)**

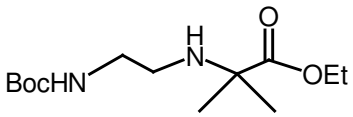

The *N1*-(Boc)-1,2-diaminoethane **2** (3.2g, 20mmol) was treated with 2-bromo-ethyl-isobutyrate (3 ml, 20mmol) in dry acetonitrile (50ml) in the presence of anhydrous K_2CO_3 (5.52g, 40mmol) and the mixture was stirred at 70^0C for 15 hrs. The reaction mixture was concentrated to remove the acetonitrile. The product was extracted from the aqueous layer with ethylacetate and was purified by column chromatography to obtain the ethyl *N*-Boc-(aminoethyl)-α,α-dimethylglycinate **7** as a yellowish oil in good yield (4.2g, 76.6% yield).

^{1}H NMR ($CDCl_3$) δ: 5.29 (br s, 1H, N*H*), 4.22-4.11 (q, 2H), 3.26-3.21 (t, 2H), 2.7-2.65 (t, 2H), 1.43 (s, 9H, C (C*H*$_3$)$_3$), 1.34 (s, 6H, C(C*H*$_3$)$_2$), 1.30-1.23 (t, 3H)

^{13}C NMR ($CDCl_3$) δ: 176.77, 171.15, 156.64, 79.72, 62.56, 61.60, 43.92, 37.75, 28.13, 22.15, 21.10, and 13.77.

$M_{calculated}$ = 274 and $M_{observed}$ = 275.21 (M+1).

***Ethyl N-(Boc-aminoethyl)-N-(chloroacetyl)- α,α-dimethylglycinate* (10)**

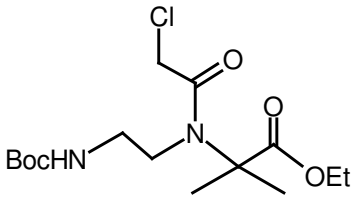

The ethyl *N*-Boc-(aminoethyl)-α,α-dimethylglycinate **7** (4.0g, 14.6mmol) was taken in 10% aqueous Na_2CO_3 (75ml) and dioxane (60ml). Chloroacetyl chloride (3.5ml, 43.8mmol) was added in two portions with vigorous stirring. The reaction was complete within an hour. The reaction mixture was brought to pH 8.0 by addition of 10% aqueous Na_2CO_3 and concentrated to remove the dioxane. The product was extracted from the aqueous layer with ethyl acetate and was purified by column chromatography to obtain the ethyl *N*-Boc-(aminoethyl)-*N*-(chloroacetyl)- α,α-dimethylglycinate **10** as a yellowish oil in good yield (4.2g, 82.35% yield).

^{1}H NMR ($CDCl_3$) δ: 5.13 (br s, 1H, N*H*), 4.27-4.17 (q, 2H), 4.13 (s, 2H), 3.57-3.5 (t, 2H), 3.36-3.30 (t, 2H), 1.49 (s, 6H, C(CH_3)$_2$, 1.43 (s, 9H, C(CH_3)$_3$, 1.27-1.20 (t, 3H)

^{13}C NMR ($CDCl_3$) δ: 173.92, 167.31, 156.01, 79.84, 72.62, 61.65, 61.18, 43.69, 41.78, 41.15, 28.19, 23.81, and 13.90.
$M_{calculated}$ = 350 and $M_{observed}$ = 352.01 (M+2).

***N-(Boc-aminoethyl-α,α-dimethyl glycyl)-thymine ethyl ester* (11)**

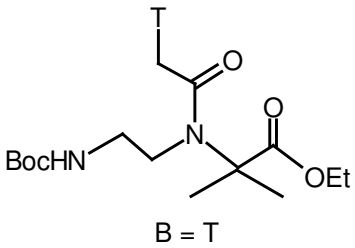

Ethyl *N*-Boc-(aminoethyl)-*N*-(chloroacetyl)-α,α-dimethyl-glycinate **10** (4.0g, 11.4mmol) was stirred with anhydrous K_2CO_3 (1.73g, 12.5mmol) in DMF (50ml) with thymine (1.58g, 12.5mmol) to obtain the desired compound in good yield. DMF was removed under reduced pressure and the *N*-Boc-(aminoethyl-α,α-dimethyl glycyl)-thymine ethyl ester **11** as white solid obtained was purified by column chromatography (4.8gm, 96%).
^{1}H NMR ($CDCl_3$) δ: 6.94 (s, 1H), 5.43 (br s, 1H.N*H*), 4.57 (s, 2H), 4.17-4.06 (q, 2H), 3.57-3.50 (t, 2H), 3.41-3.34 (t, 2H), 1.87 (s, 3H, CH_3), 1.48 (s, 6H, C(CH_3) $_2$, 1.42 (s, 9H, C(CH_3)$_3$, 1.23-1.16 (t, 3H).

$M_{calculated}$ = 440 and $M_{observed}$ = 463 (M+Na).

N1-Boc-1,3-diaminopropane **(14)**

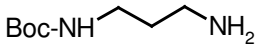

1,3-diaminopropane **13** (20g, 0.27mol) was taken in dioxane: water (1:1, 500ml) and cooled in an ice-bath. Boc-anhydride (5.9g, 27mmol) in dioxane (50ml) was slowly added with stirring and the pH was maintained at 10.0 by continuous addition of 4M NaOH. The mixture was stirred for 8h and the resulting solution was concentrated to 100ml. The *N*1, *N*3-di-Boc derivative not being soluble in water, precipitated, and it was removed by filtration. The corresponding *N*1-mono-Boc derivative **14** was obtained by repeated extraction from the filtrate in ethyl acetate. Removal of solvents yielded the mono-*N*-Boc-diaminopropane **14** (4g, 60% yield).

Ethyl N-Boc-(aminopropyl)- α,α-dimethylglycinate **(15)**

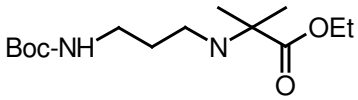

The *N1*-Boc-1,3-diaminopropane **14** (3.12g, 18mmol) was treated with 2-bromo-ethyl-isobutyrate (2.64ml, 18mmol) in dry acetonitrile (100ml) in the presence of anhydrous K_2CO_3 (2.48g, 18mmol) and the mixture was stirred at 70^0C for 15 hrs. The reaction mixture was concentrated to remove the acetonitrile. The product was extracted from the aqueous layer with ethylacetate and purified by column chromatography to obtain the ethyl *N*-Boc-(aminopropyl)-α,α-dimethylglycinate **15** as yellowish oil in good yield (4.5g, 87% yield).

^{1}H NMR ($CDCl_3$) δ: 5.02 (br s, 1H, N*H*), 4.18-4.07 (q, 2H), 3.17-3.11 (t, 2H), 2.51-2.45 (t, 2H), 1.63-1.56 (t, 2H), 1.40 (s, 9H, C(C*H*$_3$)$_3$, 1.26 (s, 6H, C(C*H*$_3$)$_2$, 1.23-1.20 (t, 3H).

^{13}C NMR ($CDCl_3$) δ: 176.84, 155.94, 60.66, 58.84, 41.93, 38.96, 30.48, 28.34, 25.20, and 14.19.

$M_{calculated}$ = 288 and $M_{observed}$ = 289.17 (M+1).

***Ethyl N-Boc-(aminopropyl)-N-(chloroacetyl)-α,α-dimethylglycinate* (16)**

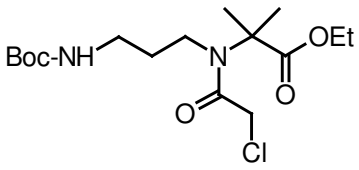

The ethyl *N*-Boc-(aminopropyl)-α,α-dimethylglycinate **15** (3.6g, 12.5mmol) was taken in 10% aqueous Na_2CO_3 (75ml) and dioxane (60ml). Chloroacetyl chloride (5ml, 62.5mmol) was added in two portions with vigorous stirring. The reaction was complete within 5 min. The reaction mixture was brought to pH 8.0 by addition of 10% aqueous Na_2CO_3 and concentrated to remove the dioxane. The product was extracted from the aqueous layer with dichloromethane and was purified by column chromatography to obtain the ethyl *N*-Boc-(aminopropyl)-*N*-(chloroacetyl)-α,α-dimethylglycinate **16** as a yellowish oil in good yield (3.8g, 83.5% yield).

^{1}H NMR ($CDCl_3$) δ: 4.77 (br s, 1H, N*H*), 4.17-4.06 (q, 2H), 4.04 (s, 2H), 3.48-3.40 (t, 2H), 3.17-3.10 (t, 2H), 1.91-1.82 (t, 2H), 1.46 (s, 6H, $C(CH_3)_2$, 1.43 (s, 9H, $C(CH_3)_3$, 1.23-1.17 (t, 3H).

^{13}C NMR ($CDCl_3$) δ: 173.64, 166.22, 156.09, 61.66, 61.05, 42.19, 41.70, 32.33, 28.30, 23.75, and 13.97.

$M_{calculated}$ = 364 and $M_{observed}$ = 365.13 (M+1).

***N-Boc-(aminopropyl-α,α-dimethyl glycyl)-thymine ethyl ester* (17)**

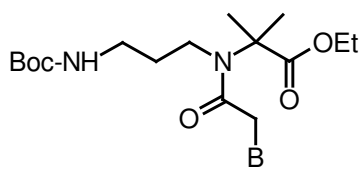

B = T

Ethyl N-Boc-(aminopropyl)-N-(chloroacetyl)-α,α-imethyl-glycinate **16** (2.0g, 5.5mmol) was stirred with anhydrous K_2CO_3 (0.84g, 6.1mmol) and thymine (0.76g, 6.1mmol) in DMF to obtain the

desired compound in good yield. DMF was removed under reduced pressure and the N-Boc-(aminopropyl)-α,α-dimethyl-glycyl-thymine ethyl ester **17** obtained as white solid was purified by column chromatography (2.2g, 88%yield).

^{1}H NMR ($CDCl_3$) δ: 6.98 (s, 1H), 4.95 (br s, 1H, N*H*), 4.49 (s, 2H), 4.16-4.06 (q, 2H), 3.49-3.41 (t, 2H), 3.24-3.18 (t, 2H), 1.89 (s, 3H), 1.47 (s, 6H, C(CH_3)$_2$, 1.42 (s, 9H, C(CH_3)$_3$, 1.23-1.16 (t, 3H).

^{13}*C* NMR (*C*DCl_3) δ: 173.71, 166.36, 164.16, 156.39, 151.21, 110.60, 61.99, 61.19, 41.49, 31.92, 28.39, 23.98, 14.03, 12.32.

$M_{calculated}$ = 454 and $M_{observed}$ = 477.18 (M+Na).

Ethyl N-Boc-(aminoethyl)-glycinate **(19)**[39]

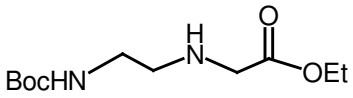

The *N1*-Boc-1,2-diaminoethane **2** (3.2g, 20mmol) was treated with ethylbromoacetate (2.25ml, 20mmol) in acetonitrile (100ml) in the presence of K_2CO_3 (2.4g, 20mmol) and the mixture was stirred at ambient temperature for 5h. The solid that separated was removed by filtration and the filtrate was evaporated to obtain the ethyl *N*-(2-Boc-aminoethyl)-glycinate **19** (4.3g, 83% yield) as a colourless oil.

^{1}H NMR ($CDCl_3$) δ: 5.02 (br s, 1H, N*H*), 4.24-4.20 (q, 2H, J=8Hz), 3.35 (s, 2H), 3.24-3.20 (t, 2H, J=6Hz), 2.80-2.76 (t, 2H, J=6Hz), 1.46 (s, 9H, C(CH_3)$_3$), 1.34-1.28 (t, 3H, J=8Hz).

Ethyl N-Boc-(aminoethyl)-N-(chloroacetyl)-glycinate **(20)** [39]

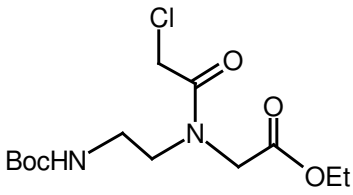

The ethyl *N*-Boc-(aminoethyl)-glycinate **19** (4.0g, 14mmol) was taken in 10% aqueous Na_2CO_3 (75ml) and dioxane

(60ml). Chloroacetyl chloride (6.5ml, 0.75mmol) was added in two portions with vigorous stirring. The reaction was completed within 5 min. The reaction mixture was brought to pH 8.0 by addition of 10% aqueous Na_2CO_3 and concentrated to remove the dioxane. The product was extracted from the aqueous layer with dichloromethane and was purified by column chromatography to obtain the ethyl *N*-Boc-(aminoethyl)-*N*-(chloroacetyl)-glycinate **20** as colourless oil in good yield (4.2g, 80% yield).

^{1}H NMR ($CDCl_3$) δ: 5.48 (br s, 1H), 4.25-4.14 (m, 2H), 4.03 (s, 2H), 3.54 (t, 2H), 3.33-3.28 (q, 2H), 1.45 (s, 9H, $C(CH_3)_3$), 1.34-1.26 (t, 3H, J=8Hz).

***N-Boc-(aminoethylglycyl)-thymine ethyl ester* (21a)** [39]

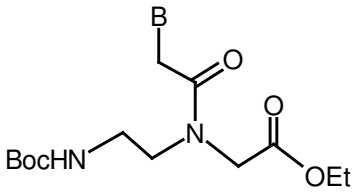

21a B = T
21b B = C^{CBz}
21c B = A
21d B = 2-amino-6-chloropurine

Ethyl *N*-Boc-(aminoethyl)-*N*-(chloroacetyl)-glycinate **20** (4.0g, 11.6mmol) was stirred with anhydrous K_2CO_3 (1.56g, 11.8mmol) in DMF with thymine (1.4g, 11.2mmol) to obtain the desired compound **21a** in good yield. DMF was removed under reduced pressure and the oil obtained was purified by column chromatography.

^{1}H NMR ($CDCl_3$) δ: 8.75 (br s, 1H, *T*-N*H*), 7.97 (maj) (s, 1H, *T*-*H*6), 5.66 (maj) & 5.09 (min) (br s, 1H, N*H*), 4.55 (maj) & 4.40 (min) (s, 1H, *T*-CH_2), 4.20 (m, 2H, OCH_2), 3.48 (m, 2H), 3.28 (m, 2H), 1.85 (s, 3H, *T*-CH_3), 1.39 (s, 9H), 1.23 (m, 3H).

^{13}*C* NMR ($CDCl_3$) δ: 170.8, 169.3, 167.4, 164.3, 156.2, 151.2, 141.1, 110.2, 79.3, 61.8, 61.2, 48.5, 48.1, 47.7, 38.4, 28.1, 13.8, 12.2.

N^4-benzyloxycarbonylcytosine [32]

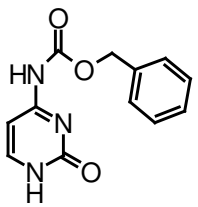

Cytosine (1.0g, 9.0mmol) was suspended in dry pyridine (100ml) at 0^{o}C. CBz-Cl (3.2ml, 22.5mmol) was added and the reaction was stirred under nitrogen overnight. The pyridine suspension was evaporated to dryness. Water (10ml) and dilute HCl were added to bring the pH to 4.0. The resulting

white precipitate was filtered off, washed with water and partially dried under vacuum. The wet precipitate was boiled in absolute ethanol (10ml), cooled to 0^oC, filtered, washed thoroughly with ether and dried under vacuum (1.1g, 50% yield).

***N-Boc-(aminoethylglycyl)-(N^4-benzyloxycarbonyl cytosine)ethyl ester* (21b)** [32]

A mixture of NaH (0.25g, 6.2mmol) and N^4-benzyloxycarbonyl cytosine (1.24g, 6.2mmol) was taken in DMF and stirred at 75°C till the effervescence ceased. The mixture was cooled and ethyl *N*-Boc-(aminoethyl)-*N*-(chloroacetyl)-glycinate **20** (2.0g, 6.2mmol) was added. Stirring was then continued at 75°C to obtain the cytosine monomer, *N*-Boc-(aminoethylglycyl)-(N^4-benzyloxycarbonyl cytosine) ethyl ester **21b**, in moderate yield (1.62g, 50% yield).

^{1}H NMR ($CDCl_3$) δ: 7.63 (d, 1H, *C-H6*, J=8Hz), 7.32 (s, 5H, Ar), 7.22 (d, 1H, *C-H5*, J=8Hz), 5.68 (br s, 1H, N*H*), 5.20 (s, 2H, Ar-CH_2), 4.69 (maj) & 4.22 (min) (br s, 2H), 4.12 (q, 2H), 4.01 (s, 2H), 3.49 (m, 2H), 3.29 (m, 2H), 1.44 (s, 9H, $C(CH_3)_3$), 1.23 (t, 3H).

***N-Boc-(aminoethylglycyl)-adenine ethyl ester* (21c)** [39]

NaH (0.25g, 6.1mmol) was taken in DMF (15ml) and adenine (0.8g, 6.1mmol) was added. The mixture was stirred at 75°C till the effervescence ceased and the mixture was cooled before adding ethyl *N*-Boc-(aminoethyl)-*N*-(chloroacetyl)-glycinate **20** (2.0g, 6.1mmol). The reaction mixture was heated once again to 75°C for 1h, when TLC analysis indicated the disappearance of the starting ethyl *N*-Boc-(aminoethyl)-*N*-(chloroacetyl)-glycinate. The DMF was removed under vacuum, the resulting thick oil was taken in water and the product was extracted in ethyl acetate. The organic layer was then concentrated to obtain the crude product which was purified by column chromatography to obtain the pure *N*-Boc-(aminoethylglycyl)-adenine ethyl ester **21c**.

^{1}H NMR ($CDCl_3$) δ: 8.34 (s, 1H), 7.97 (min) & 7.93 (maj) (s, 1H), 5.82 (maj) & 5.75 (min) (br, 2H), 5.11 (maj) & 4.96 (min), 4.27 (min) & 4.07 (maj) (s, 2H),

4.22 (m, 2H), 3.66 (maj) & 3.56 (min) (m, 2H), 3.41 (maj) & 3.54 (min) (m, 2H), 1.42 (s, 9H, $C(CH_3)_3$), 1.27 (m, 3H).

***N-Boc-(aminoethylglycyl)-2-amino-6-chloropurine ethyl ester* (21d)** [39]

A mixture of 2-amino-6-chloropurine (1.14g, 6.8mmol), K_2CO_3 (0.93g, 7.0mmol) and ethyl *N*-Boc-(aminoethyl)-*N*-(chloroacetyl)-glycinate **20** (2.4g, 7.0mmol) was taken in dry DMF (20ml) and stirred at room temperature for 4h. K_2CO_3 was removed by filtration, and the DMF, by evaporation under reduced pressure. The resulting residue was purified by column chromatography to obtain the *N*-Boc-(aminoethylglycyl)-2-amino-6-chloropurine ethyl ester **21d** in excellent yield (2.65g, 98% yield).
^{1}H NMR ($CDCl_3$) δ: 7.86 (min) & 7.82 (maj) (s, 1H), 7.30 (s, 1H), 5.76 (br s, 1H, N*H*), 5.18 (br, 2H), 4.96 (maj) & 4.81 (min) (s, 2H), 4.17 (min) & 4.02 (maj) (s, 2H), 3.58 (maj) & 3.48 (min) (m, 2H), 3.36 (maj) and 3.26 (min) (m, 2H), 1.38 (s, 9H, $C(CH_3)_3$), 1.22 (m, 3H).

Hydrolysis of the PNA ethyl ester monomers

General method

The ethyl esters were hydrolyzed using 2N aqueous NaOH (5ml) in methanol (5ml) and the resulting acid was neutralized with activated Dowex-H^+ till the pH of the solution was 7.0. The resin was removed by filtration and the filtrate was concentrated to obtain the resulting Boc-protected acid in excellent yield (>85%).

Functionalization and Picric Acid Estimation of the MBHA [(4-methyl benzhydryl) Amine] Resin

The loading value (amine function) 0.85 mmol/g of the MBHA resin (Sigma, 100-200 mesh) was lowered to 0.25mmol/g by capping the excess 0.6 mmol/g of amine functionalization in dry DMF/DCM using acetic anhydride and pyridine as a base. The loading value of 0.25mmol/g was found to be optimum for the synthesis of oligomers. The MBHA resin with loading value 0.25mmol/g was functionalized by coupling di-protected L-lysine carboxylic group (N^{α}-amino group protected with Boc and N^{ω}- amino group by Cl-Cbz) to

the free amines on the resin using coupling reagents. Then the final loading value of the so functionalized resin was estimated using picric acid. The procedure for estimation of the loading value of the resin was carried out with 5 mg of the resin and comprised the following steps:

The resin was swollen in dry CH_2Cl_2 for at least 30min. The CH_2Cl_2 was drained off and a 50% solution of TFA in CH_2Cl_2 was added (1ml x 2, 15min each). After washing thoroughly with CH_2Cl_2, The TFA salt was neutralized with a 5% solution of DIPEA in CH_2Cl_2 (1ml x 3, 2min each) and further washing was carried out with CH_2Cl_2. The free amine was treated with a 0.1M picric acid solution in CH_2Cl_2 (2ml x 2, 3min each). The excess picric acid was eliminated by extensively washing the resin with CH_2Cl_2. The adsorbed picric acid was displaced from the resin by adding a solution of 5% DIPEA in CH_2Cl_2. The eluant was collected and the volume was made up to 10ml with CH_2Cl_2 in a volumetric flask. The absorbance was recorded at 358nm in ethanol and the concentration of the amine groups on the resin was calculated using the molar extinction coefficient of picric acid as 14,500$cm^{-1}M^{-1}$ at 358nm.

Kaiser's Test

Kaiser's test was used to monitor the Boc-deprotection and amide bond (peptide bond) formation steps in the solid phase peptide synthesis. Three solutions were used, viz. (1) ninhydrin (5.0g) dissolved in ethanol (100ml),

(2) phenol (80g) dissolved in ethanol (20ml) and

(3) KCN: 2ml of a 0.001M aqueous solution of KCN in 98ml pyridine.

To a few beads of the resin to be tested taken in a test tube, were added 3-4 drops of each of the three solutions described above. The tube was heated at 100°C for ~ 2 min, and the color of the beads was noted. A blue color on the beads, which slowly comes in the solution, indicated successful deprotection, while colorless beads and the solution confirmed

the completion of the amide coupling reaction. The blank solution should remain yellow.

Synthesis of PNA-oligomers incorporating modified monomers

The modified PNA monomers were built into PNA oligomers using standard procedure on an L-lysine derivatized (4-methyl benzhydryl) amine (MBHA) resin (initial loading 0.25 meq/g) with HBTU/HOBt/DIPEA in DMF/NMP as a coupling reagent. The PNA oligomers were cleaved from the resin with TFMSA. The oligomers were purified by RP-HPLC (C 18 column) and characterized by MALDI-TOF mass spectrometry. The overall yields of the crude products were 70-80%. The control PNAs were prepared similarly as discussed above.

Cleavage of the PNA oligomers from the solid support

A typical cleavage reaction was carried out with 5 or 10mg of resin-bound PNA oligomer. The resin-bound PNA oligomer (10mg) was stirred in an ice-bath with thioanisole (20µl) and 1,2-ethanedithiol (8µl) for 10min, TFA (120µl) was added and stirring was continued for another 10min. TFMSA (16µl) was added and stirring continued for 2h. The reaction mixture was filtered through a sintered funnel. The residue was washed with TFA (3 x 2ml) and the combined filtrate and washings were evaporated under vacuum and co-evaporated with ether, avoiding heating during this process. The residue was precipitated using dry ether and centrifuged to obtain a white pellet. The pellet was re-dissolved in methanol (~0.1ml) and re-precipitated by adding ether. The pellet collected after centrifugation was subjected to this re-precipitation process at least thrice, when a white precipitate was obtained of the crude PNA oligomer.

Gel Filtration

The crude PNA oligomer obtained after ether precipitation was dissolved in water (~0.5ml) and loaded on a gel filtration column. This column consisted of G25 Sephadex and had a void volume of 0.5/1ml. The oligomer was eluted with water and six fractions of 0.5/1ml volume each were collected. The presence of the PNA oligomer was detected by measuring the absorbance at 260nm. The fractions containing the oligomer were freeze-dried. The purity of the cleaved crude PNA oligomer was determined by RP HPLC on a C18 column. If found to be above 90%, the oligomers were used as such for experiments without further purification. If the purity was not satisfactory, the oligomers were purified by HPLC/FPLC.

FPLC

The crude PNA oligomers were dissolved in water containing 0.1% TFA, the starting buffer for injection. The polypyrimidine T_8 sequences were purified using a gradient of 0 to 60% buffer B in 40min at a flow rate of 1.0ml/min, where buffer A = water with 0.1% TFA and buffer B = 60% CH_3CN in water containing 0.1% TFA. The mixed sequence PNAs eluted earlier and hence had to be purified using a gradient of 0 to 30% B in 30min at a flow rate of 1.0ml/min, when good resolution of the peaks was obtained. The purity of the oligomer after FPLC was ascertained by HPLC on a C18 RP column.

HPLC

The purity of the PNA oligomers was ascertained on an analytical RP C18 column using a gradient of 5 to 50% CH_3CN in water containing 0.1% TFA at a flow rate of 1.5ml/min.

MALDI-TOF Mass Spectrometry

Literature reports the analysis of PNA purity by MALDI-TOF mass spectrometry in which several matrices have been explored, *viz.* sinapinic acid (3,5-dimethoxy-4-hydroxycinnamic acid), CHCA (α-cyano-4-hydroxycinnamic acid) and DHB (2,5-

dihydroxybenzoic acid). Of these, sinapinic acid was found to give the best signal to noise ratio with all the other matrices typically producing higher molecular ion signals.

For all the MALDI-TOF spectra recorded for the *aeaib*-PNAs reported in this Chapter, sinapinic acid was used as the matrix and was found to give satisfactory results.

UV studies

All the UV spectrophotometric studies were performed either on a Perkin Elmer λ15 UV-VIS spectrophotometer equipped with a Julabo temperature programmer and a Julabo water circulator or a Perkin Elmer λ35 UV-VIS spectrophotometer with peltier to maintain the temperature. The samples were degassed by purging nitrogen or argon gas through the solution for 2-3min prior to the start of the experiments. Nitrogen gas was purged through the cuvette chamber below 15^{o}C to prevent the condensation of moisture on the cuvette walls.

UV-titration

To a solution of DNA **1** in 0.01M sodium phosphate at pH 7.4, were added fixed portions of the complementary PNA oligomer **2 & 7**. The temperature of the circulating water was maintained at 10^{o}C (i.e., well below the melting temperature of the complexes) and the absorbance at each step was recorded at 260nm. This was plotted as a function of the PNA mole fraction.

UV-T_m

The PNA oligomers and the appropriate DNA oligomers were mixed together in stoichiometric amounts (2:1, PNA:DNA for oligothymine-T_8 PNAs or 1:1 for the duplex forming PNAs, *viz*., the mixed base sequences) in 0.01M sodium phosphate buffer, pH 7.3 to achieve a final strand concentration of either 0.5 or 1μM each strand. For the AT-rich PNAs, *antiparallel* and *parallel* complexes were constituted by employing DNA. The samples were heated at 85^{o}C for 5 min. followed by slow cooling to room temperature. They were allowed to remain at room temperature for at least half an hour and refrigerated overnight prior to running the melting experiments. Each melting experiment was repeated at least twice. The absorbance or the percent hyperchromicity at 260 nm was plotted as a function of the temperature. The T*m* was determined from the peaks in the first derivative plots and is accurate to ±0.5^{0}C. The concentration of DNA, RNA and PNA were calculated with the help of extinction coefficients, A= 15.4, T= 8.8, C= 7.3 and G= 11.7.

Mismatch studies

DNA **2** was used to probe the specificity of the PNA-oligothymine-T_8 interaction with DNA. The relevant PNA and DNA strands were mixed together in a 2:1 molar ratio and subjected to UV-melting.

Circular Dichromism

CD spectra were recorded on a Jasco J-715 spectropolarimeter. The CD spectra of the PNA:DNA complexes and the relevant single strands were recorded in 0.01M sodium

phosphate buffer, pH 7.4. The temperature of the circulating water was kept below the melting temperature of the PNA:DNA complexes, i. e., at 10^{o}C.

The CD spectra of the oligothymine T_8 single strands were recorded as an accumulation of 10 scans from 320 to 200nm using a 1cm cell, a resolution of 0.1nm, band-width of 1.0nm, sensitivity of 2mdeg, response 2sec and a scan speed of 100nm/min. For the PNA_2:DNA complexes, spectra were recorded as an accumulation of 10 scans, response of 1sec and a scan speed of 200nm/min.

The CD spectra of the mixed base PNAs and the derived PNA:DNA duplexes were recorded as an accumulation of 5 scans and a scan speed of 200nm/min.

2.8. APPENDIX

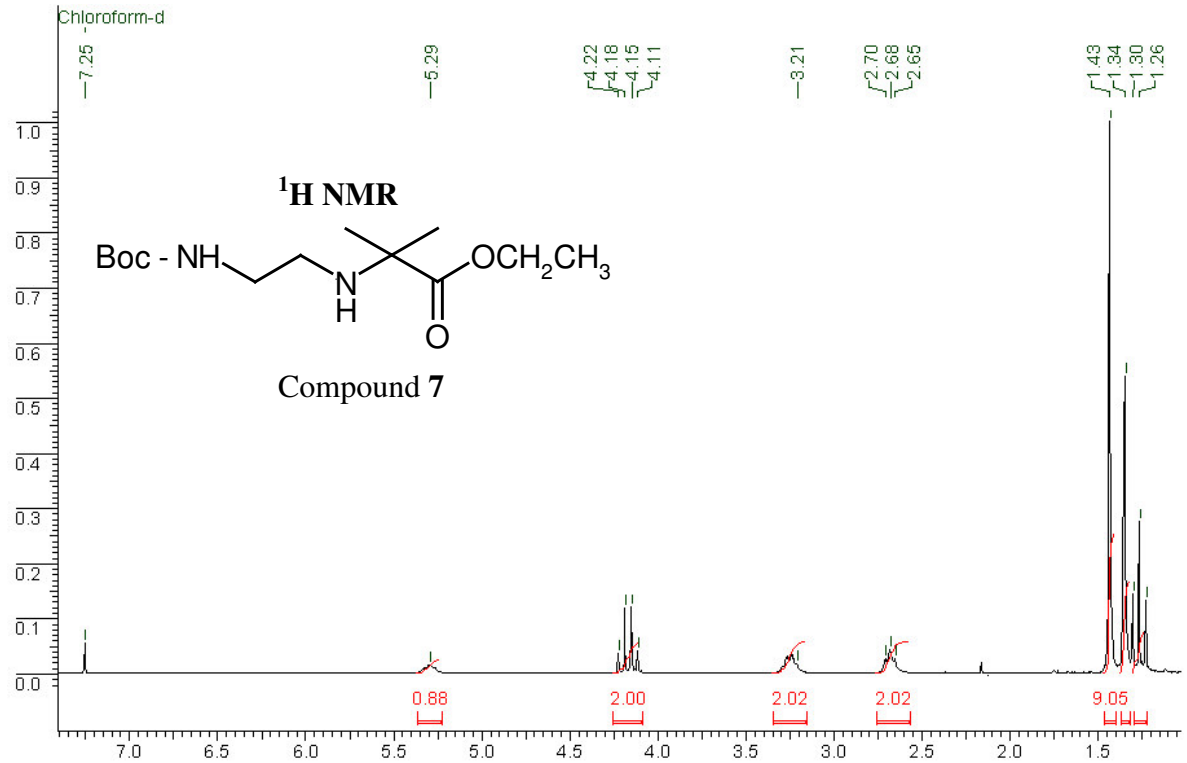

^{1}H NMR

Compound **7**

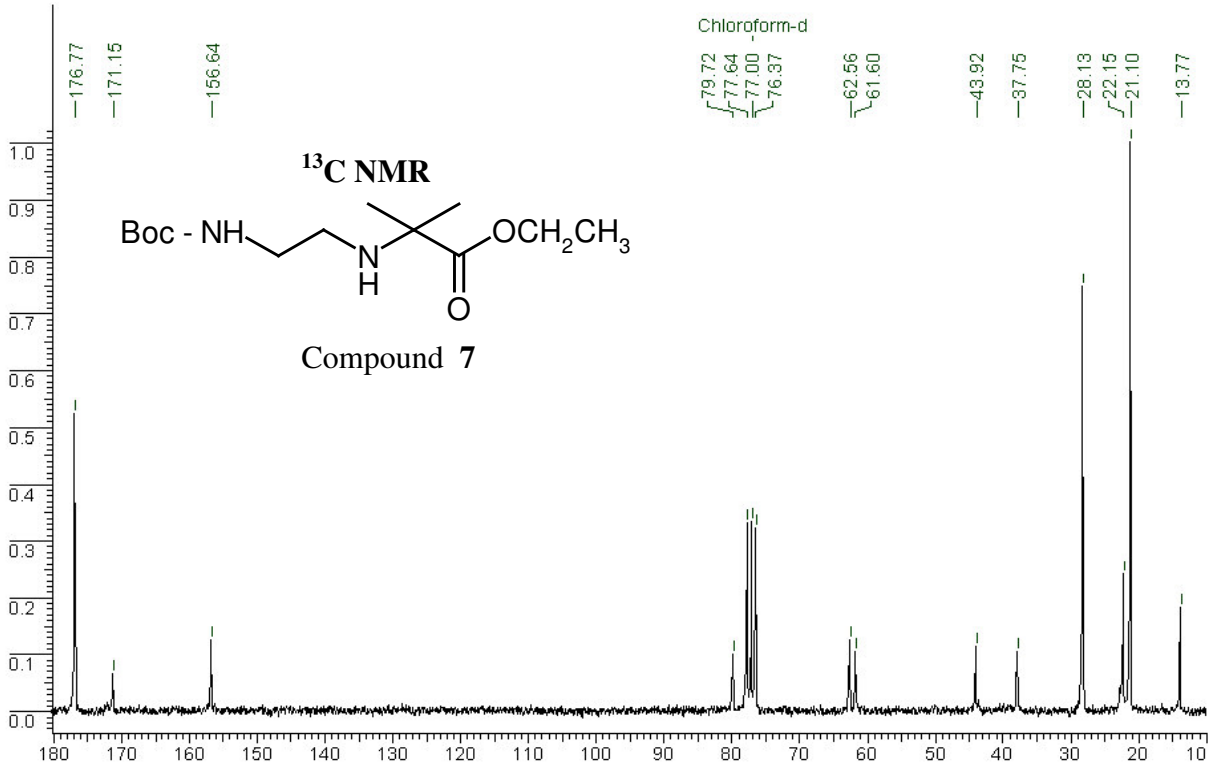

^{13}C NMR

Compound **7**

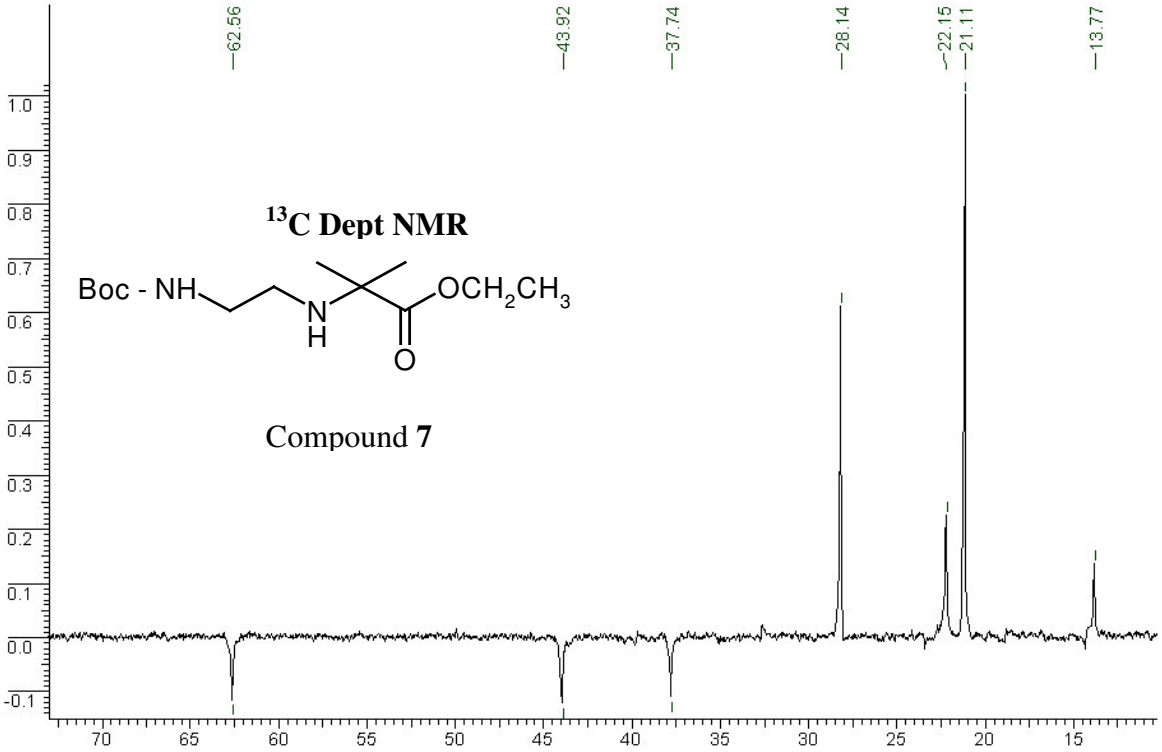

^{13}C Dept NMR

Compound **7**

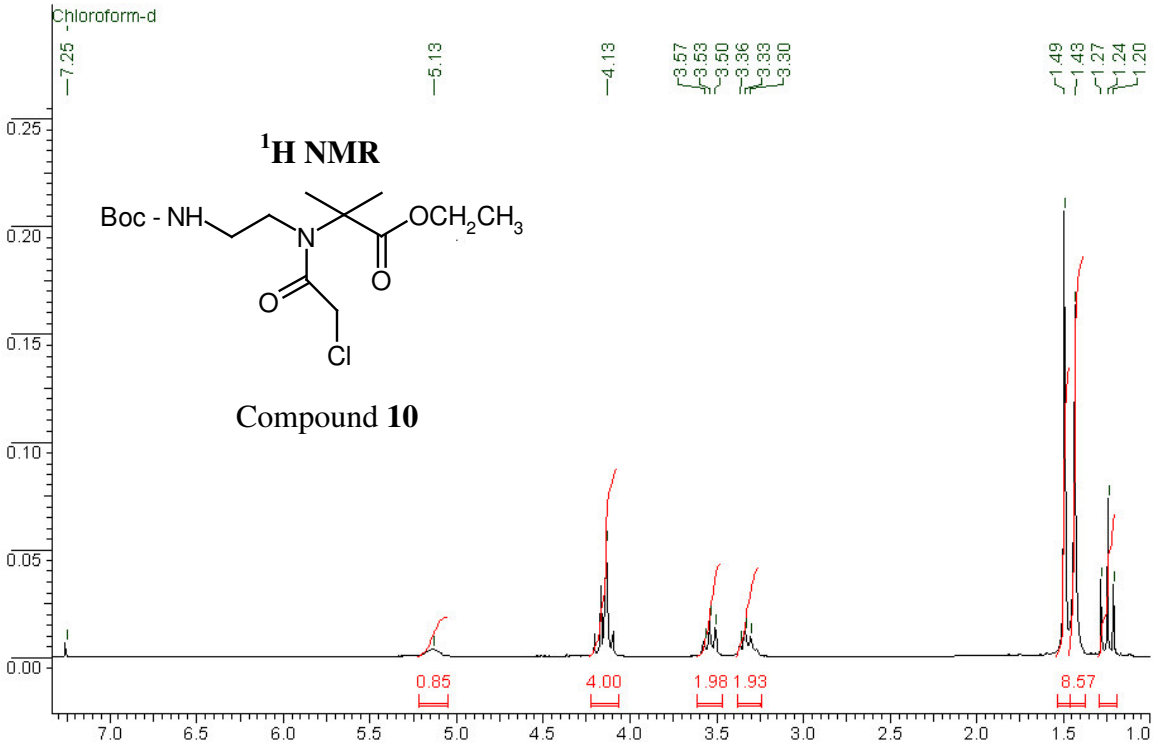

^{1}H NMR

Compound **10**

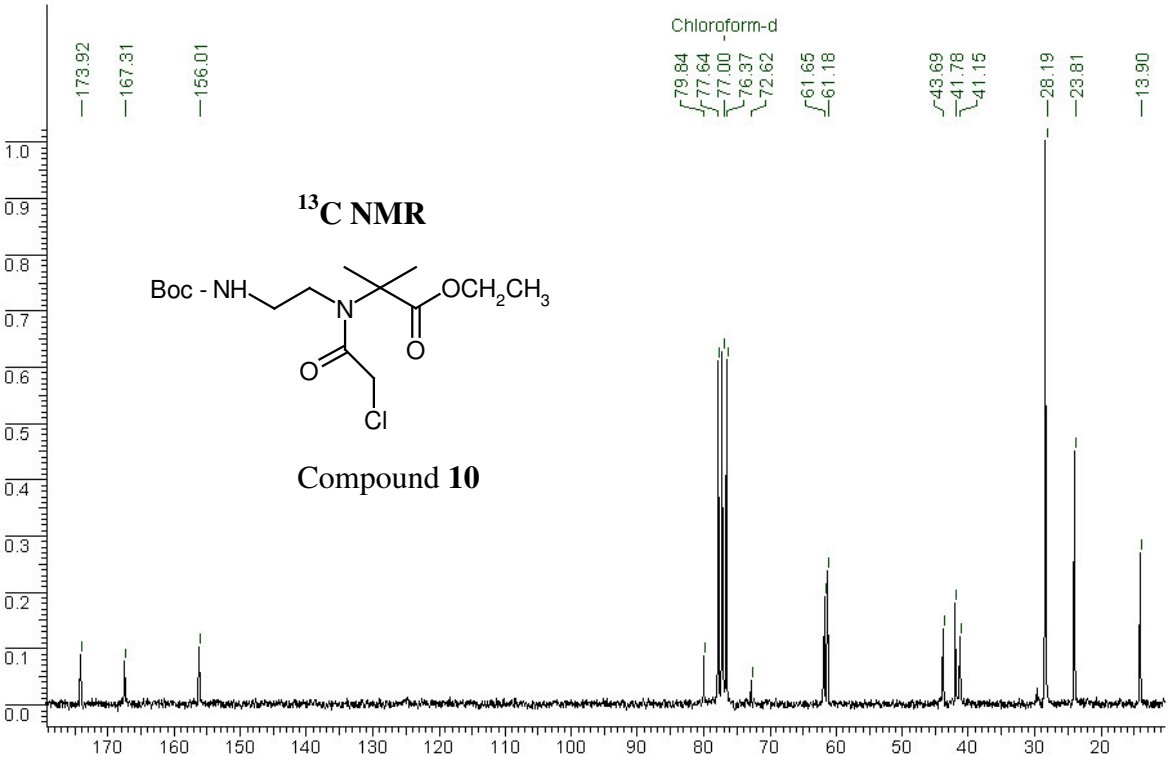

^{13}C NMR

Compound **10**

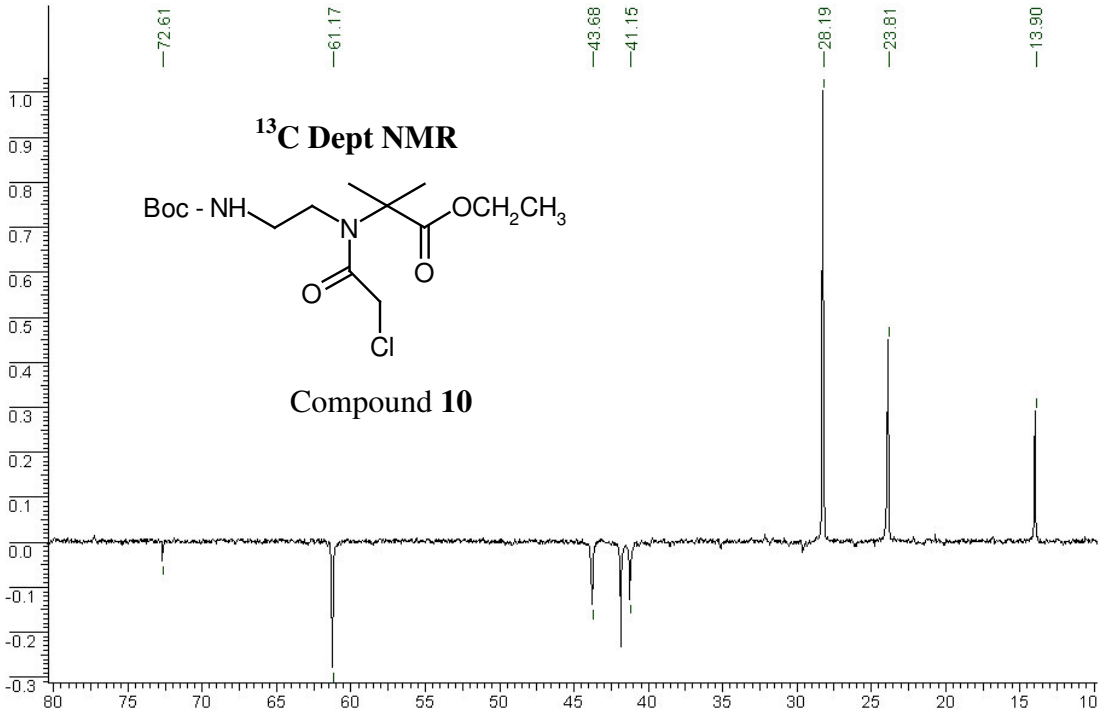

^{13}C Dept NMR

Compound **10**

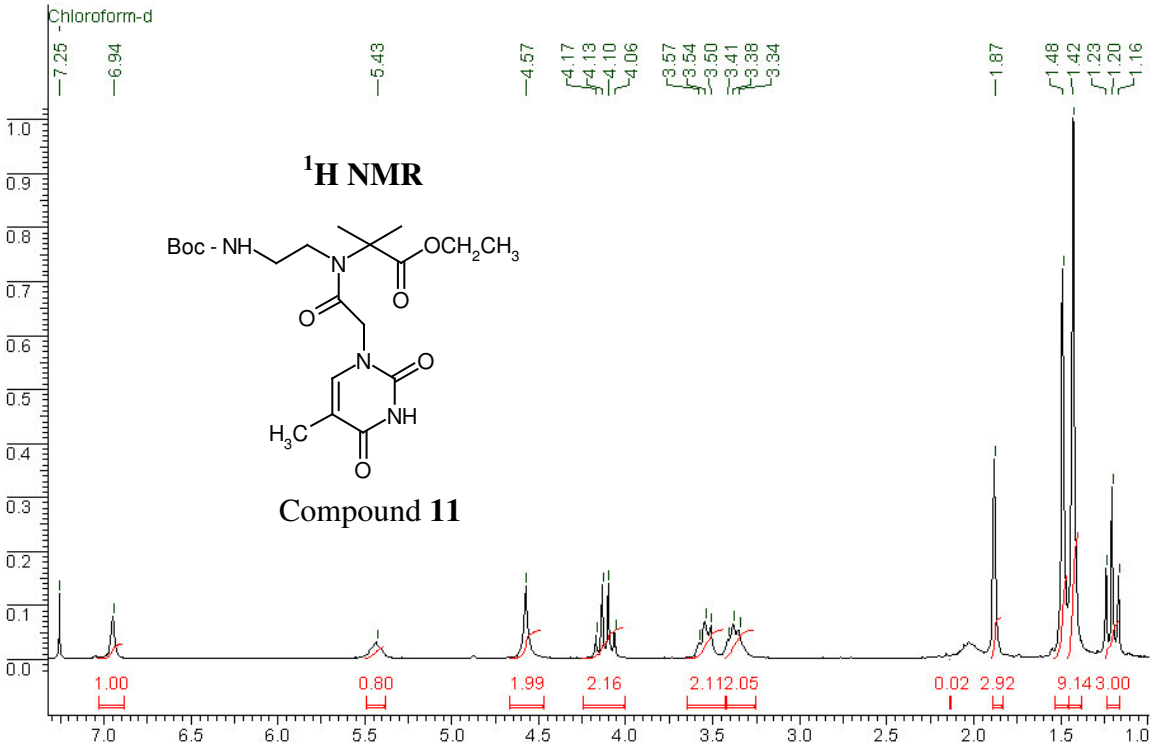

^{1}H NMR

Compound **11**

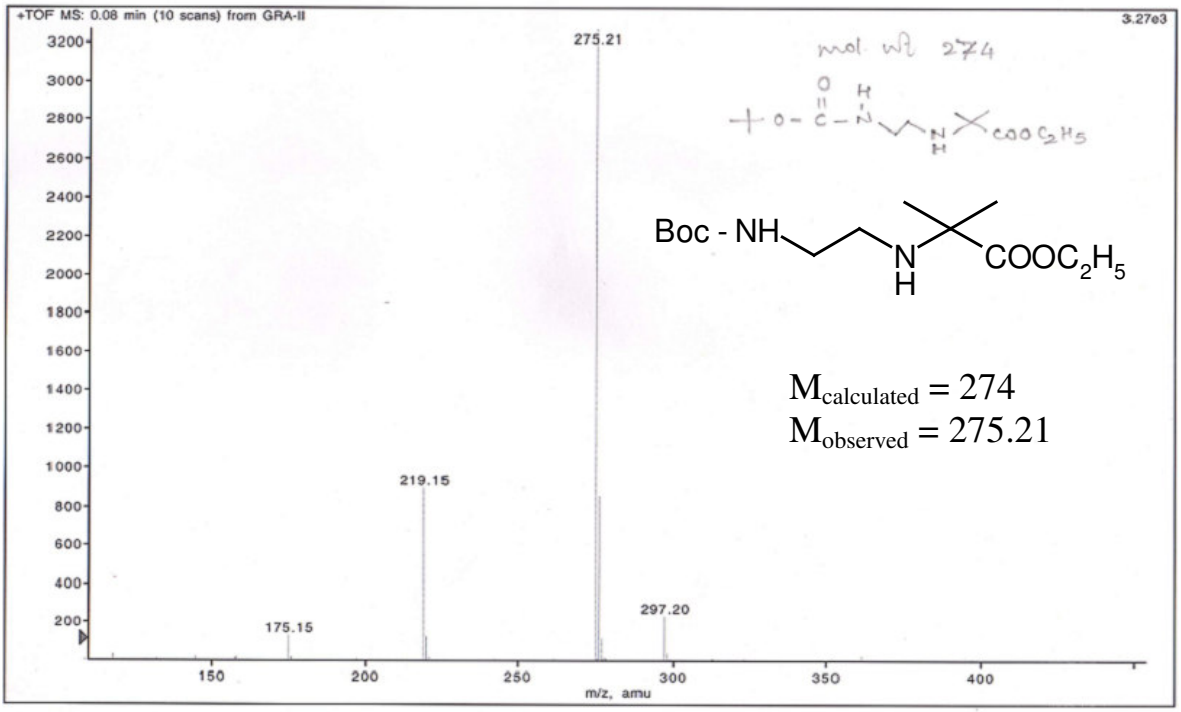

$M_{calculated} = 274$

$M_{observed} = 275.21$

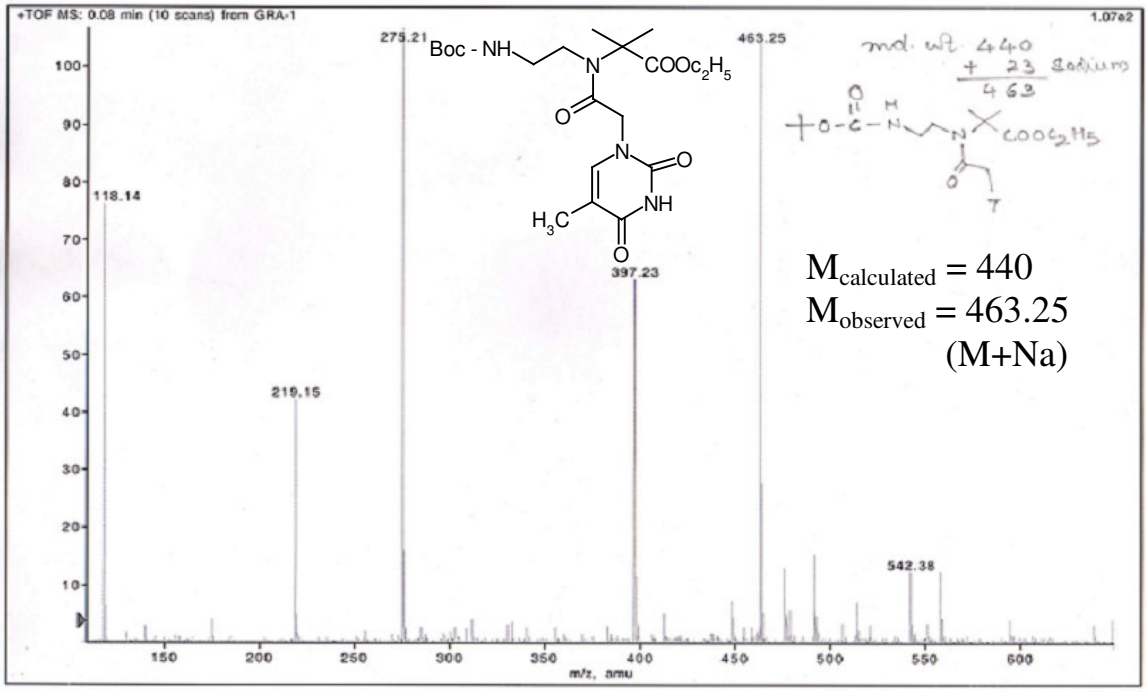

$M_{calculated}$ = 440
$M_{observed}$ = 463.25
(M+Na)

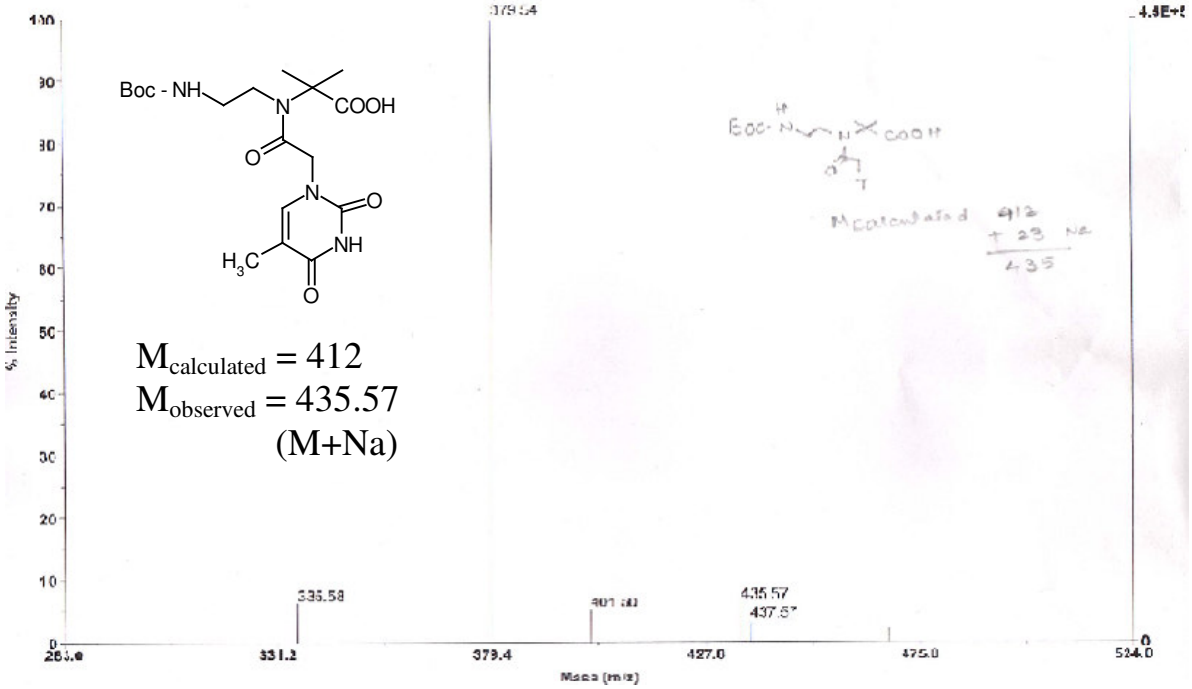

$M_{calculated}$ = 412
$M_{observed}$ = 435.57
(M+Na)

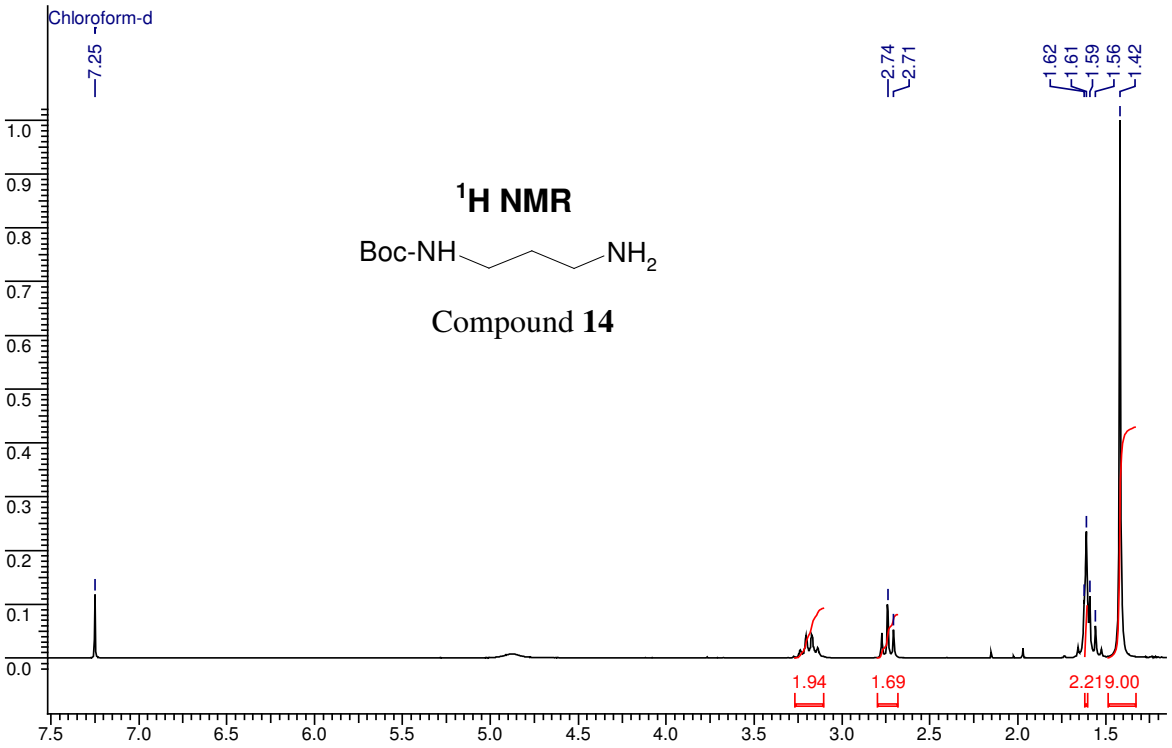

^{1}H NMR

Compound **14**

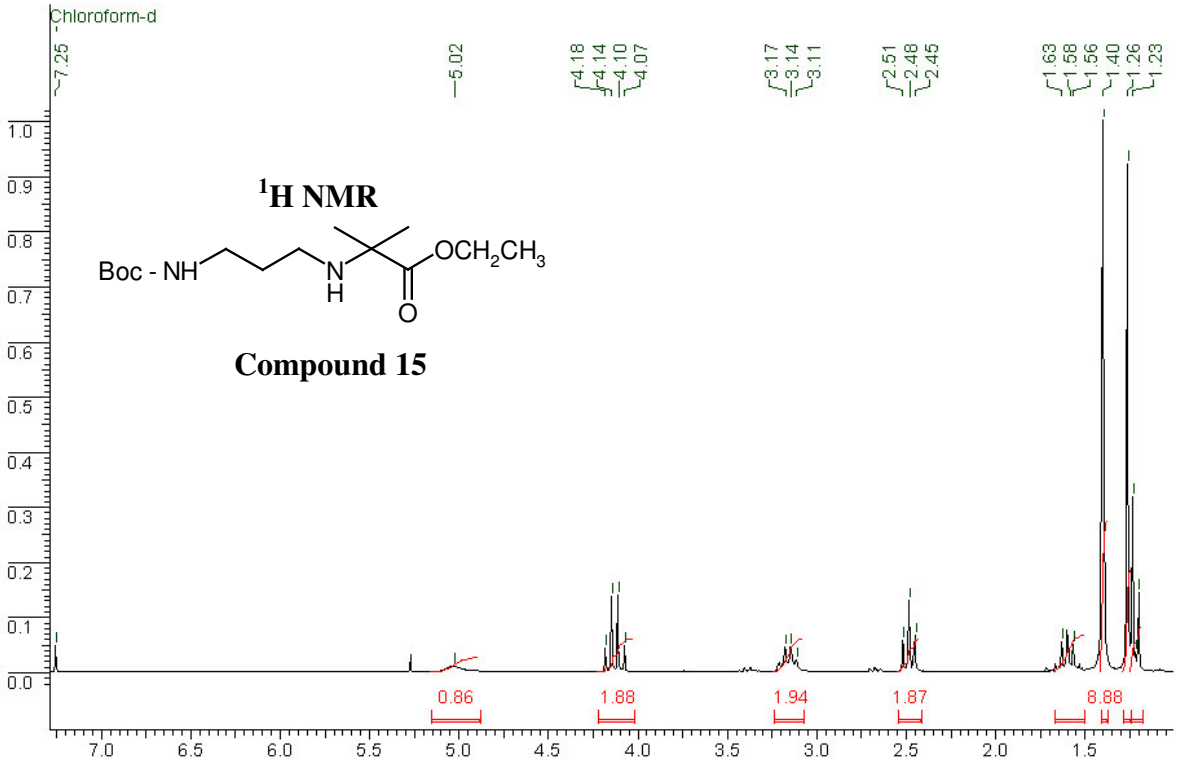

^{1}H NMR

Compound 15

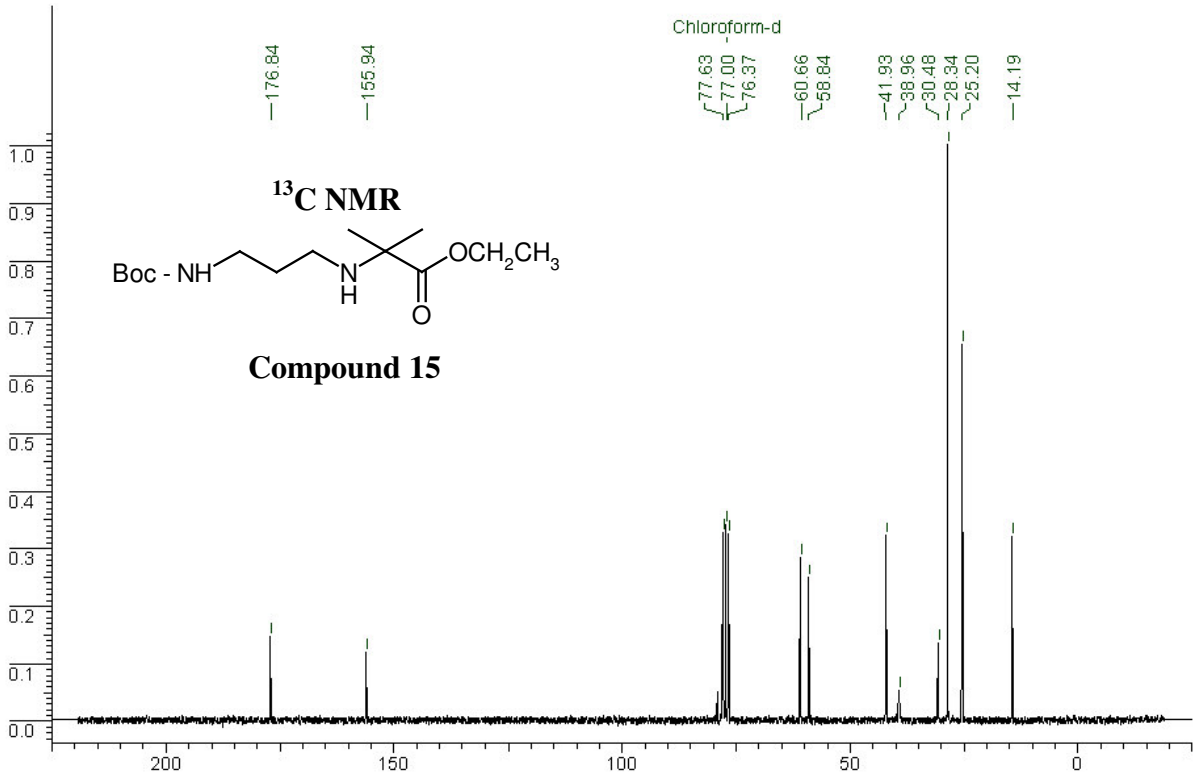

^{13}C NMR

Compound 15

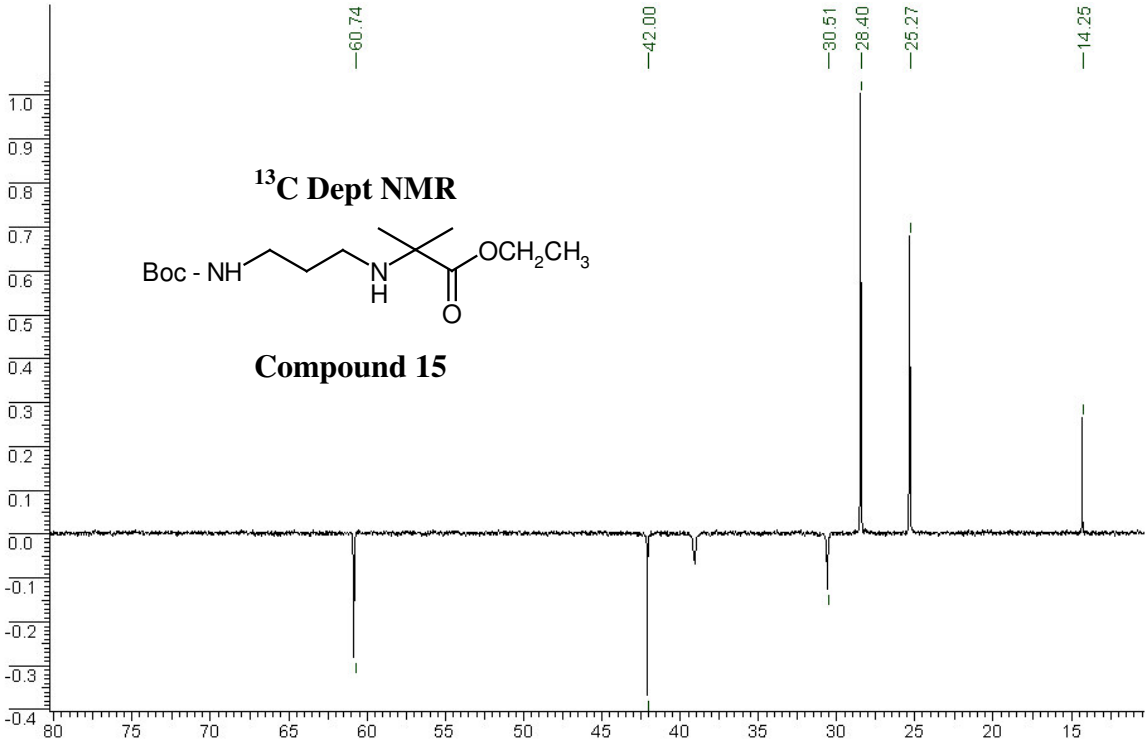

^{13}C Dept NMR

Compound 15

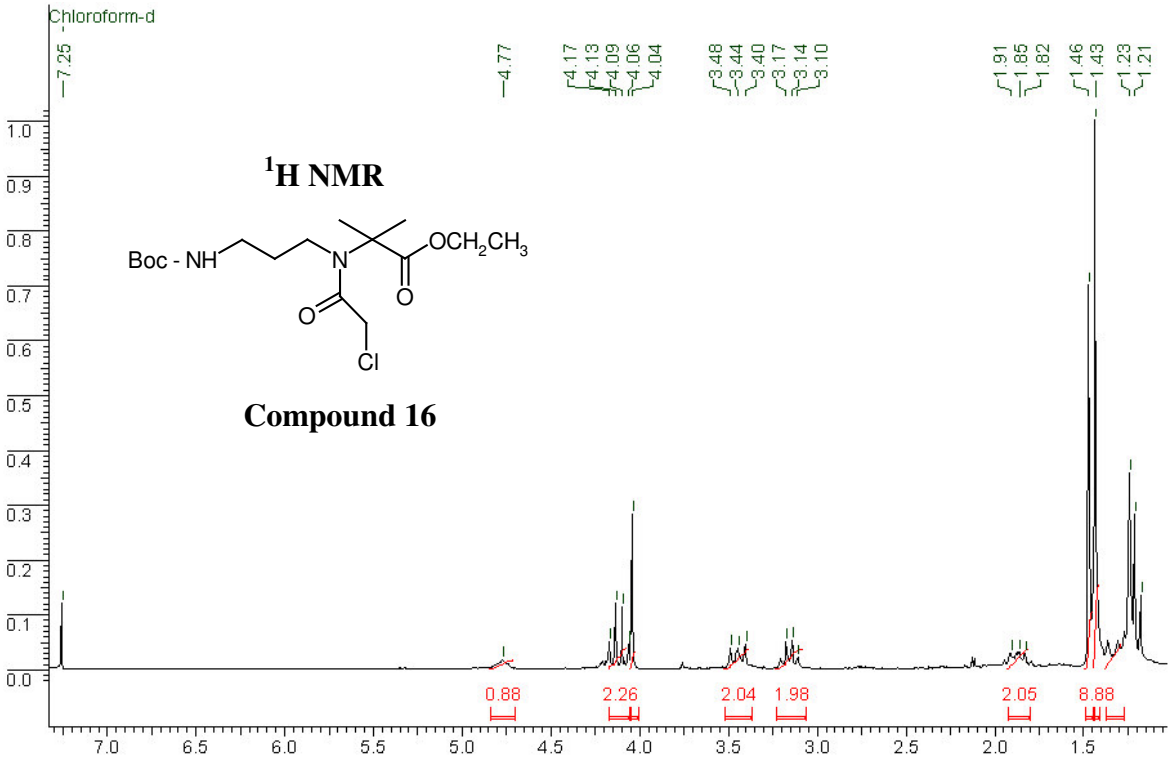

^{1}H NMR

Compound 16

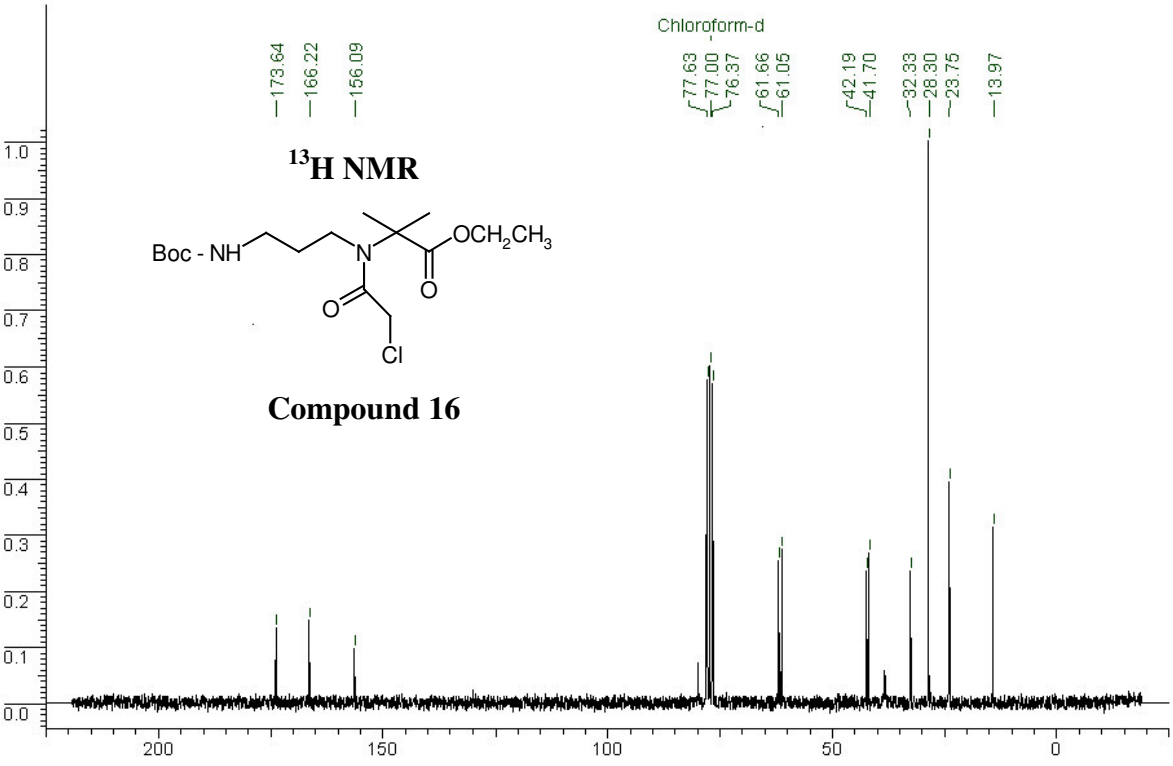

^{13}H NMR

Compound 16

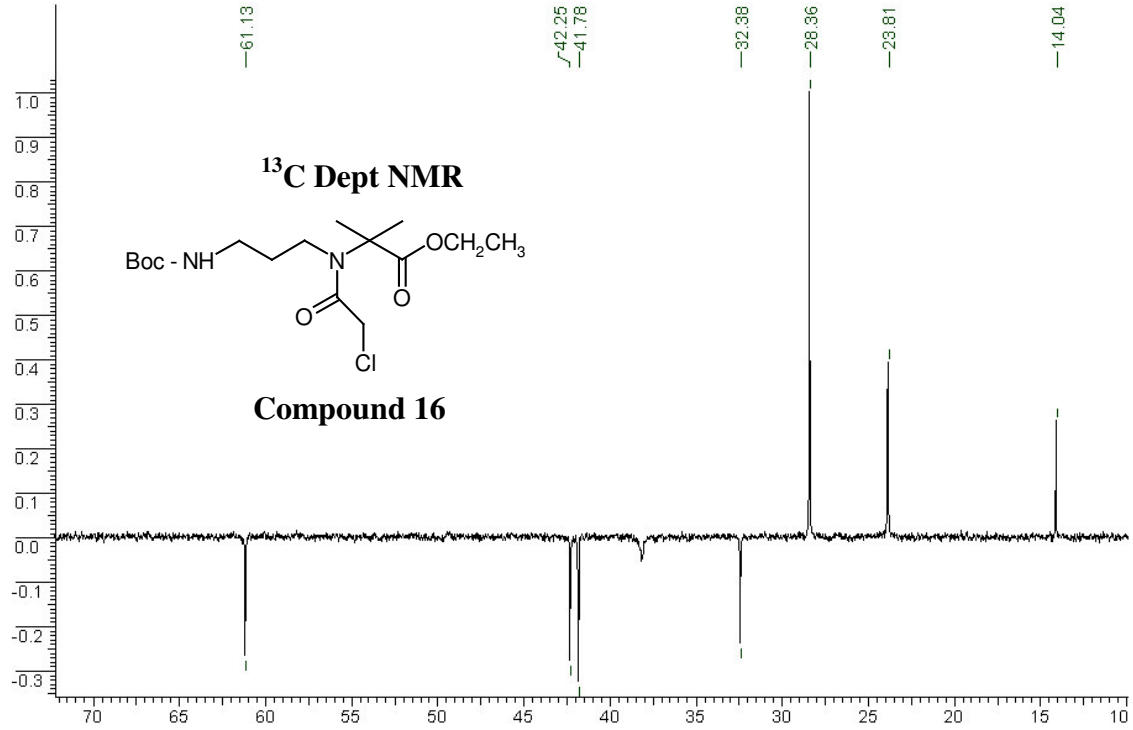
61.13
42.25
41.78
32.38
28.36
23.81
14.04
^{13}C Dept NMR
Boc - NH
N
OCH$_2$CH$_3$
O
O
Cl
Compound 16

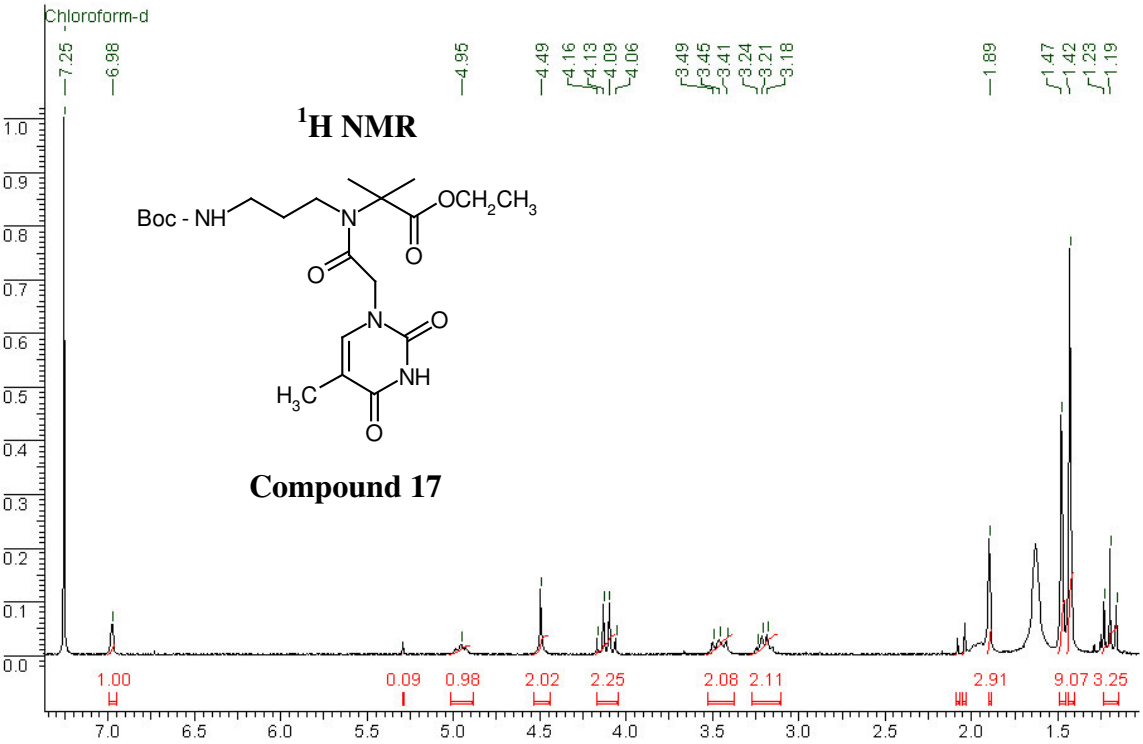
Chloroform-d
7.25
6.98
4.95
4.49
4.16
4.13
4.09
4.06
3.49
3.45
3.41
3.24
3.21
3.18
1.89
1.47
1.42
1.23
1.19
^{1}H NMR
Boc - NH
N
OCH$_2$CH$_3$
O
O
N
O
NH
H$_3$C
O
Compound 17
1.00
0.09
0.98
2.02
2.25
2.08
2.11
2.91
9.07
3.25

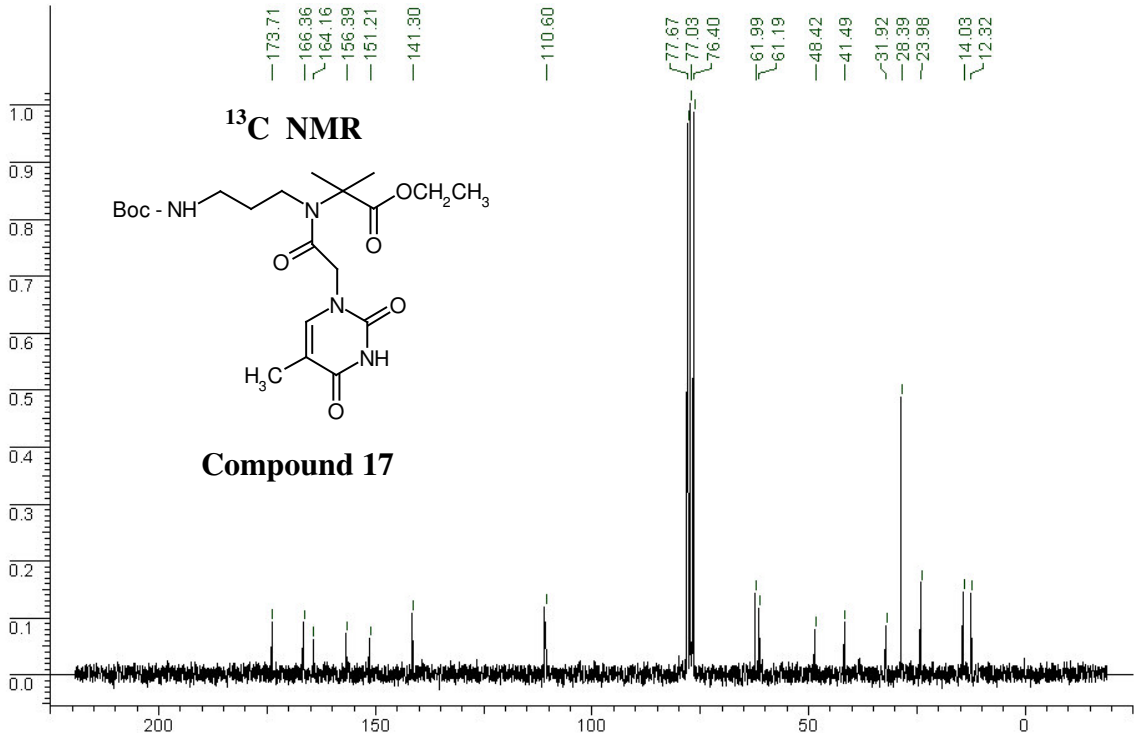

^{13}C NMR

Compound 17

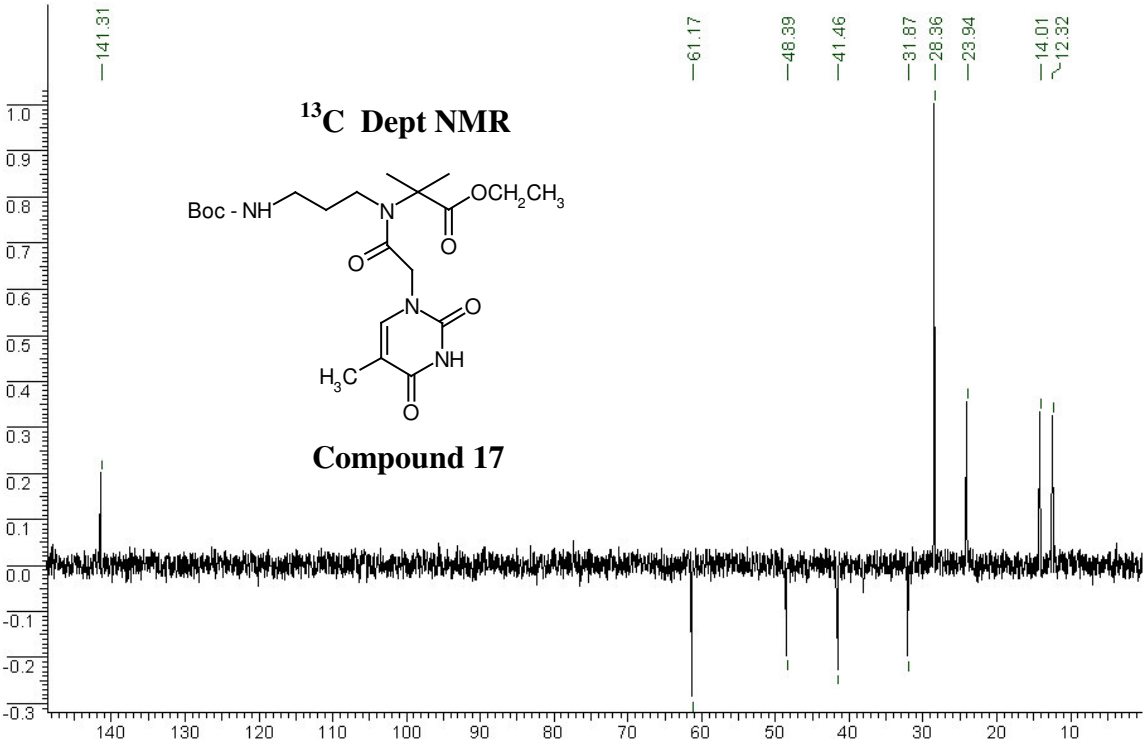

^{13}C Dept NMR

Compound 17

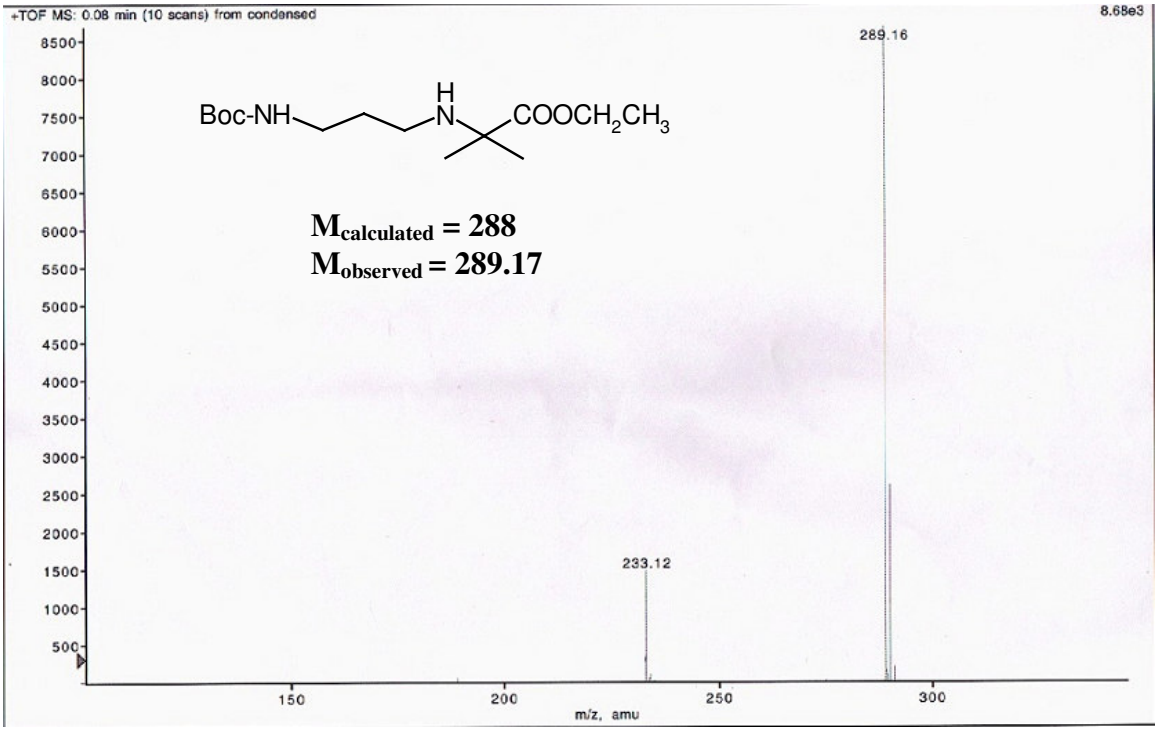

$M_{calculated}$ = 288
$M_{observed}$ = 289.17

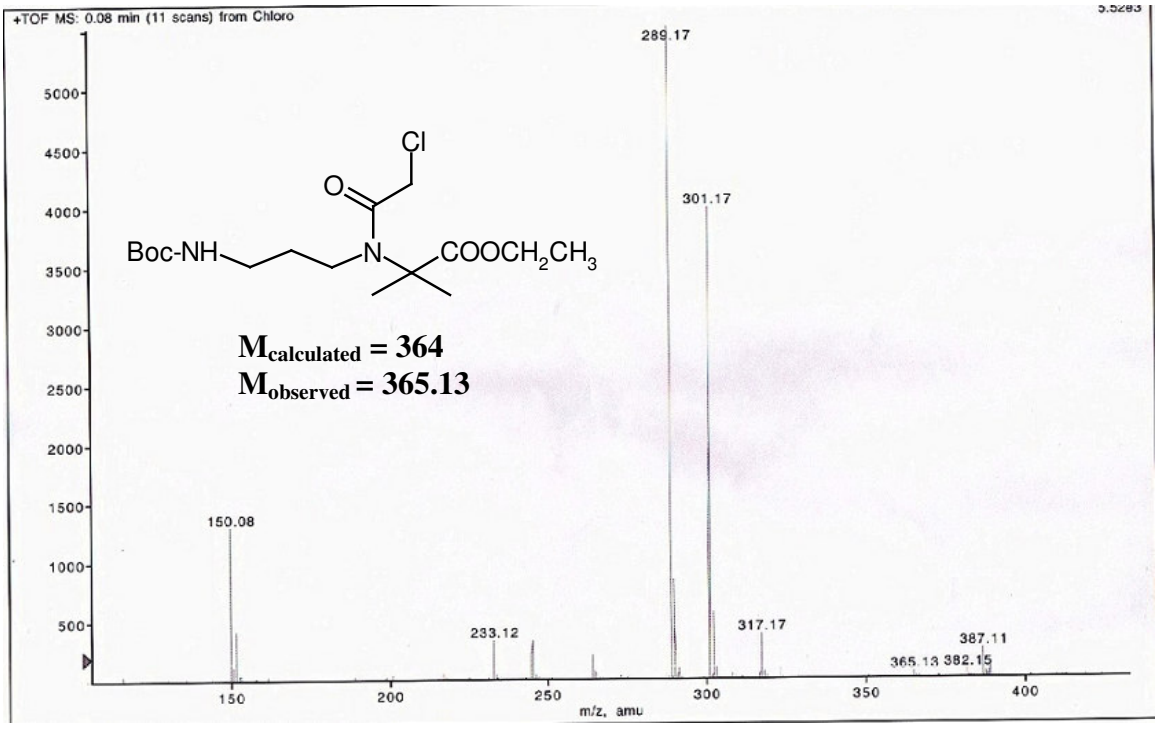

$M_{calculated}$ = 364
$M_{observed}$ = 365.13

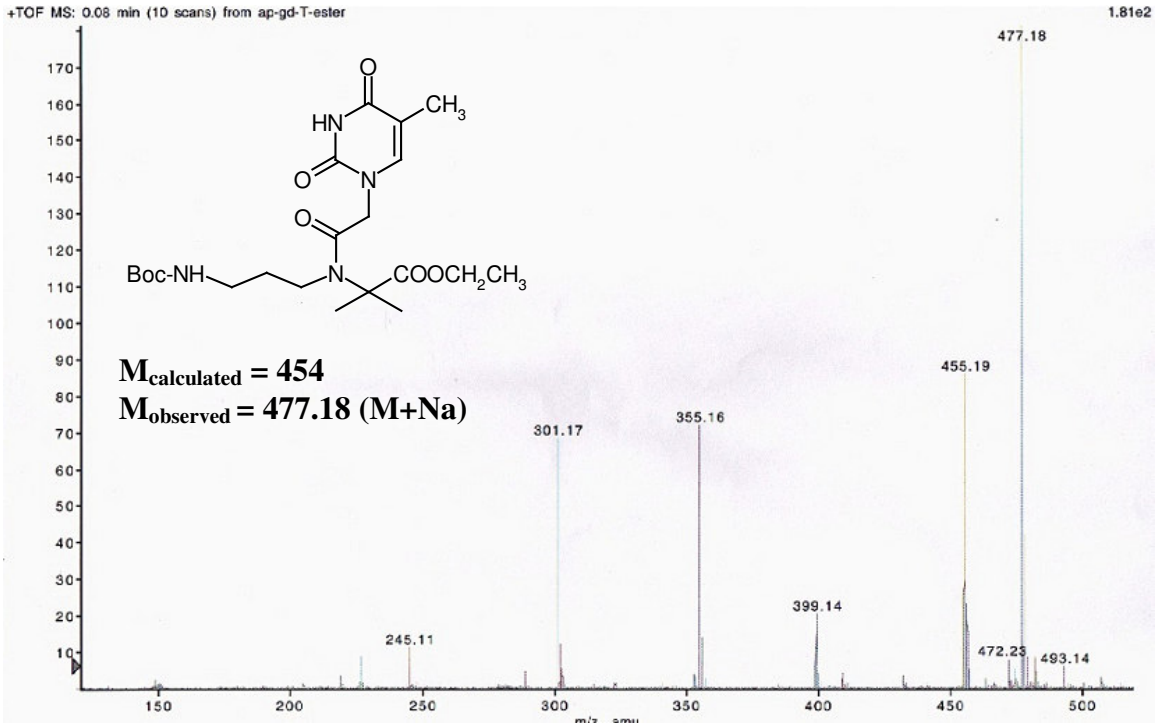
+TOF MS: 0.08 min (10 scans) from ap-gd-T-ester
1.81e2
477.18
455.19
355.16
301.17
399.14
245.11
472.23
493.14
Boc-NH
COOCH2CH3
CH3
HN
O
N
Mcalculated = 454
Mobserved = 477.18 (M+Na)

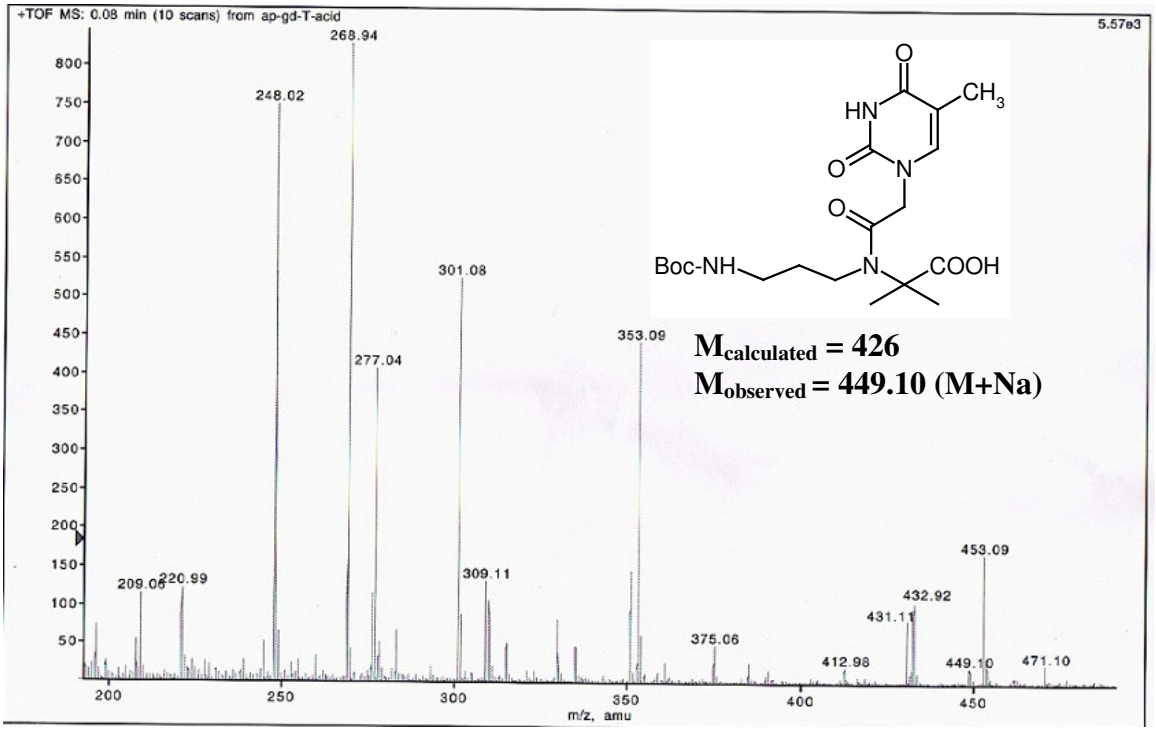
+TOF MS: 0.08 min (10 scans) from ap-gd-T-acid
5.57e3
268.94
248.02
301.08
353.09
277.04
453.09
209.08
220.99
309.11
432.92
431.11
375.06
412.98
449.10
471.10
m/z, amu
Boc-NH
COOH
CH3
HN
O
N
Mcalculated = 426
Mobserved = 449.10 (M+Na)

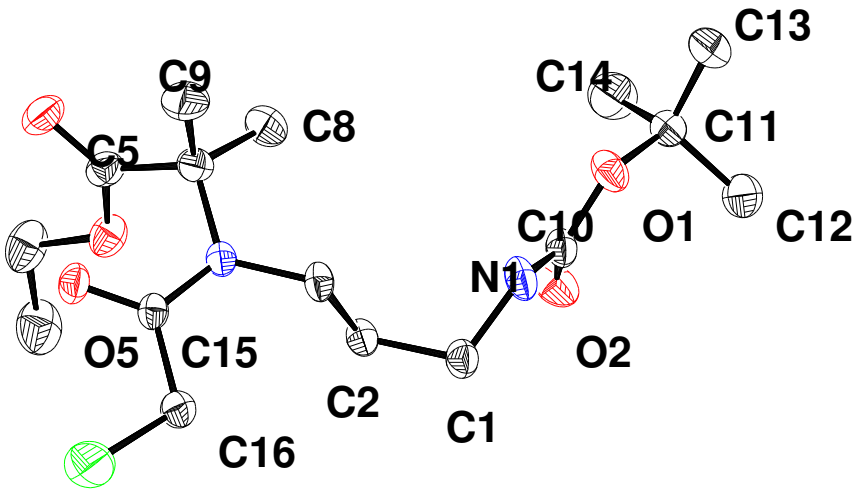

Crystal structure data for Compound **15**

Empirical Formula	$C_{16}H_{29}ClN_2O_5$
Formula weight	364.86
Crystal form, colour	Flat, colourless
Crystal size (mm)	0.34 × 0.16 × 0.14
Wavelength	0.71073
Temperature (K)	293(2) K
Crystal system, space group	Monoclinic, *P*2(1)/*n*
Unit cell Dimensions	a = 12.431 (1) Å; α = 90º b = 11.909 (1) Å; β = 92.26(1) º c = 13.448 (1) Å; γ = 90º
Volume	1989.5 (3) $Å^3$
Z, Calculated density	4, 1.218 Mg/m^3
F(000)	784
Absorption coefficient (μ)	0.22 mm^{-1}
Maximum and minimum transmission	0.970 and 0.930
Reflection collected / unique/ observed	18877 / 3503 / 3131
θ range for data collection	2.3-26.5
Limiting indices	-14⇐h⇒14; -14⇐k⇒14; -15⇐l⇒15
Goodness-of-fit on F^2	1.07
Final R indices [I >2σ(I)]	R1 = 0.047, wR2 = 0.125
R indices [all data]	R1 = 0.0379, wR2 = 0.0920
Data / parameters	3503 / 227
H-atom treatment	From difference Fourier map
Largest diff. Peak and hole (ρ_{max}, & ρ_{min})	0.28 & -0.28 $eÅ^{-3}$

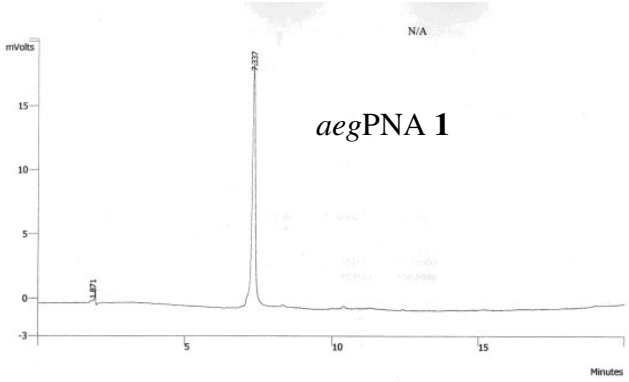

*aeg*PNA **1**

Peak No	Ret. Time (min)	Width 1/2 (sec)	Peak Area (counts)	Result ()
1	1.871	11.6	2935	1.9322
2	7.337	6.7	148949	98.0678
			151884	**100.0000**

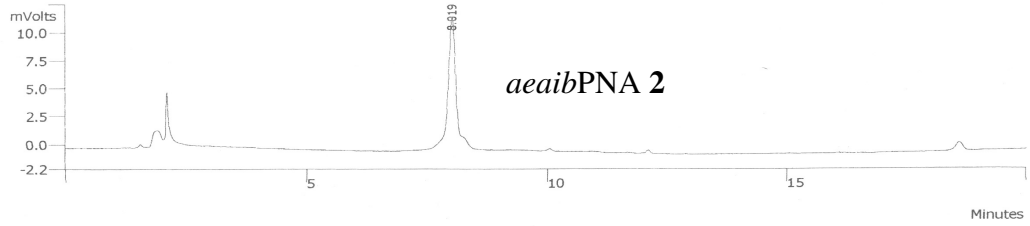

*aeaib*PNA **2**

Peak No	Ret. Time (min)	Width 1/2 (sec)	Peak Area (counts)	Result ()
1	8.019	10.1	154914	100.0000
			154914	**100.0000**

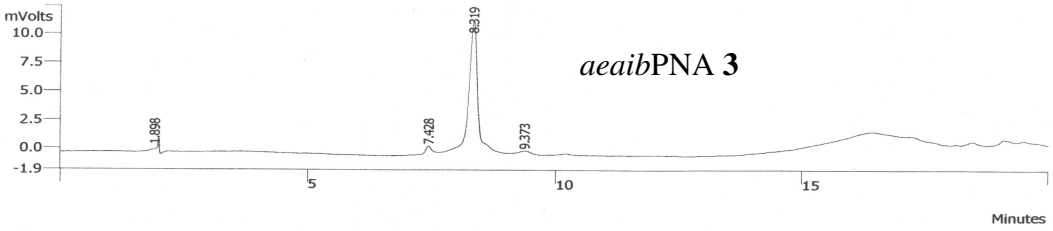

*aeaib*PNA **3**

Peak No	Ret. Time (min)	Width 1/2 (sec)	Peak Area (counts)	Result ()
1	1.898	0.1	3457	1.8842
2	7.428	8.3	8563	4.6674
3	8.319	10.4	167114	91.0930
4	9.373	0.0	4321	2.3555
			183455	**100.0001**

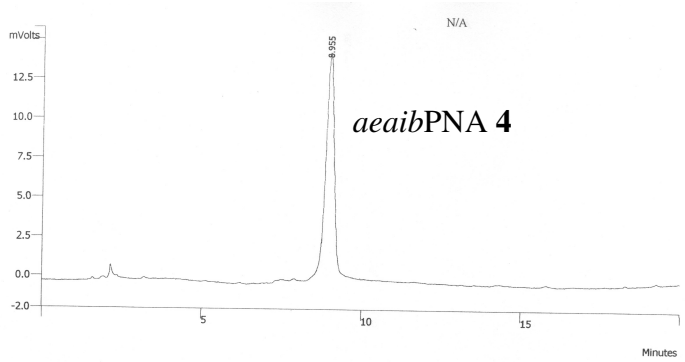

*aeaib*PNA **4**

Peak No	Ret. Time (min)	Width 1/2 (sec)	Peak Area (counts)	Result ()
1	8.955	17.0	286585	100.0000
			286585	**100.0000**

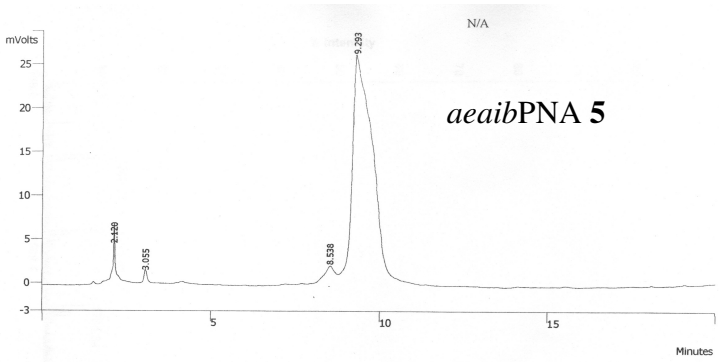

*aeaib*PNA **5**

Peak No	Ret. Time (min)	Width 1/2 (sec)	Peak Area (counts)	Result ()
1	2.120	5.4	49856	4.1305
2	3.055	7.6	34795	2.8827
3	8.538	22.1	46200	3.8276
4	9.293	40.6	1076163	89.1592
			1207014	**100.0000**

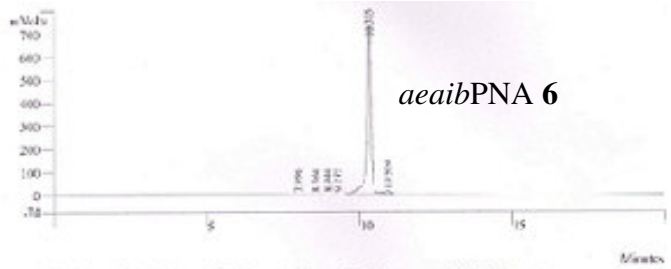

*aeaib*PNA **6**

Peak No	Result ()	Ret Time (min)	Peak Area (counts)	Width 1/2 (sec)
1	0.2382	7.995	1591.5	5.2
2	0.2647	8.568	17644	5.9
3	0.3382	8.944	37291	9.0
4	0.3272	9.272	35219	8.4
5	96.3219	10.315	6434736	5.6
6	2.4880	10.904	139003	3.0
	99.9999		**6668430**	

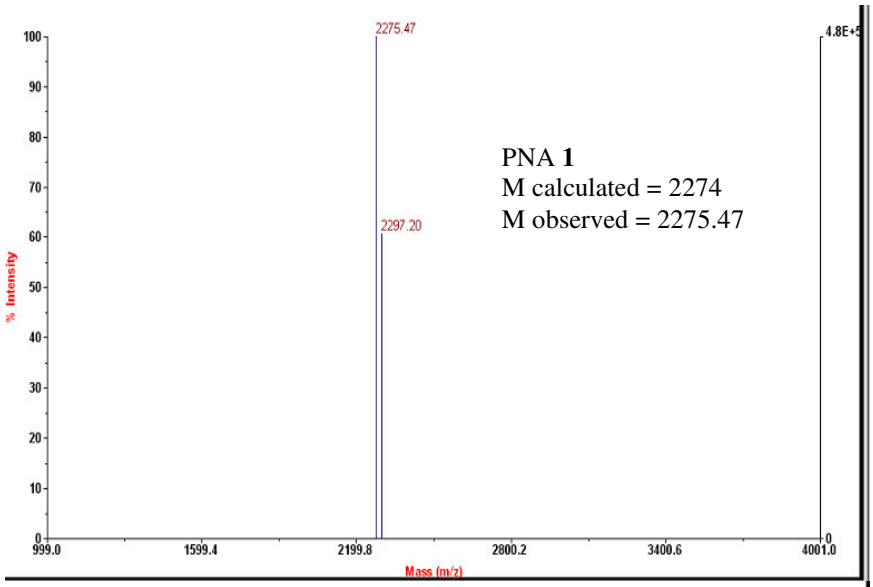

PNA **1**
M calculated = 2274
M observed = 2275.47

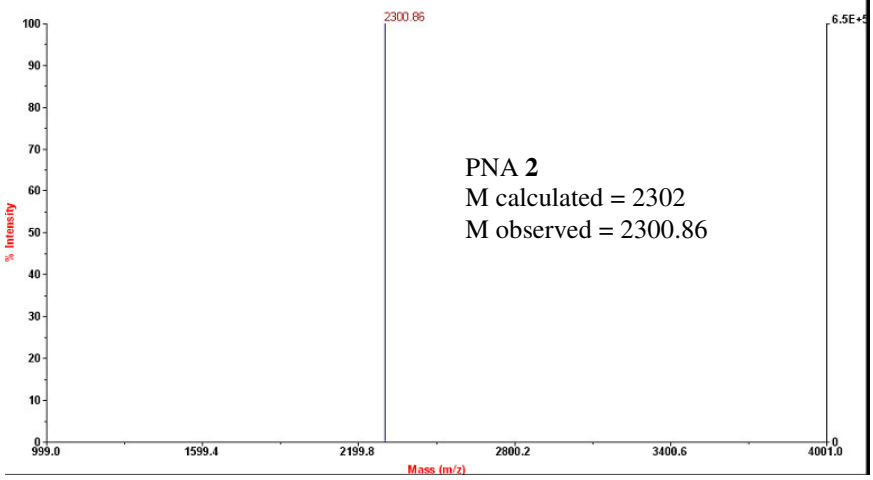

PNA **2**
M calculated = 2302
M observed = 2300.86

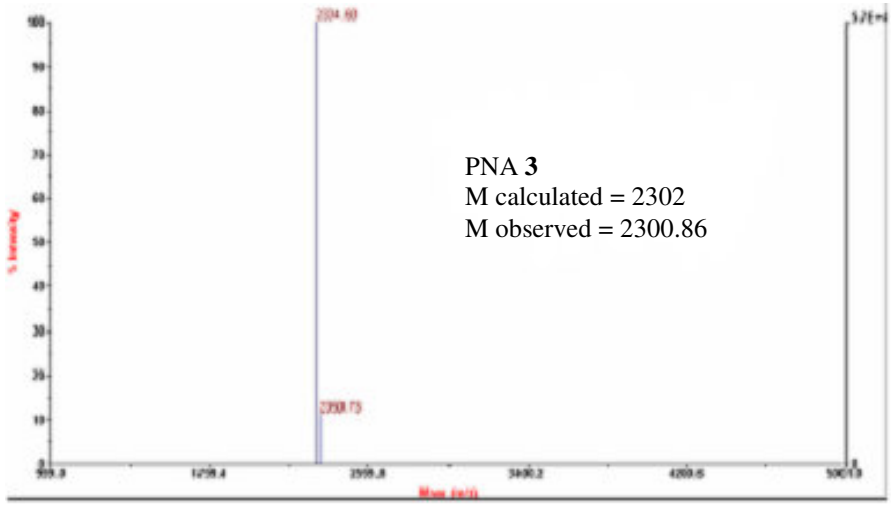

PNA **3**
M calculated = 2302
M observed = 2300.86

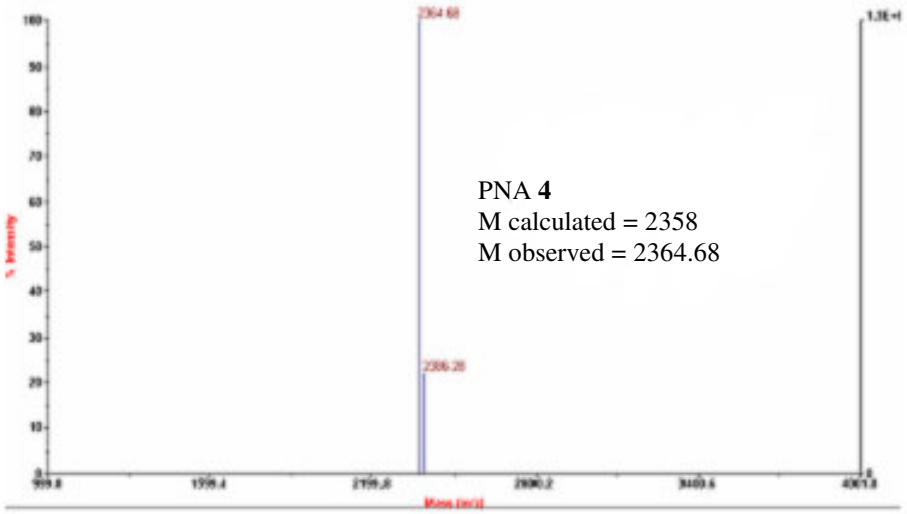

PNA **4**
M calculated = 2358
M observed = 2364.68

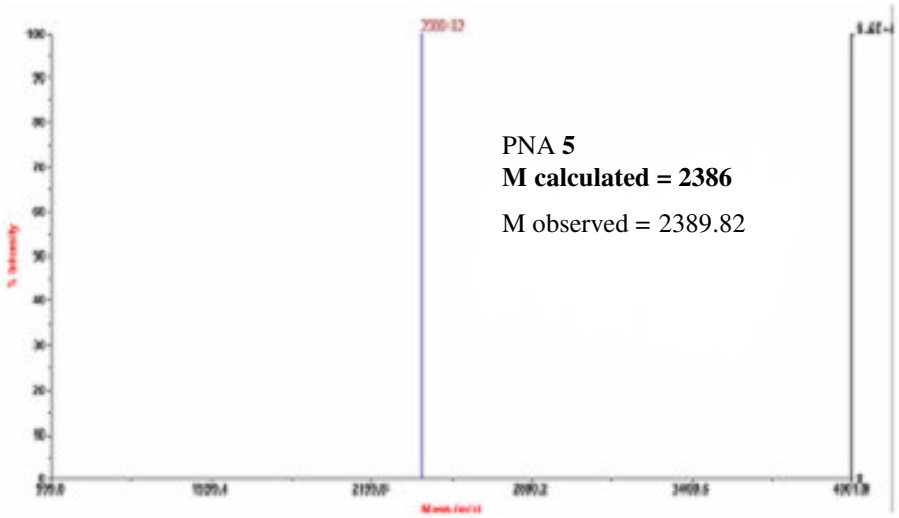

PNA **5**
M calculated = 2386
M observed = 2389.82

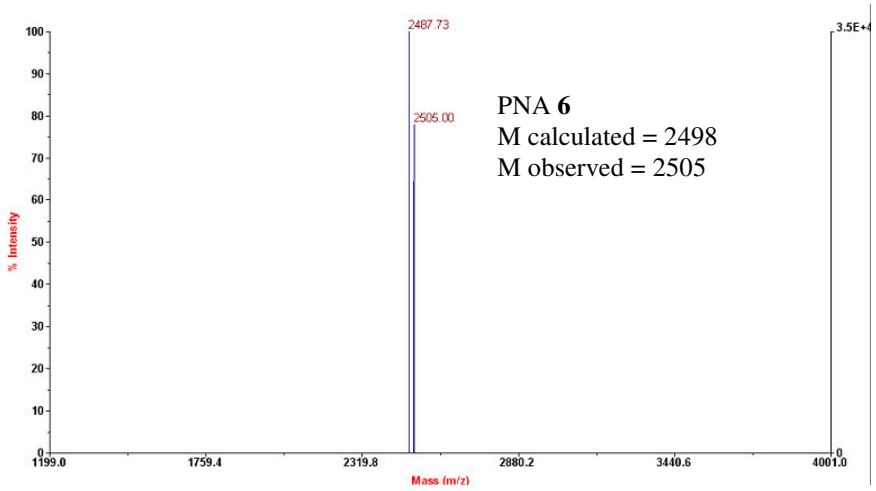

PNA **6**
M calculated = 2498
M observed = 2505

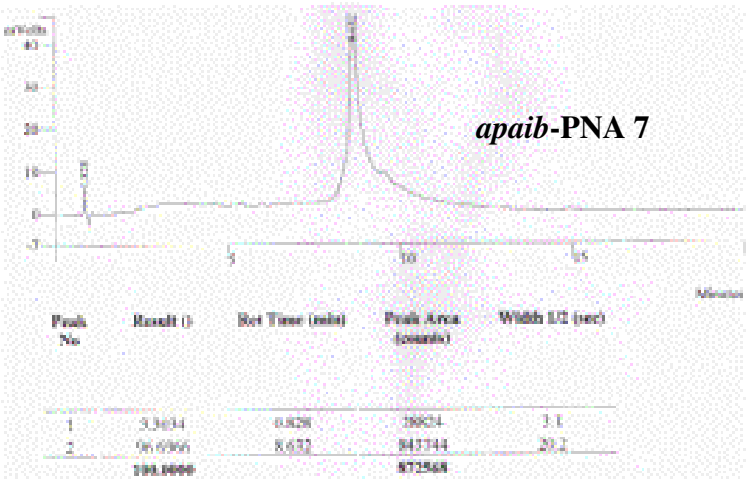

***apaib*-PNA 7**

Peak No	Result ()	Ret Time (min)	Peak Area (counts)	Width 1/2 (sec)
1	3.3034	0.828	28824	3.1
2	96.6966	8.632	843744	20.2
	100.0000		872568	

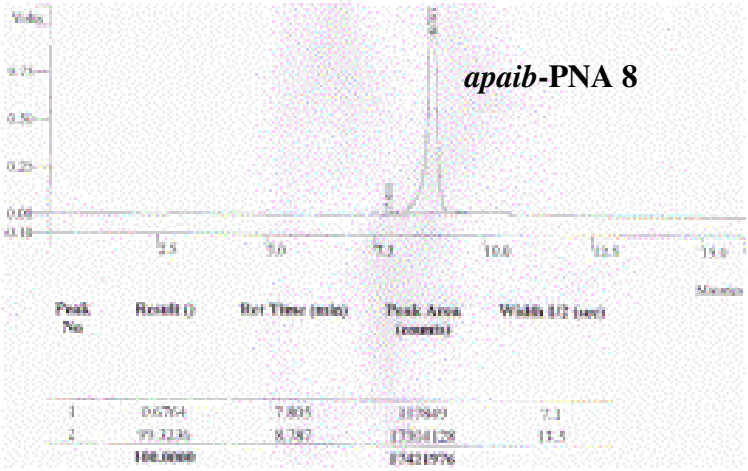

***apaib*-PNA 8**

Peak No	Result ()	Ret Time (min)	Peak Area (counts)	Width 1/2 (sec)
1	0.6794	7.805	117849	7.1
2	99.3206	8.787	17304128	15.5
	100.0000		17421976	

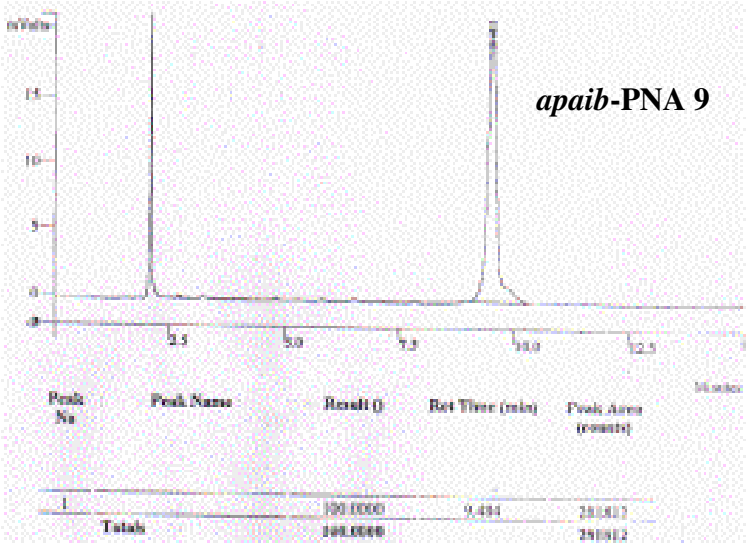

***apaib*-PNA 9**

Peak No	Peak Name	Result ()	Ret Time (min)	Peak Area (counts)
1		100.0000	9.484	281812
Totals		100.0000		281812

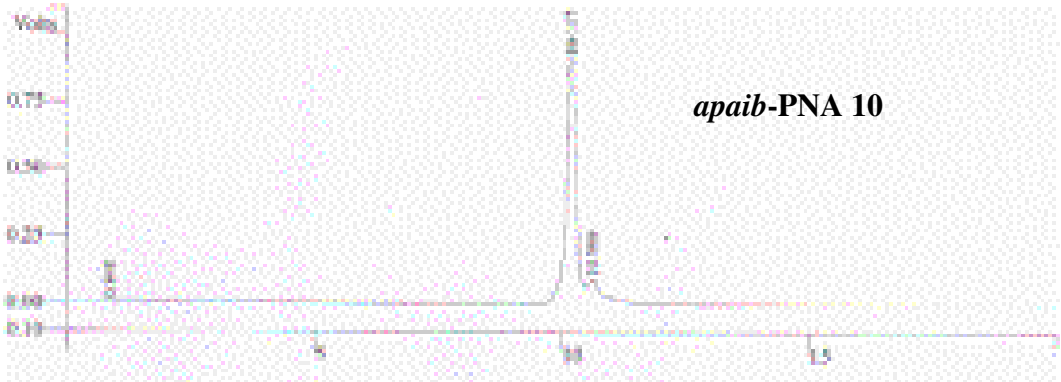

***apaib*-PNA 10**

Peak No	Result ()	Ret Time (min)	Peak Area (counts)	Width 1/2 (sec)
1	0.2312	0.848	29865	4.2
2	97.5216	10.167	13550656	10.4
3	2.4472	10.599	339471	0.0
	100.0000		13759192	

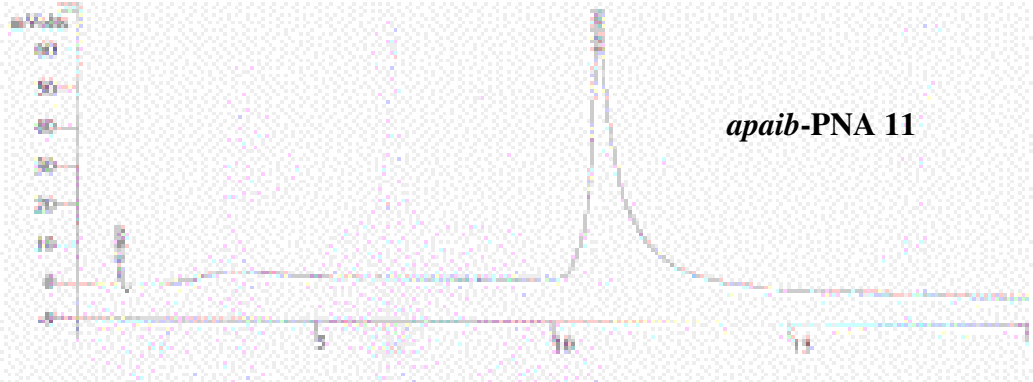

***apaib*-PNA 11**

Peak No	Result ()	Ret Time (min)	Peak Area (counts)	Width 1/2 (sec)
1	1.3601	0.869	35408	5.6
2	98.6399	10.906	3016453	25.4
	100.0000		3052061	

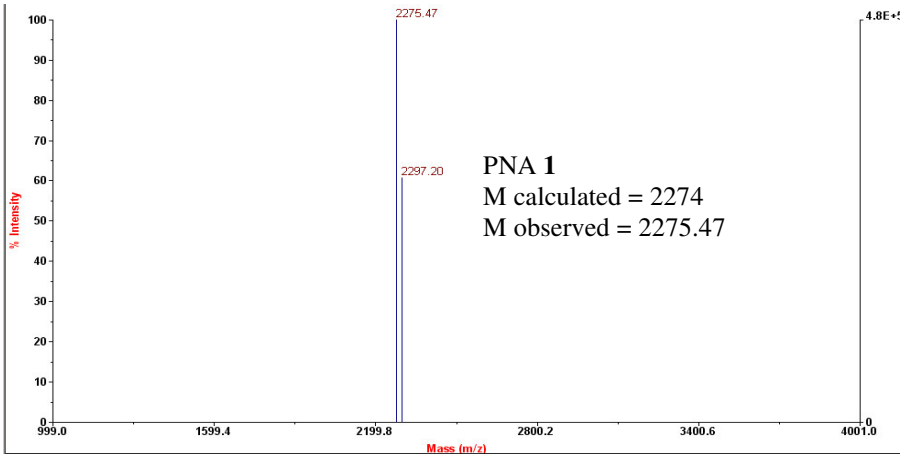

PNA **1**
M calculated = 2274
M observed = 2275.47

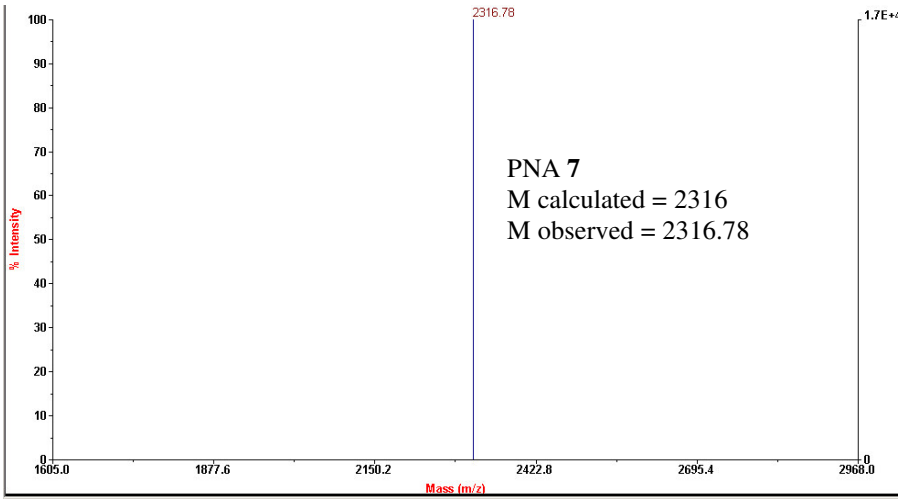

PNA **7**
M calculated = 2316
M observed = 2316.78

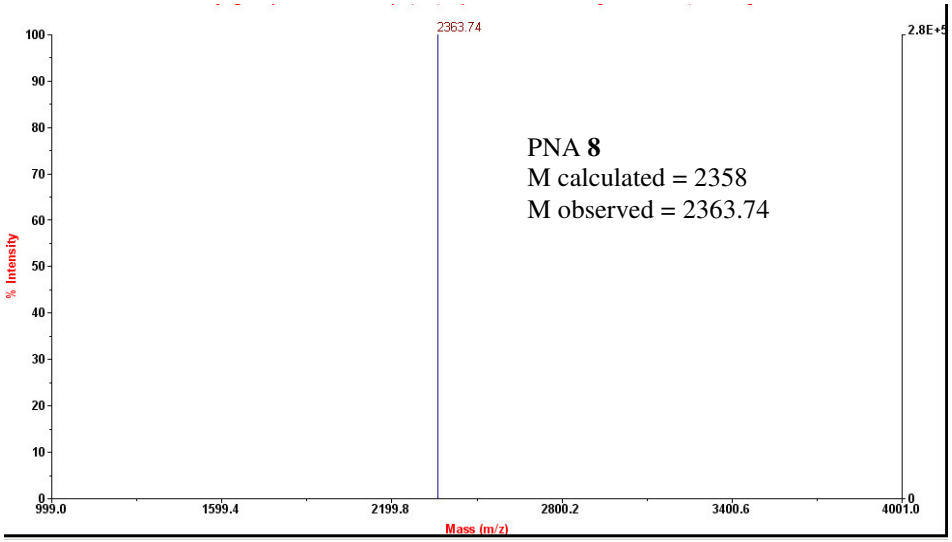

PNA **8**
M calculated = 2358
M observed = 2363.74

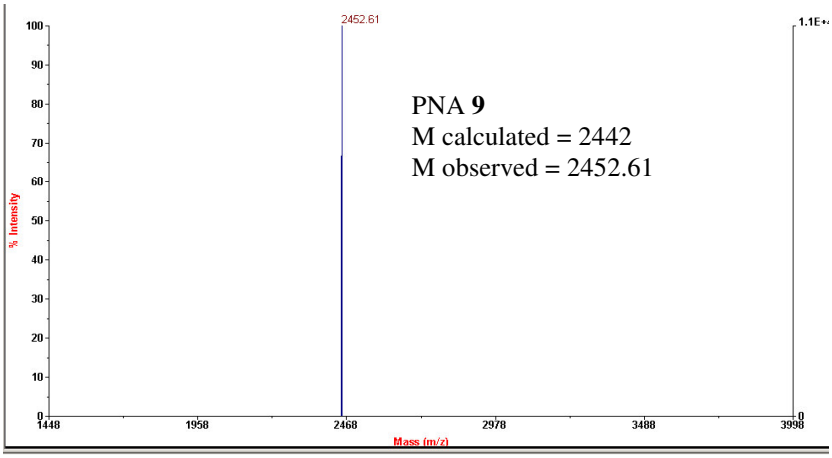

PNA **9**
M calculated = 2442
M observed = 2452.61

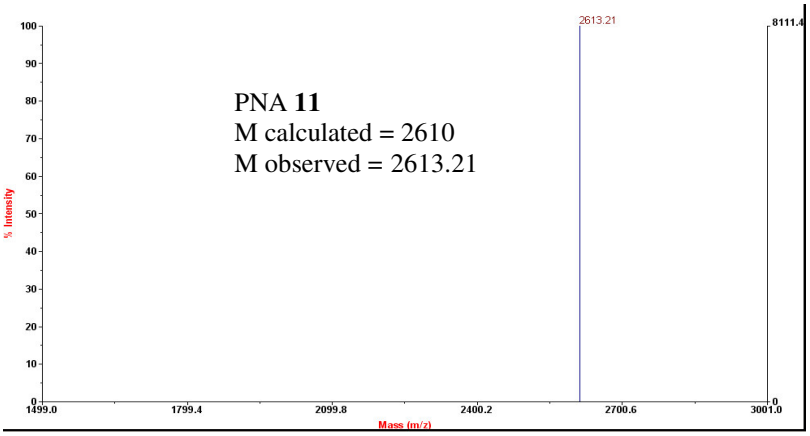

PNA **11**
M calculated = 2610
M observed = 2613.21

***aeg*-PNA 12**

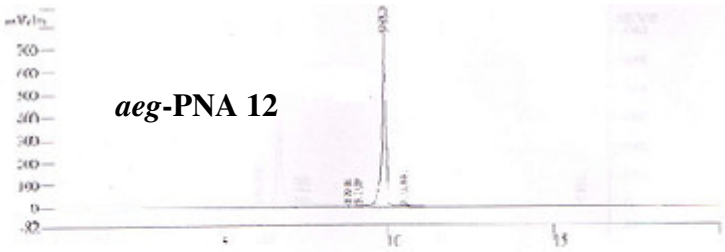

Minutes

Peak No	Result ()	Ret Time (min)	Peak Area (counts)	Width W2 (sec)
1	0.4135	5.805	26641	7.8
2	0.4898	9.102	31511	8.3
3	96.3502	9.360	620930	5.0
4	2.7251	10.481	17544	3.0
	100.0000		643626	

***aeaib*-PNA 13**

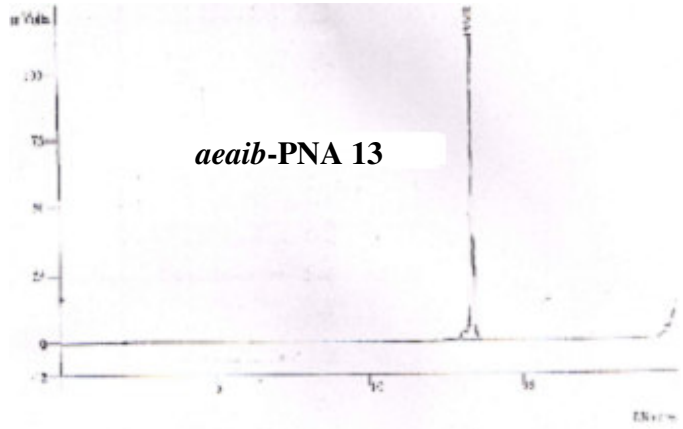

Peak No	Peak Name	Result %	Ret Time (min)	Peak Area (counts)
1		100.0000	13.848	86240
	Totals	100.0000		86240

***apaib*-PNA 14**

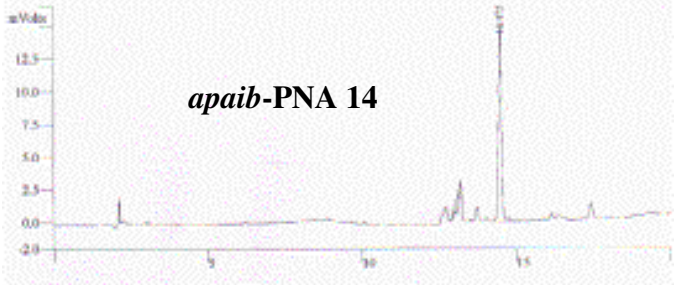

Minutes

Peak No	Peak Name	Result ()	Ret Time (min)	Peak Area (counts)
1		100.0000	14.472	93627
	Totals	100.0000		93627

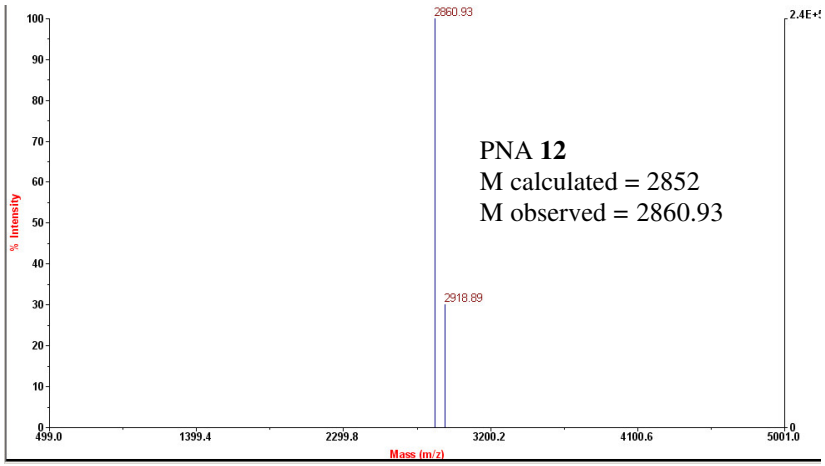

PNA **12**
M calculated = 2852
M observed = 2860.93

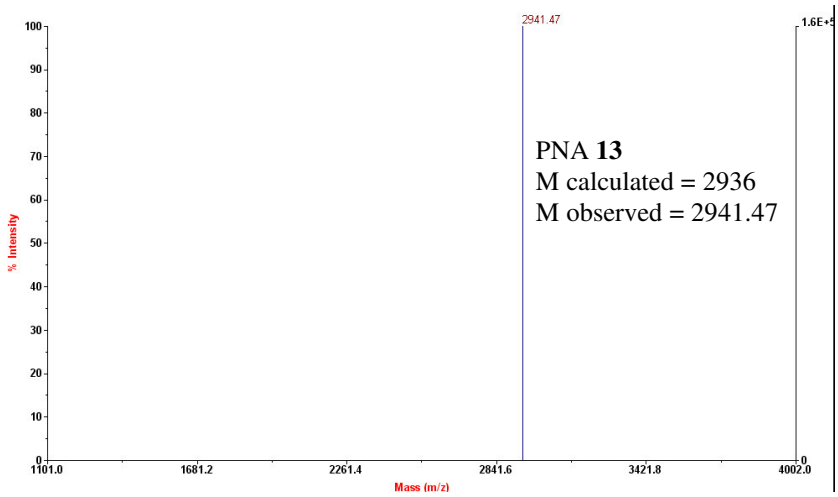

PNA **13**
M calculated = 2936
M observed = 2941.47

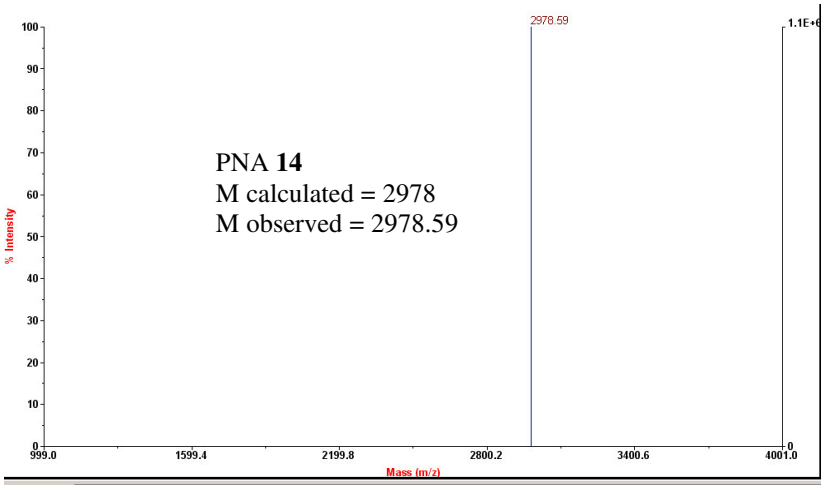

PNA **14**
M calculated = 2978
M observed = 2978.59

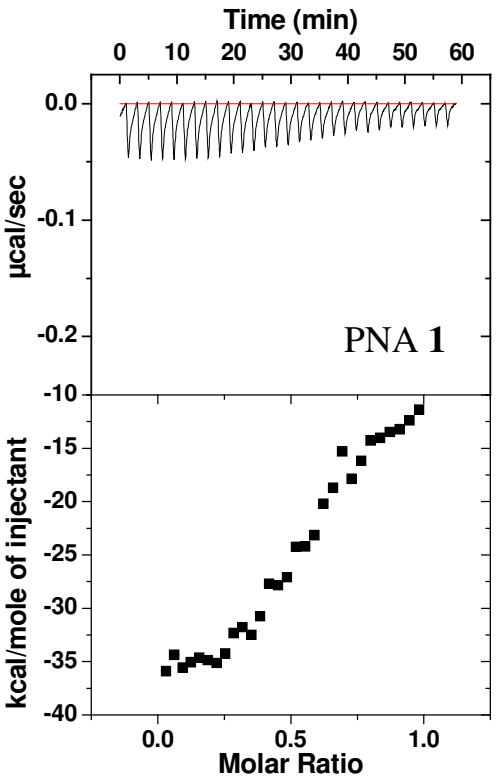
Time (min)
0 10 20 30 40 50 60
µcal/sec
0.0
-0.1
-0.2
PNA 1
kcal/mole of injectant
-10
-15
-20
-25
-30
-35
-40
0.0 0.5 1.0
Molar Ratio

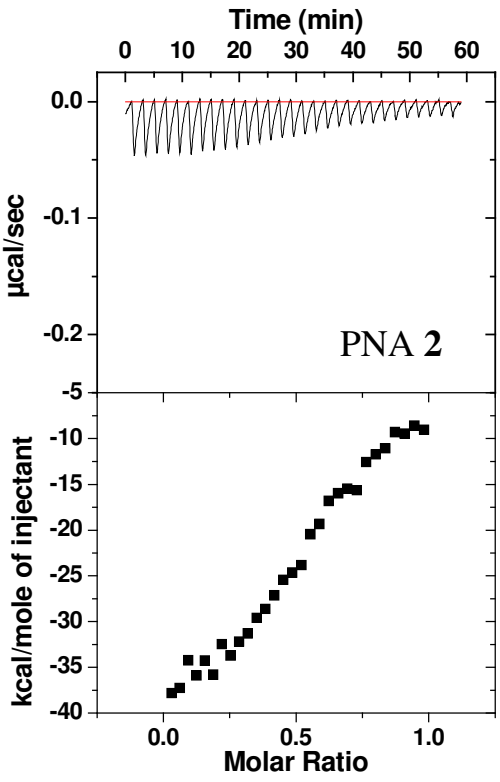
Time (min)
0 10 20 30 40 50 60
µcal/sec
0.0
-0.1
-0.2
PNA 2
kcal/mole of injectant
-5
-10
-15
-20
-25
-30
-35
-40
0.0 0.5 1.0
Molar Ratio

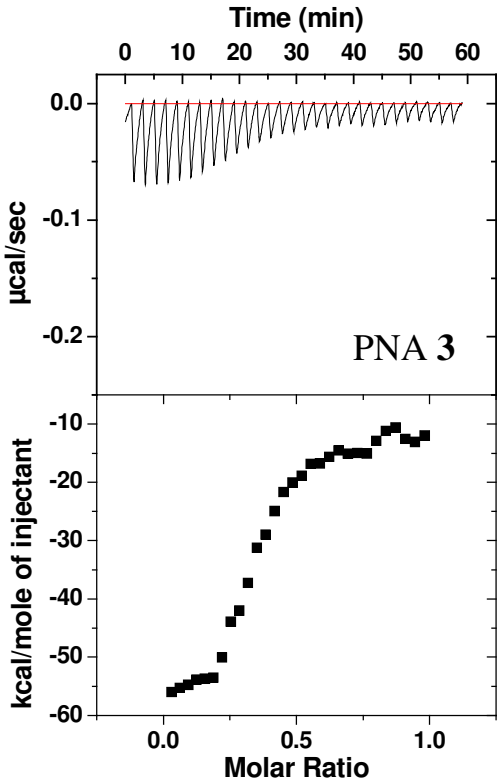
Time (min)
0 10 20 30 40 50 60
µcal/sec
0.0
-0.1
-0.2
PNA 3
kcal/mole of injectant
-10
-20
-30
-40
-50
-60
0.0 0.5 1.0
Molar Ratio

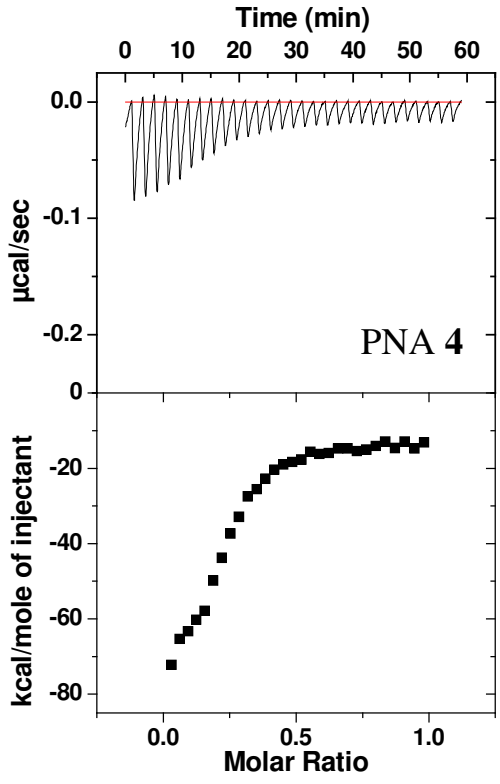
Time (min)
0 10 20 30 40 50 60
µcal/sec
0.0
-0.1
-0.2
0
PNA 4
kcal/mole of injectant
-20
-40
-60
-80
0.0 0.5 1.0
Molar Ratio

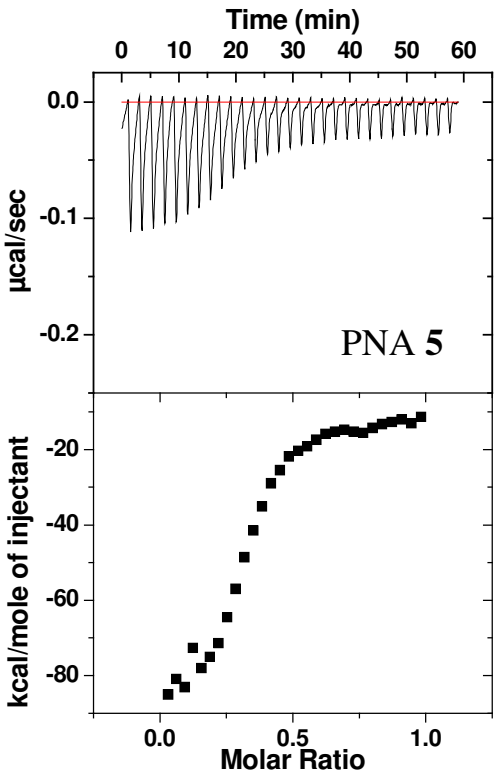
Time (min)
0 10 20 30 40 50 60
µcal/sec
0.0
-0.1
-0.2
PNA 5
kcal/mole of injectant
-20
-40
-60
-80
0.0 0.5 1.0
Molar Ratio

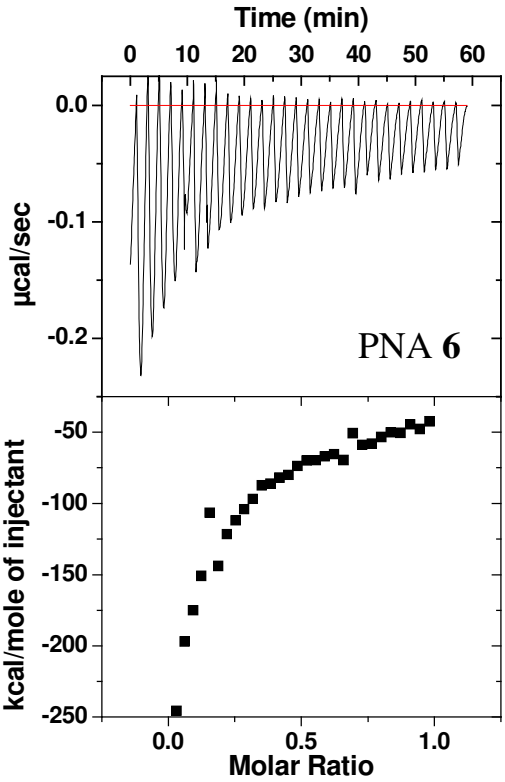
Time (min)
0 10 20 30 40 50 60
µcal/sec
0.0
-0.1
-0.2
PNA 6
kcal/mole of injectant
-50
-100
-150
-200
-250
0.0 0.5 1.0
Molar Ratio

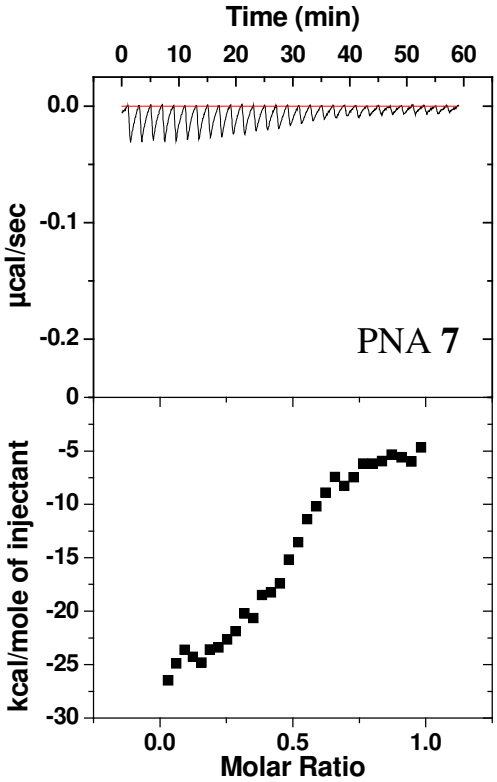
Time (min)
0 10 20 30 40 50 60
µcal/sec
0.0
-0.1
-0.2
0
PNA 7
kcal/mole of injectant
-5
-10
-15
-20
-25
-30
0.0 0.5 1.0
Molar Ratio

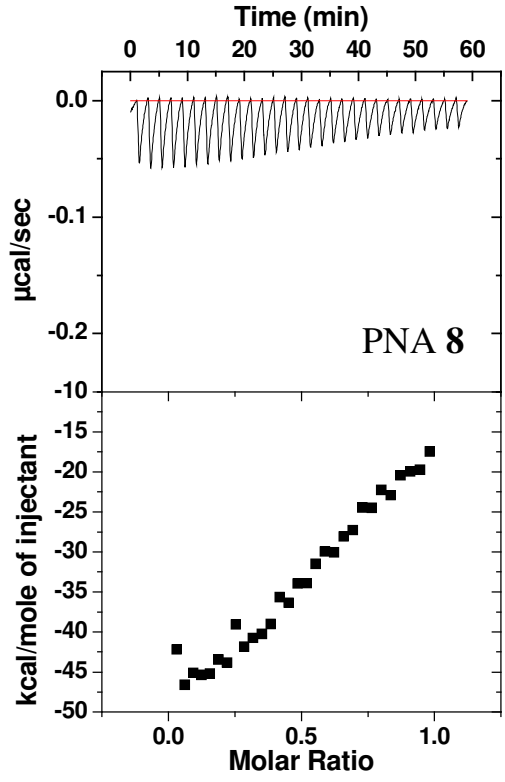
Time (min)
0 10 20 30 40 50 60
µcal/sec
0.0
-0.1
-0.2
-10
PNA 8
kcal/mole of injectant
-15
-20
-25
-30
-35
-40
-45
-50
0.0 0.5 1.0
Molar Ratio

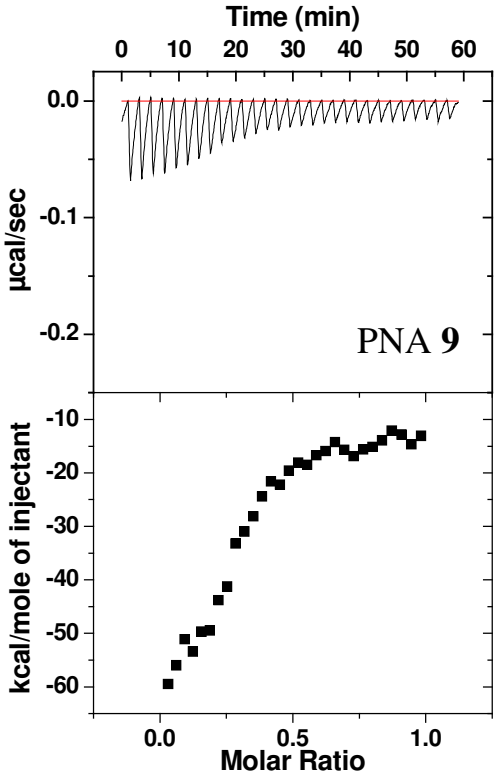
Time (min)
0 10 20 30 40 50 60
µcal/sec
0.0
-0.1
-0.2
PNA 9
kcal/mole of injectant
-10
-20
-30
-40
-50
-60
0.0 0.5 1.0
Molar Ratio

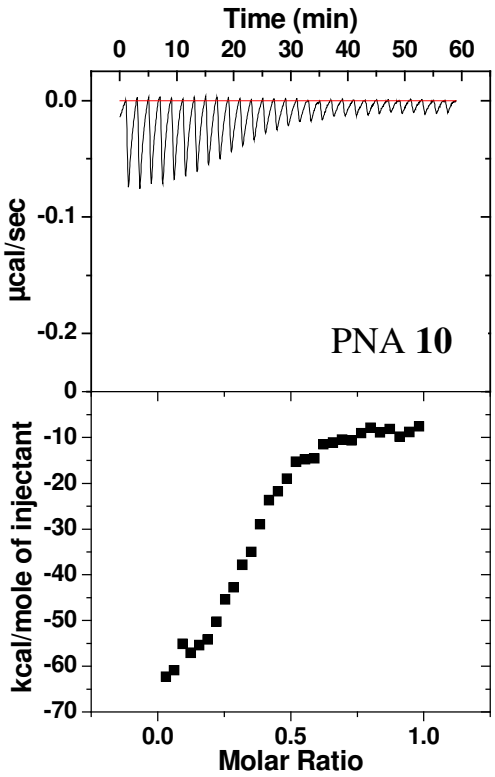
Time (min)
0 10 20 30 40 50 60
µcal/sec
0.0
-0.1
-0.2
PNA 10
kcal/mole of injectant
0
-10
-20
-30
-40
-50
-60
-70
0.0 0.5 1.0
Molar Ratio

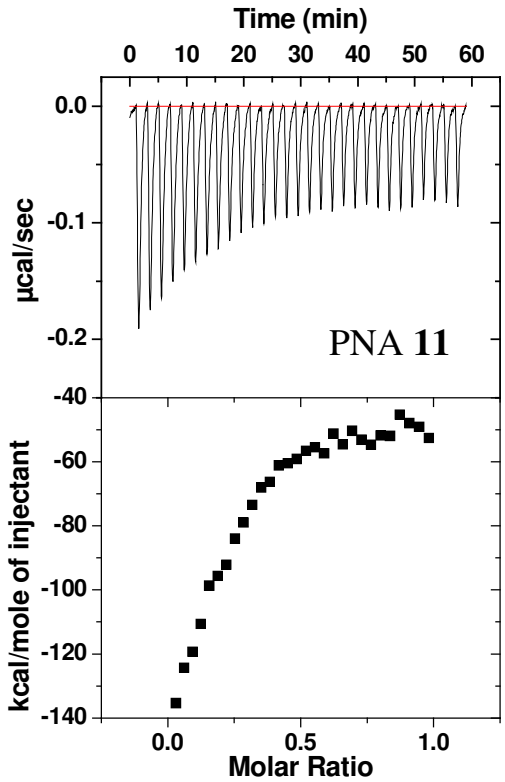
Time (min)
0 10 20 30 40 50 60
µcal/sec
0.0
-0.1
-0.2
-40
PNA 11
kcal/mole of injectant
-60
-80
-100
-120
-140
0.0 0.5 1.0
Molar Ratio

2.9. REFERENCES

[1] Uhlmann, E.; Peyman, A. Antisense oligonucleotides: A new therapeutic principle. *Chem. Rev.* **1990**, *90*, 543-584.

[2] *Antisense Research and Applications* (Eds.: Crooke, S. T.; Lebleu, B.), CRC Press, Boca Raton, FL, 1993.

[3] Uhlmann, E.; Peyman, A. Antisense Oligonucleotides - Chemical Modifications. In *Encyclopaedia of Molecualr Biology and Biotechnology* (Ed.: Meyer, E.), VCH, New York, 1995.

[4] De Mesmaeker, A.; Haner, R.; Mertin, P.; Moser, H. E. Antisense Oligonucleotides. *Acc. Chem. Res.* **1995**, *28*, 366-374

[5] *Methods in Molecular Biology, Vol. 20: Protocols for Oligonucleotides and Analogs* (Ed.: Agrawal, S.), Humana Press, New Jersey, Totowa, Chapter 16, 1993, pp. 355-389.

[6] Nielsen, P. E. DNA analogues with nonphosphodiester backbones. *Annu. Rev. Biophys. Biomol. Struct.* **1995**, *24*, 167-183.

[7] De Mesmaeker, A.; Altmann, K. -H.;Waldner, A.; Wendeborn, S. Backbone modifications in oligonucleotides and peptide nucleic acid systems. *Curr. Opin. Struct. Biol.* **1995**, *5*, 343-355.

[8] Stirchak, E. P.; Summerton, J. E.; Weller, D. D. Uncharged stereoregular nucleic acid analogs: 2- Morpholino nucleoside olgiomers with carbamate internucleoside linkages. *Nucleic Acids Res.* **1989**, *17*, 6129-6141.

[9] Nielsen, P. E.; Egholm, M.; Berg, R. H.; Buchardt, O. Sequence-selective recognition of DNA by strand displacement with thymine-substituted polyamide. *Science,* **1991**, *254*, 1497-1500.

[10] Nielsen, P. E.; Egholm, M.; Buchardt, O. Peptide nucleic acid (PNA). A DNA mimic with a peptide backbone. *Bioconj. Chem.* **1994**, *5*, 3-7.

[11] Hyrup, B.; Egholm, M.; Buchardt, O.; Nielsen, P. E. A flexible and positively charged PNA analogue with an ethylene-linker to the nucleobase: Synthesis and hybridization properties. *Bioorg. Med.Chem. Lett.* **1996**, *6*, 1083-1088.

[12] Good, L.; Nielsen, P. E. Progress in developing PNA as a gene-targeted drug. *Antisense & Nucleic Acids Drug Dev.* **1997**, *7*, 431-437.

[13] Nielsen, P. E.; Haaima, G. Peptide nucleic acid. A DNA mimic with a pseudopeptide backbone. *Chem. Soc. Rev.* **1997**, 73-78.

[14] Uhlmann, E.; Peyman, A.; Breipohl, G.; Will, D. W. PNA: Synthetic Polyamide Nucleic Acids with Unusual Binding Properties. *Angew. Chem. Int. Ed. Engl.* **1998, *37*,** 2796-2823

[15] Egholm, M.; Buchardt, O.; Christensen, L.; Behrens, C.; Freier, S. M.; Driver, D. A.; Berg, R. H.; Kim, S. K.; Norden, B.; Nielsen, P. E. PNA hybridizes to complementary oligonucleotides obeying the Watson-Crick hydrogen-bonding rules. *Nature,* **1993**, *365*, 566-568.

[16] Hanvey, J. C.; Peffer, N. J.; Bisi, J. E.; Thomson, S. A.; Cadilla, R.; Josey, J. A.; Ricca, D. J.; Hassman, C. F.; Bonham, M. A.; Au, K. G.; Carter, S. G.; Bruckenstein, D. A.; Boyd, A. L.; Noble, S. A.; Babiss, L. E. Antisense and antigene properties of peptide nucleic acids. *Science,* **1992**, *258*, 1481- 1485.

[17] D'Costa, M.; Kumar, V. A.; Ganesh, K. N. Aminoethylprolyl peptide nucleic acids (aepPNA): Chiral PNA analogues that form highly stable DNA: aepPNA$_2$ triplexes. *Org. Lett.* **1999**, *1*, 1513-1516.

[18] D'Costa, M.; Kumar, V. A.; Ganesh, K. N. Aminoethylprolyl (*aep*) PNA: Mixed purine/pyrimidine oligomers and binding orientation preferences for PNA:DNA duplex formation. *Org. Lett.* **2001**, *3*, 1281-1284.

[19] Kumar, V. A. Structural preorganization of peptide nucleic acids: Chiral cationic analogues with five- or six-membered ring structures. *Eur. J. Org. Chem.* **2002**, 2021-2032.

[20] (i).Vilaivan, T.; Lowe, G. A novel pyrrolidinyl PNA showing high sequence specificity and preferential binding to DNA over RNA. *J. Am. Chem. Soc*. **2002**, 124, 9326-9327. (ii) Hickman, D. T.; King, P. M.; Cooper, M. A.; Slater, J. M.; Mickelfield, J. Unusual RNA and DNA binding properties of a novel pyrrolidine-amide oligonucleotide mimic (POM). *Chem. Comm*un. **2000**, 2251-2252. (iii). Puschl, A.; Boesen, T.; Zuccarello, G.;

Dahl, O.; Pitsch, S.; Nielsen, P. E. Synthesis of pyrrolidinone PNA: A novel conformationally restricted PNA analogue. *J. Org. Chem*. **2001**, *66*, 707-712.

[21] Alema´n, C.; Roca, R.; Luque, F. J.; Orozco, M. Helical Preferences of Alanine, Glycine, and Aminoisobutyric Homopeptides. *PROTEINS: Structure, Function, and Genetics* **1997**, *28*, 83–93.

[22] MacArthur M. W.; Thornton, J. M. Deviations from Planarity of the Peptide Bond in Peptides and Proteins. *J. Mol. Biol.* **1996**, *264*, 1180–1195.

[22a] Park, J.; Tian, G. R.; Kim, D. H. Synthesis of Optically Active 2-Alkyl-3,4-iminobutanoic Acids.β-Amino Acids Containing an Aziridine Heterocycle. *J. Org. Chem.* **2001**, *66,* 3696-3703.

[23] Nielsen, P. E.; Egholm, M**.;** Berg, R. H.; Buchardt, 0. In *Antisense Research and Applications*. CRC Press: Boca Raton, FL, **1992**, pp 363-372.

[24] Synthesis **1995**, 1205-1222.

[25] Buchardt, O.; Egholm, M.; Nielsen, P. E.; Berg, R. H. *Int. PCT Appl. wo 92/20702* **1992**.

[26] Ando, T.; Yamawaki, J. Potassium fluoride on Celite: A versatile reagent for C-, N-, O-, and S-alkylations. *Chem. Lett.* **1979**, 45-46.

[27] Christensen, L.; Fitzpatrick, R.; Gildea, B.; Petersen, K.; Hansen, H. F.; Koch, C.; Egholm, M.; Buchardt, O.; Nielsen, P. E.; Coull, J.; Berg, R. H. Solid-phase synthesis of peptide nucleic acids. *J. Peptide Sci.* **1995**, *3*, 175-183.

[28] Dueholm, K. L.; Egholm,M.; Behrens, C.; Christensen, L.; Hansen, H. F.; Vulpius T.; Petersen, K. H.; Berg, R.; H.; Nielsen, P. E.; Buchardt, O. Synthesis of peptide nucleic acid monomers containing the four natural nucleobases: Thymine, cytosine, adenine, and guanine and their oligomerization. *J. Org. Chem.* **1994**, *59*, 5767-5773.

[29] Kaiser, E.; Colescott, R. L.; Bossinger, C. D.; Cook, P. I. Color test for detection of free terminal amino groups in the solid-phase synthesis of peptides. *Anal. Biochem.* **1970**, *34*, 595-598.

[30] Puglisi, J. D.; Tinoco, I. Jr. Absorbance melting curves of RNA. *Methods Enzymol.* **1989**, *180*, 304-325.

[31] Barawkar, D. A.; Bruice, T. C. Deoxynucleic guanidines/PNA (DNG/PNA) chimeras: Oligonucleoside analogue containing cationic guanidinium and neutral amide linkages. *J. Am. Chem. Soc.* **1999**, *121*, 10418.

[32] Egholm, M.; Buchardt, O.; Nielsen, P. E.; Beg, R. H. Recognition of guanine and adenine in DNA by cytosine and thymine containing peptide nucleic acids (PNA). *J. Am. Chem. Soc.* **1992**, *114*, 9677-9678.

[33] Gray, D. M.; Ratliff, R. L.; Vaughan, M. R. Circular dichroism spectroscopy of DNA. *Methods Enzymol.* **1992**, *211*, 389-396.

[34] Gray, D. M.; Hung, S. –H.; Johnson, K. H. Absorption and circular dichroism spectroscopy of nucleic acid duplexes and triplexes. *Methods Enzymol.* **1995**, *246*, 19-34.

[35] Wittung, P.; Nielsen, P. E.; Buchardt, O.; Egholm, M.; Nordén, B. DNA-like double helix formed by peptide nucleic acid. *Nature,* **1994**, *368*, 561-563.

[36] Ganesh, K. N.; Nielsen, P. E. Peptide Nucleic Acids: Analogs and Derivatives. *Curr. Org. Chem.* **2000**, *4*, 931-943.

[37] Kumar, V. A.; Ganesh, K. N. Conformationally Constrained PNA analogues: Structural Evolution toward DNA/RNA Binding Selectivity. *Acc. Chem. Res.* **2005**, *38*, 404-412.

[38] Aravinda, S.; Shamala, N.; Roy, R. S.; Balaram, P. Non-protein amino acids in peptide design. *Proc. Indian Acad. Sci.* (*Chem. Sci.*), **2003**, *115*, 373-400.

[39] Egholm, M**.;** Buchardt, 0. Nielsen, P. E.; Berg, R. H.; Buchardt, 0. Peptide Nucleic Acids (PNA). Oligonucleotide analoues with achiral peptide backbone. *J. Am. Chem. Soc.*, **1992**, *114*, 1895-1897.

Chapter 3: Section A

Introduction

to

DNA/PNA Nano-Biotechnology

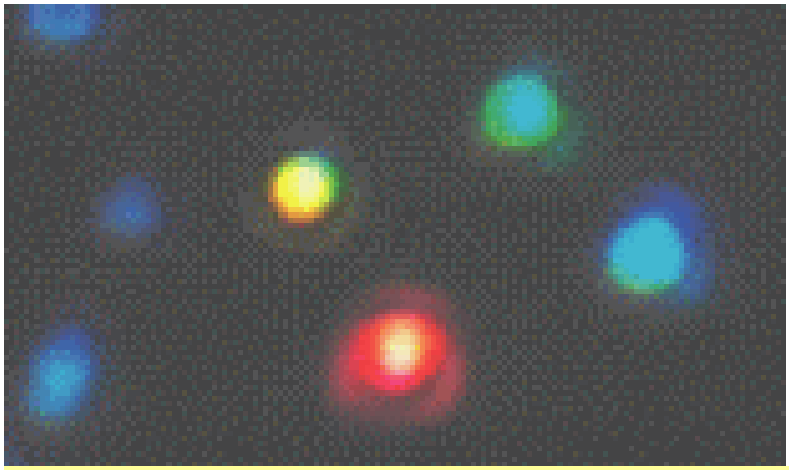

There's plenty of room at the bottom.
Richard P. Feynman (1959)

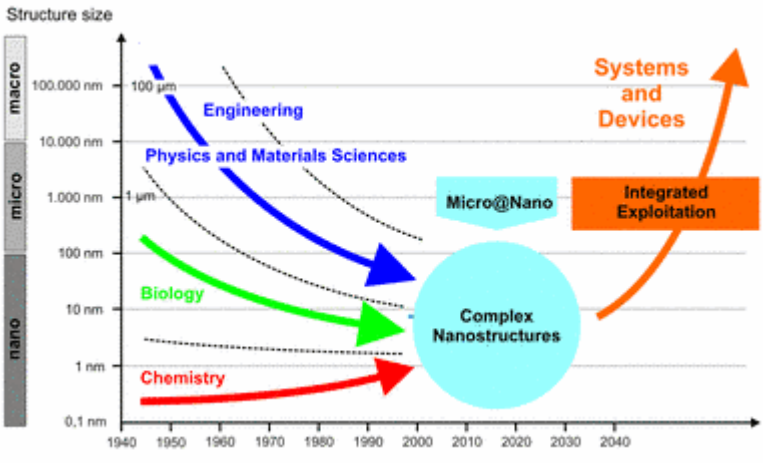

3.1. INTRODUCTION

The science and technology of nanomaterials has created great excitement and expectations in the last few years. By its very nature, the subject is of immense research interest, having to do with very tiny objects in the nanometer regime. There has already been much progress in the synthesis, assembly and fabrication of nanomaterials, and, equally importantly, in the potential applications of these materials in a wide variety of technologies. The next decade is likely to witness major strides in the preparation, characterization and exploitation of nanoparticles, nanotubes and other nanounits, and their assemblies. In addition, there will be progress in the discovery and commercialization of nanotechnologies and devices. These new technologies are bound to have an impact on the chemical, energy, electronics and space industries. They will also have applications in medicine and health care, drug and gene delivery being important areas. Since synthesis, structure, properties and simulation are important ingredients of nanoscience; chemists have a major role to play.

Nanotechnology is the term used to describe the creation and exploitation of materials with structural features in between those of atoms and bulk materials, with at least one dimension in the nanometer range (1 nm = 10^{-9} m). Table 1 lists typical nanomaterials of different dimensionalities. The properties of materials with nanometric dimensions are significantly different from those of atoms or bulk materials. Suitable control of the properties of nanometer-scale structures can lead to new science as well as new products, devices and technologies. The underlying theme of nanotechnology is

miniaturization, the importance of which was pointed out by Feynman as early as 1959 in his often-cited lecture entitled ‘‘There is plenty of room at the bottom’’. The challenge is to beat Moore’s law[1] and accommodate 1000 CDs in a wristwatch.[2] There has been explosive growth of nanoscience and technology in the last decade, primarily because of the availability of new methods of synthesizing nanomaterials, as well as tools for characterization and manipulation (Table 2).

Several innovative methods for the synthesis of nanoparticles and nanotubes, and their assemblies, are now available. There is a better understanding of the size-dependent electrical, optical and magnetic properties of individual nanostructures of semiconductors, metals and other materials. Besides the established techniques of

Table 1. Typical Nanomaterials

	Size (approx.)	**Materials**
(a) Nanocrystals and clusters (Quantum Dots)	Diameter 1-10nm	Metals, Semiconductors, Magnetic materials
Other Nanoparticles	Diameter 1-100nm	Ceramic oxides
(b) Nanowires	Diameter 1-100nm	Metals, Semiconductors, Oxides, sulfides, Nitrides
Nanotubes	Diameter 1-100nm	Carbon, layered metal chalcogenides
(c) 2-Dimensional arrays (of nanoparticles)	Several $nm^2 - \mu m^2$	Metals, Semiconductors, Magnetic materials
Surfaces and thin films	Thickness 1–1000 nm	Various materials
(d) 3-Dimensional structures (superlattices)	Several nm in all three dimensions	Metals, Semiconductors, Magnetic materials

Table 2. Different methods of synthesis and investigation of nanomaterials

Scale	**Synthetic Methods**	**Structural Methods**	**Theory and Simulation**
0.1–10 nm	Covalent synthesis	Vibrational spectroscopy, NMR, Diffraction methods, Scanning probe microscopies (SPM)	Electronic structure
<1–100 nm	Self-assembly techniques	SEM, TEM, SPM	Molecular Dynamics and mechanics

100nm - 1μm	Processing, modifications	SEM, TEM	Coarse grained models, hopping *etc.*

electron microscopy, crystallography and spectroscopy, Scanning probe microscopies have provided powerful tools for the study of nanostructures.

Novel methods of fabricating patterned nanostructures, as well as new device and fabrication concepts, are constantly being discovered. Nanostructures have also been ideal for computer simulation and modeling, their size being sufficiently small to accommodate considerable rigour in treatment. In computations on nanomaterials,[3] one deals with a spatial scaling from 1 Å to 1 μm and temporal scaling from 1 fs to 1 s, the limit of Quantum computing[4,5] has made a good start and appropriate quantum algorithms have been developed.

3.1.1 Biological Significance in Nanotechnology

Biological self-assembly has stimulated biomimetic "bottom-up" approaches for the development of artificial nanometer-scaled materials which has potential commercial applications in microelectronics and micromechanical devices of increasingly small dimensions in the range of ~ 5 to 100 nm as shown in Figure 1. In this regard, researchers had suggested that the synthetic nanometer-sized elements might be fabricated from biomolecular building blocks.[6] In biologically integrated devices, multiple biomolecules are organized on surfaces with resolution from micron to nanometer scale. The fabrication of supramolecular structures and devices require molecules that are capable of interlocking in a predictable, well-defined manner. Molecular self-assembly systems that

exploit molecular-scale manufacturing precision of biological systems are prime candidates for supramolecular engineering.

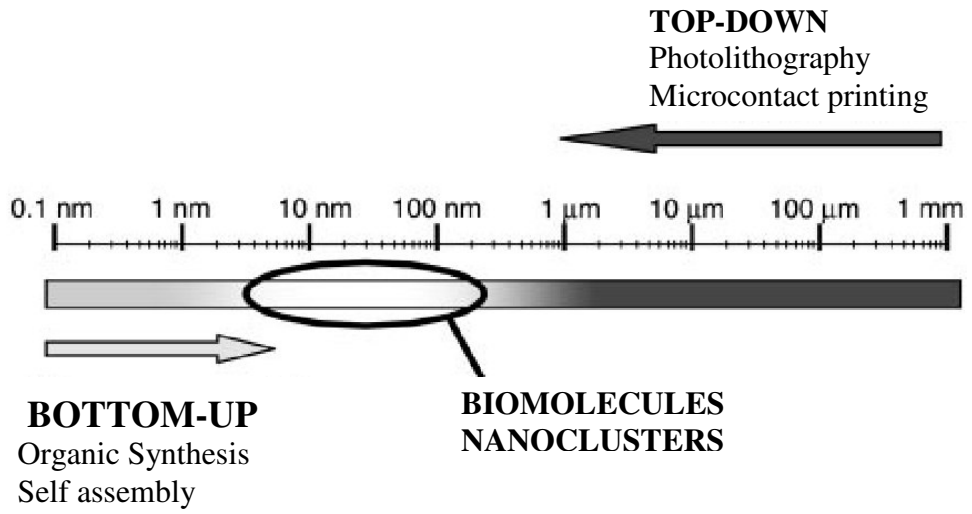

Figure 1. A gap currently exists in the engineering of small-scale devices. Whereas conventional top-down processes hardly allow the production of structures smaller than about 200 ± 100 nm, the limits of regular bottom-up processes are in the range of about 2 ± 5 nm. As a result of their own dimensions, two different types of compounds appear to be suited for addressing that gap: 1) biomolecular components, such as proteins and nucleic acids, and 2) colloidal nanoparticles comprised of metal and semiconductor materials.

3.1.2. Building blocks in nanotechnology

Nature has provided a limited number of basic building blocks such as amino acids, lipids and nucleic acids. The chemical diversity of these molecules and the different ways in which they can be polymerized or assembled provides an enormous range of possible structures. Furthermore, advances in chemical synthesis and biotechnology enable one to combine these building blocks to produce new materials and structures that have not been made by nature. These materials often have enhanced properties as well as unique applications. Moreover, one can understand nature and try to mimic nature for the development of new materials. Biological molecules and systems

have a number of attributes that make them highly suitable for nanotechnology applications. For example, proteins fold into precisely defined three-dimensional shape, and nucleic acids assemble according to well-understood rules. Antibodies are highly specific in recognizing and binding their ligands and biological assemblies such as molecular motors can perform transport operations.

3.2. BIOMOLECULE-NANOPARTICLE INTERACTIONS

The conjugation of nanoparticles with biomolecules is a tempting research project as it may provide new dimensions into the area of nanobiotechnology.[7] The integration of nanotechnology with biology and medicine is expected to produce major advances in medical diagnostics, therapeutics, molecular biology and bioengineering.[8] Moreover, bioelectronics is also a rapidly progressing research field in modern science. It involves the integration of biomaterials such as enzymes,[9] antigen-antibodies,[10] DNA[11] or cells[12] with electronic elements such as electrodes, field effect transistors and piezo-electric crystals with the aim to transduce biological events occurring on these elements by electronic signals.

Ensuring an ordered arrangement of nanoparticles in two- and three-dimensional structures is an important research challenge with great practical implications.[13] In the past few years, the use of thiolated oligonucleotides immobilized onto gold surfaces has received a considerable amount of attention, due in part to the control and flexibility in forming self-assembled monolayers (SAMs) of DNA and/or mixed DNA/alkanethiol SAMs.[14,15] Thiolated DNA probes have also been immobilized onto thin gold films for

gravimetric analysis,[16,17] electrochemical detection[18,19] and AFM imaging[20] of DNA targets. Thiolation is normally done at the 5'-terminus and organizing such DNA strands into duplexes or overlapping duplexes, enables one to organize the gold particles bound to thiol function into well-defined configurations. Such duplex bound gold nanoparticles have been used to generate supramolecular nanoparticle structures in solution[21] (Figure 2).

All these applications involve thiol functionalized DNA and exploit the ability of DNA to form wide varieties of geometrically defined structures such as duplexes, triplexes, hairpins, tetraplexes and cruciforms dictated by the nature of the base sequence. However, DNA (Figure 3-I) is also a polyanion, with negatively charged phosphates arranged uniformly on the backbone and the nature of DNA secondary structures determines the spatial distribution of the negative charges. The potential of underivatised DNA molecules as templates to realize linear nanoparticle assemblies has not been much examined, although they have been used to arrange cationic lipids.[22,23] Although self-assembly of nanoparticles in hexagonal close packed structures of thin films is known, the programmed organization of nanoparticles in superstructures of

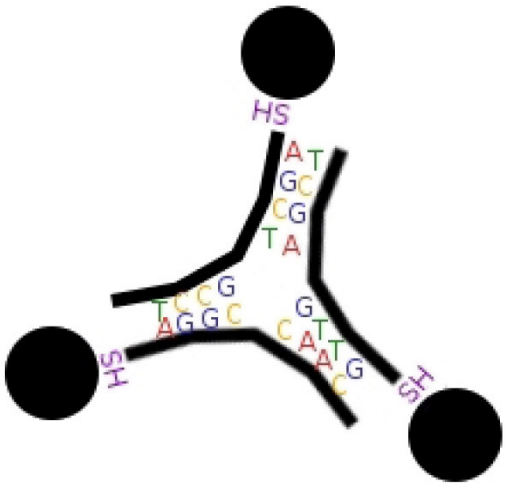

Figure 2. By matching half of each thiolated DNA strand to half of each of the other two DNA strands in an appropriate sequence with AuNPs, a triangle is formed.

desired shape and morphology is relatively unexplored.

Previous work in this laboratory on synergistic assembly of cationic lipids on anionic DNA template led us to explore assembling cationic gold nanoparticles on anionic DNA.[22,23] The complexation is mediated by the electrostatic or coulomb interactions between the two oppositely charged components. DNA also forms sequence specific hybrids with uncharged complementary peptide nucleic acids (PNA),[24] (Figure 3-II), which are an emerging class of DNA mimics. DNA:PNA hybrids, in principle can also organize gold nanoparticles electrostatically, but only the anionic DNA strand is involved in templating activity. This chapter describes efforts in exploring the templating ability of DNA, PNA and their conjugates to form nanoassemblies via electrostatic interaction between anionic DNA and cationic lysine capped gold nanoparticles. The DNA surface immobilized gold nanohybrids are morphologically characterized by TEM and STM techniques and it was observed that the coating of gold nanoparticles on DNA/DNA:PNA hybrids significantly stabilize these complexes in solution. Phosphorothiaote DNA (PS-DNA) is shown to form interesting organizing features with DNA forming interconnects between the nanoparticles.[25]

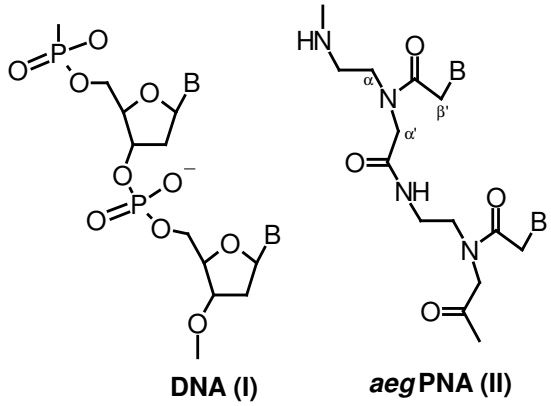

Figure 3. The basic structures of DNA (I) and PNA (II)

DNA-based nanotechnology has generated interest in a number of applications due to the specificity, programmability, and reproducibility of DNA interaction with nanoparticles. Gold nanoparticles (AuNPs) modified with DNA find use in diverse fields such as DNA chips,[26] DNA sensors,[27] drug/DNA delivery,[28] imaging,[29] and biodiagnostics[30] and in structured nanoparticle assemblies for electronics.[31] Similar applications are envisaged for the DNA analogue- peptide nucleic acids (PNAs), wherein the sugar-phosphate backbone is replaced by a polyamide backbone.[24,32] The remarkable utility and versatility of such systems is attributed to the very nature of AuNP-DNA interaction, which in turn is determined by the differential affinity of the nucleobases (adenine, guanine, thymine, and cytosine), nucleosides, nucleotides and oligonucleotide sequences to the gold nanoparticles.[33] Previous studies on understanding the nature of interaction of nucleobases with nanogold have made use of various spectroscopic techniques such as surface-enhanced Raman spectroscopy (SERS),[34] Fourier transform infrared (FTIR),[35] and reflection absorption infrared (RAIR) spectroscopies,[36] which are somewhat indirect methods for estimation of the strength of the abovementioned interactions.

3.2.1. DNA:Gold nanoparticle composites: Synthesis and characterization

Biological molecules and systems have a number of attributes that make them highly suitable for nanotechnology applications. The well-defined double-stranded structure of the DNA molecule provides a practical platform for the assembly of nanoparticles into structured nanomaterials. Biomacromolecules such as DNA is of great

interest. DNA is an excellent template for nanoassembly because of its physicochemical stability, linearity of the molecular structure and mechanical rigidity.

Sequence-specific assembly motifs involving the hybridization of complementary DNA strands conjugated to nanoparticles have been extensively employed to produce nanoparticle chains or networks. DNA-templated nanoparticle assemblies in the solid state are of particular interest, as the controlled deposition of nanoparticles on surfaces plays an important role in fabrication of nanoscale electronics as shown in Figure 4.

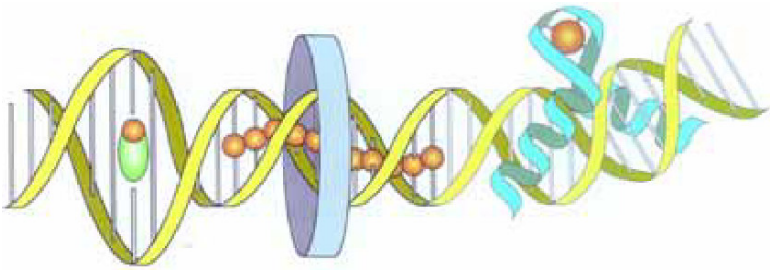

Figure 4. Novel combinations of DNA, metal ligands, DNA templating, and proteins are being investigated for molecular wires, inductors, and switches (Photo courtesy of Shionoya and coworkers, Inst. for Molecular Science).

Diverse cationic nanoparticles have been subjected to the assembly with DNA on surfaces, affording nanoparticle wires and threads. By changing the nanoparticle–DNA ratio, assemblies of network structures can be generated instead of linear assemblies.

Upon addition of lysine-capped gold colloidal solution to 15/30-mer ODN duplexes, the color of solution changed rapidly from ruby red to blue (Figure 5). This indicates aggregation of gold nanoparticles in presence of DNA.[37]

After equilibration, ultracentrifugation and redispersion in H_2O (pH 7.0), the samples were drop-coated as film on carbon-coated grids for transmission electron microscopy (TEM) and on Si wafer for imaging by scanning tunneling microscopy

(STM).[38] The TEM picture (Figure 6) shows parallel dark bands, obtained with a high degree of order in alignment of duplex chains over the film surface. The dark bands arise from electron scattering from gold particles and the observed length of the bands 80Å is in close agreement with the expected length of the DNA molecule (55Å). The average separation between the longer black bands was 90Å, corresponding to DNA double helix-gold nanoparticle sandwich assembly.

The STM image (Figure 7) shows individual gold nanoparticle assembly as a regular, linear pattern on DNA template in a lamellar fashion. The surface height

Figure 5. (A) Ruby red color of colloidal gold solution (B) Blue color of colloidal gold solution with DNA. (Photo courtesy of Mirkin C. A. International Inst. for Nanotechnology).

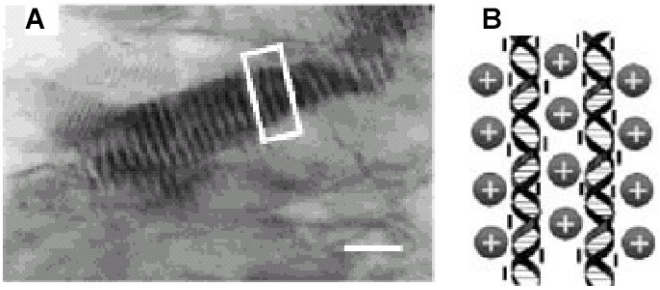

Figure 6. (A). TEM picture of the synthetic DNA + gold nanoparticle complex film showing the linear gold supercluster assemblies organised on the DNA template. (B) Expected templating action of the DNA double helical molecules leading to the condensed, layered gold nanoparticle-DNA-gold nanoparticle-DNA structures observed in the TEM. Reproduced from Ref. 38.

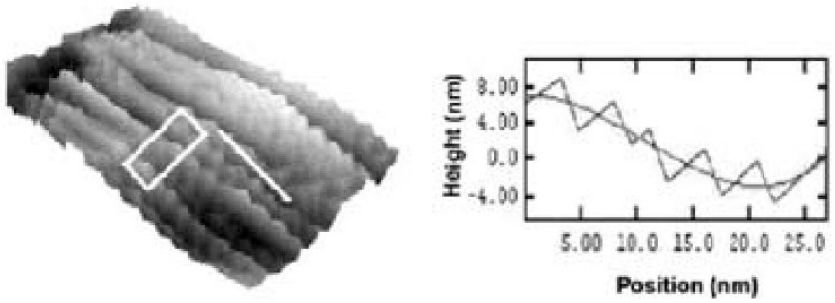

Figure 7. STM image of a synthetic DNA + gold nanoparticle complex film drop-coated on a highly conducting Si substrate showing the linear gold nanoparticle assemblies (left). The length of the line in this image corresponds to 27.5 nm. Surface height variation with distance along the line shown for the STM image (right). Reproduced from Ref. 38.

variation- distance plot indicated a highly periodic variation in height and the observed periodicity of 4 nm is in excellent agreement with the size of gold nanoparticle (3.5±0.7 nm) arranged in linear arrays. No such ordered structure was seen with uncapped gold particle-DNA films.

Similar linear superstructures arising from gold nanoparticle on DNA template could be realized from a simpler protocol in which drop-dried films of DNA duplexes were first deposited on a substrate followed by the addition of lysine-capped gold colloidal particles to the film (Figure 8). The formation of nanoparticle assembly on DNA was also supported by UV-Visible spectra of the film, which showed appearance of a strong band at 685 nm upon addition of DNA. It is well known that aggregation of noble metal colloidal particles such as silver and gold into quasi-linear superstructures leads to the appearance of a longitudinal surface plasmon resonance (685 nm), red shifted with respect to the transverse component resonance (545 nm). Attractive electrostatic interaction between the positive charges on the lysine molecules bound to the gold

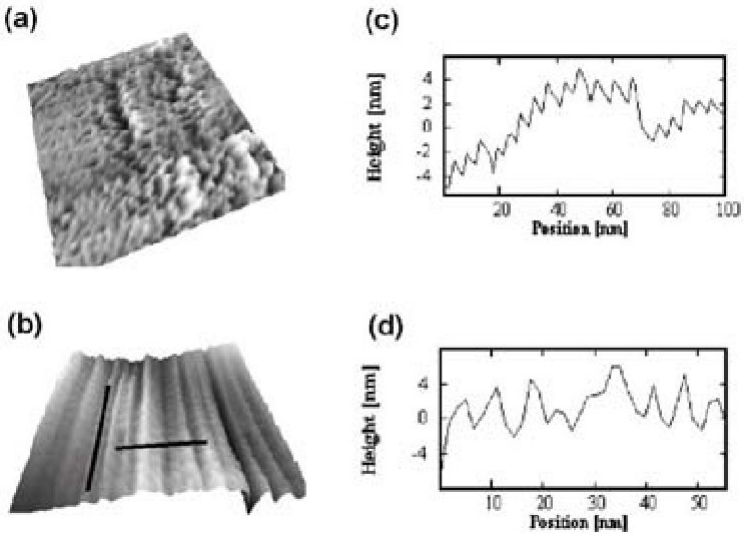

Figure 8. (a) STM image of a drop-dried DNA film deposited on a conducting Si substrate. (b) STM image of a drop-dried DNA film deposited on a conducting Si substrate after addition of lysinecapped gold nanoparticles. The extent of the imagse is 100 nm x 100 nm. (c) Surface height variation with distance along the vertical line shown in the STM image of the DNA-gold nanoparticle film as in (a). (d) Surface height variation with distance along the horizontal line shown in the STM image of the gold nanoparticle-DNA film as in (b). Reproduced from Ref. 27.

nanoparticles and the negative charges on the phosphate groups of the DNA molecules drives the assembly of the gold nanoparticles on DNA template. The DNA acts like counterions and screen the repulsive interactions between the positively charged gold nanoparticles, thus enabling their assembly into close-packed superstructures.[39]

3.2.2. Phosphorothioate DNA-gold nanoparticles

Phosphorothioate DNA (PS-DNA) analogs have the anionic oxygen of the DNA phosphate uniformly replaced by sulphur and it would be interesting to study their interaction with gold nanoparticles in comparison to end-monothiolated DNA. Single stranded dT_{12}–PS DNA was treated with gold nanoparticles as per standard procedures and the resulting complexes were examined by UV-VIS and TEM techniques. A smaller

red shift was observed in surface plasmon resonance band from 516 nm in free gold particles to 530 nm in DNA. A comparison of Figure 9A and 9B, indicates that the parent gold nanoparticles assemble into a dense close-packed structure and consequent to complexation with S-DNA assemble into loose, open structures.[25] Thus, the S-DNA molecules bound to the surface of gold nanoparticles prevent their rapid assembly and hold them in place in quasi-linear, open structures. In some regions, fairly long and linear arrangement of nanoparticles is observed.

An important observation is the larger and more uniform separation between the gold nanoparticles (32 ± 6 Å) after complexation with PS-DNA molecules as compared to that before complexation (12 ± 2 Å). The interparticle edge to edge separation of 32Å between gold nanoparticles complexed with PS-DNA is in good agreement with the length of PS-DNA molecule of ~40 Å. This suggests that the PS-DNA molecules bind to the gold nanoparticles through terminal sulphur atoms in the DNA, as depicted in Figure 9C. PS-DNA acts like a rigid linker between the gold nanoparticles leading to superstructures. This is unlike the case of other thiol-DNA based gold nanoparticle cross-

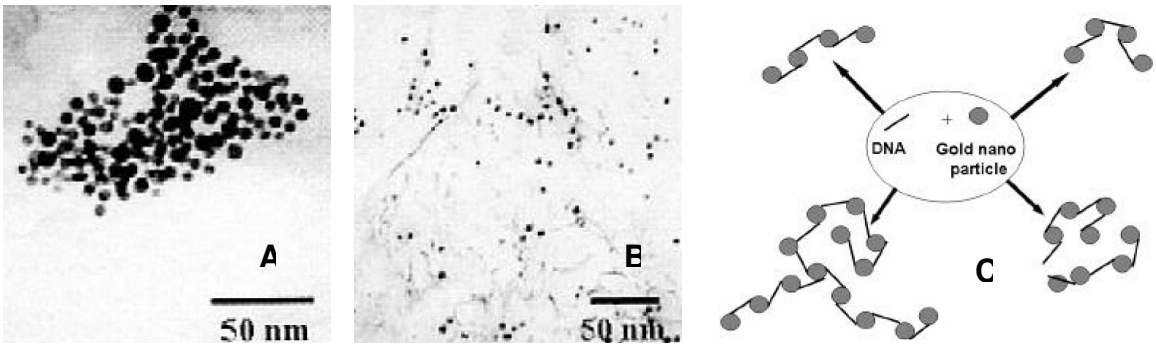

Figure 9. (A) and (B) TEM picture of drop-coated film of borohydride-reduced gold nanoparticles before complexation with S-DNA on a carboncoated TEM grid (C) Schematic of possible gold nanoparticle superstructures formed in solution using S-DNA interconnects. Reproduced from Ref. 13.

linking strategies that rely on hybridization of complementary DNA molecules for superstructure formation. PS-DNA covalently cross-links the gold nanoparticles conceivably leading to greater stability.[25]

3.2.3. DNA –Based molecular nanotechnology

The integration of nanotechnology with biology and bioengineering is producing many advances. The essence of nanotechnology is to produce and manipulate well-defined structures on the nanometer scale with high accuracy. Conventional technologies based on the "top-down" approaches, such as the photolithographic method, are difficult to continue to scale down due to real physical limitations including size of atoms, wavelengths of radiation used for lithography, and interconnect schemes. While engineers and scientists have long aspired to controllably manipulate structures at the micrometer and nanometer scale, nature elegantly performs these tasks and assembles structures with great accuracy and high efficiency using specific biological molecules.

Biological molecules, such as DNA, have shown great potential in fabrication and construction of nanostructures and devices. DNA molecules can be used for the assembly of devices and computational elements, for the assembly of interconnects, or as the device element itself. There are several advantages to use DNA for these constructions. First, DNA is the molecule whose intermolecular interactions are the most readily programmed and reliably predicted. Many properties that make DNA so effective as genetic material also make it an excellent molecule for programmed self-assembly. Second, DNA of arbitrary sequences is available by convenient solid support synthesis. The needs of the biotechnology industry have also led to reliable chemistries to produce

modifications, such as biotin groups, fluorescent labels, and linking functions. Third, DNA can be manipulated and modified by a large battery of enzymes that include DNA ligases, restriction endonucleases, kinases, and exonucleases.

Nanotechnology has helped the development of novel biosensors for biological and medical applications. Nanobioconjugates that consists of various functional nanoparticles linked to biological molecules have been used in many areas such as diagnostics, therapeutics, sensors, and bioengineering. Detection methods based on these nanobioconjugates show increased selectivity and sensitivity as compared with many conventional assays that rely on molecular probes.[8]

Attachment of DNA to surfaces

The first step toward DNA-based nanotechnology is to attach DNA molecules to surfaces. So far, the most widely used attachment scheme utilizes the covalent bond between sulfur and gold.[40-46] Nuzzo and Allara first reported the formation of long chain ω-substituted dialkyl-disulfide molecules on a gold substrate.[40] Bain *et al.* demonstrated a model system consisting of long-chain thiols that adsorb from solution onto gold to form densely packed, oriented monolayers.[44] The bonding of the sulfur head group to the gold substrate is in the form of a metal thiolate, which is a very strong bond (~ 44 kcal/mol), and hence the resulting films are quite stable and very suitable for surface attachment of functional groups. For example, the DNA molecule can be functionalized with a thiol (S-H) or a disulfide (S-S) group at the 3' or 5' end. Hickman *et. al.* also demonstrated the selective and orthogonal self-assembly of disulfide with gold and isocyanide with platinum.[45] It should be noted that there are also other strategies to attach DNA to surfaces, for example, the covalent binding of DNA oligonucleotides to a preactivated

particle surface[46] and adsorption of biotinylated oligonucleotides on a particle surface coated with avidin.[47,48] These attachment schemes have served as the fundamental base for DNA-related self-assembly of artificial nanostructures.

Self Assembly and construction of nanostructure using DNA

There has been a tremendous interest in recent years to develop concepts and approaches for self-assembled systems. While significant work continues along this direction, it has also been recognized that the exquisite molecular recognition of various natural biological materials can be used to form a complex network of potentially useful particles for a variety of optical, electronic, and sensing applications. This approach can be considered a bottom-up approach rather than the top-down approach of conventional scaling. DNA is a particularly promising candidate to serve as a construction material in nanotechnology. Despite its simplicity, the highly specific Watson-Crick hydrogen bonding allows convenient programming of artificial DNA receptor moieties. The power of DNA as a molecular tool is enhanced by automated methods and by the PCR technique to amplify any DNA sequence from microscopic to macroscopic quantities. Another attractive feature of DNA is the great mechanical rigidity of short double helices, so that they behave effectively like a rigid rod spacer between two tethered functional molecular components on both ends. Moreover, DNA displays a relatively high physicochemical stability. Finally, nature provides a complete toolbox of highly specific enzymes that enable the processing of the DNA material with atomic precision and accuracy.

Nanostructures from DNA

Seeman and co-workers[49] were the first to exploit DNA's molecular recognition properties to design complex mesoscopic structures based solely on DNA. In their work, branched DNA was used to form stick figures by properly choosing the sequence of the complementary strands. Macrocycles, DNA quadrilateral, DNA knots, Holliday junctions, and other structures were designed. Figure 10 shows a four-armed stable branched DNA junction made by DNA molecules and the use of the branched junctions to form periodic crystals.[50] The same group also reported the design of two-dimensional crystalline forms of DNA double crossover molecules that are programmed to self-assemble by the complementary binding of the sticky ends of the DNA molecules.[51] These lattices can also serve as scaffolding material for other biological materials.[52]

Other researchers also have put effort on using DNA to design complex architectures. Bergstrom and co-workers have designed rigid tetrahedral linkers with arylethynylaryl spacers to direct the assembly of attached oligonucleotide linker arms into novel DNA macrocycles.[53] Unlike Seeman's approach where the DNA serves as both

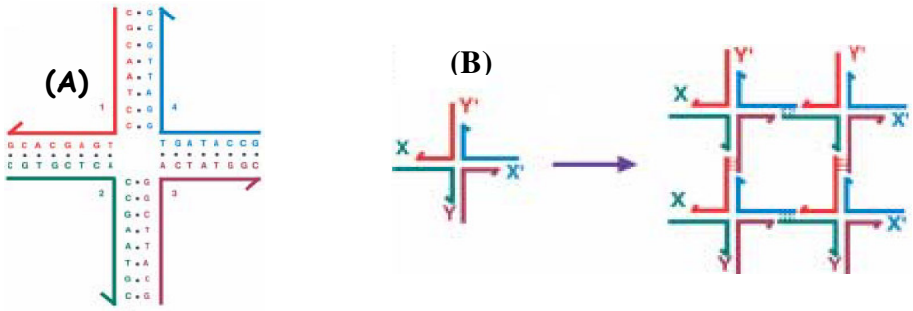

Figure 10. (A) A branched molecule with four arms. The four strands labeled with Arabic numerals combine to produce four arms, labeled with Roman numerals. Arrowheads indicate strand polarity. (B) Formation of a two-dimensional lattice from a four-arm junction with sticky ends. X is a sticky end and X' is its complement. The same relationship exists between Y and Y'. Four of the monomeric junctions on the left are complexed in parallel orientation to yield the structure on the right. Note that the complex has maintained open valences, so it could be extended by the addition of more monomers.

the vertices and the edges of the assembled architectures, Bergstrom's approach utilizes rigid tetrahedral organic vertices, where the attached oligonucleotides serve as the connectors for the design of more complex architectures. In principle, a variable number of oligonucleotide arms could be attached to the core tetrahedral organic linkers, thereby allowing for the construction of different types of DNA structures.

DNA-based assembly of metal nanoparticles

In 1996, Mirkin and co-workers[54] first described a method of assembling colloidal gold nanoparticles into macroscopic aggregates using DNA as linking elements. As illustrated in Figure 11, this method involved attaching non-complementary oligonucleotides to the surfaces of two batches of gold particles capped with thiol groups,

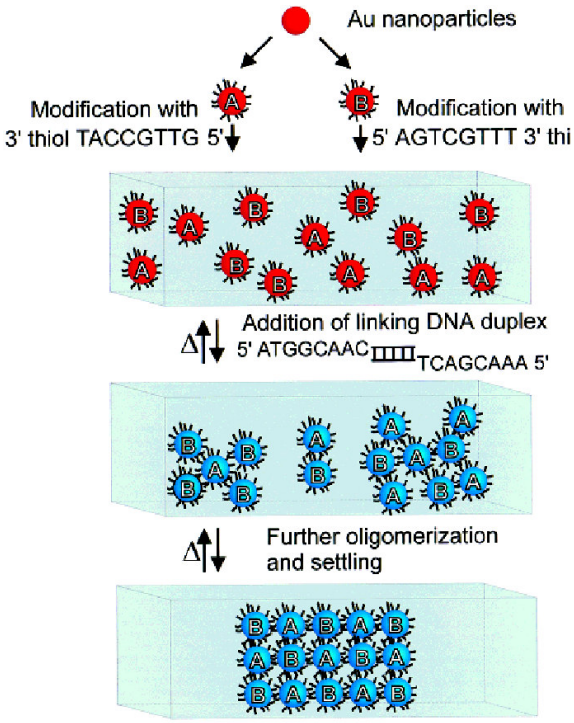

Figure 11. Scheme showing the DNA-based gold nanoparticle assembly strategy. The scheme is not meant to imply the formation of a crystalline lattice but rather an aggregate structure that can be reversibly annealed.

which bind to gold. When another oligonucleotide, which is complementary to the two grafted sequences, is introduced, the nanoparticles self-assemble into aggregates. This process could also be reversed when the temperature was increased due to the melting of the DNA oligonucleotides. Because of the molecular recognition properties associated with the DNA interconnects, this strategy al lows one to control interparticle distance, strength of the particle interconnects, and size and chemical identity of the particles in the targeted macroscopic structure.

In the same time, Alivisatos *et al.*[47] also reported DNA-based techniques to organize gold nanocrystals into spatially defined structures. In their work, gold particles were attached to either the 3' or 5' end of 19 nucleotide long single-stranded DNA molecules through the well-known thiol attachment scheme. Then, 37 nucleotide long single stranded DNA template molecules were added to the solution containing the gold nanoparticles functionalized with single-stranded DNA. The authors showed that the nanocrystals could be assembled into dimers (*parallel* and *antiparallel*) and trimers upon hybridization of the DNA molecules with that of the template molecule. Due to the ability to choose the number of nucleotides, the gold particles can be placed at defined positions from each other.

Based on the work of Alivisatos and co-workers, Loweth *et al.*[55] have studied further details of the formation of the hetero-dimeric and hetero-trimeric nonperiodic nanocluster molecules. They showed exquisite control of the placement of 5 nm and 10 nm gold nanoclusters that were derivatized with single-stranded DNA.

Mucic *et al.*[56] have made the construction of binary nanoparticle networks composed of 9 nm particles and 31 nm particles, both composed of citrate-stabilized colloidal gold. These 9 and 31 nm particles are coated with different 12-mer oligonucleotides via a thiol bond. When a third DNA sequence (24-mer), which is complementary to the oligonucleotides on both particles is added, hybridization led to the association of particles. When the ratio of 9 nm to 31 nm particles is large, a binary assembly of the nanoparticles is formed. Figure 12 shows the scheme and a TEM image of the binary nanoparticle assembly.[56]

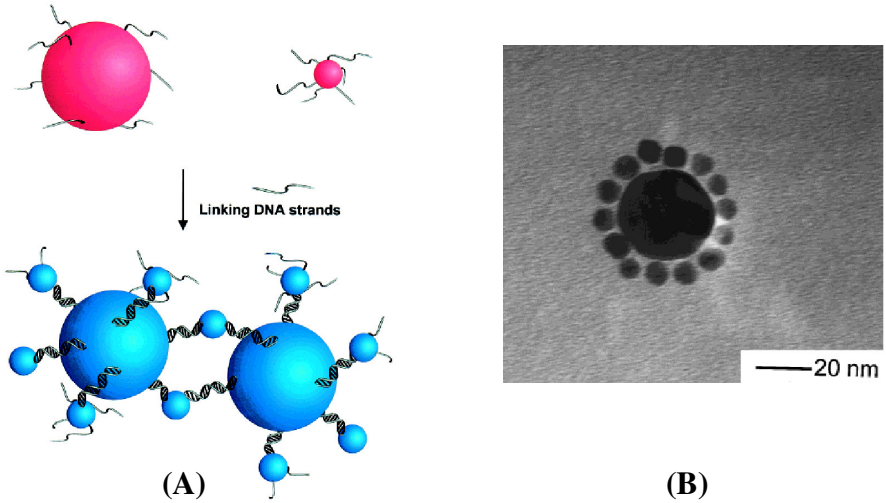

Figure 12. (A) DNA-directed synthesis of binary nanoparticle networks. (B) The panel shows a TEM image of a nanoparticle satellite structure.

Simultaneously, people also tried to use covalent chemistry to link DNA with nanotubes because covalent interaction is expected to provide the best stability, accessibility, and selectivity during competitive hybridization. Hamers and co-workers have developed a multi-step route to the formation of covalently linked adducts of SWNT and DNA oligonucleotides.[57] Figure 13 shows an overview of the covalent attachment

process. Purified SWNTs were oxidized to form carboxylic acid groups at the ends and sidewalls. These were reacted with thionyl chloride and then ethylenediamine to produce amine-terminated sites. The amines were then reacted with the heterobifunctional cross-

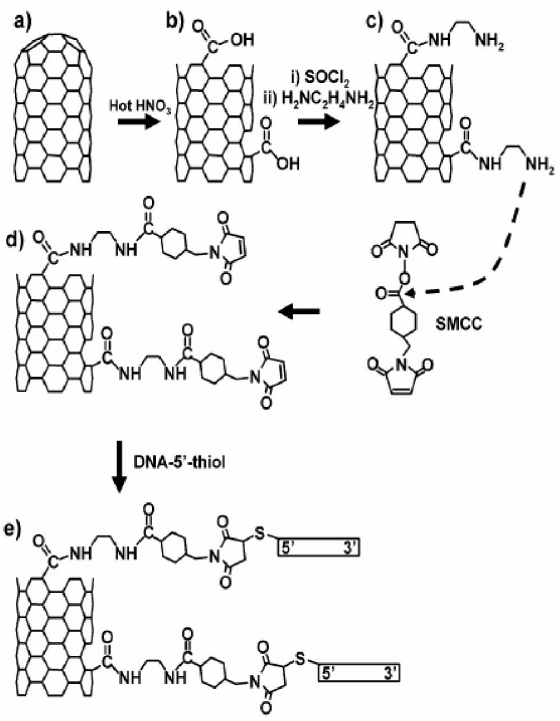

Figure 13. An overview of the covalent attachment of DNA with SWNT.

linker succinimidyl 4-(N-maleimidomethyl)-cyclohexane-1-carboxylate, (SMCC), leaving the surface terminated with maleimide groups. Finally, thiol-terminated DNA was reacted with these groups to produce DNA-modified SWNTs. It is found that DNA molecules covalently linked to SWNTs are accessible to hybridization as evidenced by strong tendency in hybridization with molecules having complementary sequences compared with non-complementary sequences.

Williams *et. al.*[58] recently developed a way to couple SWNTs covalently to peptide nucleic acid (PNA, an uncharged DNA analogue[59]) and to hybridize these macromolecular wires with complementary DNA. This technique is shown in Figure 14.

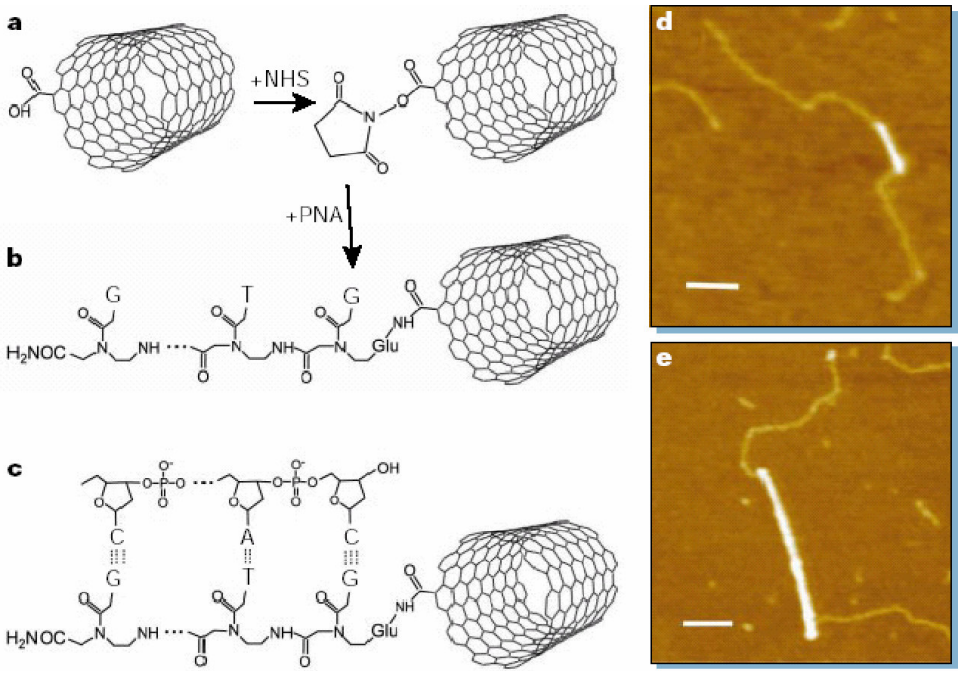

Figure 14. Attachment of DNA to carbon nanotubes. **a**, **b**, N-hydroxysuccinimide (NHS) esters formed on carboxylated, SWNTs are displaced by peptide nucleic acid (PNA), forming an amide linkage. **c**, A DNA fragment with a single-stranded, 'sticky' end hybridizes by Watson–Crick base-pairing to the PNA–SWNT. **d**, **e**, Atomic-force microscope (TappingMode) images of PNA–SWNTs.

Self assembly using artificial DNA

Among the variety of approaches to DNA-based supramolecular chemistry, the strategy of replacing DNA natural bases by alternative bases that possess distinct shape, size, or function has allowed the modification of DNA in a highly specific and site-selective manner.[60-64] One good example is the replacement of the natural bases by

artificial nucleosides or nucleoside mimics.[61] However, this approach is restricted to molecules with shapes and sizes that are commensurate to normal bases to ensure that the DNA modifications occur highly specifically and site selectively.[92] Recently, a new generation of such nucleoside mimics was reported in which the hydrogen bonding interactions were replaced by metal-mediated base pairing.[65-70] The advantage of this modification strategy is that it allows the metal ions to be replaced in the interior of the DNA duplex. This represents an important structural prerequisite for the development of new molecular devices based on interacting metal centers.[63-65]

3.3. PROPERTIES OF DNA - LINKED GOLD NANOPARTICLES

The DNA-linked gold nanoparticle assembly is a prototype of DNA-based nanostructures. The optical and melting properties of this system have attracted considerable interest because the understanding of these properties is essential for DNAbased nanotechnology.[71-73]

3.3.1. Aggregation of DNA-modified gold nanoparticles

UV-visible absorption spectroscopy is a suitable tool to study the optical properties of DNA-linked gold nanoparticle aggregation because DNA bases and gold nanoparticles have strong absorption in the UV region (~ 260 nm) and the visible light region (~ 520 nm), respectively. The extinction coefficient of a collection of gold particles is sensitive to the size of the aggregates. Thus, the change in the gold extinction reflects the aggregation of the gold nanoparticles. The kinetics of aggregation of DNA-linked gold nanoparticles is studied by measuring the UV-visible spectrum as a function

of time at room temperature.[73] Upon adding linker DNA, the DNA hybridization leads to aggregation of gold nanoparticles, indicating in the gold surface plasmon peak (520 nm) shift of the DNA-modified gold nanoparticles.[74-75] The aggregation starts with the wavelength shift of the plasmon band, followed by broadening and more shifting of the peak as hybridization continues. These results indicate that the initial aggregation takes place with increasing volume fraction, followed by increasing network size.[76,77]

3.3.2. Melting of DNA-linked gold nanoparticle aggregations

The UV-visible spectrum is also used to monitor the melting properties of the DNA linked aggregates. The DNA double helix has a smaller extinction coefficient than does single-stranded DNA due to hypochromism, and, therefore, the absorption intensity at 260 nm increases as a result of DNA melting. Meanwhile, the melting will also cause sharp changes in the gold nanoparticle extinction coefficient due to the dissociation of the aggregate. Therefore, the melting can be monitored at either 260 nm or 520 nm as a function of temperature. The 260 and 520 nm melting curves are very similar, indicating that DNA and gold nanoparticle melting are closely correlated.[73] The melting transition width is about 5 K, compared to 12 K for melting of free DNA. The transition width as well as the melting temperature has been dramatically modified by the binding to gold particles. It is also clear that the melting properties are highly dependent on the gold nanoparticle size. For bigger gold particles the melting temperature is higher.[73]

3.3.3. Effects of external variables on the melting properties

Besides the particle size, the melting properties of DNA-linked gold nanoparticles are also strongly dependent on other variables, including the DNA density on the gold surface, the interparticle distance, and the salt concentration in the solution. Jin et al. recently performed a series of experiments to systematically study the effects of various external variables.[72] A high DNA surface density on the Au nanoparticle is expected to provide advantage in particle stabilization as well as to increase the hybridization efficiency. The Experimental results showed that for temperature below 70 ºC, the melting temperature is proportional to the DNA surface density when the nanoparticle and target concentrations are kept constant. Also, a slight broadening of the melting transition was observed as the DNA density decreases.

The interparticle distance is another key parameter to control the melting properties. As gold nanoparticles are linked together via DNA hybridization, electromagnetic coupling between the nanoparticles result in significant damping of their surface plasmon resonances. The interparticle spacing also influences the amount of extinction due to scattering. Interparticle distance also influences Van der Waals and electrostatic forces between the particles, weakly affecting duplex DNA stability and hybridization/dehybridization properties. Experimental results showed that the melting temperature increases with the length of the interparticle distance for temperatures below 70 ºC, and there is a linear relationship between the two.

The melting behavior of DNA-linked nanoparticle aggregation also depends on the salt concentration. In Jin et al's study, the melting temperature increased from 41 to

61.5 ºC as the salt concentration was increased from 0.05 to 1.0 M while keeping the nanoparticle and linker DNA concentration constant. Moreover, increasing salt concentration also causes larger aggregates as evidenced by a larger absorption change during melting. It is believed that the salt brings about a screening effect that minimizes electrostatic repulsion between the DNA-DNA bases and between the nanoparticles, hence, strengthening the effect of the linker bond.[72]

3.4. APPLICATIONS OF NANOTECHNOLOGY TO BIOTECHNOLOGY

The ability to systematically modify the properties of nanostructures by controlling their structure and their surface properties at a nanoscale level makes them extremely attractive candidates for use in biological contexts, from fundamental scientific studies to commercially viable technologies.

The expanding availability of a variety of nanostructures with highly controlled properties in the nanometer size range has sparked widespread interest in their use in biotechnological systems. Size does matter - the fact that nanoparticles are similar in size range to many common bio-molecules makes them appear to be natural companions in hybrid systems. More importantly, however, are the new and unique properties that nanostructures bring to biotechnological applications. By controlling structure precisely at nanoscale dimensions, one can control and tailor properties of nanostructures, such as semiconductor nanocrystals and metal nanoshells, in a very accurate manner. In addition, one can make modifications to nanostructures to better suit their integration with biological systems; for example, modifying their surface layer for enhanced aqueous solubility, biocompatibility, or bio-recognition. With selected biomolecules bound to

nanostructure surfaces, new 'hybrid' nanostructures can be obtained for applications such as bio-sensing and imaging, or nanostructures can be embedded in other biocompatible materials to modify material properties or impart new functionality.

The idea of merging biological and non-biological systems at the nanoscale level is not a new one. The broad field of bioconjugate chemistry is based on combining the functionalities of biomolecules and non-biologically derived molecular species for specialized use in applications ranging from markers for research in cell and molecular biology to bio-sensing, bio-imaging and masking of immunogenic moieties to targeted drug delivery. Many current applications of nanostructures in biotechnology are a natural evolution of this approach. In fact, several of the 'breakthrough' applications recently demonstrated using nanostructure–biomolecular hybrids are in fact traditional applications originally addressed by standard molecular bioconjugate techniques that have been revisited with these newly designed nanostructure hybrids.

So one might argue, why replace conventional molecular tags, such as fluorescent chromophores, with nanostructures? Typically, nanostructures possess properties far superior to the molecular species they replace - higher quantum efficiencies, greater scattering or absorbance cross sections, optical activity over more biocompatible wavelengths, and significantly increased chemical or photochemical stability. The systematic control of nanostructure properties obtained by controlled variations in particle size and dimension is in direct contrast to molecular tags, whose properties vary non-systematically between molecular species. This systematic variation of properties via structure variation not only improves traditional applications, but also leads to new, unique applications well beyond the scope of conventional molecular bioconjugates. A

prime example is the optical properties of semiconductor nanocrystals and metal nanoshells, which are new and robust fluorophores, absorbers and scatterers in the near infrared, a region of the electromagnetic spectrum where tissue is essentially transparent. The availability of these new nanostructures will greatly facilitate new *in situ* probes and sensor methods.

The use of bioconjugate semiconductor nanocrystals, or 'quantum dots', as fluorescent biological labels, a new and powerful assay based on the optical properties of bioconjugate gold nanoparticles, a new innovation on a traditional bioconjugate technology, the biotechnologically friendly properties of gold nanoshells and a novel photo-thermally triggered drug delivery system based on a new nanoshell–polymer composite are the examples of nanostructures which have been integrated with biomolecular species and applied to relevant problems in biotechnology.

3.4.1. Bioconjugate quantum dots as fluorescent biological labels

Semiconductor nanocrystals are highly light absorbing, luminescent nanoparticles whose absorbance onset and emission maximum shift to higher energy with decreasing particle size, due to quantum confinement effects.[77] These nanocrystals are in the size range of 2–8 nm in diameter. Unlike molecular fluorophores, which typically have very narrow excitation spectra, semiconductor quantum dots absorb light over a very broad spectral range. This makes it possible to optically excite a broad spectrum of quantum dot colors using a single excitation laser wavelength, which enables one to simultaneously probe several markers. Although the luminescence properties of semiconductor nanocrystals have historically been sensitive to their local environment and nanocrystal

surface preparation, recent core-shell geometries where the nanocrystal is encased in a shell of a wider band gap semiconductor have resulted in increased fluorescence quantum efficiencies (> 50%) and greatly improved photochemical stability. In the visible region, CdSe–CdS core-shell nanocrystals have been shown to span the visible region from 550 nm (green) to 630 nm (red). Other materials systems, such as InP and InAs, provide quantum dot fluorophores in the near infrared region of the optical spectrum, a region of high physiological transmissivity. Although semiconductor nanocrystals are water insoluble, let alone biocompatible, surface functionalization with molecular species such as mercaptoacetic acid or the growth of a thin silica layer on the nanoparticle surface facilitate aqueous solubility.[78] Both the silica layer and the covalent attachment of proteins to the mercaptoacetic acid coating permit the nanoparticles to be biocompatible. Specific binding to cell surfaces, insertion into cells, and binding to cell nuclei have all been demonstrated following conjugation of the nanoparticle with the appropriate targeting protein.

3.4.2. A gold nanoparticle bioconjugate-based colorimetric assay

The use of gold colloid in biological applications began in 1971, when Faulk and Taylor invented the immunogold staining procedure. Since that time, the labeling of targeting molecules, especially proteins, with gold nanoparticles has revolutionized the visualization of cellular or tissue components by electron microscopy.[79] The optical and electron beam contrast qualities of gold colloid have provided excellent detection qualities for such techniques as immunoblotting, flow cytometry, and hybridization assays. Conjugation protocols exist for the labeling of a broad range of biomolecules with

gold colloid, such as avidin, streptavidin, glucose oxidase, horseradish peroxidase, and IgG.[80]

Gold nanoparticle conjugation was recently applied to polynucleotide detection in a manner that exploited the change in optical properties resulting from plasmon–plasmon interactions between locally adjacent gold nanoparticles.[81] The characteristic red of gold colloid has long been known to change to a bluish-purple color upon colloid aggregation. In the case of polynucleotide detection, mercaptoalkyl-oligonucleotide modified gold nanoparticle probes were prepared. When a single-stranded target oligonucleotide was introduced into solution, a polymer network was formed consisting of the target oligonucleotide and the conjugated nanoparticles. This condensed network brought the nanoparticles into close enough vicinity to induce a dramatic red-to-blue macroscopic color change. Because of the extremely strong optical absorption of gold colloid, this colorimetric method can be used to detect ~10 fmol of an oligonucleotide, which is 50 times more sensitive than sandwich hybridization detection methods based on fluorescence detection.

3.4.3. A gold nanoshell–polymer composite photo-thermally triggered drug delivery system

Gold nanoshells are new composite nanoparticles that combine infrared optical activity with the uniquely biocompatible properties of gold colloid. Metal nanoshells are concentric sphere nanoparticles consisting of a dielectric (typically gold sulfide or silica) core and a metal (gold) shell.[82] By varying the relative thickness of the core and shell layers, the plasmon-derived optical resonance of gold can be dramatically shifted in

wavelength from the visible region into the infrared over a wavelength range that spans the region of highest physiological transmissivity as shown in Figure 15.[83]

By varying the absolute size of the gold nanoshell, it can be made to either selectively absorb (for particle diameters <~75 nm) or scatter incident light. Because the gold shell layer is deposited using the same chemical methods used to grow gold colloid, the surface properties of gold nanoshells are virtually identical to those of gold colloid.

The same conjugation protocols used to bind a wide variety of biomolecules to gold colloid are therefore readily transferable to gold nanoshell conjugation. Successful gold nanoshell conjugation with enzymes and antibodies has been demonstrated. Gold nanoshells also take advantage of the inherent biocompatibility of gold, not requiring further surface functionalization or protective layer growth.

When optically absorbing gold nanoshells are embedded in a matrix, illuminating them at their resonance wavelength causes the nanoshells to transfer heat to their local environment. This photothermal effect can be used to optically 'remote control' drug release in a nanoshell–polymer composite drug delivery material.[84] Copolymers of *N*-

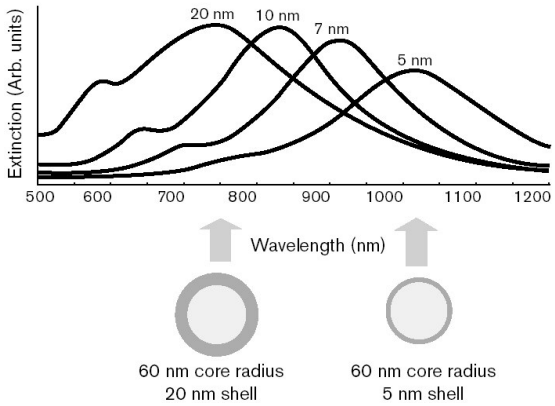

Figure 15. Optical resonances of gold-shell–silica-core nanoshells, as a function of their core : shell ratio, for particles of 120 nm core diameter. Respective spectra correspond to the nanoparticles depicted beneath.

isopropylacrylamide (NIPAAm) and acrylamide (AAm) exhibit a critical solution temperature (LCST) that is slightly above body temperature. When the temperature of the copolymer exceeds the LCST, the material collapses causing a burst release of any soluble material held within the polymeric matrix. Gold nanoshells that had been designed to strongly absorb near infrared light have been incorporated into poly(NIPAAm–co-AAm) hydrogels; light at these wavelengths (800–1200 nm), which can be transmitted through tissue with relatively little attenuation, is absorbed by the nanoparticles and converted to heat, thus causing the copolymer to collapse as its temperature exceeds its LCST. Significantly enhanced drug release has been achieved in response to irradiation by Nd:YAG laser light at 1064 nm. The triggered release of methylene blue and proteins of varying molecular weight has also been demonstrated. The nanoshell–composite hydrogels can also release multiple bursts of protein in response to repeated near IR irradiation.

Nanotechnology in the form of nanoparticles whose properties can be precisely tailored by chemical methods is rapidly becoming an important new tool in the arsenal of the biotechnologist. Nanostructures will no doubt lead to new and improved assays and sensing methods, new optically controlled functional materials, new highly specific color-coded probes of cellular function, and new optically based therapeutic methods.

3.3.4. Surface plasmon resonance

Optical biosensors capable of exploiting surface plasmon resonance (SPR), waveguides and resonant mirrors have been used a lot over the past decade to analyze biomolecular interactions. These sensors determine the affinity and kinetics of a wide

variety of molecular interactions in real time, without the need for a molecular tag or label.[85] Conventional SPR is applied in specialized biosensing instruments that use expensive sensor chips of limited reusable capacity and require complex chemistry for ligand or protein immobilization. SPR has also been successfully applied with colloidal gold particles in a buffered solution.[86] This application offers many advantages over conventional SPR because the support is cheap, easily synthesized and can be coated with various proteins or protein–ligand complexes, by charge adsorption. Using colloidal gold, the SPR phenomenon can be monitored in any UV–visible spectrophotometer. For high-throughput applications, the technology has been adapted in an automated clinical-chemistry analyzer. Among the label-free systems currently available, the use of metal nanocolloids offers enhanced throughput and flexibility for real-time biomolecular-recognition monitoring, at a reasonable cost.[87] A sensitive technique is being developed for the optical detection of gold nanoparticle- labeled molecules on protein microarrays by applying the SPR and specific molecular binding using rolling-circle amplification.[88]

3.5. THE ROLE OF NANOBIOTECHNOLOGY IN DRUG DISCOVERY

The current drug discovery paradigm constantly needs to progress, increasing efficiency and reducing time to market. The post-genomic era has uncovered many potentially important targets. However, to exploit their value in full, the efficiency of screening and validation processes must be improved. Today, Nanotechnology play a role in improving the drug discovery process. Given the inherent nanoscale functions of the biological components of living cells, it was inevitable that nanotechnology would be applied to the life sciences. Such applications give rise to the term nanobiotechnology.

Analyses of signaling pathways by nanobiotechnology techniques might provide new insights into disease processes, thus identifying more efficient biomarkers and understanding the mechanisms of action of drugs. This will help in designing new approaches to drug discovery.

Technical achievements in nanotechnology are being applied to improve drug discovery, drug delivery and pharmaceutical manufacturing. It is a common misconception that most of the applications of nanobiotechnology in drug discovery involve the use of nanoparticles. Currently, there are several fundamental nanotechnologies and nanodevices that can be used in drug discovery.

3.5.1. Nanotechnological applications in target identification and validation: *Proteomic applications*

Proteomics is playing an important role in the target identification and validation phases of the drug discovery process. Most current protocols, including protein purification and/or display and automated identification schemes, yield unacceptably low recoveries, thus, limiting the overall process with respect to sensitivity, speed and the requirement of large amounts of starting material. Less abundant proteins and proteins that can only be isolated from source materials that are limited in quantity (e.g. biopsies, body fluids) can be subjected to nanoscale protein analysis, nanocapture of the specific proteins and/or complexes and the optimization of all subsequent sample-handling steps, leading to the molecular-mass determination of the peptide fragments.

3.5.2. Nanodevices

Use of nanotube electronic biosensors in proteomics

Single-walled carbon nanotubes have been used as a platform for investigating surface–protein and protein– protein binding, as well as to develop highly specific electronic biomolecule detectors.[88] Non-specific binding on nanotubes, a phenomenon found with a wide range of proteins, is overcome by the immobilization of polyethylene-oxide chains. A general method is followed that enables the selective recognition and binding of target proteins, conjugating their specific receptors to polyethylene-oxide functionalized nanotubes. These arrays are attractive because no labeling is required and the entire assay can be done in the solution phase. This scheme, combined with the sensitivity of nanotube electronic devices, provides highly specific electronic sensors for detecting clinically important biomolecules (such as antibodies associated with human autoimmune diseases).

3.6. NANOBIOTECHNOLOGY FOR COMBINATION OF DRUG DESIGN AND DRUG DELIVERY

Many drugs discovered in the past could not be used in patients because a suitable method of drug delivery was lacking. Nanotechnology is also used to facilitate drug delivery. A product incorporating the NanoCrystal® technology of Elan Drug Delivery (King of Prussia, PA, USA), a solid-dose formulation of the immunosuppressant sirolimus, was approved by the FDA in 2000. Abraxane™ (Abraxis™ Oncology), containing paclitaxel as albumin bound particles in an injectable suspension, is approved

for the treatment of breast cancer after the failure of combination chemotherapy for metastatic disease or after relapse within six months of adjuvant chemotherapy. It is based on nanoparticle technology, which integrates biocompatible proteins with drugs to create the nanoparticle form of the drug (with a size ~100–200 nm) to overcome the insolubility problems encountered with paclitaxel.

Now, the trend is to consider drug-delivery issues at the earlier stages of drug discovery and design. Potential applications of nanotechnology to facilitate drug delivery can be taken into consideration at the stage of drug design. A carrier nanoparticle can be designed simultaneously with the therapeutic molecule. An example is the approach of Calando Pharmaceuticals (Duarte, CA, USA), to design siRNAs as anticancer agents using nanoparticle delivery. Proprietary technology uses sequence selection and construction of effective siRNA molecules that bind to (and self-assemble with) the siRNA to form uniform colloidal-sized particles ~50 nm in diameter. As they are administered by intravenous injection, larger particles cannot get out of the blood and penetrate the tumor. If the drug particles are smaller than 10 nm they are quickly excreted through the kidneys.

3.7. SUMMARY

Due to its unique recognition capabilities, physicochemical stability, mechanical rigidity, and high precision processibility, DNA is a promising material for "biomolecular nanotechnology." Though significant progress has been made, the study of DNA/PNA-based nanostructures is still at its early stage. The catalytic, electrical, magnetic, and electrochemical properties of such structures have not yet been systematically

investigated, and they, therefore, represent new frontiers in this field. It is anticipated that new phenomena and useful structures will continue to emerge over the next few years. Advanced study in this field will not only provide valuable fundamental information about the collective physical and chemical properties of nanoparticles and DNA, but also may provide access to new and useful electronic and photonic materials applicable to the industry.

3.8. FUTURE DIRECTIONS

As it stands now, the majority of commercial nanoparticle applications in medicine are geared towards drug delivery. There are some developments in directing and remotely controlling the functions of nanoprobes, for example driving magnetic nanoparticles to the tumor and then making them either to release the drug load or just heating them in order to destroy the surrounding tissue. The major trend in further development of nanomaterials is to make them multifunctional and controllable by external signals or by local environment thus essentially turning them into nano-devices.

3.19. REFERENCES

[1] Packman, P. L. Device Physics: Pushing the limits. *Science* **1999**, *285*, 2079-2081.

[2] Whitesides, G. M. Nanotechnology: Art of the Possible, Technology Review, Technology Review Inc., Cambridge, MA, Nov/Dec **1998**.

[3] Nanostructure Science and Technology, National Science & Technology Council Report, ed. R. W. Seigel, E. Hu, M. C. Roco, Kluwer Academic Publishers, Boston, **1999**.

[4] Gershenfeld N. A.; Chuang, I. L. Bulk Spin-Resonance Quantum Computation. *Science* **1997**, *275*, 350-356.

[5] Orlav, A. O.; Amlani, I.; Bernstein, G. H.; Lent, C. S.; Snider, G. L. Realization of a Functional Cell for Quantum-Dot Cellular Automata. *Science* **1997**, *277*, 928-930.

[6] Drexler, K. E. molecular Engineering: An Approach to the development of General Capabilities for molecular Manipulation. *Proc. Natl. Acad. Sci. USA* **1981**, *78*, 5275-5278. (b) Haddon, R.C.; Lamola, A. A. The Molecular Electronic device and the Biochip Computer: Present Status *Proc. Natl. Acad. Sci. USA* **1985**, *82*, 1874-1878.

[7] Niemeyer, C. Nanoparticles, Proteins and Nucleic Acids: Biotechnology Meets Material Science. *Angew. Chem. Int. Ed.* **2001**, *40*, 4128-4158.

[8] (a) Heller, A. *J. Phys. Chem.* ***1992,*** 96, 3579-3587. (b) Willner, I.; Riklin, A.; Shoham, B.; Rivenzon, D.; Katz, E. *Adv. Mater.* **1993**, *5*, 912-915. (c) Bardea, A.; Katz, E.; Buckmann, A. F.; Willner, I. NAD^+ -Dependent Enzyme Electrodes: Electrical Contact of Cofactor-Dependent Enzymes and Electrodes. *J. Am. Chem. Soc.* **1997**, *119*, 9114-9119.

[9] Willner, I.; Riklin, A.; Shoham, B.; Rivenzon, D.; Katz, E. *Adv. Mater.* **1993**, *5*, 912-915.

[10] Bardea, A.; Katz, E.; Willner, I. *Electroanalysis* **2000**, *12*, 1097-1106.

[11] Patolsky, F.; Katz, E.; Willner, I. Amplified DNA Detection by Electrogenerated Biochemiluminescence and by the Catalyzed Precipitation of an Insoluble Product on Electrodes in the Presence of the Doxorubicin Intercalator. *Angew. Chem. Int. Ed.* **2002**, *41*, 3398-3402.

[12] Park, T. H.; Shuler, M. L. Integration of Cell Culture and Microfabrication Technology. *Biotechnol. Prog.* **2003**, *19*, 243-253.

[13] Jin, R.; Cao, Y. W. C.; Mirkin, C. A.; Kelly, K. L.; Schatz, G. C.; J. G. Zheng. Photoinduced conversion of silver nanospheres to nanoprisms. *Science* **2000**, *294* , 1901–1903.

[14] Steel, A. B.; Herne, T. M.; Tarlov, M. J. Electrochemical Quantitation of DNA immobilized on gold. *Anal. Chem.* **1998**, *70*, 4670–4677.

[15] Kelley, S. O.; Barton, J. K.; Jackson, N. M.; McPherson, L. D.; Porter, A. B.; Spain, E. M.; Allen, M. J.; Hill, M. G. Orienting DNA helices on gold using applied electric fields. *Langmuir* **1998**, *14*, 6781–6784.

[16] Okahata, Y.; Matsunobu, Y.; Ijiro, K.; Mukae, M.; Murakami, A.; Makino, K. Hybridization of nucleic acids immobilized on a quartz crystal microbalance. *J. Am. Chem. Soc.* **1992**, *114*, 8299–8300.

[17] Patolsky, F.; Lichtenstein, A.; Willner, I. Amplified microgravimetric quartz-crystal-microbalance assay of DNA using oligonucleotide-functionalized liposomes or biotinylated liposomes. *J.Am. Chem. Soc.* **2000**, *122*, 418–419.

[18] Takenaka, S.; Takagi, M.; Uto, Y.; Kondo, H. DNA sensing on a DNA probe-modified electrode using ferrocenylnaphthalene diimide as the electrochemically active ligand. *Anal. Chem.* **2000**, *72*, 1334–1341.

[19] Hittemore, N. A.; Mullenix, A. N.; Inamati, G. B.; Manoharan, N.; Cook, P. D.; Tuinman, A. A.; Baker, D. C.; Chambers, J. Q. Synthesis and Electrochemistry of Anthraquinone-Oligodeoxynucleotide Conjugates. *Bioconjugate Chem.***1999**, *10*, 261–270.

[20] Han, S.; Lin, J.; Zhou, F.; Vellanoweth, R. L. Oligonucleotide-capped gold nanoparticles for improved atomic force microscopic imaging and enhanced selectivity in polynucleotide detection. *Biochem. Biophys. Res. Comm.* **2000**, *279*, 265–269.

[21] Storhoff, J. J.; Lazarides, A. A.; Mucic, R. C.; Mirkin, C. A.; Letsinger R. L.; Schatz, G. C. What controls the optical properties of DNA-linked gold nanoparticle assemblies? *J. Am. Chem. Soc.* **2000**, *122*, 4640–4650.

[22] Sastry, M.; Ramakrishnan, V.; Pattarkine, M. V.; Gole, A.; Ganesh, K. N. Hybridization of DNA by sequential immobilization of oligonucleotides at the air-water interface. *Langmuir* **2000**, *16*, 9142-9146.

[23] Sastry, M.; Ramakrishnan, V.; Pattarkine, M. V.; Ganesh, K. N. Studies on the formation of DNA–cationic lipid composite films and DNA hybridization in the composites. *J. Phys. Chem. B* **2001**, *105*, 4409-4414.

[24] Ganesh, K. N.; Nielsen, P. E. Peptide nucleic acids: Analogs and derivatives. *Curr. Org. Chem.* **2000**, *4*, 916-928.

[25] Kumar, A.; Phadtare, S.; Paschricha, R.; Guga, P.; Ganesh K. N.; Sastry, M. Assembling gold nanoparticles in solution using phosphorothioate DNA as structural interconnects. *Curr. Sci.* **2003**, *84*, 71-74.

[26] Moller, R.; Csaki, A.; Kohler, J. M.; Fritzche, W. DNA probes on chip surfaces studied by scanning force microscopy using specific binding of colloidal gold *Nucleic Acid Res.* **2000**, *28*, e91(1-5).

[27] Liu, T.; Tang, J.; Jiang, L. The enhancement effect of nanoparticles as a surface modifier on DNA sensor sensitivity. *Biochem. Biophys. Res. Commun.* **2004**, *313*, 3-7.

[28] Woffendin, C.; Yang, Z.; Udaykumar; Xu, L.; Yang, N.; Sheehy, M. J.; Nabel, G. J. nonviral and viral delivery of a Human Immunodeficiency Virus protective gene into primary human T cells. *Proc. Natl. Acad. Sci. U.S.A.* **1994**, *91*, 11581-11585.

[29] Niemeyer, C. M. Nanoparticles, proteins and nucleic acids: Biotechnology meets Materials Science. *Angew. Chem., Int. Ed.* **2001**, *40*, 4128-4158.

[30] Bielinska, A.; Eichman, J. D.; Lee, I.; Baker, J. R. Jr.; Balogh, L. Imaging {Au^0-PAMAM} gold dendrimer nanocomposites in cells. *J. Nanopart. Res.* **2002**, *4*, 395-403.

[31] Nakao, H.; Shiigi, H.; Yamamoto, Y.; Tokonami, S.; Nagaoka, T.; Sugiyama, S.; Ohtani, T. Highly ordered assemblies of Au nanoparticles organized on DNA. *Nano Lett.* **2003**, *3*, 1391-1394.

[32] Chakrabarti, R.; Klibanov, A. M. Nanocrystals modified with Peptide nucleic acids (PNAs) for selective self-assembly and DNA detection. *J. Am. Chem. Soc.* **2003**, *125*, 12531- 12540.

[33] Storhoff, J. J.; Elghanian, R.; Mirkin, C. A.; Letsinger, R. L. Sequence-dependent stability of DNA-modified gold nanoparticles. *Langmuir* **2002**, *18*, 6666-6670.

[34] Jang, N. H. The Co-ordination chemistry of DNA nucleosides on gold nanoparticles as a probe by SERS. *Bull. Korean Chem. Soc*. **2002**, *23*, 1790-1800.

[35] Hiromi, K.; Petrovykh, D. Y.; Tarlov, M. J.; Whitman, L. J. Base-dependent competitive adsorption of single-stranded DNA on gold. *J. Am. Chem. Soc.* **2003**, *125*, 9014-9015.

[36] Demers, L. M.; Ostblom, M.; Zhang, H.; Jang, N. H.; Liedberg, B.; Mirkin, C. A. Thermal desorption behavior and binding properties of DNA bases and nucleosides on gold. *J. Am. Chem. Soc.* **2002**, *124*, 11248-11249.

[37] Rongchao Jin, Guosheng Wu, Zhi Li, Chad A. Mirkin, and George C. Schatz. What Controls the Melting Properties of DNA-Linked Gold Nanoparticle Assemblies? *J. Am. Chem. Soc.* **2003**, *125*, 1643 –1654.

[38] Kumar, A.; Pattarkine, M.; Bhadbhade, M.; Mandale, A. B.; Ganesh K. N.; Sastry, M. Linear Superclusters of Colloidal Gold Particles by Electrostatic Assembly on DNA Templates *Adv. Mater.* 2001, *13*, 341-344.

[39] Sastry, M.; Kumar, A.; Datar, S.; Dharmadhikari, C. V.; Ganesh, K. N. DNA-mediated electrostatic assembly of gold nanoparticles into linear arrays by a simple drop-coating procedure. *Appl. Phys. Lett.* **2001**, *78*, 2943-2945.

[40] Nuzzo R. G.; Allara, D. L. Adsorption of Bifunctional Organic Disulfides on Gold Surfaces. *J. Am. Chem. Soc.* **1983**, *105*, 4481-4483.

[41] L. H. Dubois and R. G. Nuzzo, *Annu. Rev. Phys. Chem.* **1992**, *43*, 437.

[42] Peterlinz, K. A.; Georgiadis, R. M.; Herne T. M.; Tarlov, M. J. Observation of Hybridization and Dehybridization of Thiol-Tethered DNA Using Two-Color Surface Plasmon Resonance Spectroscopy. *J. Am. Chem. Soc.* **1997**, *119*, 3401-3402.

[43] Yang, M.; Yau, H. C. M.; Chan, H. L. Adsorption Kinetics and Ligand-Binding Properties of Thiol-Modified Double-Stranded DNA on a Gold Surface. *Langmuir* **1998**, *14*, 6121-6129.

[44] C. D. Bain and G. M. Whitesides, *Agnew. Chem. Int. Ed. Engl.* **1989**, *28*, 506.

[45] Hickman, J. J.; Laibinis, P. E.; Auerbach, D. I.; Zou, C.; Gardner, T. J.; Whitesides, G. M.; Wrighton, M. S. Toward Orthogonal Self-Assembly of Redox Active Molecules on Pt and Au: Selective reaction of Disulfide with Au and Isocyanide with Pt. *Langmuir* **1992**, *8*, 357-359.

[46] S. Pathak, S. K. Choi, N. Arnheim, and M. E. Thompson, *J. Am. Chem. Soc.* **2001**, *123.*

[47] A. P. Alivisatos, K. P. Johnsson, X. Peng, T. E. Wilson, C. J. Loweth, M. P. Bruchez; P. G. Schultz, *Nature* **1996**, *382*, 609.

[48] Niemeyer, C. M.; Burger, W.; Peplies, J. Covalent DNA – Streptavidin Conjugates as Building Blocks for Novel Biomettalic Nanostructures. *Angew. Chem. Int. Ed.* **1998**, *37*, 2265-2268.

[49] N. C. Seeman, *J. Theor. Biol.* **1982**, *99*, 237.

[50] N. C. Seeman, *Nanotechnology* **1991**, *2*, 149.

[51] E. Winfree, F. Liu, L. Wenzler, and N. C. Seeman, *Nature* **1998**, *394*, 539.

[52] N. C. Seeman, *Annu. Rev. Biophys. Biomol. Struct.* **1998**, *27*, 225.

[53] J. Shi and D. E. Bergstrom, *Angew. Chem., Int. Ed. Engl.* **1997**, *36*, 111.

[54] C. A. Mirkin; R. L. Letsinger; R. C.; Mucic; J. J. Storhoff. *Nature* **1996**, *382*, 607.

[55] Loweth, C. J.; Caldwell, W. B.; Peng, X.; Alivisatos, A. P.; Schultz, P. G. DNA – Based Asembly of Gold Nanocrystals. *Agnew. Chem. Int. Ed.* **1999**, *38*, 1808-1812.

[56] Mucic, R. C.; Storhoff, J. J.; Mirkin, C. A.; Letsinger, R. L. DNA – Directed Synthesis of Binary Nanoparticle Network Materials. *J. Am. Chem. Soc.* **1998**, *120*, 12674-12675.

[57] Baker, S. E.; Cai, W.; Lasseter, T. L.; Weidkamp, K. P.; Hamers, R. J. Covalently Bonded Adducts of Deoxyribonucleic Acid (DNA) Oligonucleotides with Single-Wall Carbon Nantube: Synthesis and Hybridization. *Nano Lett.* **2002**, *2*, 1413-1417.

[58] K. A. Williams; P. T. M. Veenhuizen; B. G. de la Torre; R. Eritja; G. Dekker. *Nature* **2002**, *420*, 761.

[59] P. E. Nielsen; M. Engholm. R. H. Berg; O. Buchardt. *Science* **1991**, *254*, 1497.

[60] D. E. Bergstrom, in Current Protocols in Nucleic Acid Chemistry, S. L. Beaucage, D. E. Bergstrom, G. D. Glick, and R. A. Jones, Eds. (Wiley, New York, 2001).

[61] Kool, E. T. Replacing the Nucleobases in DNA with Designer Molecules. *Acc. Chem. Res.* **2002**, *35*, 936-943.

[62] Popescu, D.-L.; Parolin, T. J.; Achim, C. Metal Incorporation in Modified PNA Duplexes. *J. Am. Chem. Soc.* **2003**, *125*, 6354-6355.

[63] Wagenknecht, H.-A. Metal-Modified DNA Base Pairing and Metal Arrays in Artificial DNA: Towards New Nanodevices. *Angew. Chem. Int. Ed.* **2003**, *42*, 3204-3206.

[64] T. Carell, C. Behrens, and J. Gierlich, *Org. Biomol. Chem.*, **2003,** *1*, 2221.

[65] Tanaka, K.; Shionoya, M. Synthesis of a Novel Nucleoside for Alternative DNA Base Pairing through Metal Complexation. *J. Org. Chem.*, **1999**, *64*, 5002-5003.

[66] Tanaka, K.; Yamada, Y.; Shionoya, M. Formation of Silver (I)-Mediated DNA Duplex and Triplex through an Alternative Base Pair of Pyridine Nucleobases. *J. Am. Chem. Soc.*, **2002**, *124*, 8802-8803.

[67] Meggers, E.; Holland, P. L.; Tolman, W. B.; Romesber, F. E.; Schultz, P. G. *J. Am. Chem. Soc.*, **2000**, *122*, 10714-10715.

[68] Weizman, H.; Tor, Y. 2,2'-Bipyridine Ligandiside: A Novel Building Block for Modifying DNA with Intra-Duplex Metal Complexes. *J. Am. Chem. Soc.*, **2001**, *123*, 3375 –3376.

[69] Atwell, S.; Meggers, E.; Spraggon, G.; Schultz, P. G. Structure of a Copper-Mediared Base Pair in DNA. *J. Am. Chem. Soc.*, **2001***, 123*, 12364-12367.

[70] Tanaka, K.; Tengeiji, A.; Kato, T.; Toyama, N.; Shionoya, M. A Discrete Self-Assembled Metal Array in Artificial DNA. *Science*, **2003**, *299*, 1212-1213.

[71] Storhoff, J. J.; Lazarides, A. A.; Mucic, R. C.; Mirkin, C. A.; Letsinger, R. L.; Schatz, G. C. What Controls the Optical Properties of DNA-Linked Gold Nanoparticle Assemblies? *J. Am. Chem. Soc.*, **2000**, *122*, 4640-4650.

[72] Jin, R.; Wu, G.; Li, Z.; Mirkin, C. A.; Schatz, G. C. What Controls the Melting Properties of DNA-Linked Gold Nanoparticle Assemblies? *J. Am. Chem. Soc.*, **2003**, *125*, 1643-1654.

[73] C.-H. Kiang, *Physica A*, **2003**, *321*, 164.

[74] S. Link and M. A. El-Sayed, *J. Phys. Chem.*, **1999**, *103*, 8410.

[75]A. A. Lazarides and G. C. Schatz, J. Phys. Chem., **2000**, *104*, 460.

[76] S. Y. Park and D. Stroud, *Phys. Rev. B*, **2003**, *67*, 212202.

[77] Bruchez, M. Jr.; Moronne, M.; Gin, P.; Weiss, S.; Alivisatos, A.P. Semiconductor nanocrystals as fluorescent biological labels. *Science*, **1998**, *281*:2013-2016.

[78] Chan, WCW.; Nie, S.; Quantum dot bioconjugates for ultrasensitive nonisotopic detection. *Science*, **1998**, *281*, 2016-2018

[79] Hayat, M. (Ed): *Colloidal Gold: Principles, Methods and Applications.* San Diego: Academic Press; **1989**.

[80] Anonymous: *Immunochemistry Labfax*. Oxford, UK: BIOS Scientific Publishers; **1994.**

[81] Elghanian, R.; Storhoff, J. J.; Mucic, R. C.; Letsinger, R. L.; Mirkin, C. A. Selective colorimetric detection of polymucleotides based on the distance-dependent optical properties of gold nanoparticles. *Science*, **1997**, *277*, 1078-1081

[82] Averitt, R. D.; Sarkar, D.; Halas, N. J. Plasmon resonance shifts of Au-coated Au2S nanoshells: insight into multicomponent nanoparticle growth. *Phys Rev Lett*, **1997**, *78*, 4217-4220.

[83] Oldenburg, S. J.; Averitt, R. D.; Westcott, S. L.; Halas, N. J. Nanoengineering of optical resonances. *Chem Phys Lett* **1998**, *288*, 243-247.

[84] Sershen, S; Westcott, S. L.; Halas, N. J.; West, J. L. Temperature-sensitive polymer-nanoshell composites for photothermally modulated drug delivery. *J Biomed Mater Res* **2000***, in press*.

[85] Cooper, M.A. Optical biosensors in drug discovery. *Nat. Rev. Drug Discov.* **2002***, 1*, 515–528.

[86] Englebienne, P. *et al.* Advances in highthroughput screening: biomolecular interaction monitoring in real-time with colloidal metal nanoparticles. *Comb. Chem. High Throughput Screen.* **2003***, 6*, 777–787.

[87] Englebienne, P. *et al.* Surface plasmon resonance: principles, methods and applications in biomedical science. *Spectroscopy* **2003,** *17*, 255–273.

[88] Chen, R.J. *et al.* Noncovalent functionalization of carbon nanotubes for highly specific electronic biosensors. *Proc. Natl. Acad. Sci. U. S. A.*, **2003***, 100*, 4984–4989

Chapter 3: Section B

Present Work

Studies on interactions of DNA:PNA-Gold nanoparticles (AuNPs) by spectroscopy, microscopy and microcalorimetry

3.10. PRESENT WORK - I : A RATIONALE

The directed assembly of nanoparticles (particularly gold nanoparticles, AuNPs) using DNA as a natural template is gaining increasing popularity.[1-4] The base pairing interaction of complementary DNA strands (Figure 1A), which is mediated by hydrogen bonds, facilitates this process in a straightforward manner. The use of DNA as a structural interconnect for gold nanoparticle assembly, (Figure 1B) has a number of advantages:

(1) DNA sequences may be suitably designed to precisely control the extent of aggregation and inter-particle separation and thereby, the collective optical properties of the assembly.[2] Such assemblies may have important implications in nanomaterials science.

(2) DNA is an excellent anionic one-dimensional template for promoting the growth of metal nanowires either by a process of ion entrapment and reduction or direct attachment of metal nanoparticles[5] and

(3) The sequence-specific denaturation of DNA duplexes enables the use of gold nanoparticles as colorimetric DNA detectors with immense application in diagnosis of genetic disorders.[6]

In all studies pertaining to the assembly of nanoparticles by DNA hybridization, conjugation of the single stranded DNA sequences with gold nanoparticles has been achieved by thiolation of the DNA at the 3' end of the sequence. While this has been shown to be an excellent strategy for anchoring DNA at a single point to the nanoparticle via the strong gold-thiolate covalent bond, exploring the binding of DNA to the

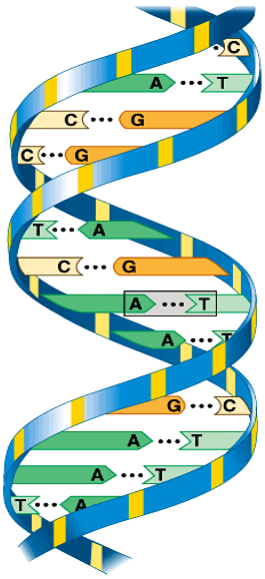

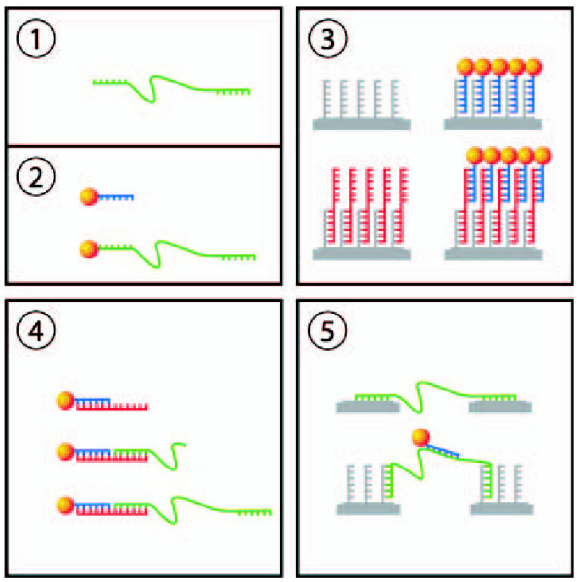

nanoparticles through the nucleobases is also worthwhile. Direct binding of free nucleobases to gold nanoparticles could provide an excellent strategy for using the particles as nanoelectrodes for sensing, electron transport studies and as carriers in gene therapy.

The specific objectives of this chapter are:

(i) To carry out the interaction studies and thermodynamic analysis for the interaction of the nucleobases (Figure 2A) (Adenine, Guanine, Cytosine and Thymine) as well as the corresponding PNA monomers (Figure 2B) with AuNPs at molecular level by

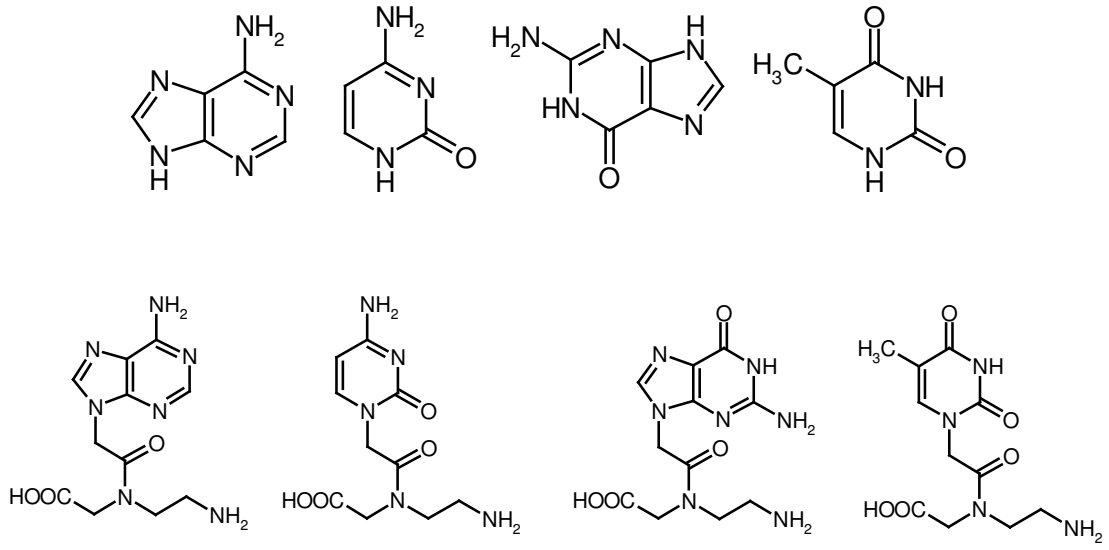

UV-visible Spectroscopy, Isothermal Titration Calorimetry (ITC) and Transmission Electron Microscopy (TEM).

(ii) The synthesis and characterization of DNA/PNA/DNA:PNA-gold nanoparticle composites using TEM and UV-T_m techniques at oligomeric level.

3.11. CHARACTERIZATION TECHNIQUES

Several different characterization techniques have been used during the course of present work to characterize the biocomposites. These comprise of UV-visible spectroscopy, Transmission Electron Microscopy (TEM) and Isothermal Titration Calorimeter (ITC).

3.11.1. UV-Visible Spectroscopy

UV-visible spectroscopy is used for diagnosing the spectral signatures of gold nanoparticles and their complexes with free nucleobases/*aeg*PNA monomers.

Absorption spectroscopy in the visible region (Figure 3) has long been an important tool to the analyst.[8] The spectroscopic transitions arise due to molecular and structural changes in the substances being examined, leading to corresponding changes in the ability to absorb light in the visible region of the electromagnetic spectrum. Absorption of electromagnetic radiation leads to a transition of electron from the ground state to one of the several excited states. Most of the electronic spectra are very broad smooth curves and not sharp peaks. This is because changes in the electronic energy are also accompanied by changes in the vibrational and rotational energy levels (Figure 4).

A variety of energy absorption occurs in molecules arising from different types of electrons within a molecule. For instance, electrons in strong σ bonds, weaker π-bonds or non-bonded (n) orbitals can be elevated to excited antibonding states represented as σ* and π*. Most σ to σ* absorptions for individual bonds take place below 200 nm in the vacuum ultraviolet region and transitions in σ bonds are transparent in the near UV/vis region. $\pi \rightarrow \pi^*$ and $n \rightarrow \pi^*$ absorptions occur in the near UV/vis region, and these are present in molecules possessing unsaturated groups known as chromophores.

The intensity of light passing through a sample is given by the relation:

$$I = I_0 \exp(-\alpha k x) \quad \text{.....Equation (1)}$$

The Electromagnetic Spectrum

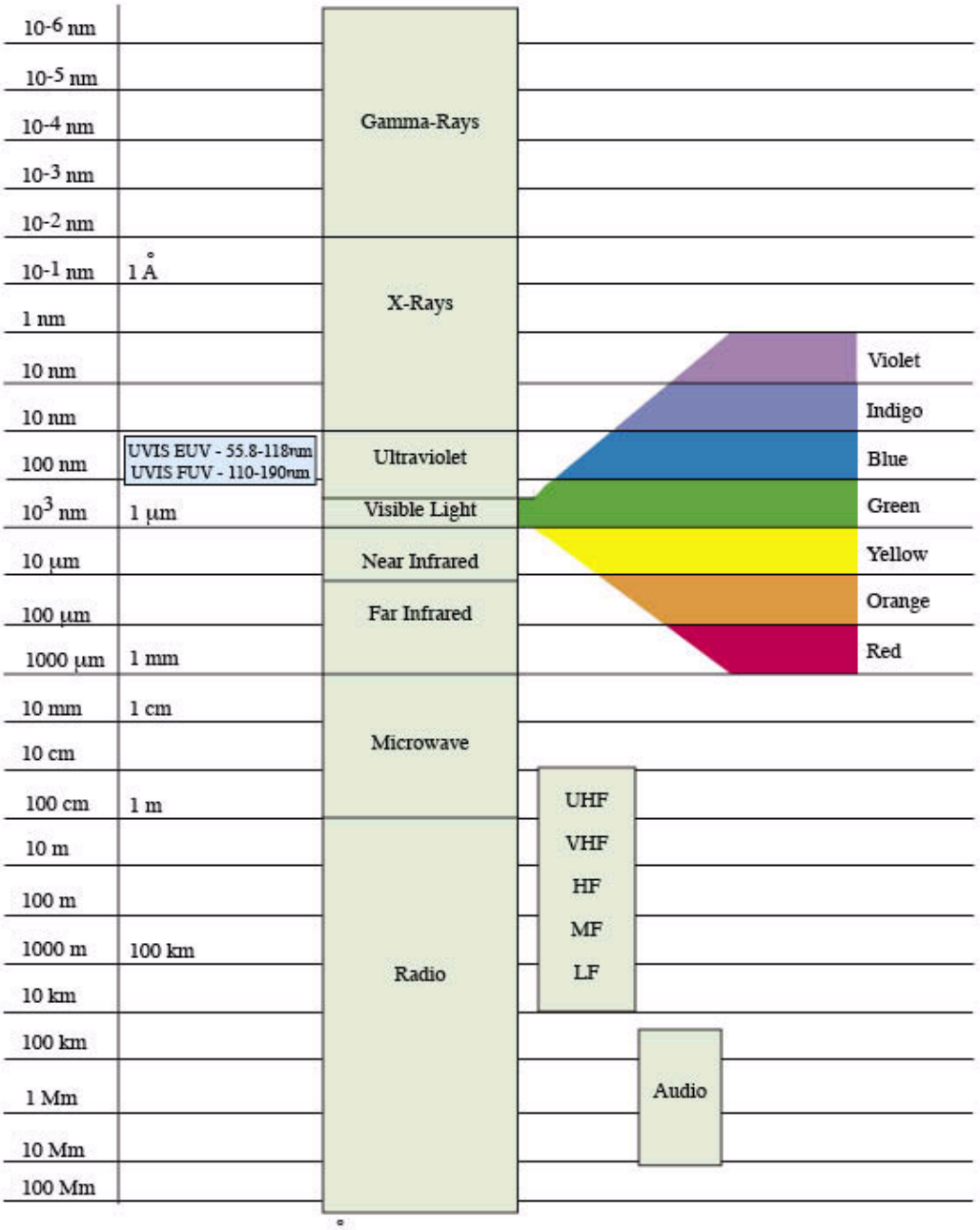

nm=nanometer, Å=angstrom, μm=micrometer, mm=millimeter,
cm=centimeter, m=meter, km=kilometer, Mm=Megameter

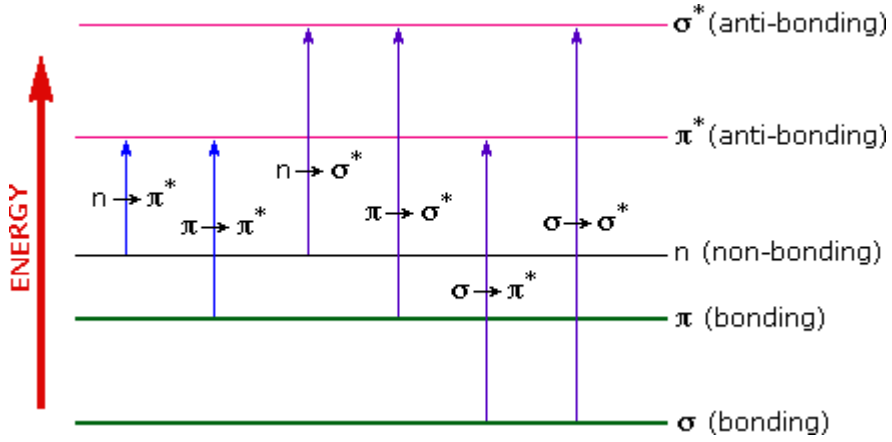

where I = intensity of transmitted light; I_0 = intensity of incident light; α = molar absorption coefficient; k = constant; x = path length.

The combined Beer-Lambert law is used for quantification of exact concentration of unknown species in a mixture using UV-vis spectroscopy. This can be done by drawing a graph of intensities of absorption for different concentrations of the sample and comparing with a standard graph.[9]

The Beer-Lambert law is:

$A = \varepsilon c l$…….. Equation (2)

where ε = proportionality constant known as the molar extinction coefficient.

A shift of absorption to a longer wavelength is called red shift or bathochromic shift, while a shift of absorption to a shorter wavelength is called blue shift or hypochromic shift.

A surface plasmon (SP) is a collective excitation of the electrons at the interface between a conductor and an insulator. Surface plasmon phenomena emerge in a number of different scenarios: the energy loss of electrons propelled through thin metal foils; the

colorful appearance of suspensions of small metallic particles; and the dips in the intensity of light reflected from metal coated diffraction gratings. When the interface between the media is coated with a thin layer of metal (gold), and light is monochromatic and p-polarized, the intensity of the reflected light is reduced at a specific incident angle producing a sharp shadow called surface plasmon resonance (SPR). This is due to the resonance energy transfer between evanescent wave and surface plasmons. The resonance conditions are influenced by the material adsorbed onto the thin metal film.

The frequency and width of the surface plasmon absorption depends on the size and shape of the metal nanoparticles as well as on the dielectric constant of the metal itself and the surrounding medium. Noble metals such as copper, silver and gold have a strong visible-light plasmon resonance, whereas most other transition metals show only a broad and poorly resolved absorption band in the ultraviolet region. This difference is attributed to the strong coupling between the plasmon transition and the interband excitation. In addition, the conduction band electrons of the noble metals can move freely, independently from the ionic background, and the ions act only as scattering centers. This gives the electrons in the noble metals a higher polarizability, which shifts the plasmon resonance to lower frequencies with a sharp bandwidth.

The surface plasmon resonance was theoretically explained by Mie in 1908, including linear optical properties such as extinction and scattering of small spherical metal particles. Mie's theory and experimental spectra agree well in the size regime >20 nm until the normal incidence absorption no longer shows a plasmon resonance for bulk metals. The spectrum is composed of the sum of size-dependent absorption and scattering modes. Higher order modes become more dominant with increasing particle size, causing

the plasmon absorption band to red shift and resulting in increased bandwidth, because for larger particles, the light cannot polarize the nanoparticles homogeneously and retardation effects lead to the excitation of higher order modes. The optical absorption spectra depend directly on the size of the nanoparticles, which is called the extrinsic size effect.

$$\alpha = \frac{18\,\pi}{\ln 10}\ \frac{10^5}{\lambda}\ \frac{M\,n_0^3}{\rho}\ \frac{\varepsilon_2}{(\varepsilon_1 + 2\,n_0^2) + \varepsilon_2^2}$$

where λ is the wavelength of light in nanometers, M and ρ are the molecular weight and density of the metal, n_o is the refractive index of the solvent and ε_1 and ε_2 are the real and imaginary parts of the dielectric constant of the metal. When the size of the particles becomes smaller than the mean free path of the electrons, the absorption bands are broadened; this is accounted for by using size-corrected values of ε_2. [9-11]

$$\varepsilon_2 = \varepsilon_{2\,(bulk)} + (\omega_p^{\,2} / \omega^3)(V_F/R) \quad \text{..... Equation (4)}$$

where, ω is the light frequency, ω_p is the plasmon frequency, V_F the electron velocity at the Fermi level and R the particle radius (R/V_F, mean time of the free movement of the electrons). Resonance with the incident light is reached at the wavelength, where the negative value of ε_1 of the metal is equal to twice the dielectric constant of the medium.

Gold particles possess plasmon resonances in the visible range (~514 nm). Resonance is produced by a collective excitation of all the free electrons in the particles. As is shown in Figure 5, the movement of the electrons under the influence of the electric field vector of the incoming light leads to a dipole excitation across the particle sphere,

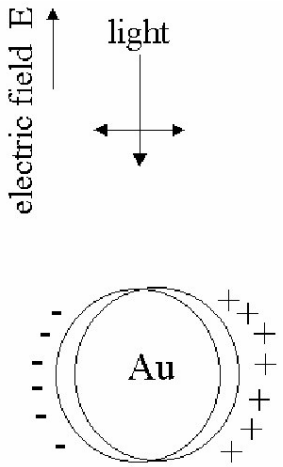

the positive polarization charge acting as a restoring force, which makes the electrons oscillate.

Thus, the electron density within a surface layer, whose thickness equals the screening length of a few angstroms, oscillates, whereas the density in the interior of the particle remains constant (surface plasmon). Therefore, any changes in the electron density of this surface layer will lead to changes in the plasmon absorption. For example, the surface sensitivity of colloidal nanoparticles has been used to study adsorption/chemisorption of thiols.[12-14]

UV-visible spectroscopy was used for monitoring gold nanoparticles and their biocomposite signatures. Noble metal particles are ideal candidates for study with UV-vis spectroscopy, since they exhibit strong surface plasmon resonance absorption in the visible region, and are highly sensitive to surface modification.

3.11.2. Transmission electron microscopy

Transmission electron microscopy (TEM) is an imaging technique whereby a beam of electrons is focused onto a specimen causing an enlarged version to appear on a fluorescent screen or a photographic film or to be detected by a camera. TEM is widely used to characterize a lot of materials both from a morphological point of view and from the crystallographic but also for the elemental composition. Using TEM, a large variety of materials as ceramics, alloys, biocomposites, polymers, metals and semiconductors can be observed.

This technique requires that the thickness of the films under study will be less than 300 Å; however, direct observation of one monolayer is not possible because of lack of contrast. The electron energy in TEM is very high (100 KeV) and the resolution ranges from 1000 Å to a few tens of Angstroms. Samples for TEM analysis are prepared by drop coating films of the re-dispersed powder in de-ionized water on carbon-coated copper TEM grids, allowing the grid to stand for 2 minutes following which the extra solution is removed using a blotting paper.

TEM set up consists of a diffraction camera with an electron gun, an aperture to define a small beam cross-section, a specimen holder, a fluorescent screen and a plate camera[15] (Figure 6).

The virtual source is an electron gun, producing a stream of monochromatic electrons. This stream is focused to a small, thin, coherent beam by the use of condenser lenses 1 and 2. The first lens largely determines the spot size; while the second lens controlled by the intensity or brightness knob help change in the nature of the spot from

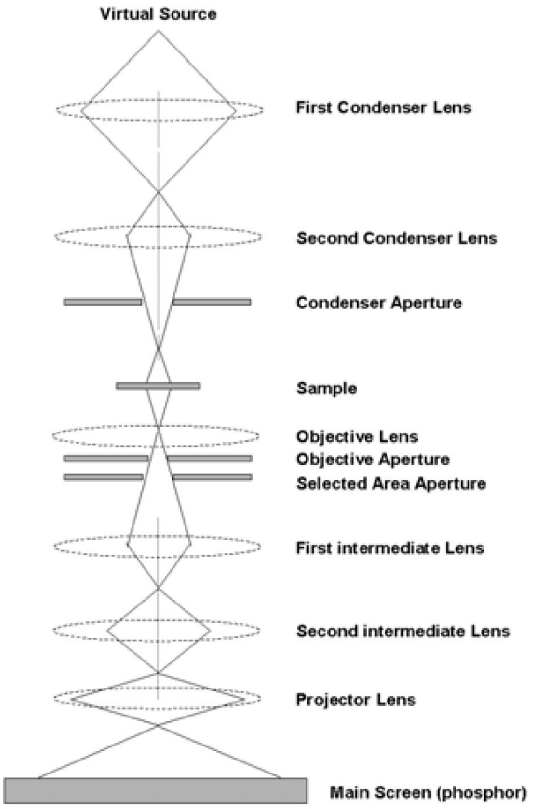

a wide dispersed spot to a pinpoint beam.

The beam is restricted by the condenser aperture, which knocks out high angle electrons and upon striking the specimen, parts of it are transmitted. This transmitted part is focused by the objective lens into an image. The objective aperture enhances the contrast by blocking out high-angle diffracted electrons, while the selected area aperture enables the user to examine the periodic diffraction of electrons by ordered arrangements of atoms in the sample. The image is passed down the column through the intermediate and projector lenses, and enlarged all the way.

The image strikes the phosphor image screen and the generated light allows the seeing of the image. The darker areas of the image represent those areas of the sample that fewer electrons were transmitted through (they are thicker or denser). The lighter

areas of the image represent those areas of the sample that more electrons were transmitted through (they are thinner or less dense).

The TEM image gives the information on its structure and composition. For example, Figure 7A showing TEM micrograph of a nanoparticle/DNA assembly made up of a single λ-DNA scaffold. The linear assemblies were observed to have an extended structure, with some of the larger assemblies reaching nearly 1μm in length. Over these distances the particles are observed to be closely and evenly spaced along the DNA scaffold. Figure 7B depicts TEM micrograph of an expanded portion of the assembly showing that the average interparticle spacing is uniform along the DNA scaffold consistent with a close-packed arrangement of the nanoparticles along the DNA scaffold. The average diameter of the nanoparticles Y=1.9±0.8 nm (n=790).[16]

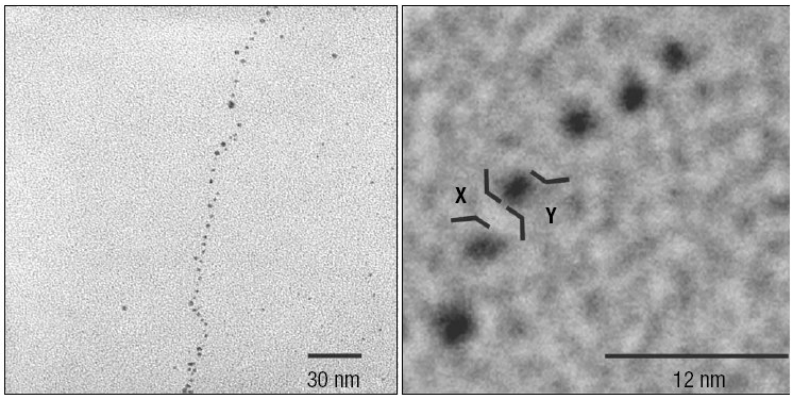

3.11.3. Isothermal Titration Calorimetry (ITC)

Molecular recognition is a fundamental but complex process, which is essential to delineate the molecular basis of life. Understanding the thermodynamics underlying such recognition processes is of enormous interest and still remains a challenge. Due to significant improvements in instrument sensitivity, isothermal titration calorimetry (ITC), (Figure 8) is now becoming a routine method for the generation of thermodynamic data relating to biomolecular association. Heat changes are associated with every molecular interaction and the ultra sensitive Isothermal Titration Calorimetry (ITC) technique can detect small changes in heat accompanying a specific event.[17]

Recent advances in ITC systems permit complete characterization of molecular interactions with as little as a few nanomoles of material. An ITC experiment takes 30–60 min to complete and is highly automated, in terms of instrument operation, data

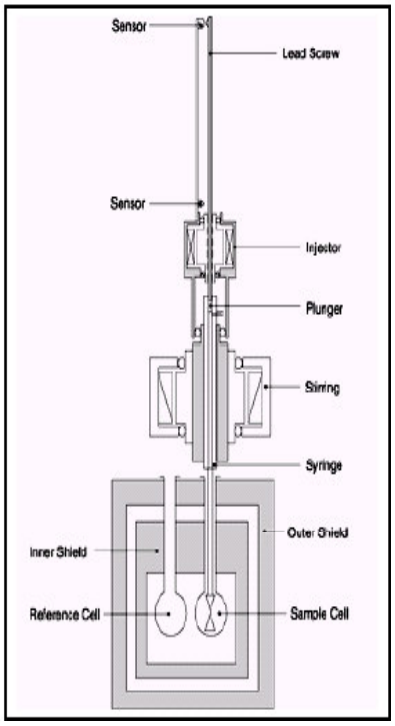

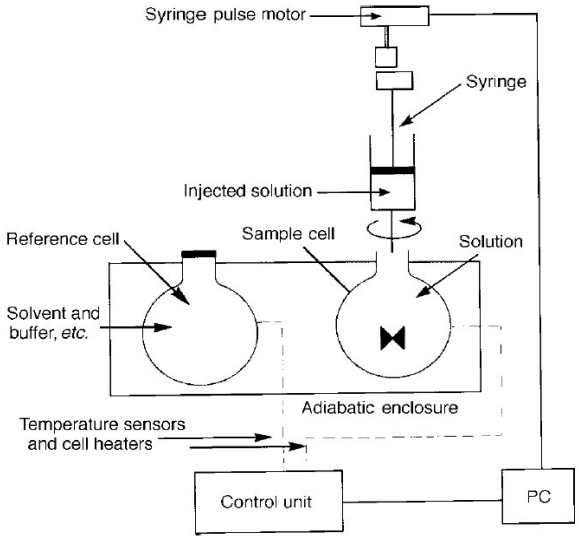

collection and analysis and provides a complete thermodynamic profile of the interaction consisting of the binding constant (K_A), the number of binding sites (*n*), enthalpy (H), entropy (S) and free energy (G). ITC may be used to study molecular interactions in native, modified, or immobilized substances and directly measures enthalpy.[17]

The instrument utilizes a differential design with two identical cells (Figure 10). All binding processes occur in the sample cell, whose temperature is continuously compared to that of the reference cell, where no reaction takes place. The cells are surrounded by an inner shield, which is maintained at the same temperature as the cells in order to minimize any heat flow to or from the cells. The outer shield is also maintained at the same temperature, to compensate for any changes in room temperature. During the operation, amount of power supplied to the sample cell (feedback power) is continuously adjusted so that its temperature is always identical to that of the reference cell. If, for example, an exothermic reaction occurs in the sample cell, then the feedback power to the sample cell will be automatically reduced to null the temperature difference caused by the heat released within the sample cell. The precise amount of heat released by the exothermic process can then be determined since it is exactly equal to the reduction in the amount of feedback heat necessary to re-establish the temperature null between the cells.[17]

ITC has been used with much success in understanding biomolecular binding processes[18-22] such as protein-ligand,[18] protein-protein,[19] DNA-RNA,[20] DNA-protein[21] and protein-lipid[22] interactions. However, not many reports exist in literature on application of ITC to characterize nanoparticle interactions.

ITC is the only technique which allows direct measurement of the values of K_A, n, and ΔH° in a single experiment. ΔH° is actually an apparent (or observed) value since the binding reaction is accompanied by many linked equilibria yielding heat changes. The observed value of ΔH must be corrected for the heat of ionization of the buffer, when the binding interaction is associated with changes in protonation. The magnitudes of ΔG° and ΔS° are then obtained from the relationship:

$$\Delta G^\circ = \Delta H^\circ - T\Delta S^\circ = -RT\ In\ K_a \quad \text{.....Equation (5)}$$

ITC also allows measurement of ΔCp, the change in heat capacity (also known as specific heat) by measuring ΔH as a function of temperature.

$$\Delta Cp = d(\Delta H^\circ)/dT = T.d(\Delta S^\circ)/dT \quad \text{.....Equation (6)}$$

In order to fully characterize the thermodynamics of a binding interaction it is necessary to measure, not only ΔG°, ΔH° and ΔS°, but also ΔCp, since this parameter allows the prediction of the changes in the other three parameters with temperature. ΔC_p is usually measured from the change in enthalpy with temperature, using the relationship:

$$\Delta Cp = (\Delta H^\circ_{T2} - \Delta H^\circ_{T1})/\ T2 - T1 = (\Delta S^\circ_{T2} - \Delta S^\circ_{T1})/\ In\ (T2\ /\ T1) \text{..Equation (7)}$$

where T1 and T2 are two temperatures at which separate determinations have been made.

3.11.3a. Interpretation of Thermodynamics: Binding Parameters

The standard Gibb's free energy change, ΔG°, is the most important energetic parameter measured by ITC. ΔG° determines the direction in which biomolecular binding equilibrium will spontaneously proceed, with more negative values of ΔG° favoring higher binding. It is important to realize that ΔG° and its enthalpic and entropic

constituents depend upon differences between free and bound states for both of the interacting partners. The standard enthalpy change, ΔH°, reflects changes in the interactions between atoms. An overall increase in binding strength is associated with the release of heat, or a negative enthalpy change, and the reaction is termed exothermic. A negative value of ΔH° is hallmark of a favorable reaction. Although the meaning of ΔH° appears simple, the bond energy changes associated with a particular binding reaction, is actually the resultant value of formation and breakage of many individual bonds. These individual changes may produce positive or negative contributions, which means that the observed enthalpy represents the net of many of these individual components.[23] The standard entropy change, ΔS°, is associated with the disorder in a system, with an increase in binding tending to decrease disorder. A positive value of ΔS° is favourable. It can be seen that increased binding tends to produce negative ΔH° values, and negative ΔS° values, which lead to opposing contributions to ΔG°. This enthalpy/entropy compensation, which appears due to effects of perturbing the weak intermolecular binding occurring in solvent water, may lead to smaller changes in ΔG°. The change in heat capacity, ΔCp controls how ΔH° and ΔS°, and hence how ΔG° change with temperature.[24-25]

3.11.3b. Hydrophobic Interactions

The classical understanding of hydrophobic interactions is that non-polar groups wishing to minimize contact with polar solvent molecules associate with each other. Hydrophobic interactions often are characterized by small (frequently positive) enthalpy

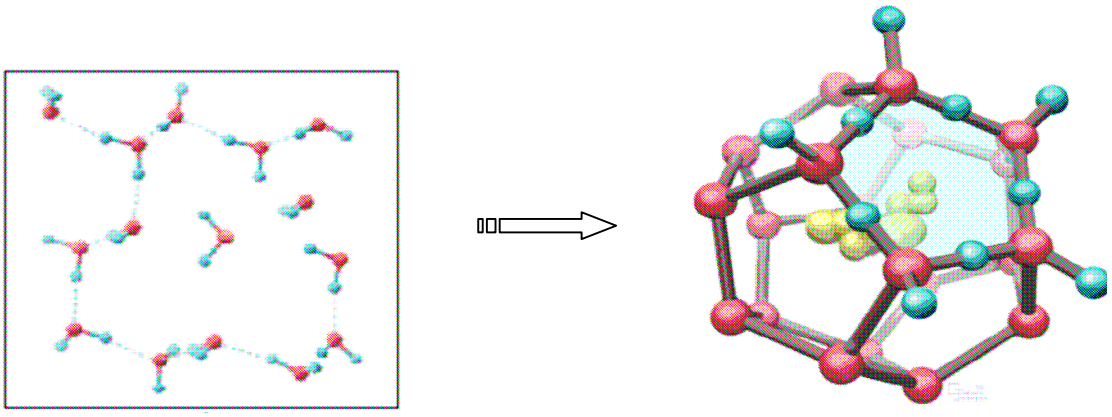

changes, large positive entropy changes, and often a negative contribution to ΔCp.[26,27] This may be explained by considering the interactions of solvent water around a non-polar solute. In the presence of a non-polar compound, the normal hydrogen bond network of water is re-organized. In an effort to maximize the number of inter-solvent hydrogen bonds, water molecules align themselves around the apolar compound. The binding thermodynamics of hydrophobic interactions are thus explained by an increase in entropy, which results from the release of relatively highly ordered water molecules surrounding the apolar surfaces of the two interacting molecules. These water molecules return to bulk where they re-establish hydrogen bonds, a process that is entropically favorable and slightly endothermic.

Hydrophobic effect in DNA: Similar to hydrophobic side chains in proteins, the hydrophobic groups in nucleic acids (the aromatic bases) are buried, and the hydrophilic groups (the sugar and phosphates) are exposed.

3.11.3c. Electrostatic Interactions

Electrostatic interactions arise from the attractive forces between charged or dipolar ligands and the counter-charged binding site on a macromolecule. The dielectric constant at a binding site may be considerably lower than the dielectric constant of bulk solvent, and would thus favor strong charge-charge interactions upon binding, but transferring a charged group to a low dielectric environment is unfavorable. This is because buried charged groups must be stabilized by local dipoles.[28] The binding of charged groups to macromolecules often is entropically driven, with low values of ΔH°.[29] An entropic advantage is also expected for displacement of the water molecules solvating the free charged groups.

3.11.3d. Hydrogen Bonds

Hydrogen bond formation is thought to be particularly important in biological binding interactions. However, it is often overlooked that hydrogen bond formation between a macromolecule and ligand, is at the cost of disrupting hydrogen bonds between the macromolecule and water and also between the ligand and water. Thus, hydrogen bond formation in a complex is accompanied by a relatively small net contribution to binding thermodynamics.[30] Though the energy of a single hydrogen bond is estimated to be around 21 kJ/mol (5 kcal/mol), net contributions to binding thermodynamics are often much smaller than this due to the nature of hydrogen bond exchange. However in terms of binding strength, a single hydrogen bond may contribute from 10 to around 10,000 fold to affinity. This illustrates that it is extremely difficult to make generalizations

regarding the contribution of a single hydrogen bond to overall binding affinity, or to characterize strength of binding in terms of the enthalpy of hydrogen bond formation. The properties of hydrogen bond donor and acceptor, as well as their local surroundings in both the free and complexed states must be taken into account in order to assign parameterizations.[31]

Base pairing in DNA: Each base pair makes two or three hydrogen bonds. Since these are shielded from solvent, they should stabilize DNA base pairing. However, there's an entropy cost to adopting this very ordered state, and the enthalpy gain is partially offset by an entropy penalty.

3.11.3e. Conformational Changes

Ligand induced conformational changes are important in many binding interactions, and are responsible for several significant functional roles. Conformational changes may be responsible for correct orientation of active site residues involved in catalysis, or may facilitate the subsequent binding of ligands such as other substrates or allosteric effectors. It is likely that conformational changes occurring on ligand binding are subtle changes rather than the large changes exemplified by unfolding or refolding reactions. These subtle changes are therefore expected to exhibit relatively low magnitudes for both ΔH° and ΔS° (usually with strong enthalpy-entropy compensation), with negative values anticipated for ΔCp.[32]

3.11.3f. The Role of Water in Binding Interactions

It is evident from the discussion above that solvent water plays a key role in governing biomolecular-binding interactions. Water molecules interact with both the free partners and the complex, and any changes in the number of water molecules located at a binding interface may have a dominant effect on binding affinity. These locally structured water molecules can potentially be retained or released during binding interaction with very different thermodynamic consequences. The release of bound water molecules from a binding interface is associated with a favourable gain in entropy as these molecules are displaced back into bulk. However this is an enthalpically unfavorable process as the strong bonds made with the macromolecule are broken. Conversely, retention of water may be associated with a favourable enthalpy resulting from increased hydrogen bonding, but an unfavorable entropy penalty.

3.11.3g. Enthalpy-Entropy Compensation

The phenomenon of enthalpy-entropy compensation appears in many, if not all biochemical thermodynamic binding studies. Enthalpy-entropy compensation is characterized by the linear relationship that is observed between the enthalpy change and the entropy change in a binding interaction. Hence, large changes in ΔH° are compensated by large and opposing changes in ΔS°, which almost cancel leading to much smaller variations in the observed ΔG°. Enthalpy-entropy compensation in these systems, seems at first to be connected to the properties of solvent water, but actually

appears to be an almost inescapable general consequence of perturbing most weak intermolecular interactions.[33,34]

At the thermodynamic level, the binding affinity is dictated by the Gibbs free energy (ΔG), which in turn depends on the enthalpy and entropy changes, associated with binding. In principle, many combinations of enthalpy and entropy changes are consistent with any ΔG, and therefore the corresponding binding affinity. In reality, the situation is different because ΔH and ΔS reflect different types of interactions, and for small molecule binding to proteins, the ensemble of interactions is finite and dictated by the type of interactions that can be established between the constituent atoms. Enthalpic contributions reflect the strength of H-bonds, van der Waals interactions relative to those with the solvent (water). Entropic contributions to the binding affinity, on the other hand, are mainly due to a large increase in solvent entropy arising from the burial of hydrophobic groups upon binding, and the loss of conformational degrees of freedom associated with binding. In this regard, it must be noted that the binding of conformationally constrained, highly hydrophobic ligands is entropically driven because their binding affinity is dominated by the burial of hydrophobic groups coupled to a minimal loss of conformational degrees of freedom.[35-37]

3.12. RESULTS AND DISCUSSION

In the research field of nanotechnology, DNA is recognized as nanomaterial, not as a biological material. It is obvious that DNA molecule is one of the most promising functional nanomaterial. However, the application of DNA molecules is still under study because of the big gap that exists between theory and practice.

3.12.1. Studies on interactions of nucleobases and *aeg*PNA monomers with Gold nanoparticles by Spectroscopy, microscopy and calorimetry

The specific objective of this section is to carry out the interaction studies and thermodynamic analysis for the interaction of the nucleobases (Figure 2A) (A, G, C and T) as well as the corresponding PNA monomers (Figure 2B) with AuNPs at molecular level by UV-visible Spectroscopy, Isothermal Titration Calorimetry (ITC) and Transmission electron microscopy (TEM).

3.12.1.1. Synthesis of Gold nanoparticles (AuNP) and *aeg*PNA monomers

Chloroauric acid ($HAuCl_4$), sodium borohydride, adenine (A), guanine (G), cytosine (C), and thymine (T) were obtained from Aldrich Chemicals and used as received. Aqueous gold nanoparticles were synthesized by borohydride reduction of chloroauric acid (10^{-4} M of aqueous solution of $HAuCl_4$) resulting in a ruby red solution with gold nanoparticles of dimensions 65 ± 7 Å[38] (Figure 9). The pH of the solution was adjusted to physiological pH using dilute hydrochloric acid, and the solution was dialyzed for 24 h. All four amino ethyl glycyl (*aeg*)-PNA monomers (Figure 2B) were synthesized in the laboratory as described earlier.[39] The capping of the gold nanoparticles with the PNA base monomers and nucleobases was achieved by mixing 1.47 mL of 10^{-4} M AuNPs with 300 μL of 0.25 mM PNA monomers and 2.5 mM DNA bases. It is also

noted that nucleobase, guanine is almost insoluble in water, 5% methanolic aqueous solution of guanine is used.

3.12.1.2. Interaction *aeg*PNA monomers and nucleobases with Gold nanoparticles: Studies by UV-visible Spectroscopy

Figures 10A & 10B show the UV-vis absorption spectra recorded from AuNPs modified with *aeg*PNA monomers and nucleobases, respectively. It is seen that upon addition of *aeg*PNA-A **5**, *aeg*PNA-C **6**, and *aeg*PNA-G **7** monomers, the UV-visible band of the AuNPs at 520 nm was red shifted to 670 nm (Figure 10A). However, such a shift was not seen with *aeg*PNA-Thymine monomer **8**. A similar trend is seen in the interaction of nucleobases with AuNPs (Figure 10B); while a longitudinal plasmon band was not observed. The transverse plasmon band at ca. 520 nm broadens upon complexation with nucleobases adenine **1**, cytosine **2** and guanine **3**. However, these UV-

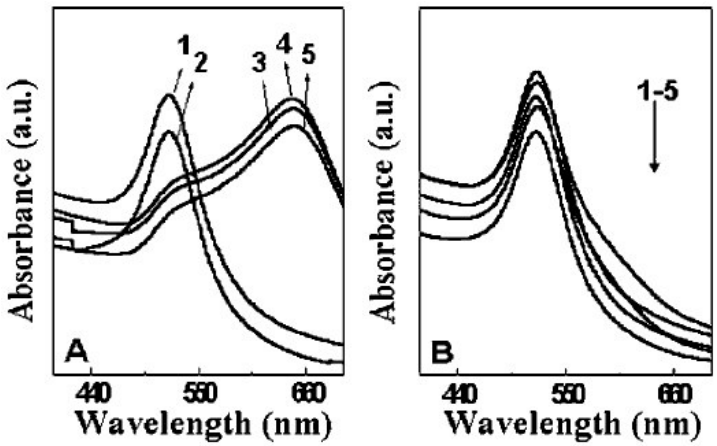

visible spectroscopy results are only qualitative and unable to differentiate the strength of interaction of the nucleobases/*aeg* PNA monomers with AuNPs.

3.12.1.3. Interaction of nucleobases and *aeg*PNA monomers with Gold nanoparticles: Studies by Transmission Electron Microscopy (TEM)

The TEM images were recorded on a JEOL Model 1200EX instrument operated at an accelerating voltage of 120 kV. STM images were obtained using a low-current, home-built instrument operated at a current of 17 pA and a bias voltage of 1V. The solution of the samples are prepared by capping of the gold nanoparticles with the *aeg*PNA base monomers **5**-**8** and nucleobases **1**-**4** which was achieved by mixing 1.47 mL of 10-4 M AuNP with 300 μL of 0.25 mM *aeg*PNA monomers and 2.5 mM

nucleobases. These samples for TEM analysis are prepared by drop coating films of the re-dispersed powder in de-ionized water on carbon-coated copper TEM grids, allowing the grid to stand for 2 minutes following which the extra solution was removed using a blotting paper.

Figures 11 & 12 show the TEM images nucleobases **1**-**4** and *aeg*PNA monomers **5**-**8** with AuNPs respectively. It is observed that free nucleobases upon interaction with AuNPs induce diminutive uniformly packed nanoorganization of gold particles (Figure 11). The nanoorganization of free nucleobases with AuNP involves the branched assemblies wherein a ribbon structure splits into narrower ribbon assemblies. In contrast, *aeg*PNA monomers with AuNPs exhibit clusters in an aggregated form with no particular ordering of gold nanoparticles (Figure 12). The TEM images though show a distinct difference in assembly structures do not highlight the differential binding affinities among four nucleobases **1**-**4** and *aeg*PNA monomers **5**-**8**.

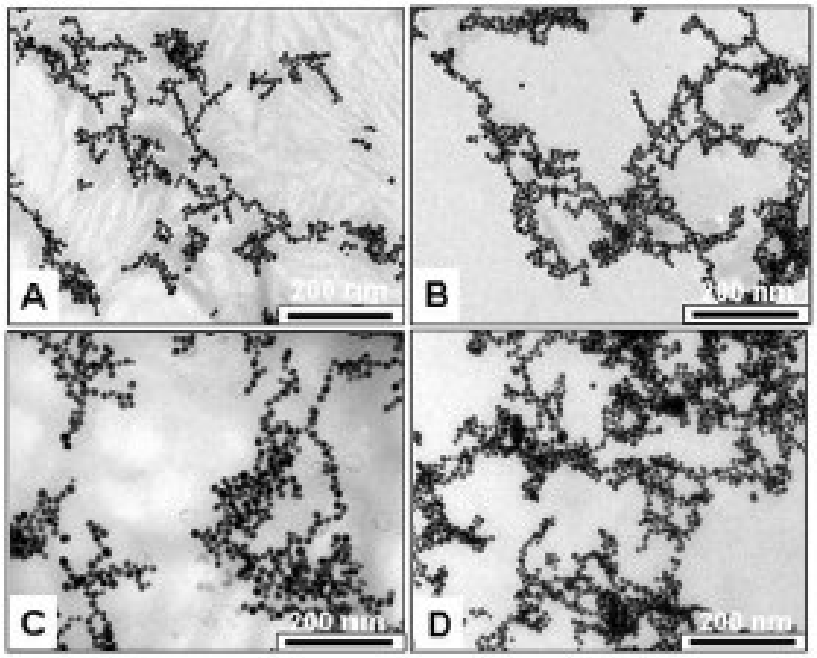

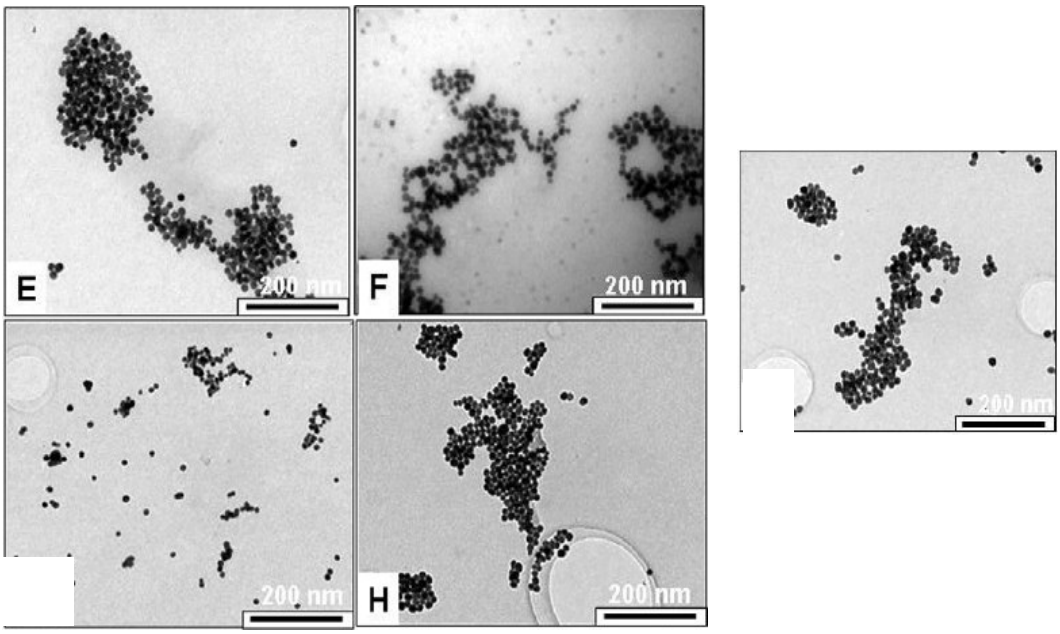

3.12.1.4. Interaction of nucleobases and *aeg*PNA monomers with Gold nanoparticles: Studies by Isothermal titration Calorimetry

The interaction between nucleobases and *aeg*PNA monomers with gold nanoparticles were studied directly by using isothermal titration calorimetry (ITC). The calorimeter consists of two cells: a reference cell filled with pure solvent (de-ionized water) and a sample titration cell filled with 1.47ml of dialyzed borohydride reduced gold hydrosol (10^{-4} M). The aqueous solution of nucleobases (2.5 mM) and PNA monomers (0.25 mM) were prepared and added from the syringe into the titration cell containing the dialyzed AuNPs in small steps of 10µl at an interval of 120s at 4^0C and at pH 7. The heat evolved/absorbed during interaction of nucleobases and *aeg*PNA monomers was recorded as positive or negative signals on a function of the added substrate.

Each negative peak shown in the heat signal curves from the interaction of AuNPs with free nucleobases **1**-**4** and *aeg*PNA monomers **5**-**8** (Figure 13 & 14) represents an exothermic process, representing the heat released in one injection of the nucleobases and *aeg*PNA monomers into the dialyzed borohydride reduced gold hydrosol as a function of time. The raw calorimetric data obtained during titration is shown in Figure 13 & 14, A-D, while the plots of the integrated calorimetric response obtained from the raw data plotted against the total volume of aqueous nucleobase solution added to the reaction vessel containing the AuNPs is shown in Figure 13 & 14, E-H. It should be pointed out that the data shown in Figure 13 & 14 has been corrected for heat effects arising due to dilution of the nucleobases **1**-**4** and *aeg*PNA monomers **5**-**8** (Figure 15 & 16) during titration. In all experiments, the interaction was found to be exothermic as seen by the negative calorimetric response. However, the magnitude of the response was a strong function of the type of nucleobase/*aeg*PNA monomer-AuNP complex and thus enabling a direct evaluation of the strength of the interaction in terms of calories of heat involved in such interaction.

The three nucleobases namely, adenine **1**, cytosine **2** and guanine **3** (Figure 13 E-G) and corresponding *aeg*PNA monomers **5**-**7** (Figure 14 E-G) respectively showed a classical binding behavior with a sigmoidal response. The exothermicity of the interaction of free nucleobases **1**-**4** was much lower than for the *aeg*PNA monomers **5**-**8**. The sigmoidal nature of the binding curves may be accounted on the basis of increasing coverage of gold nanoparticles by nucleobases/aegPNA monomers, which lowers the available surface area for the complexation during succeeding titrations. On the other hand, the titration of thymine **4** (Figure 13H) and *aeg*PNA-Thymine monomer **8** (Figure

14H) did not elicit a strong calorimetric response, with a fair degree of scatter existing in the data. The exothermic tail in each case perhaps arises from the dilution of the nucleobases/*aeg*PNA monomers during titration and upon completion of nanoparticle surface coverage by nucleobases/*aeg*PNA monomers. Primarily, the strength of interaction of free nucleobases **1**-**4** and *aeg*PNA monomers **5**-**8** with AuNPs are evaluated on the basis of exothermicity during initial stages of interaction. The strength of interaction of nucleobases and *aeg*PNA monomers with AuNPs decreases in the order C > G > A > T, are given in Table 1.

Table 1. AuNP-nucleobase/*aeg*PNA Interaction Exothermicity in Cal/mol

Entry		**Nucleobases**	**PNA monomers**
1.	Cytosine	- 732.2	- 2445.0
2.	Guanine	- 427.2	- 1148.0
3.	Adenine	- 249.3	- 518.5
4.	Thymine	----	----

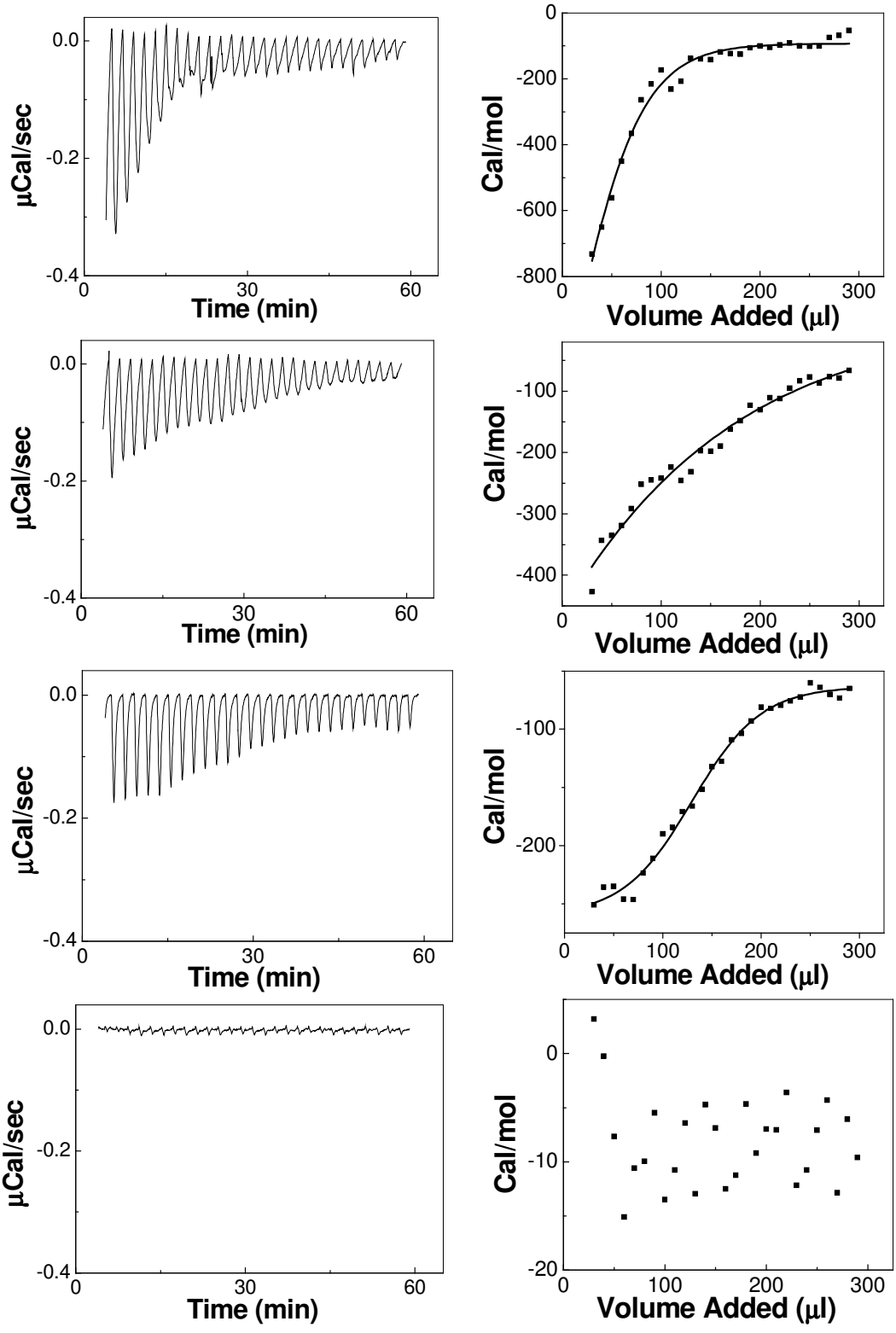
µCal/sec
Time (min)
Cal/mol
Volume Added (µl)
0.0
-0.2
-0.4
0
30
60
-200
-400
-600
-800
100
200
300
-100
-300
-10
-20

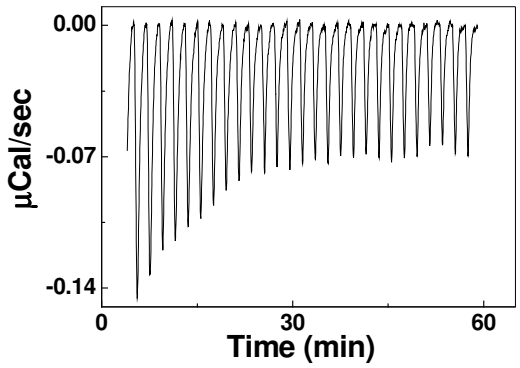
0.00
-0.07
-0.14
µCal/sec
0
30
60
Time (min)

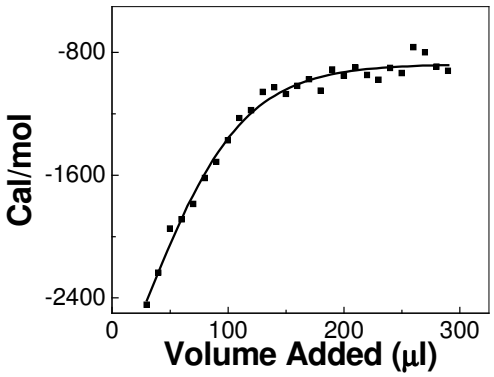
-800
-1600
-2400
Cal/mol
0
100
200
300
Volume Added (µl)

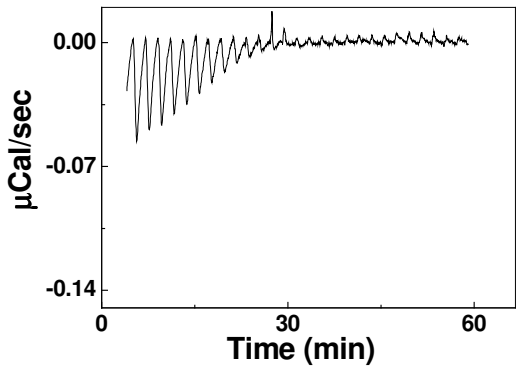
0.00
-0.07
-0.14
µCal/sec
0
30
60
Time (min)

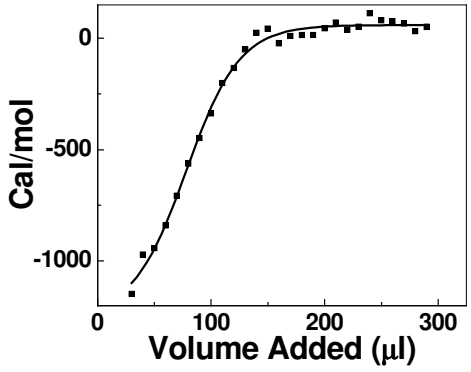
0
-500
-1000
Cal/mol
0
100
200
300
Volume Added (µl)

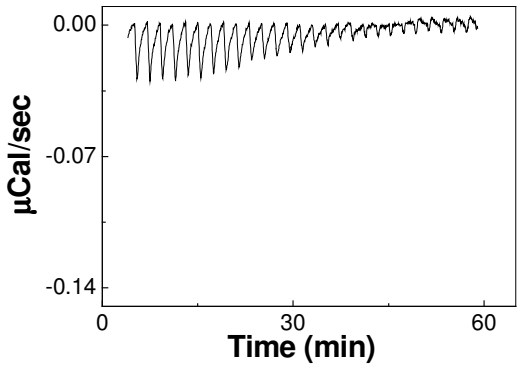
0.00
-0.07
-0.14
µCal/sec
0
30
60
Time (min)

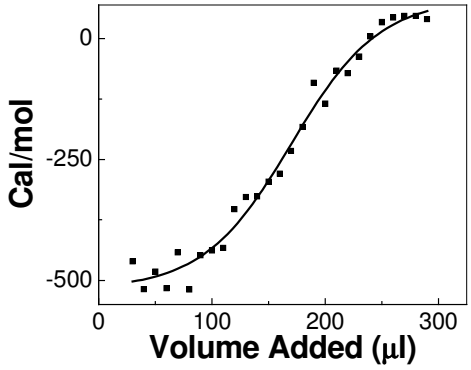
0
-250
-500
Cal/mol
0
100
200
300
Volume Added (µl)

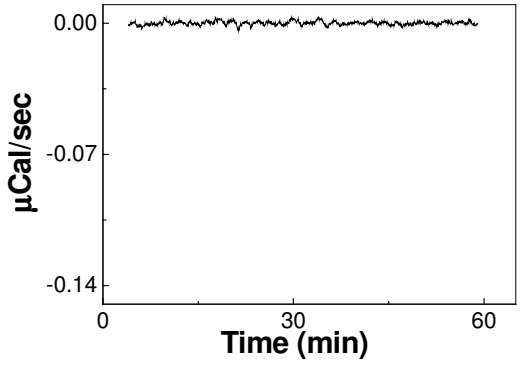
0.00
-0.07
-0.14
µCal/sec
0
30
60
Time (min)

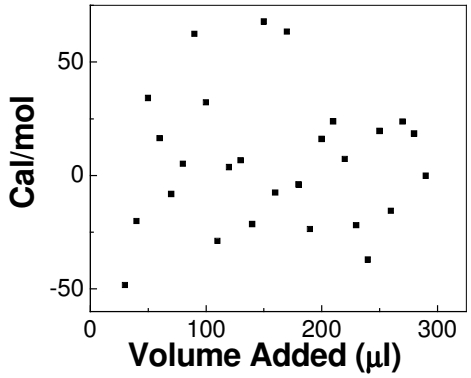
50
0
-50
Cal/mol
0
100
200
300
Volume Added (µl)

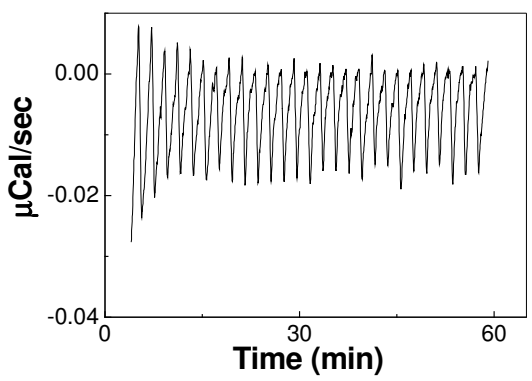
µCal/sec
0.00
-0.02
-0.04
0
30
60
Time (min)

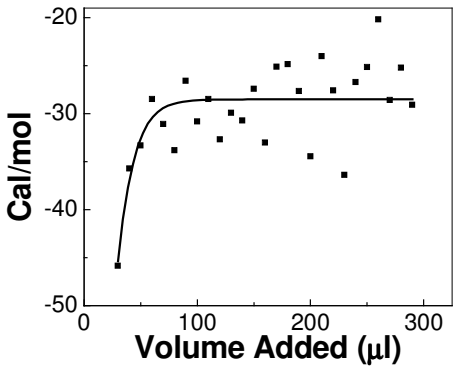
Cal/mol
-20
-30
-40
-50
0
100
200
300
Volume Added (µl)

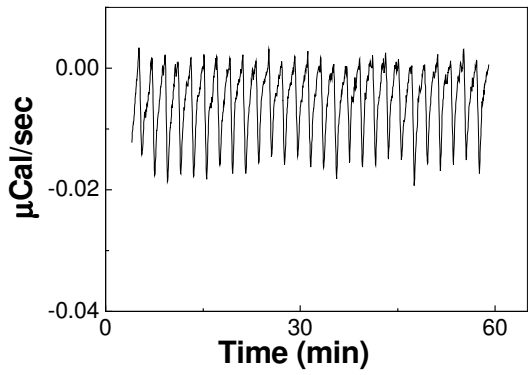
µCal/sec
0.00
-0.02
-0.04
0
30
60
Time (min)

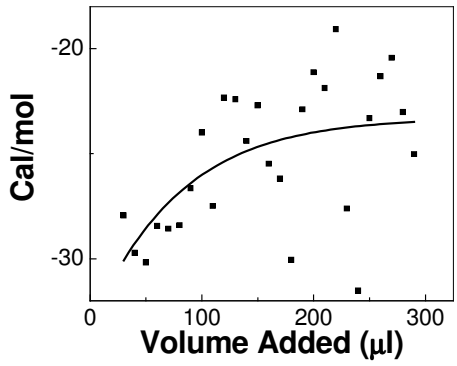
Cal/mol
-20
-30
0
100
200
300
Volume Added (µl)

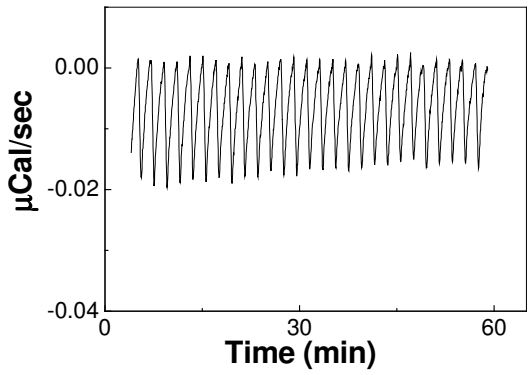
µCal/sec
0.00
-0.02
-0.04
0
30
60
Time (min)

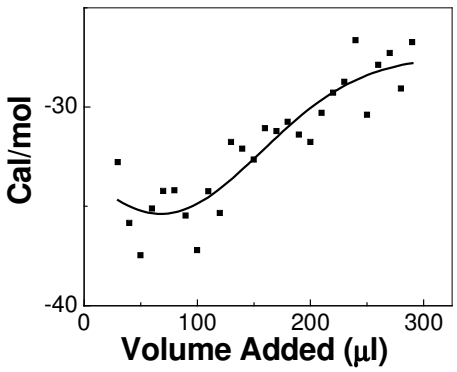
Cal/mol
-30
-40
0
100
200
300
Volume Added (µl)

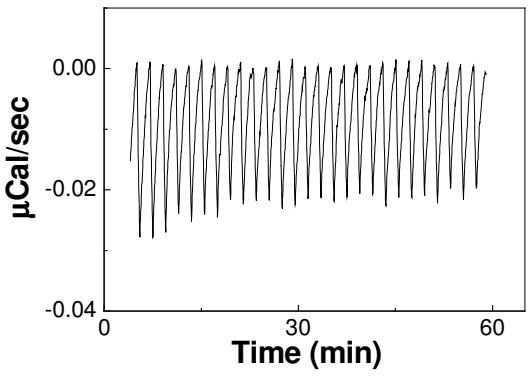
µCal/sec
0.00
-0.02
-0.04
0
30
60
Time (min)

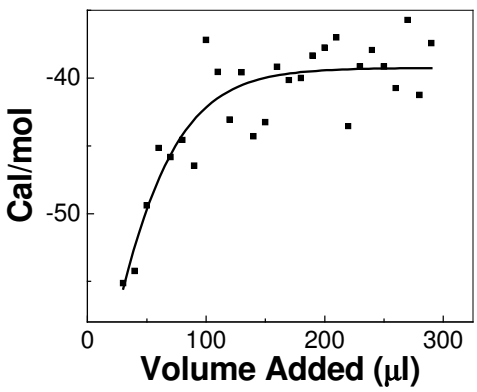
Cal/mol
-40
-50
0
100
200
300
Volume Added (µl)

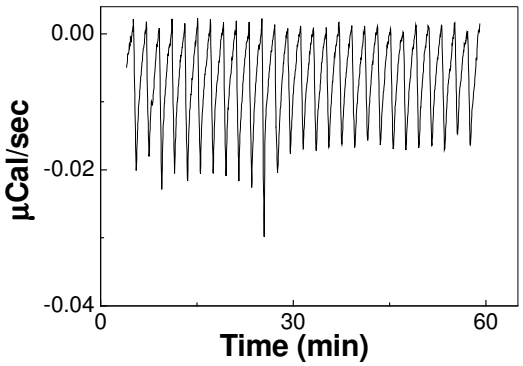
µCal/sec
0.00
-0.02
-0.04
0
30
60
Time (min)

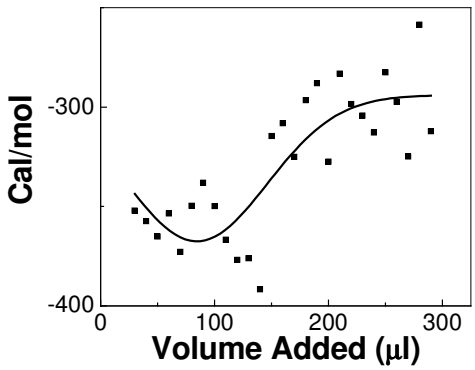
Cal/mol
-300
-400
0
100
200
300
Volume Added (µl)

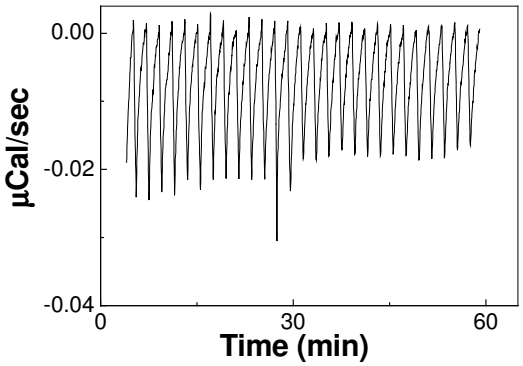
µCal/sec
0.00
-0.02
-0.04
0
30
60
Time (min)

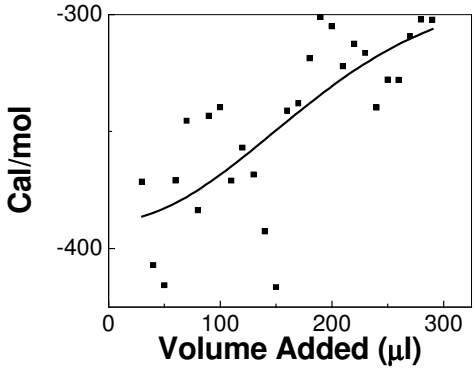
Cal/mol
-300
-400
0
100
200
300
Volume Added (µl)

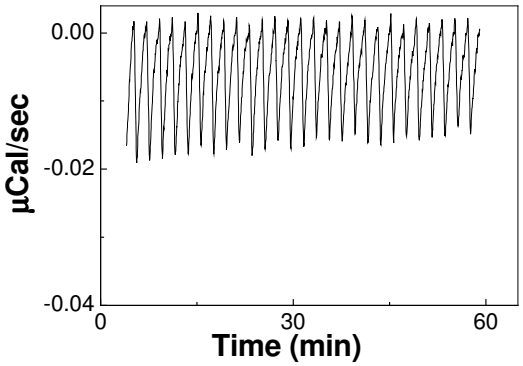
µCal/sec
0.00
-0.02
-0.04
0
30
60
Time (min)

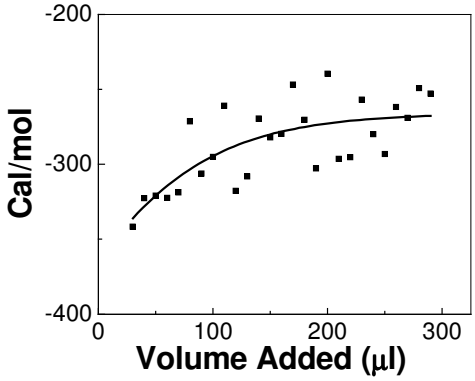
Cal/mol
-200
-300
-400
0
100
200
300
Volume Added (µl)

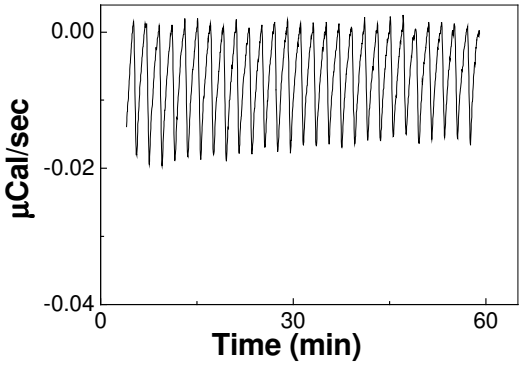
µCal/sec
0.00
-0.02
-0.04
0
30
60
Time (min)

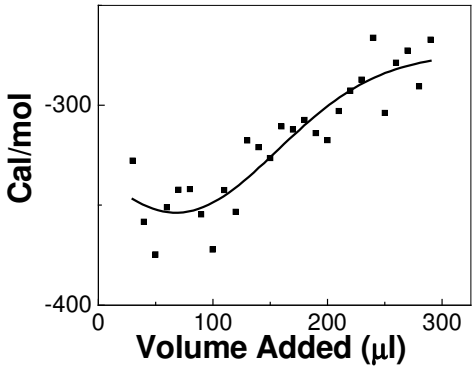
Cal/mol
-300
-400
0
100
200
300
Volume Added (µl)

3.12.1.4a. Thermodynamic analysis of the interaction of AuNPs with Nucleobases

ITC measured the heats of interaction of free nucleobases **1**-**4** and *aeg*PNA monomers **5**-**8** with AuNPs and indicated that binding is in the order C > G > A > T. The exothermicity of the first few injections of nucleobases into the AuNPs represents a measure of the strength of the interaction. By studying of nucleobases/*aeg*PNA monomers complexation with AuNPs, a model can be derived to analyze the ITC binding isotherms of nucleobase association with AuNPs and derive accurate thermodynamic parameters from the data.

The integrated area of peaks of binding are plotted as a function of concentration of the nucleobases. As seen from these plots, cytosine 2 **displays the largest interaction, while thymine** 4 **shows minimal interaction. Replacing the nucleobases** 1-3 **with corresponding *aeg*PNA** 5-7 **causes substantial increase in the strength of the interaction with AuNPs, as seen from much larger values on Y-axis.**

It is noted that the sequence of interaction seen from these plots is C > G > A > T for both free nucleobases (Figure 17a) and *aeg*PNA monomers (Figure 17b) suggesting

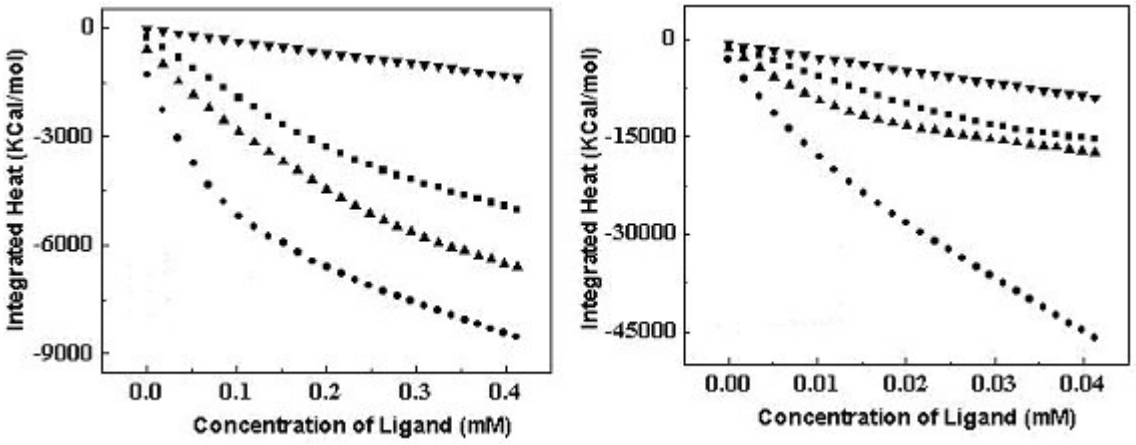

that the predominant interactions of *aeg*PNA with AuNPs are mediated between the nucleobases and the AuNPs.

In Figure 18a (Page 38), the integral heat data for the adenine-AuNP system has been converted to a plot of fractional loading (surface coverage θ) Vs concentration of the free ligand. This is a typical Langmuir, Michaelis Menton (MM) type of concave binding isotherm. The necessary mathematical derivation steps have been outlined in Annexure 1, Eqs 8-10. In Figure 18b, the corresponding inverse loading Vs inverse concentration plot is shown (a Lineweaver-Burke type plot) which is excellently linear. Cytosine also showed (Figure 19a and 19b) qualitatively similar features; even though the binding constants are much larger.

For thymine, as has been mentioned earlier, the binding is relatively weak, as seen earlier from the integral heat data. In the experimental range of ligand concentrations employed, the binding isotherm for thymine **4** is essentially linear, as shown in Figures 23a and 23b and is distinctly different from the concave nonlinear isotherms observed for the other three bases (Figure 18a-20a).

The derivation steps shown in Annexure I enable computation of the geometric factor, α and the binding constant, K_A and these are shown in Table 2**.** The geometric factor, α signifying to take into account the different areas of the nitrogenous bases and the site for the binding on gold nanoparticles whereas the binding constant $K_A$is a measure of extent of an association between two molecular species, nucleobases/aegPNA monomer with gold nanoparticle. The binding constant that expresses the propensity of the species to form from its component parts. The larger the binding constant, the more

stable is the species. The binding constant is reciprocal of an instability constant or dissociation constant.

Table 2. Binding parameters for nucleobases
[See eq 9]

Base	α	K_A (mol/ Litre)	Residual
Cytosine	1.177 ± 0.034	1.060 (± 0.103) x 10^4	0.0412
Guanine	1.723 ± 0.068	3.328 (± 0.249) x 10^3	0.0257
Adenine	2.036 ± 0.056	2.358 (± 0.109) x 10^3	0.0137
Thymine	8.41 ± 1.250	3.226 (± 0.530) x 10^2	0.011

3.12.1.4b. Thermodynamic analysis of the interaction of AuNP-*aeg*PNA monomers

As estimated by the ITC measurements, the AuNP–*aeg*PNA monomers **5**-**8** interaction is much stronger in comparison with that with free nucleobases **1**-**4**. This is in agreement with the integral heat plots (Figure 17a and Figure 17b) and further substantiated by the surface coverage plots of Figures 22a-25a and 22b-25b. In every case, excellent isotherm fits are obtained for all these *aeg*PNA monomers.

The various parameters, α and K_A for *aeg*PNA monomers obtained from the analysis are listed in Table 3. One surprising feature is the enhanced value of the binding for the *aeg*PNA-G monomer **7** in comparison to *aeg*PNA-C **6**. In *aeg*PNA monomers, guanine showed the highest binding constant K_A of 7.5 x 10^4 that is several folds higher than that of the other nucleobases.

Table 3: Binding parameters for *aeg*PNA monomers.
[See eq 9]

*aeg*PNA	α	K_A (mol/ Litre)	Residual
Cytosine	1.918 ± 0.10	2.519 (± 0.223) x 10^4	0.0264
Guanine	1.329 ± 0.022	7.051 (± 0.305) x 10^4	0.0181
Adenine	2.158 ± 0.077	2.204 (± 0.126) x 10^4	0.0166
Thymine	3.438 ± 0.45	9.790 (± 1.650) x 10^3	0.0234

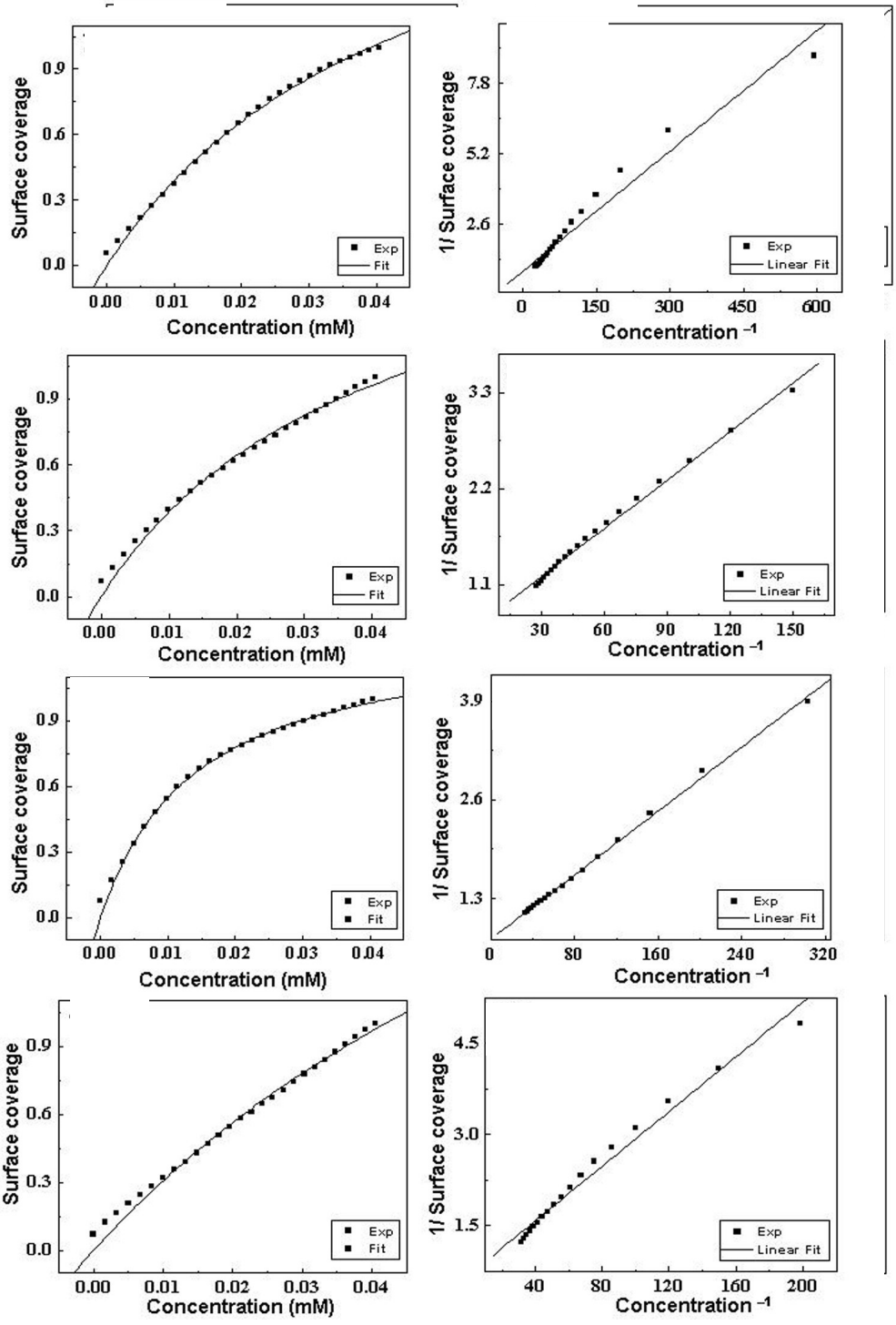
Surface coverage
Concentration (mM)
Exp
Fit
1/ Surface coverage
Concentration $^{-1}$
Linear Fit

3.12.1.4c. Thermodynamic analysis of Interaction of nucleobases and *aeg*PNA monomers with AuNPs

The statistical factor, α showed considerable variation among the nucleobases **1**-**4** and *aeg*PNA monomers **5**-**8** as seen in the data in Tables 2 and 3. A molecular level interpretation of the α parameter is not possible. It is noticed that for adenine (both for nucleobase itself **1** and with *aeg*PNA-adenine monomer **5** the α parameter is ~ 2. By assuming that two molecules are adsorbed on every AuNP surface atom, $(K_a C_L)^2$ should replace the $K_a C_L$ term in the undissociated molecular adsorption model (Annexure 1, Equation 8) amounting to a square dependence on the concentration term. However, this is not noticed in the best-fit model and thus the two-molecule/site model is effectively ruled out.

For cytosine, the α value is closer to 1 for the nucleobase itself **2** and approximately equals 2 for the *aeg*PNA-C monomer **6**. This suggests that the molecularity of the adsorption process is changed from one in nucleobase **2** to two *aeg*PNA-C **6** backbone which is highly unlikely since **6** is bulkier than **2**.

For guanine, the association constant, K_A parameter varies almost by 50 percent. But the highest difference is observed for thymine where, the α value for nucleobase **4** is 8.41 and for the *aeg*PNA-Thymine monomer **8** is 3.44. Thus in all probability, α is best interpreted as a geometric factor (and not a fudge factor), which effectively represents the predominance of molecular orientation over other proportion in binding. All nucleobases **1**-**4** and their corresponding *aeg*PNA monomers **5**-**8** holding on to a single receptor site is inconceivable.

It should be pointed out that since the exact surface area provided by the nanoparticles is unknown, only the average concentration of all nanoparticles (with a narrow size distribution) is estimated. What is known precisely is the concentration of gold atoms/ liter from the extinction measurements. How they are distributed on the surface, or whether the surface is indeed atomically rough (from the adsorption point of view) or whether there are kinks and edges additionally involved that influence the binding kinetics, are questions that cannot be speculated from present work.

The enthalpy of the process (ΔH) is obtained from the slope of the integrated heat Vs surface coverage and estimated using a simple least squares procedure. This plot is not shown in this work and the estimated heats are presented in the Tables 4 & 5.

Table 4 : Thermodynamic parameters of the DNA – GNP system at T = 283 ^{0}K

Base	**ΔG (Kcal/mol)**	**ΔH (Kcal/mol)**	**ΔS/R e.u**
Cytosine	-5.2148	-1.695	6.256
Guanine	-4.56	-0.505	7.2125
Adenine	-4.369	-0.319	7.198
Thymine	-3.25	-0.008	5.761

Table 5 : Thermodynamic parameters of the PNA – GNP system at T = 283 ^{0}K

Base	**ΔG (Kcal/mol)**	**ΔH (Kcal/mol)**	**ΔS/R e.u.**
Cytosine	-5.702	-2.473	5.7388
Guanine	-6.281	-2.538	6.6526
Adenine	-5.627	-0.676	8.799
Thymine	-5.170	-0.102	9.008

Tables 3 and 4 delineate the free energy functions into its constituent entropy and enthalpy factors. It is interesting to compare the free energies (affinity spectrum) for each

of the DNA/AuNP system and the entropies of adsorption. The enthalpy values are significant only for guanine and cytosine, and for Adenine and Thymine, the enthalpy values are minimal, with thymine displaying almost zero enthalpy of binding. For nucleobases **1**-**4** the affinity spectrum follows the sequence: C > G > A > T which is same as the order of enthalpy of binding. The entropy factors seem significant and drive the overall process of binding. The entropies of binding are all large and positive and follow the trend G > A > C > T and in contrast to the heats of adsorption, there are only marginal differences in the entropy values. If the result is attributed to entropy changes due to loss of degrees of freedom (like the rotational and vibrational modes), then the only slight differences in overall positive entropy values cannot be explained for since significant changes must occur between the pyrimidine and purine bases. In all probability, the large positive values arise may from the effects of desolvation on binding. This is only a speculation since under the conditions of the experiment; the state of the residual ions bound to the free nucleobases is unknown.

3.13. DISCUSSION

DNA-based nanotechnology has generated considerable interest in a number of applications due to the specificity, programmability and reproducibility of DNA interaction with nanoparticles. This section demonstrates the possible molecular basis of interaction of free nucleobases **1**-**4** and *aeg*PNA monomers **5**-**8** with gold nanoparticles

studied competently with a combination of UV-Visible spectroscopy, Transmission electron Microscopy (TEM) and Isothermal Titration calorimetry (ITC).

For the *aeg*PNA monomers **5**-**7** interaction with AuNPs, binding is indicated by the appearance of a longitudinal plasmon band at ca. 670 nm, indicative of aggregation of the nanoparticles. In the case of *aeg*PNA-thymine monomer **8** interaction with AuNPs, the 670 nm band does not arise, suggesting weak interaction with the particles. A similar trend is seen in the reaction of free nucleobases **1**-**4** with gold nanoparticles in which a longitudinal absorption band is not observed (suggesting that the *aeg*PNA monomers **5**-**8** interact more strongly with AuNPs than the corresponding free nucleobases **1**-**4**) or lead to more aggregation. The transverse plasmon band at ca. 520 nm broadens upon AuNP complexation with A, C, and G **1**-**3**. These results show that both the thymine nucleobase **4** and *aeg*PNA-thymine monomer **8** interact much more weakly with AuNPs than the A, C and G **1**-**3**/*aeg*PNA monomers **5**-**7**. UV-visible spectroscopy is, however, unable to differentiate between the strength of interaction of the remaining three nucleobases/*aeg*PNA monomers with AuNPs. The TEM images for the composites of nucleobases **1**-**4** and *aeg*PNA monomers **5**-**8** with AuNPs are different from the free AuNPs, but are unable to highlight the differential binding affinities among the four nucleobases **1**-**4** and *aeg*PNA monomers **5**-**8**.

The concentration of *aeg*PNA monomers (0.25 mM) which was 10 times smaller than that of the nucleobases (2.5 mM) is enough to bring about the saturation of the gold nanoparticle surface. Since the integral heat is directly proportional to the surface coverage, it is used as a measure of the relative surface coverage. Further, the thermodynamic analysis of nucleobases/aegPNA monomers with AuNPs proposed a

novel transformation to relate the free equilibrium concentration of the ligand and the fractional loading.

The strengths of interaction of the nucleobases **1**-**4** and *aeg*PNA monomers **5**-**8** with AuNPs evaluated on the basis of the exothermicity during the initial stages of interaction (i.e., when the AuNP surface is bare). The strength of interaction of the nucleobases/*aeg*PNA monomers decreases in the order C > G > A > T. Amine groups have been shown to bind exceptionally strongly with aqueous AuNPs, and the weak interaction of thymine with the AuNPs could be due to the absence of an exocyclic amino group in this nucleobase.

From the number of injections required for saturation of the calorimetric response on AuNPs, an equilibrium coverage of 0.2mM, 0.35mM and 0.39mM determined for cytosine, guanine, and adenine and 0.025mM, 0.028mM and 0.039mM for their corresponding *aeg*PNA monomers, respectively. This may be perhaps attributed to a secondary binding interaction (from backbone) between AuNPs and the *aeg*PNA monomers and their more bulky size. Amine groups have been shown to bind exceptionally strongly with aqueous AuNPs. Thus, it is believed that the weak interaction of thymine with the AuNP could be due to the absence of an exocyclic amino group in this nucleobase. The weakest interaction of thymine and *aeg*PNA-thymine monomer is in agreement with previous results (G > A > C > T).[1,2,40] Previous studies on understanding the nature of interaction of nucleobases with nanogold have made use of various spectroscopic techniques such as surface-enhanced Raman spectroscopy (SERS),[40] Fourier transform infrared (FTIR),[1] and reflection absorption infrared (RAIR) spectroscopies,[2] which are somewhat indirect methods for estimation of the strength of

the abovementioned interactions. But it is observed the different order in the strength of interaction of the other three nucleobases/*aeg*PNA base monomers (Cytosine, Guanine and Adenine) using the more direct, calorimetric evaluation.

In the study conceptually closest to present, Mirkin and co-workers have used temperature-programmed desorption (TPD) to study the interaction of DNA bases and nucleosides with gold thin films.[2] There were several striking trends that appear in their data. First, thymine interacts much more weakly with the gold surface than the other nucleobases studied. In general, the pyrimidines, thymine, and cytosine desorb at lower temperatures than the purines, adenine, and guanine in the order of G > A > C > T. It is believed that the differences in the strength of interactions of the free nucleobases in this studies and that of the Mirkin group[2] could be attributed to differences in surface chemistry; in the case of solution-based AuNPs, the role of surface-bound $AuCl_4^-/AuCl_2^-$ ions in modulating these interactions cannot be neglected. The differences could also be due the fact that free nucleobases/*aeg*PNA monomers have been used in this study, while nucleosides were studied in earlier reports. However, the difference in binding does not alter the order of interaction of the *aeg*PNA monomers with AuNPs; they mirror the results obtained with nucleobases.

From thermodynamic analysis, it was noted that the sum of entropies of binding of the A-T pair and the G-C pair (Table 1, $\Delta S(A+T) \cong 13.95$; $\Delta S(G+C) \cong 13.46$) are approximately equal, to a reasonable assumption. This cannot be coincidental as DNA duplex self-assemblies from two strands in aqueous salt media. The entropy gain is uniform in space, as it has to be, because the sugar – phosphate backbone is unchanged.

For *aeg*PNA monomers, the affinity order follows the sequence G > C > A > T, which is same as the heat changes, but only marginal difference noticed among the free energies for A, C and G. ($\Delta G \sim 1$ Kcal is seen between G and T). Thymine has the lowest heat, but a large positive entropy of binding. For *aeg*PNA monomers, the binding constants K_A are at least an order higher than the free nucleobases, but the entropy factors are also much larger and positive. Thymine, in particular has the highest entropy change value of ~ 9 e.u.

The addition of the entropy change factors of complementary base pairs, in the form of *aeg*PNA is $\Delta S(A+T) \cong 17.8 e.u.$; $\Delta S(G+C) \cong 12.38 e.u.$ suggesting a clear difference in the summed up ΔS values. This suggests that linking the nucleobase to a backbone as in *aeg*PNA monomer has consequences in binding to AuNPs. The assembly on AuNP would be more favored for the A – T pair in comparison to the G – C pair, if entropy factors were to solely determine the course of binding, as implied by the large positive values of the same. This is in sharp contrast to the pure DNA bases where A+T pair and G+C pair has the same probability of formation of AuNP complexes.

3.14. CONCLUSION

It is demonstrated that isothermal titration calorimetry can be successfully employed to study the thermodynamic parameters of nucleobase/*aeg*PNA:AuNP interaction. It is interesting to note that the *aeg*PNA monomers **5**-**8** bind much more strongly to the AuNPs than the free nucleobases **1**-**4**. The mole ratio and the corrected base concentration along with the estimated surface coverage were used to compute the

concentration of the unbound ligand. A straight forward fitting procedure using a Langmuir –Michaelis Menton type isotherm model provides an excellent picture. The validity of the above model was verified through convincing linear plots (Lineweaver – Burke plots) of the inverse surface coverage Vs the inverse ligand concentration. The binding constants were then subjected to a standard thermodynamic analysis. An attempt is carried out to understand the physical meaning of the positive entropies of adsorption for the nucleobases and complementary base pairs.

3.15. PRESENT WORK - II

PNA binds to DNA with very high affinity and selectivity and PNA:DNA hybrids are much more thermally stable than DNA:DNA hybrids. In view of this, and the fact that PNA is uncharged, it would be interesting to study the pattern of gold nanoparticle organization on PNA:DNA hybrids.

3.15.1. Interaction studies of DNA/PNA and DNA:PNA with Gold nanoparticles by Transmission Electron Microscopy (TEM)

Figure 34 shows TEM images of sodium borohydride reduced gold nanoparticles (uncapped) complexes with DNA (dA_8), PNA–T_8 and the duplex dA_8:PNA-T_8. Interestingly, it is observed that the single stranded DNA-A_8 induces a uniformly packed nano-organization of gold particles (Figure 26A & 26B) while the uncharged PNA-T_8 exhibits clusters in an aggregated form with no particular ordering of gold nanoparticles (Figure 26C & D). Upon mixing the two complementary strands, some bit of order is restored, but no linear superclustered assemblies were seen as in case of PNA_2:DNA triplexes (Figure 26E & F).

3.15.2. Interaction studies of DNA/PNA and DNA:PNA complex with Gold nanoparticles by UV-visible spectroscopy

The UV-Visible spectra showed a weak and broad red shifted surface plasmon band at nm. Thus charges present on DNA and gold nanoparticles seem to be the driving factors for formation of highly ordered linear superclusters by electrostatic complexation.

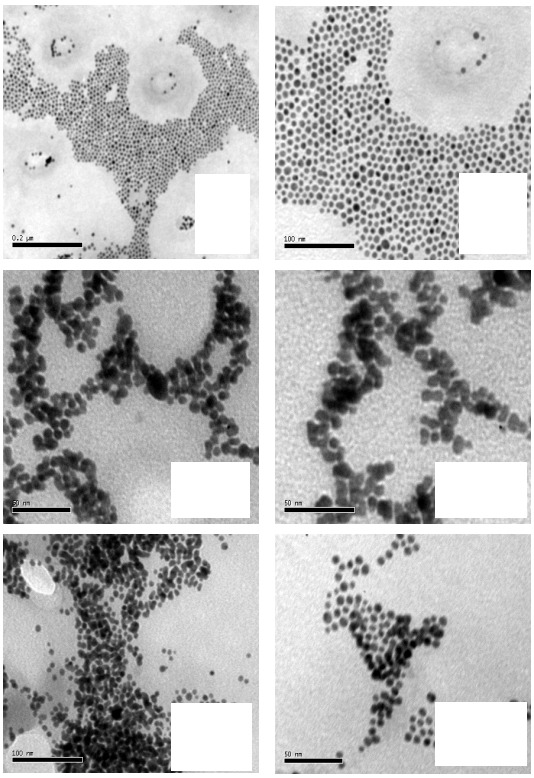

Figure 27 & 28 show the absorption spectra of AuNP composites without thiolation of DNA/PNA give the binding evidence at oligomeric level. So, without expenses of thiolation PNA/DNA are able to bind to the gold nanoparticles.

3.15.3. UV melting Studies on DNA:PNA-gold hybrids

The UV spectral data clearly suggest that there is a complex formation between AuNP-DNA A_8 with PNA T_8. A difference in λmax of AuNP, AuNP-DNA A_8 and the AuNP-DNA A_8:PNA T_8 was noticed with a red shift in absorption band upon addition of DNA-A_8 into the AuNPs. A similar trend is seen by addition of PNA-T_8. These data

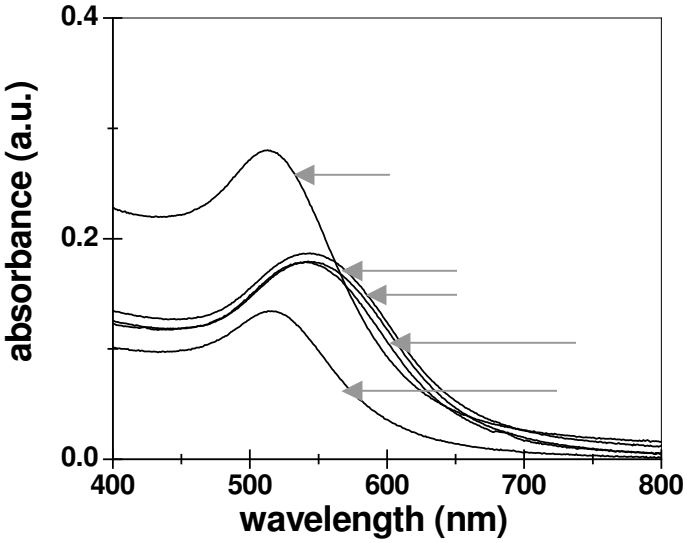

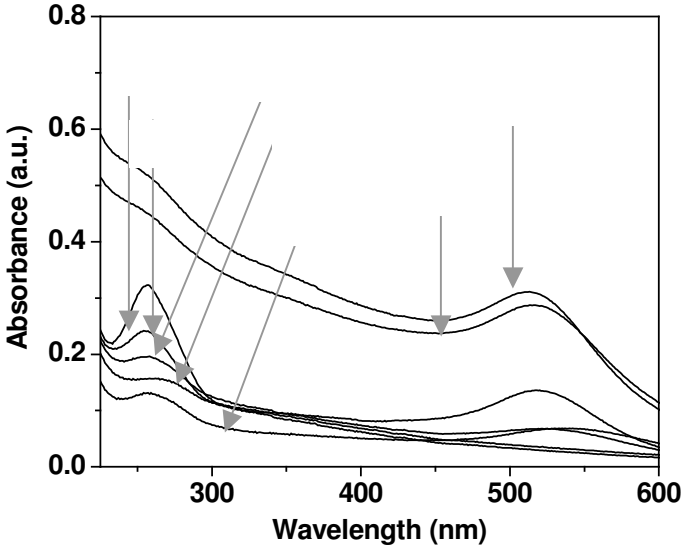

confirm the formation of DNA (T_8:A_8:T_8) triplex by attaching gold nanoparticles to the DNA without thiolation.

In order to examine the effect of gold nanoparticle complexation on the thermal stabilities of DNA:PNA hybrids, temperature dependent UV absorbance at 260 nm was

carried out. Gold nanoparticles do not have interfering absorbance in this region. The DNA:PNA duplexes both free and as gold complexes showed sigmoidal transitions characteristic of two phases and the T_m, the mid point of thermal transition obtained from first derivative of melting curves is shown in Table 6.

Table 6. UV-Tm of DNA:PNA hybrids

Entry	DNA:PNA (1:2)	T_m in ^{0}C	ΔT_m in ^{0}C
1.	d(A_8):PNA-T_8	39.1	----
2.	Au-d(A_8):PNA-T_8	74.2	35.1
3.	Au-d(A_8):Au-PNA-T_8	76.9	37.8
4.	Lys-Au-d(A_8):PNA-T_8	58.7	19.6

Significant stabilization of DNA:PNA hybrids occurs upon complexation with gold nanoparticles. When Au-DNA-A_8 is mixed with PNA–T_8, the stability is enhanced by about 35.1^{0}C (Table 6, entry 1 & 2), while mixing of DNA and PNA strands, both in gold complexed form had an improvement of about 37.8^{0}C (Table 6, entry 1 & 3). This suggested that even one strand complexation with gold nanoparticle is good enough to effect a large stabilization of hybrids. When lysine capped gold nanoparticles were used, the stability enhancement was much less (ΔT_m ~ 19^{0}C), perhaps due to the repulsive effects of positively charged lysine and the N-terminus of PNA. In addition to the observed stabilization, an interesting feature of the melting transitions were that they were much sharper compared to the uncomplexed hybrids. This is consistent with such features noticed earlier in literature and attributed to percolation transition phenomena.[61] It is also possible that the exocyclic amine groups on the nucleobase-Adenine in DNA-A_8 may directly interact with uncapped gold nanoparticles.

3.16. SUMMARY AND OUTLOOK

The DNA based nanotechnology has generated tremendous interest due to programmability, reproducibility and specificity of DNA/PNA-nanoparticle interactions. A thermodynamic analysis of the binding of Gold Nanoparticles (AuNP) with the free nucleobases A, T, G, C and also the nucleobases linked to *aeg*-backbone (PNA) was carried out using Isothermal Titration Calorimetry (ITC). For the free nucleobases the free energy of binding follows the sequence: C > G > A > T; for the *aeg*PNA monomers, the affinity order is G > C > A > T. In both cases, the entropy effects outweigh the enthalpy factors, and the overall process seems to be entropy driven.

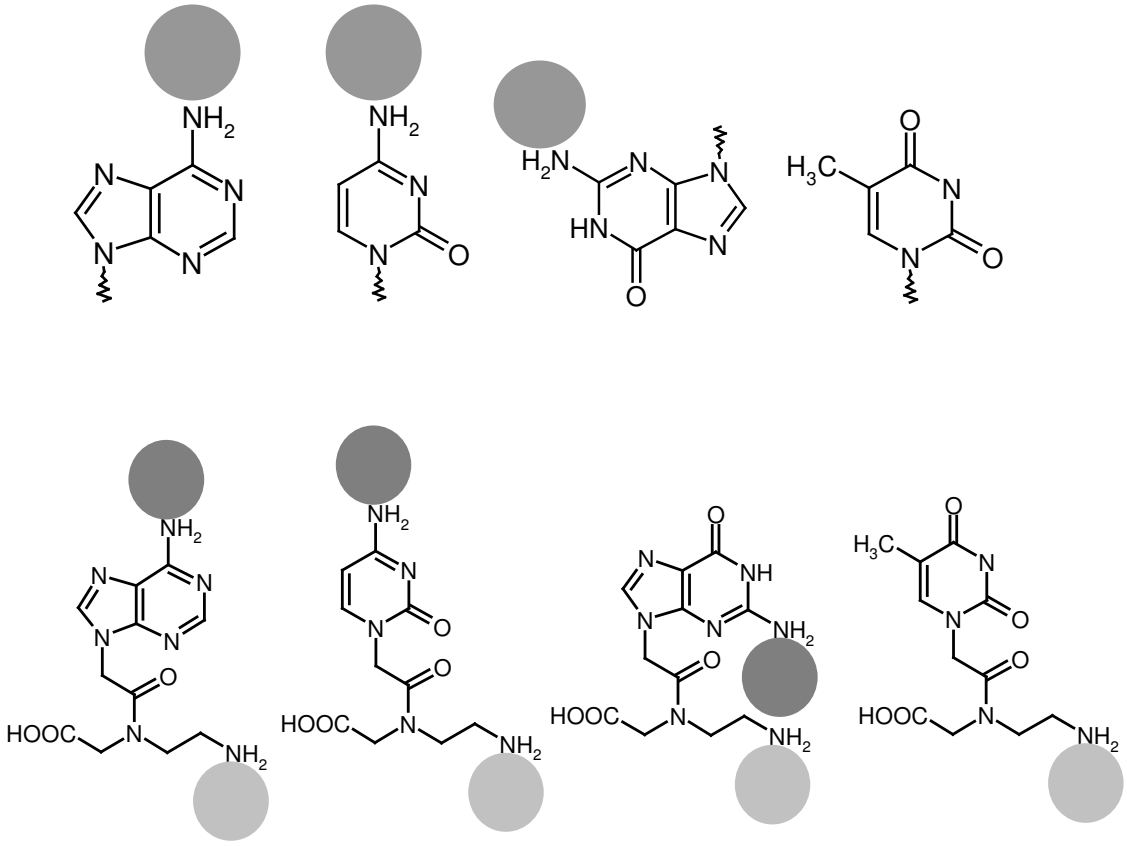

A novel transformation is proposed in which the free ligand concentration is estimated from the knowledge of the integral heat and fractional loading. This is shown to lead to a simple, reliable and stable estimation of all the thermodynamic parameters of interest.

In this chapter, the ability of nanoparticles to assemble into arrays and networks in presence of DNA/PNA template is demonstrated. This has the potential for fabrication of interesting nanodevices. Networks of nanometer–sized metal or semiconductor islands, or quantum dots, may exhibit a variety of quantum phenomena, with applications in optical devices, nanometer-sized sensors, advanced computer architectures, ultra dense memories, and quantum-information science and technology. The self-assembled nanostructures with DNA and PNA as a scaffold or templated assembly of nanoscale arrays is a useful concept for fabrication of such devices. DNA can be modified with functional groups at predetermined sites to allow for the attachment of other molecules in a specific manner. In this approach, nanoparticles bind to DNA even without thiolation. The ability to attach one or both ends of the DNA/gold complex, after generation of the desired pattern, to fixed contacts or electrodes is necessary for nanodevices fabrication.

Such organizing PNA-T_8 molecules interact weakly with gold nanoparticles, but PNA_2:DNA hybrids generated upon hybridization with complementary (DNA-A_8) can induce organization of gold nanoparticles in solution. Gold nanoparticles also remarkably stabilize the DNA:PNA hybrids against thermal denaturation.

This work also provides a number of important findings. First, the “melting transitions” observed for aggregates or individual particle layers hybridized to surfaces are indeed measurements of the entire cooperative melting processes, rather than spectroscopic

glimpses of the last stage of the melting process. Second, the melting properties of DNA linked nanoparticle aggregates are affected by a number of factors, including DNA surface density, nanoparticle size, interparticle distance, and salt concentration as well as charge on the nanoparticles. The T_m of these PNA:DNA-linked nanoparticle superstructures differing by changing the charge on nanoparticles.[58]

Solution-phase assembly of interconnected nanoparticles onto DNA/PNA is a powerful approach to patterning 1D and 2D arrangements of nanoparticles for applications in nanoelectronics. The linear, ribbon-like and branched nanoparticle assemblies prepared by this method will have a high degree of order and form close-packed, extended structures on surfaces that are readily observed by TEM. In addition, the assemblies appear to be thermally robust. Detailed analysis of the assembly structures suggests a possible mechanism for assembly that involves nucleation and growth. Higher-order structures composed of multiple nanoparticle/DNA:PNA assemblies are also formed during the assembly process through cross-linking of the DNA scaffolds by the polyvalent nanoparticles. Branched assemblies are also observed and their unique structures are attributed to the termination of one of the internal DNA strands. Further investigation of the assembly mechanism will prove useful in the development of this method for nanostructure preparation. The attributes of this system (the accessibility of diverse structural types, close-packing of nanoparticles along the scaffolds, and the thermal stability of the assemblies) offer support for the idea that such assemblies should prove useful as building blocks in the construction of integrated nanoelectronic devices.[35]

3.17. ANNEXURE

In this, it is formulated the basic equations of the ITC needed for the thermodynamic analysis for the interaction of nucleobases/ *aeg*PNA monomers with AuNPs. The raw data for this analysis was taken from nucleobase and *aeg*PNA monomer binding with AuNPs.

As is customary, microliters of the ligand (DNA bases/PNA monomers) is added to the receptor (AuNPs), through a total number of injections amounting to 30 in our case. V_O, C_i denote the cell volume and concentration of free ligand in the cell respectively and C_L denotes the total concentration of the ligand added up to 30 injections. C_R^O, C_R likewise represent the initial concentration of the receptors (AuNP) initially and after any given addition, in the same order. After taking due account of the dilution effects and corrections for the displaced volume following every addition, we have the following mass balance equation:

$$V_O C_i + N_R \theta = V_O C_L \qquad (1)$$

With the corrections given by[11-12]

$$C_R = C_O^R \frac{(1 - \Delta V / 2V_O)}{(1 + \Delta V / 2V_O)} \qquad (2)$$

$$C_L = C_L^O (1 - \Delta V / 2V_O) \qquad (3)$$

Here N_R, θ denote the total number of receptor molecules and surface coverage respectively present in the cell at any given instant. Further, we have

$$C_R^O = N_R / V_O ; C_L^O = \Delta V \times C_L^O / V_O$$

where ΔV is the total volume change (volume of the ligand receptor mixture which flows out on titration) of the titration.

$$\Delta V = \sum_i \Delta V_i \qquad (4)$$

For further developments, it is good to relate the equilibrium concentration of the free ligand in terms of the surface coverage (fractional loading of the AuNP receptors). If we assume a Michaelis- Menton (Langmuir) type model, then we have for (1:1 binding) the following expressions:

$$C_i = [\ \theta/(1-\theta)\ ]\ K_A^{-1} \qquad (5)$$

$$\frac{\theta}{1-\theta} + \beta f_1(\Delta V)\theta = \phi^O f_2(\Delta V) \qquad (6a)$$

Where

$$\beta = K_A C_R^O \qquad (6b)$$

$$f_1(\Delta V) = \frac{(1-\Delta V / 2V_O)}{(1+\Delta V / 2V_O)} \qquad (6c)$$

$$f_2(\Delta V) = (1-\Delta V / 2V_O) \qquad (6d)$$

$$\phi^O = K_A C_L^O / K_A C_R^O = C_L^O / C_R^O \qquad (6e)$$

The key factor that is of prime thermodynamic significance is the β parameter, which is defined as the product of the initial receptor concentration and the binding constant K_A. Considerable literature exists which predict the shape of the ITC curves *a*

priori (sigmoidal, concave etc.) based on the values of the β parameter. Another key parameter is the molar ratio of the ligand to the receptor at the start of the experiment and which is precisely known. $f_1(\Delta V)$ and $f_2(\Delta V)$ are the volume correction factors mentioned previously.

The foregoing considerations clearly relate the surface coverage to the correct molar ratio, a precisely known quantity. It is one of the powerful features of ITC that one can measure the integral heat of the titration directly by adding the individual heats released in a pulse of addition of the ligand. If $\overline{h_i}$ denotes the individual heat released in a pulse/unit fractional loading (akin to a differential heat) then we have

$$H^{\text{int}} = \int_0^{\theta} \overline{h_i} d\theta \qquad (7a)$$

$$= \overline{h_i}\ \overline{\theta} \qquad (7b)$$

Eq 7b of course implies constant energy of binding sites at every loading and makes the measurement of θ through H^{int}.

Once θ is known, it is a straightforward to determine β and K_A through a linear least squares procedure, as all quantities, except the β parameter is known in eq 6a. This has the advantage of avoiding the pitfalls associated with non-linear estimation, which others have employed earlier. It is to be borne in mind that customarily, the θ is fitted to a host parameters like K_A,N_R through a non –linear estimation procedure, which often give large uncertainties (confidence bands) for the parameters.

In our present work, a novel strategy is proposed. Since θ and the mole ratio ϕ^0 (see eq 6e) is known, eq 1 is transformed as:

$$C_i = C_L - \theta / \phi^0 \qquad (8)$$

Once the free ligand concentration and the surface coverage is computed it is a straightforward procedure to fit a plausible isotherm model.

The binding isotherm is postulated to be analogous to the standard MM – Langmuir model; i.e.,

$$\theta = \frac{\alpha K_A C_i}{(1 + K_A C_i)} \qquad (9)$$

Ideally we should try to physically interpret α in terms of a stoichiometric number but it is better to view it as a geometrical factor, which has to do with the way molecules are packed on the predominant crystal planes of the AuNP.

To further check the validity of eq 9 for the binding, we further transform it as follows:

$$1/\theta = 1/(\alpha K_A C_i) + 1/\alpha \qquad (10)$$

This is analogous to the Lineweaver –Burke plots. By plotting the inverse of the surface coverage Vs that of the free ligand concentration (eq 10), a straight line should result. For all the PNA base-GNP and DNA base-AuNP systems analyzed in the present work, it is shown that this is indeed the case.

3.18. REFERENCES

[1] Hiromi, K.; Petrovykh, D. Y.; Tarlov, M. J.; Whitman, L. J. Base-dependent competitive adsorption of single-stranded DNA on gold. *J. Am. Chem. Soc.* **2003**, *125*, 9014-9015.

[2] Demers, L. M.; Ostblom, M.; Zhang, H.; Jang, N. H.; Liedberg, B.; Mirkin, C. A. Thermal desorption behavior and binding properties of DNA bases and nucleosides on gold. *J. Am. Chem. Soc.* **2002**, *124*, 11248-11249.

[3] Sowerby, S.J.; Cohen, C.A.; Heckl, W.M.; Holm, N.G. Differential adsorption of nucleic acid bases: Relevance to the origin of life. *Proc. Natl. Acad. Sci. USA*. **2001**, *98*, 820-822.

[4] Friedman, R.A.; Honlig, B. A free energy analysis of nucleic acid base stacking in aqueous solution. *Biophys. J.* **1995**, *69*, 1528 – 35.

[5] Liu, T.; Tang, J.; Jiang, L. The enhancement effect of nanoparticles as a surface modifier on DNA sensor sensitivity. *Biochem. Biophys. Res. Commun.* **2004**, *313*, 3-7.

[6] Chakrabarti, R.; Klibanov, A. M. Nanocrystals modified with Peptide nucleic acids (PNAs) for selective self-assembly and DNA detection. *J. Am. Chem. Soc.* **2003**, *125*, 12531- 12540.

[7] Csaki, A.; Maubach, G.; Born, D.; Reichert, J.; Fritzsche, W. DNA-based molecular Nanotechnology. *Single Mol.* **2002**, 3, 275-280.

[8] Denney, R.C; Sinclair, R. *Visible and Ultraviolet Spectroscopy*. *Analytical Chemistry by open learning series*, John Wiley and Sons, USA.

[9] Mie, G.; *Ann. Phys*., **1908**, *25*, 377.

[19] Mulvaney, P. Surface plasmon spectroscopy of nanosized metal particles. *Langmuir*, **1996**, *12*, 788.

[11] Henglein, A. *J.Phys.B*., **1993**, *97*, 5457.

[12] (a) Brust, M.; Walker, M.; Bethell, D.; Schiffrin, D.J.; Whyman, R. *J.C.S. Chem Commun*., **1994**, 801.

[13] Malinsky, M.D.; Kelly, K.L.; Schatz, G.C.; VanDuyne, R.P. Chain length dependence and sensing capabilities of the localized surface plasmon resonance of silver

nanoparticles chemically modified with alkanethiol self-assembled monolayers. *J.Am.Chem.Soc*., **2001**, *123*, 1471.

[14] Templeton, A.C.; Wvelfing, W.P.; Murray, R.W. Monolayer-protected cluster molecules. *Acc.Chem.Res*., **2000**, *33*, 27.

[15] Knoll, M.; Ruska, E. *Z. Phys (Munich)* **1932**, *78*, 318.

[16] Warner, M.; Hutchison, J. Linear assemblies of nanoparticles electrostatically organized on DNA scaffolds. *Nature Materials*, **2003**, *2*, 272-277.

[17] Chellani, M. *Application Notes* **1999**, 14.

[18] Qin, L.; Srivastava, D. K. Energetics of Two-Step Binding of a Chromophoric Reaction Product, *trans*-3-Indoleacryloyl-CoA, to Medium-ChainAcyl-Coenzyme-A Dehydrogenase. *Biochemistry* **1998**, *37*, 3499.

[19] Pierce, M. M.; Raman, C. S.; Nall, B. T. Isothermal Titration Calorimetry of Protein-protein Interactions. *Methods* **1999**, *19*, 213.

[20] Barbieri, C. M.; Li, T. K.; Guo, S.; Wang, G.; Shallop, A. J.; Pan, W.; Yang, G.; Gaffney, B. L.; Jones, R. A.; Pilch, D. S. Aminoglycoside Complexation with a DNA·RNA Hybrid Duplex: The Thermodynamics of Recognition and Inhibition of RNA Processing Enzymes *J. Am. Chem. Soc.* **2003**, *125*, 6469.

[21] Kunne, A.; Sieber, M.; Meierhans, D.; Allemann, R. K. Thermodynamics of the DNA Binding Reaction of Transcription Factor MASH-1 *Biochemistry* **1998**, *37*, 4217.

[22] Wenk, M. R.; Seelig, J. Magainin 2 Amide Interaction with Lipid Membranes: Calorimetric Detection of Peptide Binding and Pore Formation *Biochemistry* **1998**, *37*, 3909.

[23] Fisher, H.; Singh, N. Calorimetric methods for interpreting protein-ligand interactions. *Methods Enzymol.* **1995**, *259*, 194-221.

[24] Sturtevant, J. Heat capacity and entropy changes in processes involving proteins. *Proc. Natl. Acad. Sci. U.S.A.* **1977**, *74*, 2236-2240.

[25] Eftink, M.; Biltonen, R. Thermodynamics of interacting biological systems. In A.E. Beezer (Ed.), Biological Microcalorimetry Academic Press, London, **1980**, 343-412.

[26] Lin, Z.; Schwarz, F. P.; Eisenstein, E. The hydrophobic nature of GroEL-substrate binding. *J. Biol. Chem.* **1994**, 270, 1011-1014.

[27] Srinivas, V.; B. Reddy, G.; Surolia, A. A predominantly hydrophobic recognition of H-antigenic sugars by winged bean acidic lectin: a thermodynamic study. *FEBS Lett.* **1999**, *450*, 181-185.

[28] Ward, W.; Jones, D. H.; Fersht, A. R. Effects of engineering complementary charged residues into the hydrophobic subunit interface of tyrosyl-tRNA synthetase. *Biochemistry,* **1987,** *26*, 4131-4138.

[29] Matulis, D.; Rouzina, I.; Bloomfield, V. A. Thermodynamics of DNA binding and condensation: isothermal titration calorimetry and electrostatic mechanism. *J. Mol. Biol.* **2000,** *296*, 1053-1063.

[30] Fersht, A. Structure and mechanism in protein science. **1999**, W.H. Freeman and Company, New York.

[31] Connelly, P. Acquisition and use of calorimetric data for prediction of the thermodynamics of ligand-binding and folding reactions of proteins. *Curr. Opin. Biotechnol.* **1994**, *5*, 381-388.

[32] Leder, L.; Berger, C.; Bornhauser, S.; Wendt, H.; Ackermann, F.; Jelesarov, I.; Bosshard, H. R. Spectroscopic, calorimetric, and kinetic demonstration of conformational adaptation in peptide-antibody recognition. *Biochemistry,* **1995**, *34*, 16509-16518.

[33] Dunitz, J. Win some, lose some: enthalpy-entropy compensation in weak intermolecular interactions. *Chem. Biol.* **1995**, *2*, 709-712.

[34] Gilli, P.; Ferretti, V.; Gilli, G. Enthalpy-entropy compensation in drug - receptor binding. *J. Phys. Chem.* **1994**, *98*, 1515-1518.

[35] Todd, M. J.; Luque, I.; Velazquez-Campoy, A.; Freire, E. The thermodynamic basis of resistance to HIV-1 protease inhibition. Calorimetric analysis of the V82F/I84V active site resistant mutant. *Biochemistry*, **2000**, *39*, 11876–11883.

[36] Velazquez-Campoy, A.; Kiso, Y.; Freire, E. The binding energetics of first and second generation HIV-1 protease inhibitors: Implications for drug design. *Archives of Biochimica and Biophysica*, **2001**, *390*, 169–175.

[37] Freire, E. Designing drugs against heterogeneous targets. *Nat. Biotech.* **2002**, *20*, 15-16.

[38] Patil, V.; Malvankar, R. B.; Sastry, M. Role of Particle Size in Individual and Competitive Diffusion of Carboxylic Acid Derivatized Colloidal Gold Particles in Thermally Evaporated Fatty Amine Films *Langmuir* **1999**, *15*, 8197-8206.

[39] Ganesh, K. N.; Nielsen, P. E. Peptide Nucleic Acids: Analogs and Derivatives. *Curr. Org. Chem.* **2000**, *4*, 916-928.

[40] Jang, N. H. The Co-ordination chemistry of DNA nucleosides on gold nanoparticles as a probe by SERS. *Bull. Korean Chem. Soc.* **2002**, *23*, 1790-1800.

Addendum

Chapter 3: Section A

Page 190	**Figure 1.**	Reproduced from Ref. 7.
Page 192	**Figure 2.**	Reproduced from http://zeeman.mit.edu/thesis/thesis-proposal.pdf
Page 203	**Figure 10.**	Reproduced from Ref. 49.
Page 204	**Figure 11.**	Reproduced from Ref. 54.
Page 206	**Figure 12.**	Reproduced from Ref. 56.
Page 207	**Figure 13.**	Reproduced from Ref. 57.
Page 208	**Figure 14.**	Reproduced from Ref. 58.
Page 217	**Figure 15.**	Reproduced from Ref. 83.

Chapter 3: Section A

Page 255	**Figure 11 A-D.**	Image Scale bar 200nm.
Page 256	**Figure 12 E-I.**	Image Scale bar 200nm.
Page 277	**Figure 26 A**	Image Scale bar 200nm.
	Figure 26 B	Image Scale bar 100nm.
	Figure 26 C	Image Scale bar 100nm.
	Figure 26 D	Image Scale bar 50nm.
	Figure 26 E	Image Scale bar 100nm.
	Figure 26 F	Image Scale bar 50nm.